INNOVATIVE APPROACHES IN MATERIALS SCIENCE AND APPLICATIONS

EDITORS
Hakan GÖKMEŞE
Şaban BÜLBÜL
Yusuf UZUN

ISRES Publishing

INNOVATIVE APPROACHES IN MATERIALS SCIENCE AND APPLICATIONS

EDITORS
Hakan GÖKMEŞE
Şaban BÜLBÜL
Yusuf UZUN

ISRES Publishing

Innovative Approaches in Materials Science and Applications

Edited by

Hakan GÖKMEŞE
Necmettin Erbakan University
Seydisehir Ahmet Cengiz Faculty of Engineering,
Department of Mechanical Engineering, Konya, Türkiye

Şaban BÜLBÜL
Necmettin Erbakan University,
Seydisehir Ahmet Cengiz Faculty of Engineering,
Department of Mechanical Engineering, Konya, Türkiye

Yusuf UZUN
Necmettin Erbakan University,
Seydisehir Ahmet Cengiz Faculty of Engineering,
Department of Computer Engineering, Konya, Türkiye

Language Editors
Lecturer Ceren DOĞAN
School of Foreign Languages, Necmettin Erbakan University, Türkiye
Email : cerendogan@erbakan.edu.tr

Cover Design & Layout
Resul BÜTÜNER
Directorate General for Innovation and Educational Technologies, Ankara, Türkiye
Email : resul.butuner@eba.gov.tr

ISRES Publishing

Innovative Approaches in Materials Science and Applications

Editors

Hakan GÖKMEŞE

Şaban BÜLBÜL

Yusuf UZUN

Language Editors

Ceren DOĞAN

Cover Design & Layout

Resul BÜTÜNER

This book was typeset in 10/12 pt. Times New Roman, Italic, Bold and Bold Italic.

Innovative Approaches in Materials Science and Applications
Published by ISRES Publishing, International Society for Research in Education and Science (ISRES). Includes bibliographical references and index.

ISBN
978-625-6959-94-1

Date of Issue
December, 2025

Contact
Aşkan Mah. Akınbey Sok. No: 5/A Meram/Konya/Türkiye
isresoffice@gmail.com
www.isres.org

Preface

In today's world, where the boundaries of science and technology are constantly expanding, materials science stands out as a field at the heart of this progress and forms the basis for all other disciplines.

This book aims to present the latest and most innovative approaches in materials science, combining them with their transformative applications in various engineering and scientific fields.

In addition to traditional material design approaches, it addresses pioneering topics such as nanotechnology applications, smart and adaptive materials, sustainable and recyclable materials, composite materials, advanced manufacturing techniques, and computational materials science.

Each chapter examines both fundamental scientific principles and industrial-scale applications from an integrated perspective, offering the reader both theoretical depth and practical insight.

The authors of this book are researchers known for their expertise and innovative work in their fields. They present current developments in their areas of specialization, examples from both around the world and in our country, and future perspectives in a candid style.

Without their valuable contributions and hard work, this work would not have been possible.

We offer them our deepest gratitude.

December, 2025

Prof. Dr. Hakan GÖKMEŞE
Necmettin Erbakan University
Seydisehir Ahmet Cengiz Faculty of Engineering
E-mail: hakan1440@gmail.com, **ORCID:** 0000-0003-0053-8444

Assoc. Prof. Dr. Şaban BÜLBÜL
Necmettin Erbakan University
Seydisehir Ahmet Cengiz Faculty of Engineering
E-mail: sabanbulbul@erbakan.edu.tr, **ORCID:** 0000-0002-9268-1469

Assist. Prof. Dr. Yusuf UZUN
Necmettin Erbakan University
Seydisehir Ahmet Cengiz Faculty of Engineering
E-mail: yuzun76tr@gmail.com, **ORCID:** 000-0002-7061-8784

Table of Contents

Contributors

M. Sc. Üzeyir YALMAN
Necmettin Erbakan University
E-mail: uzeyir.yalman52@hotmail.com, **ORCID:** 0000-0002-1221-5661

Prof Dr. Hakan GÖKMEŞE
Necmettin Erbakan University
Seydişehir Ahmet Cengiz Faculty of Engineering
Department of Mechanical Engineering
E-mail: hakan1440@gmail.com , **ORCID:** 0000-0003-0053-8444

Assist. Prof. Dr. Şaban BÜLBÜL
Necmettin Erbakan University
Seydişehir Ahmet Cengiz Faculty of Engineering
Department of Mechanical Engineering
E-mail: sabanbulbul42@hotmail.com , **ORCID:** 0000-0002-9268-1469

Dr. Tuba ARKAN DEMİRÖRS
KTO Karatay University
Faculty of Fine Arts and Design
Department of Interior Architecture
E-mail: tuba_arkan@hotmail.com, **ORCID:** 0000-0003-3278-9045

M. Sc. Fatma Nur ŞAHİN
Necmettin Erbakan University
E-mail: fnursahin7@gmail.com **ORCID:** 0000-0001-6071-0168

Assist. Prof. Dr. Mehmet KAYRICI
Necmettin Erbakan University,
Seydişehir Ahmet Cengiz Faculty of Engineering,
Department of Machine Engineering, Konya, Türkiye
E-mail: mkayrici@erbakan.edu.tr, **ORCID:** 0000-0001-8553-1166

M.Sc. Ahmet Faruk DOĞAN
Necmettin Erbakan University,
E-mail: 22820713012@ogr.erbakan.edu.tr, **ORCID:** 0009-0007-8712-3431

M.Sc. Okan KILINÇ
Necmettin Erbakan University
E-mail:okan@atimak.com.tr **ORCID**:0009-0007-8320-172X

Assoc. Prof. Dr. Dilek Nur ÖZEN
Necmettin Erbakan University,
Faculty of Engineering,
Department of Mechanical Engineering, Konya, Türkiye
E-mail: dnozen@erbakan.edu.tr, **ORCID:** 0000-0002-8622-4990

Prof.Dr.Melik ÇETİN
Karabük University,
Faculty of Engineering,
Department of Metallurgical and Materials Engineering
Email: mcetin@karabuk.edu.tr, **ORCID:** 0000-0002-6952-2523

Prof. Dr. Hayrettin AHLATCI
Karabük University,
Faculty of Engineering,
Department of Metallurgical and Materials Engineering
Email: hahlatci@karabuk.edu.tr, **ORCID:** 0000-0002-6766-4974

Dr. Kenza DJEBARI
Karabük University,
Faculty of Engineering,
Department of Metallurgical and Materials Engineering
Email: kenzadjebari@gmail.com, **ORCID:** ORCID: 0000-0003-0158-4741

Prof.Dr. Yavuz SUN
Karabük University,
Faculty of Engineering,
Department of Metallurgical and Materials Engineering
Email: ysun@karabuk.edu.tr, **ORCID:** 0000-0002-7336-5591

Dr. Mustafa ARAT
Directorate General of Electricity Generation Corporation, Ankara/Türkiye
Peter the Great St. Petersburg Polytechnic University, St. Petersburg/Russia
Email: mustafa.arat@euas.gov.tr, **ORCID:** 0000-0001-8783-6043

M.Sc. Selva ASTAN
Energetic Materials Research Center, R&D and Technology Directorate
Mechanical and Chemical Industries Corporation, Ankara,Türkiye
Email: selvaastan@gmail.com, **ORCID:** 0009-0007-3075-1410

Dr. Ahmet Burçin BATIBAY
Energetic Materials Research Center, R&D and Technology Directorate
Mechanical and Chemical Industries Corporation (MKE A.Ş.), Ankara,Türkiye
Email: batybay@gmail.com, **ORCID:** 0000-0002-2606-5115

Assist. Prof. Dr. Yusuf UZUN
Necmettin Erbakan University,
Seydişehir Ahmet Cengiz Faculty of Engineering,
Department of Computer Engineering, Konya, Türkiye
E-mail: yuzun76tr@gmail.com, **ORCID:** 0000-0002-7061-8784

Managing Editors

Hakan GÖKMEŞE Hakan GÖKMEŞE PhD is a Professor of Mechanical Engineering at Necmettin Erbakan University in Konya, Türkiye. He holds a master's degree in Metallurgy Education from Gazi University. His main areas of interest are casting technology, powder metallurgy, heat treatments and composites-nanocomposites applications.
E-mail: hakan1440@gmail.com , **ORCID:** 0000-0003-0053-8444

Şaban BÜLBÜL is an Associate Professor at Necmettin Erbakan University Faculty of Mechanical Engineering. Polymeric materials, manufacturing technologies and modern welding techniques are the editor's main interests.
E-mail: sabanbulbul42@hotmailcom,**ORCID:** 0000-0002-9268-1469

Yusuf UZUN PhD, is an Assistant Professor of Computer Engineering at Necmettin Erbakan University in Konya, Türkiye. He holds a PhD in Mechanical Engineering from Necmettin Erbakan University. His main areas of interest are artificial intelligence, autonomous systems and augmented reality applications. He also works as the Rector's Advisor at Selcuk University.
E-mail: yuzun76tr@gmail.com, **ORCID:** 0000-0002-7061-8784

In This Books

In Chapter 1,

In this chapter, samples taken from the wastewater treatment plant inlet were mixed with 5 different activated carbons produced by chemical activation for 2 minutes at 150 rpm and 20 minutes at 40 rpm, and then left to stand for 60 minutes. Experiments were conducted on these prepared samples to determine Chemical Oxygen Demand (COD), pH, electrical conductivity, turbidity, and color values. Additionally, Surface Analysis and Porosity (BET), density, Fourier Transform Infrared Spectroscopy (FT-IR) analysis, and Field Emission Scanning Electron Microscopy (FE-SEM) images were interpreted. The results of this study also revealed that activation with zinc chloride is a more effective method than phosphoric acid in improving micro- and mesopore structure. These findings once again demonstrate the critical impact of activation agents and process parameters used in activated carbon production on material properties. Furthermore, this study resulted in the conversion of waste products into more economical products, and showed that the produced activated carbons are more usable compared to commercial activated carbons.

In Chapter 2,

In this chapter, it was aimed to comprehensively examine 3D printing technology, to present its basic components in detail, and to define and analyze the effects of the materials and methods used in 3D printing technologies on design in furniture and interior design through examples. The descriptive method was used in the methodology of the study. Within the scope of the study, the materials used in 3D printing technologies, their technical and physical properties, areas of use, innovative production techniques, and the resulting final product design models are systematically addressed and evaluated through examples. In the conclusion section of the study, in line with the findings obtained, it has been concluded that the materials and methods used in 3D printing technologies provide significant advantages such as offering design freedom, supporting digital production processes, enabling low-cost production, making new material combinations possible, reducing waste, promoting a sustainable and environmentally friendly production approach, and enabling easy and rapid prototyping.

In Chapter 3,

This section examines the microstructure and mechanical properties obtained from the joining of S355JR and S700MC structural steels, widely used in industry, by the GMAW method. While the effects of different shielding gases were not clearly observed in microstructure examinations performed with an optical microscope, differences were detected in the weld metal and heat-affected zones (HAZ) according to the properties of the base metal. In general, grain growth in the HAZ and weld metal, as well as a dendritic structure in the weld metal, were observed in all sample steels. In addition to the

differences in metal structures, the shielding gas was one of the determining parameters in the hardness values of the materials. The fracture surfaces formed as a result of tensile tests were examined depending on the grain growth, hardness values, and mechanical properties of the base metals.

In Chapter 4,

With the widespread use of composite materials, composite materials have started to be used in the production of pressure vessels. Composite materials are preferred for pressure vessels to be both light and durable. Lightness and durability are very important in pressure vessels used especially in the space and aviation industry and in areas such as diver boats. In applications, different productions are made with various additives in order to produce pressure vessels that are lighter and more durable. The aim of this thesis; The aim of this study is to investigate the surface deformation behavior of carbon composite tubes with different carbon nanotube additive ratios produced by filament winding technique and to investigate the effects of carbon nanotube additive ratios on axial, circumferential and shear stresses. Within the scope of this thesis, three samples with different carbon nanotube additive ratios were produced and these samples were tested under internal pressure and their surface shape changing behavior was investigated. In order to investigate the effect of carbon nanotube ratio on the surface shape change, these ratios were applied as 0%, 1% and 3%. All samples were produced with filament winding technique with a winding angle of ±55°. In the study, the effect of carbon nanotube additive on the axial, circumferential and shear stresses on the surface will be compared. In experimental studies, changes in shape were observed and recorded. As a result of the study, it was determined that the carbon nanotube additive increased the strength.

In Chapter 5,

This chapter provides a detailed overview of Advanced Exergy Analysis (AEA), a method developed to overcome the limitations of conventional exergy analysis. While conventional exergy analysis reports only the total exergy destruction in system components, AEA separates these losses into avoidable/unavoidable and endogenous/exogenous parts, allowing a clearer understanding of where real improvement potential lies. The chapter explains the theoretical background of AEA and presents the main methodological approaches used in practice, including the engineering, thermodynamic, and hybrid-cycle approaches. Applications of AEA across a wide range of systems are also discussed. In addition, the integration of economic and environmental aspects through advanced exergoeconomic and exergoenvironmental analyses is described. Overall, the chapter highlights AEA as a valuable tool for the design, optimization, and sustainability assessment of modern energy systems.

In Chapter 6,

This study investigates the microstructural, mechanical, tribological, and corrosion behaviors of Al5754 matrix composites reinforced with graphene nanoplatelets (GNP), boron carbide (B_4C), and their hybrid combinations. Composites containing 0.5–1 wt.% GNP and 15 wt.% B_4C were fabricated via stir casting, followed by 30% cold rolling and recrystallization heat treatment. Characterization was performed using optical microscopy, SEM-EDAX, XRD, hardness testing, reciprocating wear tests, and immersion-based corrosion analysis. XRD confirmed the presence of Al-rich intermetallics (AlMn, AlFe) and B_4C phases. Uniform B_4C distribution enhanced hardness, while GNP improved interface bonding. The highest hardness (≈86–91 HB) was achieved in the 1% GNP + 15% B_4C composite, nearly doubling that of unreinforced Al5754. Tribological tests revealed significant wear resistance improvement with hybrid reinforcement, attributed to graphene layers reducing friction and stabilizing surfaces. Corrosion behavior varied with reinforcement type; GNP alone increased susceptibility, whereas hybrid reinforcement mitigated this effect. After rolling and recrystallization, the hybrid composite exhibited the lowest corrosion rate, indicating that appropriate thermomechanical processing enhances corrosion resistance despite rolling-induced defects.

In Chapter 7,

This chapter explains the effect of the gas nitration process on the wear behaviour of the crankshaft. For this purpose, 15 hours of gas nitration was applied to the crankshaft at a temperature of 520oC. As a result of the gas nitration, the hardness and microstructure images were taken separately from the nitrided and non-nitrided samples. In order to compare the abrasion behavior of nitrided and non-nitrided samples, a back and forth abrasion test was applied. 20N, 40N and 60N were determined as the load and subjected to an abrasive wear test. Test results vary depending on distance traveled and load applied. 100Cr6 balls are used as abrasive and nitrided and non-nitrided crankshaft is used as counter material. Compared to the wear resistance of nitrided crankshaft samples, an increase in wear resistance of about 20% was observed in non-nitrided samples.

In Chapter 8,

The purpose of this research is to compute the power distribution of contemporary Russian PWR designs (VVER), as well as to evaluate alternative fuel material compositions based on heat conductivity and power distributions. In the work, a review of currently relevant materials for emergency-resistant fuel systems was carried out, emergency-resistant materials for the VBER-300 project were selected. A thermal calculation was performed, the main geometric parameters of the core were determined, the coolant velocity was determined, and the temperature distribution over the cross-section of the fuel element for different types of fuel systems was obtained by ANSYS. The results

of the temperature distribution and the working conditions of UO_2 and UO_2+5%Cr (CERMET) fuels and whether they can operate safely or not have been obtained.

In Chapter 9,

Composite solid rocket propellants (CSRPs) are essential for contemporary propulsion systems, employed across military and civilian sectors due to their high energy output and reliability. Their heterogeneous nature facilitates the combination of various materials such as solid oxidizers and metallic fuels within a polymer matrix resulting in tailored performance characteristics important for specific mission profiles. Recent developments highlight the significance of adjusting formulations, including the use of alternative oxidizers like ammonium dinitramide (ADN), which offer environmental benefits due to the absence of toxic combustion products associated with traditional propellants. Ongoing research into CSRPs underscores advancements in enhancing burn rate, thrust, and overall stability. For instance, the optimization of ammonium perchlorate's particle size distribution plays a critical role in improving combustion rates and stability. Furthermore, the integration of energetic binders such as glycidyl azide polymer (GAP) marks a significant trend toward maximizing propellant energy density, allowing for higher performance compared to traditional hydroxy-terminated polybutadiene (HTPB). As the aerospace industry continues to prioritize environmentally responsible propulsion strategies, CSRPs remain foundational to meeting evolving demands in propulsion technology.

In summary, CSRPs embody an evolving technology that balances the needs for performance, safety, and environmental responsibility. Their continuous development is crucial for advancing both military and civilian aerospace applications.

In Chapter 10,

Energetic materials (EMs) are essential components in military and civilian applications, including munitions, explosives, propellants, and pyrotechnics. The ongoing demand for improved performance, safety, and stability has driven advancements, classifying EMs primarily into low and high explosives based on their chemical composition and behavior upon ignition. Recent research places emphasis on high-nitrogen and ionic liquid compounds, which offer high energy outputs with favorable environmental profiles. Additionally, innovations in synthetic methodologies and metal-organic frameworks (MOFs) have enhanced stability and reduced the sensitivity of EMs to external stimuli.

Characterization techniques such as X-ray crystallography and nuclear magnetic resonance provide insights into the structures and properties crucial to the performance of EMs, while dynamic mechanical analysis and thermal evaluations ensure reliability under diverse conditions. Cocrystallization emerges as a promising method for tuning

properties without requiring entirely new syntheses, enhancing both safety and performance.

Future EM research is expected to leverage computational modeling and machine learning to predict properties and accelerate material development while addressing safety challenges. The push for sustainable practices will also continue to shape EM advancements, ensuring improved functionality and compliance with environmental standards.

In conclusion, the field of energetic materials is evolving rapidly, characterized by significant chemical innovations and a focus on safety and environmental sustainability, which will define its future applications across various sectors.

A Review of Activated Carbon Production and Its Characterization in the Contect of Irrigation Field Applications

Uzeyir YALMAN
Necmettin Erbakan University

Saban BULBUL
Necmettin Erbakan University

Hakan GOKMESE
Necmettin Erbakan University

To Cite This Chapter:
Yalman, U., Bulbul, S., & Gokmese, H. (2025). A review of activated carbon production and its characterization in the context of irrigation field applications. In H. Gokmese, S. Bulbul, & Y. Uzun (Eds.), *Innovative approaches in materials science and applications* (pp. 1–17). ISRES Book Series. ISRES Publishing.

Introduction

Activated carbon is a material used in adsorption studies in many parts of the world. Its ease of obtaining and affordability make it advantageous. It is possible to commercial activated carbon from any product rich in carbon elements. Activated carbon can be produced from many different materials with a high carbon content. Generally, various organic and inorganic wastes such as coal, bone, hazelnut and olive pits, palm and chestnut shells, petroleum derivatives, coconut shells, wood residues, apricot pits, cellulosic materials, almond and orange peels are used as raw materials in activated carbon production and commercial production is carried out for this purpose (Adinata et al., 2007; Gomez-Serrano et al., 2005; Guritno et al., 2016; Hashemian et al., 2014; Hayashi et al., 2002; Kirubakaran et al.,1991; Küçükgül, 2004; Mozammel et al., 2002; Yavuz et al., 2010). Various researches carried out in recent years in the food industry have revealed that some waste materials can be evaluated in activated carbon production and these obtained activated carbons can be used for different purposes (Mohd Radhuwan et al., 2024). In addition, studies carried out in fields such as nanoscience and electrochemistry have shown that activated carbons with electrochemical properties and electromagnetic properties can be produced (Balçık et al., 2020). Activated carbon, produced from orange peels activated with phosphoric acid, was used to reduce volatile compounds such as formaldehyde produced during particleboard production. Experimental data showed that adding activated carbon to particleboards improved mechanical and physical properties and reduced formaldehyde emissions by 28.92% in the first month and 45.25% in the third month (Ergün et al., 2025). Activated carbons were produced by activating Scots pine wood waste with zinc chloride. These products aimed to reduce formaldehyde

emissions from particleboard production and to improve the physical and mechanical properties of the panels. Experiments were conducted by adding the produced activated carbons to particleboard production at 0.5%, 1%, and 1.5%. The results of the tests indicated that the particleboards' mechanical and physical properties improved, and formaldehyde emissions decreased by 24.6% in the first month and 27% in the sixth month, respectively(Ergün et al., 2024). Activated carbons produced from cellulose by activating them separately with $ZnCL_2$ and H_3PO_4 were applied to nitrile butadiene and natural rubber as fillers at 0%, 5%, 10%, 15% and 20%. According to the results obtained, the mechanical properties of rubber compounds were significantly improved after the addition of activated carbon (Bülbül and Ergün, 2024). In order to investigate the recycling and usability of waste paper, which is economically meaningless, the properties of the produced activated carbons were examined and compared with commercial activated carbons. Experimental results revealed that activated carbons derived from waste paper offer higher pore structure and surface area than commercial products (Özdemir et al., 2023) . Within the scope of the study, activated carbon production was successfully carried out from poplar tree waste treated with $ZnCL_2$ and H_3PO_4 and the results were examined. Density measurements and FE-SEM analyses revealed an activated carbon with lower density and a distinct porous structure. When the EDS results were examined, it was shown that the produced activated carbon had higher purity than the commercial product(Ergün and Bülbül, 2022). Activated carbons produced from waste paper using zinc chloride and phosphoric acid were mixed with a rubber matrix mixture. Experimental data showed that density decreased, hardness increased, and tensile strength decreased as the filler material was increased (Özdemir, 2023)

Its area of use is quite wide. In the food and beverage industry, activated carbons stand out as an effective treatment material in the removal of heavy metals, compounds that cause bad odor and color, amino acids and toxic substances (Roy, 2023). The need for more activated carbon is increasing due to the strict rules and regulations in the treatment of industrial wastewater. (González-García, 2018). The consumption of activated carbon is increasing as a result of food consumers' sensitivity to safety and quality. (Amine et al., 2006). Activated carbon production in Turkey has increased recently. Although this increase has been made, the remaining parts are filled by imports. In 2019, Turkey ranked 22nd in global activated carbon exports with a share of 0.4%. Experts predict that Turkey's activated carbon exports will increase by approximately 60% in the coming years (Orta Anadolu Kalkınma Ajansı, 2021). The global activated carbon market exceeded US$ 5 billion by 2023 (Helvacı and Korkmaz, 2024). The activated carbon market in Turkey was approximately US$ 38 million, resulting in a foreign trade deficit of US$ 35 million (Trade Map n.d.). The market is expected to reach US$ 4.58 billion in 2025 and US$ 6.11 billion in 2026. At the same time, it is predicted that the Asia-Pacific region will hold the largest market share by 2025 (mordorintelligence n.d.).

When evaluated according to usage areas, it is estimated that the water treatment sector will hold the largest market share in 2031 (Kingsresearch n.d.).

The objectives of this study are to transform low-economic waste products, such as waste paper and poplar sawdust, into high-value products. Another objective of the study is to compare the effects of zinc chloride and phosphoric acid activation agents on activated carbon properties and to determine which activation agent is most effective. Another important objective of the study is to compare the performance of laboratory-produced activated carbons with commercially available activated carbons and to determine which sample offers the most advantageous adsorption properties.

Materials and Methods

Activated carbon production consists of several processes. Production is achieved through physical and chemical activation. Both production methods have their advantages and disadvantages. If we want higher surface area, porosity, and lower temperatures for the reaction, we use chemical activation. There are multiple chemicals used as activating agents in the production of activated carbon through chemical activation. It is seen in the literature that different activation agents are used in this process. Table 1 shows the different activation agents used in the chemical activation process.

Table 1

Commonly encountered activation agents. (Gündoğdu, 2010; Wigmans, 1989).

Boric Acid	Iron (III) Chloride	Sodium Sulfate	Sulfuric Acid
Calcium Hydroxide	Potassium Carbonate	Nitrite Acid	Zinc Chloride
Calcium Chloride	Potassium Hydroxide	Sodium Chloride	Manganese (II) Chloride

Chemical compounds such as $ZnCl_2$, KOH, H_3PO_4, NaOH and K_2CO_3, which generally facilitate the formation of activated carbon by dehydrating the raw material, are among the most frequently used substances in the chemical activation process (Ahmedpour and Do, 1996; Gurten et al., 2012; Kopac and Erdogan, 2009; Kopac and Kırca, 2020; Rouquerol J. and Sing K., 1999; Ruofei et al., 2017; Xia et al., 2016). Potassium-based salts are preferred because they are environmentally friendly and offer a cleaner production process compared to compounds such as $ZnCl_2$ and H_3PO_4(Tsai et al., 2001).

Physical activation, one of the methods used in activated carbon production, consists of two main stages: the degradation of the organic structure and the activation of the carbon structure. In the first stage, the carbon skeleton is formed by removing the hydrogen

and oxygen elements in the raw material. Activation is then carried out using water vapor, carbon dioxide (CO_2), or a combination of both gases at a temperature between approximately 800-1000°C, and production is completed (Yunus et al., 2022). The chemical activation method is more widely preferred compared to the physical method because it can be applied at lower temperatures and provides higher efficiency (Güneş, 2016; İlçi, 2017).]. Activated carbon production by chemical activation is a field of study that many researchers worldwide have focused on (Özdemir et al., 2023). Activated carbons obtained by this method have larger surface areas and more developed pore structures. Differences in the physical and chemical properties of the product may occur depending on the chemical activation agent used (Heidarinejad et al., 2020). In practice, activated carbon production is generally carried out by reacting the raw material brought to appropriate sizes either directly with the chemical agent at a temperature of 400-1000 °C or by performing the same process on a pre-carbonized structure (Bülbül, 2021).

Activated Carbon Production with Phosphoric Acid

Waste paper and black poplar sawdust were divided into 3-kilogram pieces according to different processes. 1.5 liters of 50% phosphoric acid solution and 3 liters of distilled water were added to each raw material and mixed until a homogeneous state was achieved. These prepared mixtures were treated at 110°C for 2 hours. Following this process, they were kept in an 80°C oven for 24 hours and dried. These dried samples were carbonized in a 600°C annealing oven under argon gas (50 ml/min) for 1.5 hours. After this process, they were allowed to cool. The obtained products were pre-washed with 0.5 ml of KOH and then rinsed with hot deionized water to adjust the pH value between 6-6.5. Finally, they were dried in a 100°C oven for 6 hours and then ground.

Activated Carbon Production with Zinc Chloride

Waste paper and black poplar sawdust were divided into 3-kilogram pieces according to different processes. 1.5 liters of 50% zinc chloride solution and 3 liters of distilled water were added to each raw material and mixed until a homogeneous state was achieved. These prepared mixtures were treated at 110°C for 2 hours. Following this process, they were kept in an 80°C oven for 24 hours and dried. These dried samples were carbonized in a 600°C annealing oven under argon gas (50 ml/min) for 1.5 hours. After this process, they were allowed to cool. The obtained products were pre-washed with 0.5 ml of KOH and then rinsed with hot deionized water to adjust the pH value between 6-6.5. Finally, they were dried in a 100°C oven for 6 hours and then ground.

Experimental Results

Activated carbons produced using different production methods were first subjected to BET surface analyses, FE-SEM images, and density analyses. Following these studies, adsorption experiments were conducted and the results were evaluated.

Imaging With Field Scanning Electron Microscopy (FE-SEM)

FE-SEM images of the activated carbons were obtained and examined. FE-SEM images of the prepared samples are shown in Figure 1.

Figure 1

FE-SEM images of a) commercial activated carbon sample b) AKA sample c) AKT sample d) OA sample e) OT sample

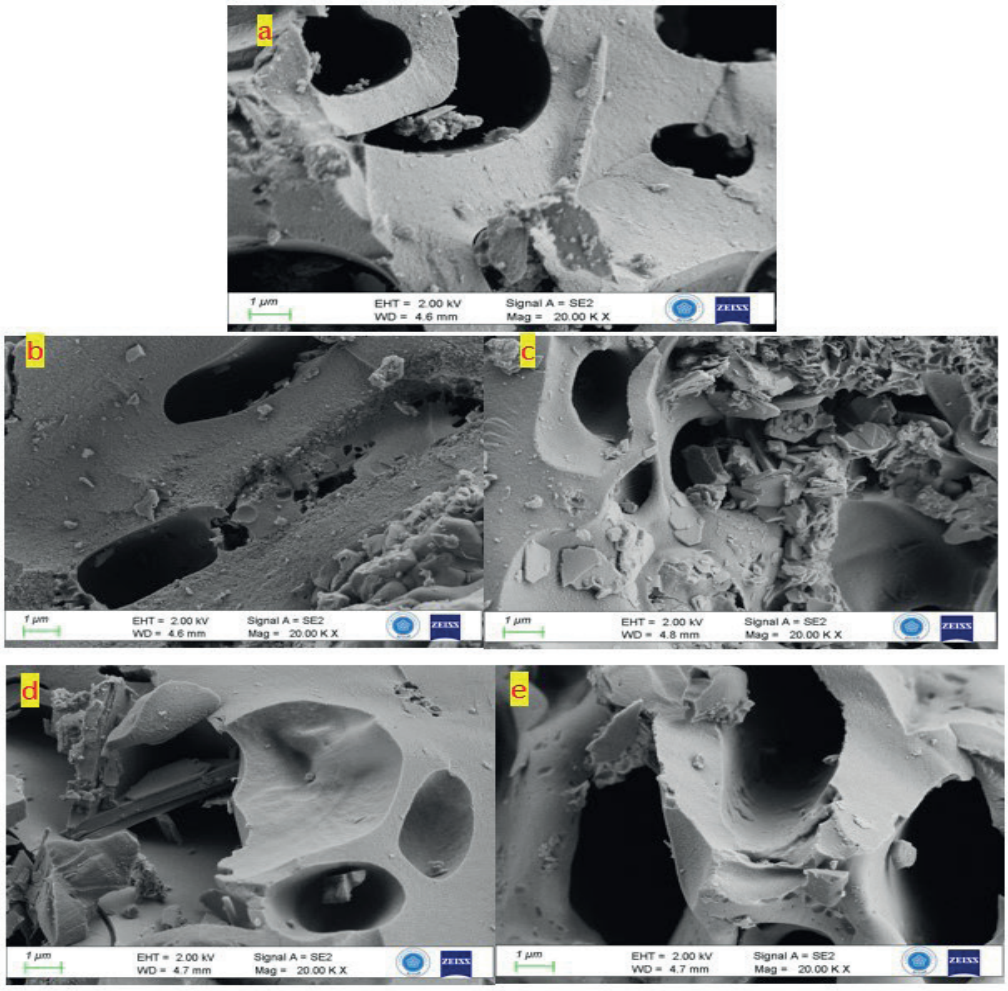

When FE-SEM images were examined, it was observed that the surface morphology of the activated carbon samples varied. While the porous structure was clearly visible in some samples, macropores were not evident in others. The images showed that the sample shapes were mostly elliptical, while some samples did not exhibit a specific geometric shape. FE-SEM analyses of the commercial activated carbon, AKT, and AKA samples revealed that their surfaces were generally rough, containing distinct indentations and protrusions; however, the amount of pores within these structures was observed to be limited. In the commercial activated carbon sample, in particular, the pores were both few in number and small in diameter, a finding confirmed by BET surface area and density analyses. The AKA sample exhibited a heterogeneous surface area, while the

AKT sample exhibited irregular voids and variously sized and irregularly shaped pores. According to BET analysis, the AKT sample had a high number of micropores, indicating a high surface area. These findings indicate that the porous structure was largely formed in the interior of the sample. In OA and OT samples, it was observed that pores were formed more clearly and distinctly and showed a more homogeneous distribution. It is thought that an increase in the number of pores occurred in carbon samples activated with zinc chloride due to the evaporation of this substance during activation (Yagmuret al., 2008). The high BET surface area and dense micropore content of these samples support the development of the porous structure in the inner regions (Jiang et al., 2021; Küçükgül, 2004). In conclusion, it can be said that zinc chloride is a more effective activation agent than phosphoric acid in the formation of micro- and mesopores (Ergün and Bülbül, 2022; Liou, 2010).

Density Analyses

Density analyses of a total of five different activated carbons were performed and interpreted. The density analyses are shown in Figure 2.

Figure 2

Density analysis results.

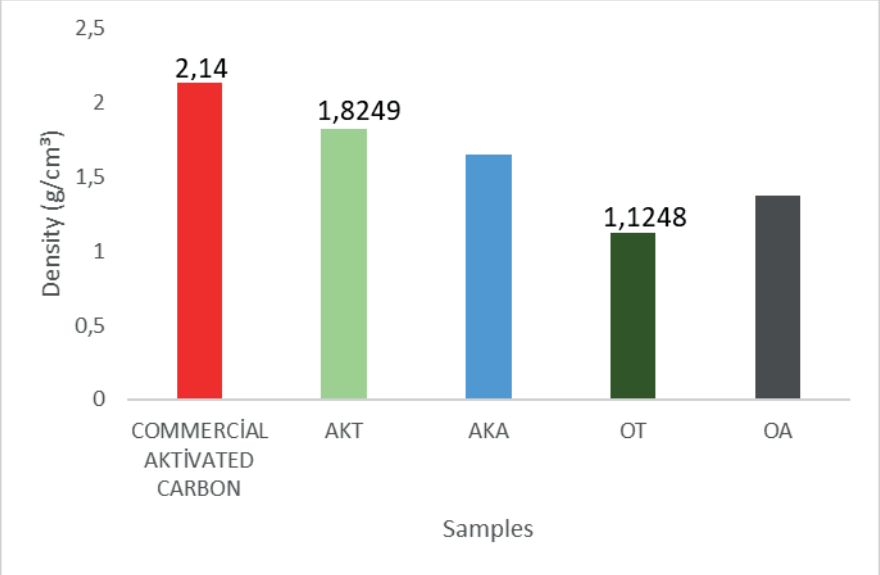

Density analyses conducted in our study showed that density decreases as porosity increases in activated carbon samples. The OT sample, in particular, provides a clear example of this inverse relationship, having the lowest density (0.24 g/cm³) and the highest total pore volume. This finding is consistent with literature examining the relationships between the physical and structural characteristics of activated carbons (Jiang et al., 2021)

The findings from these studies explain the performance of the OT sample with its low

density and high pore volume. Increasing pore volume not only increases the surface area but also improves the carbon's mass-to-area ratio, offering significant advantages in terms of cost, efficiency, and productivity in various engineering applications.

Surface Analysis And Porosity (BET) Analysis

Experiments were conducted and investigated for BET surface areas and porosities of activated carbons. Table 1 shows the results of the BET surface analysis.

Table 2

BET analysis experimental results.

	Surface Area m^2/g	V_{micro} (cm^3/g)	V_{meso} (cm^3/g)	V_{total} (cm^3/g)	D_p (nm)
Commercial Ativated Carbon	270	0.175	0.099	0.274	1.679
Black Poplar Acid OA	957	0.415	0.186	0.601	0.592
Black Poplar Salt OT	996	0.431	0.081	0.512	0.496
Waste Paper Acid AKA	400	0.254	0.099	0.342	0.868
Waste Paper Salt AKT	501	0.344	0.034	0.378	0.584

When examining the surface analyses, the highest BET was obtained in the OT sample. These were followed by the OA, AKT, AKA, and commercial activated carbon samples, respectively. The highest ratio of the number of micropores to the total pore number was obtained in the AKT sample at 91%, while the lowest was obtained in the commercial activated carbon. The high surface area makes the OT sample the most efficient sample for adsorption. The highest average pore diameter was observed with the commercial activated carbon (1.679 nm). This indicates greater macroporosity, while the other samples are more concentrated in micro and mesopores. The OT and OA samples, with the smallest pore diameters, show that they are concentrated in micropores. OA has a high surface area and total pore volume. A balanced ratio of both micro and mesopores provides an advantage for adsorption. Many studies support the effects of microporosity on surface area and adsorption performance.

The effect of activation temperature and active substance on micropore formation was examined and it was stated that more micropores were formed, especially at lower temperatures. (Lua and Yang, 2004). It was stated that phosphoric acid contributed to the formation of more mesopores and micropore development was limited. (Toles et al., 1996). $ZnCl_2$ has been shown to form micropore structures that are particularly suitable

for the removal of micropollutants (Yahya et al., 2015). It has been shown that pore accessibility decreases as a result of the accumulation of acidic groups on the surface of carbons activated with phosphoric acid. (Liou, 2010). It has been stated that $ZnCl_2$ leaves less residue after carbonization and reduces the need for cleaning. (Namane et al., 2005). Activation with $ZnCl_2$ was shown to be rapid and effective at low temperatures (Savova et al., 2001).

FT-IR Analysis Results

FT-IR analysis was performed to determine the chemical composition of the commercial activated carbons. Figure 3 shows the FT-IR results of the activated carbons.

Figure 3

FT-IR analysis results

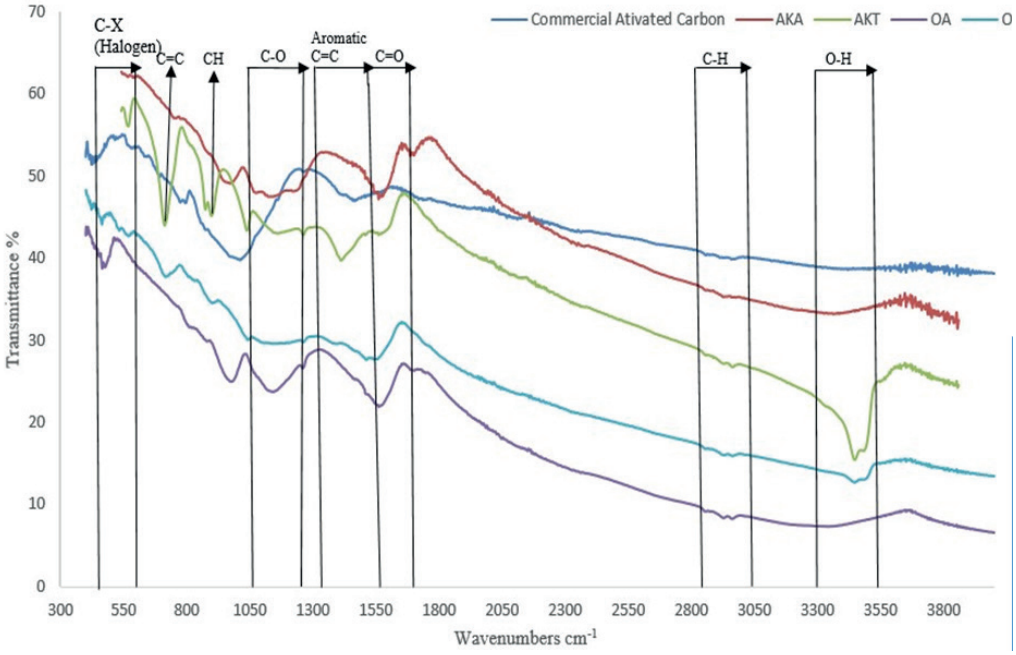

When the commercial activated carbon, OA, OT, AKA and AKT samples are examined, C-X (halogen) stretching vibrations at 450-600 cm-1 may contain halogen compounds (C-Cl or C-Br) (Mahapatra et al., 2012). C-O stretching vibrations at 1000-1300 cm-1 may indicate the presence of alcohol (R-OH), ester (R-COOR') or ether (R-O-R') groups (unitechlink.com/ftir-analysis n.d.). 1450-1600 cm-1: Aromatic C=C stretching vibrations may contain aromatic rings (benzene derivatives) (Gurten et al., 2012). 1600-1700 cm-1: C=O stretching vibrations. May contain carbonyl groups (ketone, aldehyde, carboxylic acid). 2800-3000 cm-1: C-H stretching vibrations may indicate the presence of alkanes or alkyl groups (Yagmur et al., 2008). 3300-3500 cm-1: O-H stretching vibrations may indicate the presence of alcohol or water groups (unitechlink.com/ftir-analysis n.d.).

Characteristic functional groups such as hydroxyl, aliphatic and aromatic hydrocarbons,

carbonyl groups, esters, and ethers are observed in each graph. No distinct peaks associated with inorganic compounds are present in these spectra. The presence of C=C, OH, and C-O bonds within activated carbon allowed for the reduction of color, turbidity, and COD values (Eletta et al., 2018; Mohammad Razi et al., 2018; Zhang et al., 2025).

Adsorption Experiment Results

In this study, a total of five different activated carbon samples produced using chemical activation methods and commercially available were comparatively evaluated in terms of Chemical Oxygen Demand (COD), turbidity, and color removal parameters in wastewater treatment. Adsorption experiments were conducted with our activated carbon samples. The adsorption test results are shown in Table 2.

Table 3

Adsorption experiment results

Sample Name	p H	EC_m	COD	TURBIDITY	COLOR (RES)
	PH Reading	EC Reading µS/cm	mg/L	NTU	620 nm m^{-1}
Sample	7,38	2893	725	105	1,09
Commercial Activated Carbon	7,54	2885	597	46,2	0,96
AKT	7,67	2914	682	45,5	1,42
AKA	7,64	2901	639	55,2	1,03
OT	7,64	2893	587	40,6	0,95
OA	7,64	2928	595	54,7	1,03

In the study, the OT sample stood out with the highest adsorption capacity, with 19% COD removal, 61% turbidity removal, and 13% color removal. It was reported that the improved BET surface area and porosity resulted in more efficient removal of contaminants from wastewater (Mojoudi et al., 2019). The success of the OT sample in our study supports these results. The OT sample had the highest surface area and microporosity, demonstrating the best adsorption performance. The OA and AKA samples exhibited lower microporosity and surface area due to the use of phosphoric acid. It was emphasized that phosphate residues caused pore blockage, limiting adsorption capacity (Lua and Yang, 2004)

Commercial activated carbon (HAC) performed moderately compared to laboratory-

prepared samples. This is consistent with the view that commercial carbons may not always be suitable for specific applications (Baccar et al., 2009).

It has been stated that activated carbons, especially those produced from agricultural wastes, are more effective in the adsorption of small molecules and that micropores play a dominant role here. This is true for both OT and AKT (Kalderis et al., 2008). They emphasized that surface chemistry and pore size distribution affect adsorption performance. This balance was maintained at a moderate level in the AKT and HAK samples (Rajabi et al., 2017). It has been stated that carbons with high pore volume provide faster adsorption kinetics and these structures offer advantages especially in dynamic systems (Yahya et al., 2015). It was stated that larger mesopores may also be necessary for the adsorption of colored compounds, so the commercial activated carbon sample showed similar performance in color compared to AKT (Li et al., 2008). It has been emphasized that the performance of activated carbon depends not only on the surface area but also on the functional group distribution and internal diffusion capacity (Bansal and Goyal, 2005).

As a result of this comprehensive evaluation, the OT sample activated with $ZnCl_2$ achieved the highest adsorption capacity in wastewater treatment thanks to its high microporosity, large surface area, and low density. The AKT sample, with a more stable structure, demonstrated superior results compared to HAK in COD, turbidity, and color removal. While HAK remains at the average level in terms of performance, it has advantages in terms of stability and accessibility. The OA and AKA samples exhibited limited adsorption capacity due to pore blockage caused by phosphoric acid. These findings once again demonstrate that activated carbon selection should be based on the activation method, microporosity ratio, surface area, and molecular properties of the target pollutant.

Conclusion

In this study, the densities, porosity, surface properties, morphological characteristics, and wastewater treatment performance of activated carbon samples produced using different production methods were comparatively evaluated. The following findings were obtained from the experiments:

- According to these results, the OT sample had the highest surface area. These were followed by OA, AKA, AKT, and Commercial Activated Carbon, respectively. If we sort by micropore structure, the order is OT > OA > AKT > AKA > Commercial Activated Carbon. This indicates that micropore structure is a factor affecting surface area.
- The abundance of micropores indicates that a large portion of the total pore structure occurs in the interior of the samples.

- Zinc chloride was found to be more effective in micro- and mesopore development than phosphoric acid, and its pore distribution was more homogeneous.
- FE-SEM images revealed that some samples had distinct pore structures, while others had more pronounced macropores. Specifically, the presence of fewer macropores in the AKT sample indicated that micropores were concentrated more in the interior regions of the sample. The surface morphology revealed a rough and irregular surface morphology.
- Density analyses revealed the lowest density in the OT sample. The other samples were OA, AKA, AKT, and commercial activated carbon, respectively. The results indicate an inverse relationship between porosity and density, with density decreasing as porosity increases.
- Among the samples, the OT sample achieved high removal rates, with COD (19%), turbidity (61%), and color (13%). There were no significant changes in electrical conductivity or pH across all samples.
- In activated carbons produced with phosphoric acid, samples with lower porosity and higher density were obtained due to the blockage of pores by phosphate bonds. This limited adsorption capacity.
- When comparing the OA-OT and AKT-AKA samples, it is thought that the porosity in the OA and AKA samples negatively affects the adsorption capacity. On the other hand, activated carbons activated with zinc chloride had more developed micro- and mesoporous structures. As a result, they exhibited better adsorption performance.
- Once again, it was observed that micropores play a decisive role in the adsorption process and therefore the best adsorption occurred in the OT sample..
- The high hydrophobicity of the OT sample, unlike the others, is thought to have increased adsorption efficiency. These results are consistent with previous studies. Furthermore, the presence of cellulose in the sample suggests a positive effect on adsorption performance.

The OT sample exhibited better performance compared to the other samples. Its large pore structure, low density, and high adsorption performance make it a preferred material for wastewater treatment and other industrial applications. This study demonstrated that zinc chloride is more effective than phosphoric acid.

The results of this study indicate that activated carbons produced from waste paper and wood shavings are more effective in removing COD, color, and turbidity when compared to coconut-based activated carbons commonly used in the market. Furthermore, this approach allows for the production of environmentally friendly and economically valuable products by repurposing waste materials. Future research using different activation agents could explore their effects more comprehensively.

It can be expanded by conducting different studies; optimizing the parameters such as the amount of activation agent, temperature and time used in activation, evaluating different waste materials in activated carbon production, investigating their performance in long-term use and examining the adsorption isotherms and kinetics separately.

References

Adinata, Donni, Wan Mohd Ashri Wan Daud, and Mohd Kheireddine Aroua. 2007. "Preparation and Characterization of Activated Carbon from Palm Shell by Chemical Activation with K_2CO_3." *Bioresource Technology* 98(1):145–49.

Ahmedpour, Ali, and Duong Do. 1996. "The Preparation of Active Carbons from Coal by Chemical and Physical Activation." 471–79.

Amine, Aziz, Hasna Mohammadi, Ilhame Bourais, and Giuseppe Palleschi. 2006. "Enzyme Inhibition-Based Biosensors for Food Safety and Environmental Monitoring." *Biosensors and Bioelectronics* 21(8).

Baccar, R., J. Bouzid, M. Feki, and A. Montiel. 2009. "Preparation of Activated Carbon from Tunisian Olive-Waste Cakes and Its Application for Adsorption of Heavy Metal Ions." *Journal of Hazardous Materials* 162(2–3):1522–29. doi:10.1016/J.JHAZMAT.2008.06.041.

Balçık, Eda Ülkeryılzdız, Mehmet Torun, and Hilal Şahin Nadeem. 2020. "Gıda Atıklarından Aktif Karbon Üretimi ve Aktif Karbonun Gıda Endüstrisinde Uygulamaları." *Gıda* 45:217–29.

Bansal, Roop Chand, and Meenakshi Goyal. 2005. *Activated Carbon Adsorption*.

Bülbül, Şaban, and Halime Ergün. 2024. "Investigation of the Usability of Activated Carbon as a Filling Material in Nitrile Butadiene Rubber/Natural Rubber Components and Modeling by Regression Analysis." *Journal of Elastomers and Plastics* 56(1).

Eletta, O. A. A., S. I. Mustapha, O. A. Ajayi, and A. T. Ahmed. 2018. "Optimization of Dye Removal from Textile Wastewater Using Activated Carbon from Sawdust." *Nigerian Journal of Technological Development* 15(1).

Ergün, Mehmet Emin, and Saban Bülbül. 2022. "Production and Characterization of Activated Carbon from Black Poplar (Populus Nigra) Wood Waste with Different Chemical Activation Methods." *International Advanced Researches and Engineering Journal* 6.

Ergün, Mehmet Emin, Abdullah İstek, İsmail Özlüsoylu, Filiz Koyuncu, and Şaban Bülbül. 2024. "Low Formaldehyde-Emission Particleboards with the Addition of Scots Pine Wood Waste Derived Activated Carbon." *Wood Material Science and Engineering*.

Gomez-Serrano, V., E. M. Cuerda-Correa, M. C. Fernandez-Gonzalez, M. F. Alexandre-Franco, and Macias-Garcia. 2005. "Preparation of Activated Carbons from Chestnut Wood by Phosphoric Acid-Chemical Activation Study of Microporosity and Fractal Dimension." *Study of Microporosity and Fractal Dimension.* 846–53.

González-García, P. 2018. "Activated Carbon from Lignocellulosics Precursors: A Review of the Synthesis Methods, Characterization Techniques and Applications." *Renewable and Sustainable Energy Reviews* 82.

Gündoğdu, Ali. 2010. "Fabrika Çay Atıklarından Aktif Karbon Üretimi, Karakterizasyonu ve Adsorpsiyon Özelliklerinin Incelenmesi." *Doktora Tezi, Karadeniz Teknik Üniversitesi,Fen Bilimleri Enstitüsü*.

Güneş, Sinem. 2016. *Portakal (Citrus Sinensis L.) Küspesinden Üretilen Aktif Karbonun Sulu Çözeltilerden Reaktif Boyar Madde Adsorpsiyonunda Kullanımı*.

Guritno, M. Anom, Riwandi Sihombing, and Yuni K. Krisnandi. 2016. "Synthesis of Porous Activated Carbon from Petroleum Sludge Using Mesoporous Silica Template." in *AIP Conference Proceedings*. Vol. 1729.

Gurten, I. Isil, Meryem Ozmak, Emine Yagmur, and Zeki Aktas. 2012. "Preparation and Characterisation of Activated Carbon from Waste Tea Using K_2CO_3." *Biomass and Bioenergy* 37:73–81.

Hashemian, Saeedeh, Khatereh Salari, and Zahra Atashi Yazdi. 2014. "Preparation of Activated Carbon from Agricultural Wastes (Almond Shell and Orange Peel) for Adsorption of 2-Pic from Aqueous Solution." *Journal of Industrial and Engineering Chemistry* 20(4).

Hayashi, Jun'ichi, Toshihide Horikawa, Isao Takeda, Katsuhiko Muroyama, and Farid Nasir Ani. 2002. "Preparing Activated Carbon from Various Nutshells by Chemical Activation with K_2CO_3." *Carbon* 40(13):2381–86.

Heidarinejad, Zoha, Mohammad Hadi Dehghani, Mohsen Heidari, Gholamali Javedan, Imran Ali, and Mika Sillanpää. 2020. "Methods for Preparation and Activation of Activated Carbon: A Review." *Environmental Chemistry Letters* 18(2).

Helvacı, Naciye Olcay, and Yasemin Korkmaz. 2024. "Çevre Dostu Hammaddelerden Üretilen Aktif Karbonlar ve Uygulama Alanları." *Kahramanmaraş Sütçü İmam Üniversitesi Mühendislik Bilimleri Dergisi*.

https://unitechlink.com/ftir-analysis/. n.d. "Https://Unitechlink.Com/Ftir-Analysis/."

İlçi, Ayşe. 2017. *Sulu Çözeltilerden Pestisitin Adsorpsiyonunda Zeytinyağı Katı Atığından (Pirina) Elde Edilen Aktif Karbonun Kullanılabilirliğinin*.

Jiang, Yuting, Jing Li, Zimu Jiang, Mengjiao Shi, Rui Sheng, Zheng Liu, Su Zhang, Yali Cao, Tong Wei, and Zhuangjun Fan. 2021. "Large-Surface-Area Activated

Carbon with High Density by Electrostatic Densification for Supercapacitor Electrodes." *Carbon* 175.

Kalderis, Dimitrios, Sophia Bethanis, Panagiota Paraskeva, and Evan Diamadopoulos. 2008. "Production of Activated Carbon from Bagasse and Rice Husk by a Single-Stage Chemical Activation Method at Low Retention Times." *Bioresource Technology* 99(15):6809–16. doi:10.1016/J.BIORTECH.2008.01.041.

Kingsresearch. n.d. "Activated-Carbon-Market-531." *Https://Www.Kingsresearch.Com/Tr/Activated-Carbon-Market-531*.

Kirubakaran, C. John, K. Krishnaiah, and S. K. Seshadri. 1991. "Experimental Study of the Production of Activated Carbon from Coconut Shells in a Fluidized Bed Reactor." *Industrial and Engineering Chemistry Research* 30(11):2411–16.

Kopac, Turkan, and Fatma Oğuz Erdogan. 2009. "Temperature and Alkaline Hydroxide Treatment Effects on Hydrogen Sorption Characteristics of Multi-Walled Carbon Nanotube-Graphite Mixture." *Journal of Industrial and Engineering Chemistry* 15(5):730–35.

Kopac, Turkan, and Yigit Kırca. 2020. "Effect of Ammonia and Boron Modifications on the Surface and Hydrogen Sorption Characteristics of Activated Carbons from Coal." *International Journal of Hydrogen Energy* 45(17):10494–506.

Küçükgül, Enver Yaser. 2004. *Ticari Aktif Karbon Üretimi ve Özelliklerinin Belirlenmesi*.

Liou, Tzong Horng. 2010. "Development of Mesoporous Structure and High Adsorption Capacity of Biomass-Based Activated Carbon by Phosphoric Acid and Zinc Chloride Activation." *Chemical Engineering Journal* 158(2).

Li, Wei, Libo Zhang, Jinhui Peng, Ning Li, Shimin Zhang, and Shenghui Guo. 2008. "Tobacco Stems as a Low Cost Adsorbent for the Removal of Pb(II) from Wastewater: Equilibrium and Kinetic Studies." *Industrial Crops and Products* 28(3):294–302. doi:10.1016/J.INDCROP.2008.03.007.

Lua, Aik Chong, and Ting Yang. 2004. "Effect of Activation Temperature on the Textural and Chemical Properties of Potassium Hydroxide Activated Carbon Prepared from Pistachio-Nut Shell." *Journal of Colloid and Interface Science* 274(2):594–601. doi:10.1016/J.JCIS.2003.10.001.

Mahapatra, Kalyani, D. S. Ramteke, and L. J. Paliwal. 2012. "Production of Activated Carbon from Sludge of Food Processing Industry under Controlled Pyrolysis and Its Application for Methylene Blue Removal." *Journal of Analytical and Applied Pyrolysis* 95.

Mehmet Emin Ergün, Filiz Koyuncu, Abdullah İstek, İsmail Özlüsoylu, Şaban Bülbül, and Ayben Kılıç-Pekgözlü. 2025. "Utilization of Orange Peel Waste for Activated

Carbon Production and Its Application in Particleboard for Formaldehyde Emission Reduction." *Biofuels, Bioproducts and Biorefining (Biofpr)* 690–704.

Mohammad Razi, Mohd Adib, Adel Al-Gheethi, Mohammed Al-Qaini, and Anwar Yousef. 2018. "Efficiency of Activated Carbon from Palm Kernel Shell for Treatment of Greywater." *Arab Journal of Basic and Applied Sciences* 25(3). doi:10.1080/25765299.2018.1514142.

Mohd Radhuwan, Siti Nasuha, Ahmed Saud Abdulhameed, Ali H. Jawad, Zeid A. ALOthman, Lee D. Wilson, and Sameer Algburi. 2024. "Production of Activated Carbon from Food Wastes (Chicken Bones and Rice Waste) by Microwave Assisted $ZnCl_2$ Activation: An Optimized Process for Crystal Violet Dye Removal." *International Journal of Phytoremediation* 26(5).

Mojoudi, N., N. Mirghaffari, M. Soleimani, H. Shariatmadari, C. Belver, and J. Bedia. 2019. "Phenol Adsorption on High Microporous Activated Carbons Prepared from Oily Sludge: Equilibrium, Kinetic and Thermodynamic Studies." *Scientific Reports* 9(1). doi:10.1038/s41598-019-55794-4.

mordorintelligence. n.d. "Mordorintelligence Reports Activated-Carbon-Market." *Https://Www.Mordorintelligence.Com/Industry-Reports/Activated-Carbon-Market*.

Mozammel, Hoque M., Ota Masahiro, and S. C. Bhattacharya. 2002. "Activated Charcoal from Coconut Shell Using $ZnCl_2$ Activation." *Biomass and Bioenergy* 22(5):397–400.

Namane, A., A. Mekarzia, K. Benrachedi, N. Belhaneche-Bensemra, and A. Hellal. 2005. "Determination of the Adsorption Capacity of Activated Carbon Made from Coffee Grounds by Chemical Activation with $ZnCl_2$ and H_3PO_4." *Journal of Hazardous Materials* 119(1–3):189–94. doi:10.1016/J.JHAZMAT.2004.12.006.

Orta Anadolu Kalkınma Ajansı. 2021. *Sivas İli Aktif Karbon Üretimi Ön Fizibilite Raporu*.

Özdemir Derya. 2023. "Atık Kâğıttan Üretilen Aktif Karbonun Kauçuk Matrisli Bileşiklerde Kullanımı ve Karakterizasyonu ." *Necmettin Erbakan Üniversitesi, Fen Bilimleri Enstitüsü, Yüksek Lisans Tezi*.

Özdemir, Derya, Saban Bülbül, and Mehmet Emin Ergün. 2023. "Production of Activated Carbon from the Waste Paper by Chemical Activation Method." *International Advanced Researches and Engineering Journal* 7(1). doi:10.35860/iarej.1222591.

Rajabi, M., K. Mahanpoor, and O. Moradi. 2017. "Removal of Dye Molecules from Aqueous Solution by Carbon Nanotubes and Carbon Nanotube Functional Groups: Critical Review." *RSC Advances* 7(74). doi:10.1039/c7ra09377b.

Rouquerol J., and Sing K. 1999. "Adsorption by Powders and Porous Solids Academic Press, San Diego." *Vakuum in Forschung Und Praxis* 404–404.

Roy, Glenn M. 2023. *Activated Carbon Applications in the Food and Pharmaceutical Industries*. Routledge. New York.

Ruofei, C., L. Liqing, L. Zheng, L. Mingming, W. Chunhao, L. Hailong, M. Weiwu, and W. Shaobin. 2017. "Preparation and Characterization of Activated Carbons from Tobacco Stem by Chemical Activation." *Journal of the Air and Waste Management Association* 67(6):713–24.

Şaban BÜLBÜL. 2021. "Portakal Kabuğu ve Odun Atıklardan Üretilen Aktif Karbonun Ayakkabı Tabanı Üretiminde Değerlendirilmesi." *Necmettin Erbakan Üniversitesi, Fen Bilimleri Enstitüsü, BAP Projesi*.

Savova, D., E. Apak, E. Ekinci, F. Yardim, N. Petrov, T. Budinova, M. Razvigorova, and V. Minkova. 2001. "Biomass Conversion to Carbon Adsorbents and Gas." *Biomass and Bioenergy* 21(2):133–42. doi:10.1016/S0961-9534(01)00027-7.

Toles, C., S. Rimmer, and J. C. Hower. 1996. "Production of Activated Carbons from a Washington Lignite Using Phosphoric Acid Activation." *Carbon* 34(11).

Trade Map. n.d. "Trade Map." *Https://Www.Trademap.Org/Index.Aspx*.

Tsai, W. T., C. Y. Chang, S. Y. Wang, C. F. Chang, S. F. Chien, and H. F. Sun. 2001. "Preparation of Activated Carbons from Corn Cob Catalyzed by Potassium Salts and Subsequent Gasification with CO_2." *Bioresource Technology* 78(2):203–8. https://www.sciencedirect.com/science/article/abs/pii/S0960852400001115.

Wigmans, T. 1989. "Industrial Aspects of Production and Use of Activated Carbons." *Carbon* 27(1).

Xia, Hongying, Song Cheng, Libo Zhang, and Jinhui Peng. 2016. "Utilization of Walnut Shell as a Feedstock for Preparing High Surface Area Activated Carbon by Microwave Induced Activation: Effect of Activation Agents." *Green Processing and Synthesis* 5(1):7–14.

Yagmur, Emine, Meryem Ozmak, and Zeki Aktas. 2008. "A Novel Method for Production of Activated Carbon from Waste Tea by Chemical Activation with Microwave Energy." *Fuel* 87.

Yahya, Mohd Adib, Z. Al-Qodah, and C. W. Zanariah Ngah. 2015. "Agricultural Bio-Waste Materials as Potential Sustainable Precursors Used for Activated Carbon Production: A Review." *Renewable and Sustainable Energy Reviews* 46:218–35. doi:10.1016/J.RSER.2015.02.051.

Yavuz, Reha, Hanife Akyildiz, Nilgün Karatepe, and Eda Çetinkaya. 2010. "Influence of Preparation Conditions on Porous Structures of Olive Stone Activated by

H_3PO_4." *Fuel Processing Technology* 91(1).

Yunus, Zalilah Murni, G. Yashni, Adel Al-Gheethi, Norzila Othman, Rafidah Hamdan, and Nurun Najwa Ruslan. 2022. "Advanced Methods for Activated Carbon from Agriculture Wastes; a Comprehensive Review." *International Journal of Environmental Analytical Chemistry* 102(1).

Zhang, Huirong, Lijun Zhu, Zihe Pan, Jinglei Cui, Baofeng Wang, Dongke Zhang, Yanxia Guo, and Fangqin Cheng. 2025. "Exploring the Mechanisms of Enhanced Activated Carbon's Toluene Adsorption and Regeneration by Utilizing Inherent Pyrite in Coal." *Fuel* 386:134224.

About The Authors

Uzeyir YALMAN, PhD is a Machine Manufacturing Manager at the 41st Branch Directorate of the 4th Regional Directorate of the State Hydraulic Works. I have a Master's degree in Mechanical Engineering from Necmettin Erbakan University. His main areas of interest are dams, reservoirs, and irrigation facilities.
Email: uzeyir.yalman52@hotmail.com,, **ORCID:** 0000-0002-1221-5661

Saban BULBUL, PhD is an Associate Professor of Mechanical Engineering at Necmettin Erbakan University in Konya. I have a master's degree in metallurgy education from Karabük University. His main areas of interest are casting technology, powder metallurgy, polymer materials and polymer applications.
Email: sabanbulbul42@hotmail.com, **ORCID:** 0000-0002-9268-1469

Hakan GOKMESE, PhD is a Professor of Mechanical Engineering at Necmettin Erbakan University in Konya. I have a master's degree in metallurgy education from Gazi University. His main areas of interest are casting technology, powder metallurgy, heat treatments and composites-nanocomposites applications.
Email: hakan1440@gmail.com, **ORCID:** 0000-0003-0053-8444

Similarity Index

The similarity index obtained from the plagiarism software fort his book chapter is 7 %.

The Interaction of Design, Material and Production Methods in 3D Printing Technologies: An Analysis of Furniture and Interior Design Elements

Tuba ARKAN DEMİRÖRS
KTO Karatay University

To Cite This Chapter:
Arkan Demirörs, T. (2025). The interaction of design, material and production methods in 3D printing technologies: An analysis of furniture and interior design elements. In H. Gokmese, S. Bulbul, & Y. Uzun (Eds.), *Innovative approaches in materials science and applications* (pp. 18–46). ISRES Book Series. ISRES Publishing.

Introduction

Throughout the historical process, modes of production have shown a continuous change in line with technological advancements and economic transformations. While early trade methods transitioned into the mass production that became widespread during the Industrial Revolution, the digital age has now led to a preference for a personalized, low-volume production model. With the acceleration of information and digitalization in the 21st century, consumers have shifted towards unique, personalized, and specialized products rather than standardized and uniform products. This transformation has enabled users to design and produce their own products; in the field of furniture design, it has become possible for individuals to produce their own furniture with the "Do It Yourself (DIY)" approach (Kang, 2015). In this context, the DIY approach has significantly contributed to the adoption and proliferation of 3D printing technologies (Aydın, 2015). Over time, the expiration of 3D printer patents accelerated the use of 3D printers and brought the concept of "fast furniture" to the fore by encouraging low-volume but high-variety production. Thus, attempts to combine 3D printing with the design of furniture and interior elements have begun (Kang, 2015).

3D printer technology stands out as an innovative production method that expands the possibilities for unique and custom design in interiors. Thanks to its ability to produce without being tied to molds, it offers the potential to transform spaces into personalized works of art by challenging designers' imagination. Furthermore, it provides unique solutions in furniture and interior designs by enabling the rapid production of designs that are suitable for user demands (Yıldıztepe & Arabacıoğlu, 2024). In addition, this technology not only provides aesthetics and functionality but also increases efficiency in design processes (Akbaba & Akbulut, 2021).

Interior architects and designers can produce prototypes of furniture and interior design elements using 3D printing technology in both their education and professional practice; thus, they find opportunities to test their designs in a versatile manner. The three-

dimensional models created with computer-aided software are converted into physical outputs using additional digital programs. Since this method is based on a layer-by-layer process, it is referred to as "additive manufacturing (layered manufacturing)" or "rapid prototyping" (Eke, 2019; Yang & Du, 2022). This rapidly developing technology makes the production, repair, or transformation of products possible in different spaces. It also allows a product design to be downloaded from the digital environment, copied, modified, or personalized before being printed. Furthermore, existing objects can be 3D-scanned and reproduced, which brings about a radical transformation in production processes (Saad, 2016).

As a result of the literature review conducted within the scope of this study, it has been observed that existing research on 3D printing technology has largely focused on general design fields, while remaining limited specifically to furniture design and interior design elements. Therefore, this study aims to first define 3D printing technology, investigate how 3D manufacturing is used to produce furniture and interior design elements by examining the basic components of 3D printing technology, and analyze the effects of materials and modern technology on furniture and interior design through examples. In the methodology of the study, a descriptive analysis method is used to define and analyze 3D printing technologies and the materials used with these technologies in furniture and interior design elements. The findings obtained from this study are expected to contribute to raising awareness about the production of furniture and interior design elements using 3D manufacturing. It is also aimed to provide interior architects and designers with a different perspective and a guiding path.

3D Printing Technologies

3D printing is defined as the process of manufacturing an object by adding thin layers of a selected material on top of each other by using data from a three-dimensional model designed in a digital environment (El-Sayegh et al., 2020). This technology is a form of manufacturing known as rapid prototyping technology or additive manufacturing (Yang & Du, 2022). The American Society for Testing and Materials (ASTM) and the International Organization for Standardization (ISO) define Additive Manufacturing (AM) as a process in which physical objects are produced by joining materials layer by layer, based on three-dimensional model data created in a digital environment (El-Sayegh et. al., 2020). Compared to subtractive manufacturing methods, this new approach has significant advantages, such as the ability to produce solid parts with lower energy consumption, easier application of computer-aided process control compared to other production technologies, the direct production of physical parts from computer-aided design (CAD) models, significant savings in both time and cost, especially in prototyping processes, offering design optimization freedom, and being accepted as one of today's most competent manufacturing technologies (Gedik et al., 2018; El-Sayegh

et al., 2020; Cengiz & Aktepe, 2022). Due to these features, 3D printing is currently considered an alternative method to traditional manufacturing techniques by producers. Current research includes discussions that the effects of 3D printing technologies may radically change not only production methods but also our design, consumption, and living practices; thus, it could be a pioneer of a new industrial revolution (Gedik et al., 2018).

Today, 3D printers are used in a very wide range of applications and hold significant potential, especially in furniture and interior design and their production processes. This technology stands out as an innovative manufacturing method that allows for the production of personalized designs and unique products. Furthermore, the use of 3D printers is not limited to design disciplines; they are also effectively used in the medical field for the production of prosthetics, dental implants, and biomedical devices, as well as in the prototyping processes of industrial design and machine parts. The production process of 3D printers is based on a working principle that consists of 4 main stages (Figure 1). These stages are modeling, joining, production, and cooling, respectively (Yıldıztepe & Arabacıoğlu, 2024). These stages can be briefly explained as follows.

Figure 1

Working Principles of 3D Printers (Yıldıztepe & Arabacıoğlu, 2024)

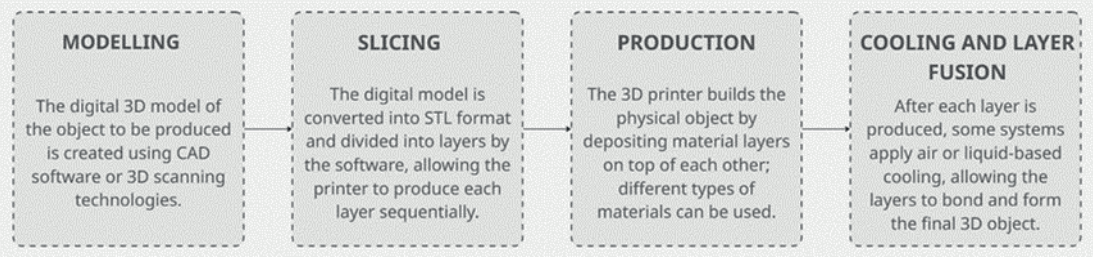

1. ***Modeling:*** The first stage of the 3D printing process is the creation of a 3D model of the object to be produced in a digital environment. This model is designed through CAD software or obtained by utilizing 3D scanning Technologies (Yıldıztepe & Arabacıoğlu, 2024).
2. ***Slicing:*** The created 3D digital model is converted into a Standard Triangle Language (STL) file type, which is a processable format for the printer. After this stage, the relevant software divides the model into layers and allows each layer to be produced sequentially by the printer (Yıldıztepe & Arabacıoğlu, 2024).
3. ***Production:*** The 3D printer creates the object by adding layers of material one on top of another until a physical object is formed. This production process is carried out with the use of different types of materials (Yıldıztepe & Arabacıoğlu, 2024).
4. ***Cooling and Layer Unification:*** After the production of each layer, some printer

systems use air or liquid-based cooling methods to solidify the layers. Following this process, the layers are integrated to produce the final 3D object (Yıldıztepe & Arabacıoğlu, 2024).

In the final stage of the production process, after the final 3D object is created, various finishing operations need to be applied. Depending on the properties of the material used and the geometric complexity of the product, some parts may require secondary processes such as sanding, filing, polishing, curing, material filling, or painting (Saad, 2016). 3D printing technologies include different production methods, and the fundamental distinction between these methods arises from the way the layers are created. The most commonly used 3D printing technologies include Selective Laser Sintering (SLS), Stereolithography Apparatus (SLA), and Fused Deposition Modeling (FDM) methods. In general, the key elements to be considered in the 3D printing process are production speed, the cost of the prototype, the economic dimension of the printer hardware, the type and cost of the material to be used, and the possibilities regarding color variety.

In the following section, a brief overview of evolving 3D printing technologies is provided. Additionally, in Table 1 created for the study, the types of 3D printing technologies are comparatively analyzed in the context of their 3D operating principles, materials used, advantages, and disadvantages.

An Overview of 3D Printing Technologies

Fused Deposition Modeling (FDM)

Fused Deposition Modeling (FDM) is a common manufacturing method based on the principle of melting a material through a heated nozzle and depositing it layer by layer. In accordance with the print paths derived from CAD data, molten plastic filaments are stacked one on top of another by a print head moving along the X, Y, and Z axes to create a solid object (Nadarajah, 2018). The advantages of this method include low hardware and material costs, ease of application, being the most common method, the ability to produce products with complex geometries, a wide range of material options, and the ability to process high-strength plastics. However, it has disadvantages such as surface roughness, low production speed, and issues with precision and material density (Saad, 2016; Şahin & Turan, 2018). In recent years, FDM's scalability has increased, and this has made it widespread in various sectors such as medicine, construction, and prototype production. In this method, thermoplastic filaments such as ABS, PLA, PETG, nylon, TPU, PC, and ULTEM are commonly used. Additionally, materials like steel, concrete, and wood have been adapted for this technology (Saad, 2016; Topal & Kavut, 2024; Eke, 2019).

Stereolithography (SLA)

Stereolithography (SLA) is an additive manufacturing method that begins with the

conversion of CAD data into STL format and is based on the layer-by-layer curing of photopolymer resin with a UV laser. The production process starts with a thin layer of photopolymer spread on a perforated platform, and this layer is selectively cured by a UV laser beam to form the first layer. The 3D model is completed by adding successive layers on top of each other using the same method, and the object is then removed from the tank. After production, the parts are cleaned with a solution to remove excess resin and then subjected to a UV curing process to complete polymerization (Nadarajah, 2018). The advantages of this method include high resolution, smooth surface quality, and the potential for rapid prototyping, while its disadvantages include high material and equipment costs, long printing times, and limited material variety (Canbolat & Aydın, 2019; Eke, 2019). SLA, which can be applied with resin-based photopolymers and materials similar to ABS, PC, and PP, is used in many sectors, especially medicine and manufacturing, for the production of prototypes and final products (Şahin & Turan, 2018; Chen et al., 2023).

Selective Laser Sintering (SLS)

Selective Laser Sintering (SLS) is an additive manufacturing method based on sintering thin layers of powdered materials with a high-power laser. In the process, which begins with the conversion of CAD files into STL format, the laser fuses the powder particles together by heating them just below their melting point and creates a layered structure. This technology, developed by Carl Deckard and Joe Beaman in the 1980s (Nadarajah, 2018), offers advantages such as strong structure, high heat and chemical resistance, fast production, durable print quality, and the ability to create complex geometries without the need for support structures (Saad, 2016; Şahin & Turan, 2018; Eke, 2019). However, this method has some disadvantages, including high costs due to the use of a high-power laser, process complexity, limited precision dependent on powder particle size, and the need for additional post-processing due to rough surfaces. The method can be applied with various powdered materials such as ceramics, glass, composites, nylon (PA), aluminum, steel, sand, paper, and wood (Eke, 2019; Saad, 2016).

Selective Laser Melting (SLM)

Selective Laser Melting (SLM) is a technology based on the complete melting of metal powders with a high-density laser and combining them in a layered manner. The method offers advantages such as superior surface quality, high performance, the production of complex geometries, and the acquisition of lightweight and large-scale parts as an alternative to welding processes (Chen et al., 2023; Saad, 2016). However, the disadvantages of the method include limited production size, high cost, the need for support structures, and the requirement for additional post-processing for a smooth surface. SLM is commonly applied with metal powders such as titanium alloys, stainless steel, and aluminum (Saad, 2016; Chen et al., 2023).

Laminated Object Manufacturing (LOM)

Laminated Object Manufacturing (LOM) is an additive manufacturing method based on laminating layers of paper, plastic, or metal with heat and pressure, then shaping them with a laser or blade. The process is repeated until the model is completed by cutting layers that have been joined with adhesive according to the CAD data. This method, developed by Helisys Inc. in the 1980s, allows for low-cost, rapid prototype production and multi-color use (Nadarajah, 2018; Eke, 2019). However, the method has some disadvantages, such as low precision (Şahin & Turan, 2018), low material durability (Eke, 2019), and inadequacy with complex geometries. In LOM, various materials like paper (new or recycled), plastic foam, ceramics, and layers impregnated with metal powder can be used (Saad, 2016; Şahin & Turan, 2018).

Direct Metal Laser Sintering (DMLS)

Direct Metal Laser Sintering (DMLS) is a powder-based additive manufacturing method that allows for the direct production of complex metal components from CAD data. In this process, a CAD model, powder material, and energy input are primarily used; parts with high density, good surface quality, and superior mechanical properties are obtained by sintering each layer selectively with a laser. DMLS provides cost and time advantages in low-volume production by eliminating the need for molds. It also offers additional benefits such as design flexibility and reduced inventory costs by allowing parts to be stored digitally and produced on demand. However, it has limitations in the production of large-scale parts and often requires additional post-processing. The method is widely applied with materials such as titanium, aluminum, nickel alloys, stainless steel, and cobalt chrome (Venkatesh & Nandini, 2013).

Digital Light Processing (DLP)

Digital Light Processing (DLP) technology is based on the principle of solidifying liquid photopolymer resin on its surface by directing ultraviolet light through micro-mirrors. The simultaneous solidification of the cross-sectional area of the layers significantly increases production speed compared to laser-based scanning methods (Eke, 2019). While the DLP method offers advantages such as high resolution, production precision, and the ability to produce complex geometries, it has certain limitations due to limited material variety and restrictions on layer thickness. This technology primarily uses liquid photopolymer materials (Saad, 2016).

Rapid Liquid Printing (RLP)

Rapid Liquid Printing (RLP) is an additive manufacturing method particularly suitable for the production of small-scale products; however, its production capacity is limited on an industrial and commercial scale. This technology, developed in collaboration between MIT and Steelcase, focuses on speed, size flexibility, and the use of high-quality materials. RLP is based on the principle of directly injecting liquid material into a special gel medium and can work with various industrial liquids such as rubber, foam, and

plastic. The gel eliminates the need for support structures by holding the material in place and prevents void formation by self-restoring after the nozzle pass. The product hardens through a chemical reaction without requiring additional light or heat treatment and can be directly removed from the gel medium. Thus, designs can be produced faster without the necessity of layered manufacturing (Canbolat & Aydın, 2019).

3D Concrete Printing (3DCP)

3D Concrete Printing (3DCP) is a production method based on the layer-by-layer deposition of cement-based materials by extrusion devices. The print head typically moves horizontally on a large frame, while the extrusion apparatus places the pre-formulated mixtures layer by layer along the desired geometric contours. This method eliminates the need for molds, saves on material and labor, offers fast production capabilities, presents design freedom, and facilitates the production of complex curved forms. Its disadvantages include high hardware and initial costs, limited material variety, and weak inter-layer bonding (Girskas & Kligys, 2025). Besides concrete, materials such as plastic, sand, metal, clay, and recycled or local materials can be used in 3DCP. The technology has various applications, including the production of residential and infrastructure structures, bridges, panels, artificial reefs, furniture, and sculptures (Nadarajah, 2018).

Binder Jetting (BJ)

Binder Jetting (BJ) technology is an additive manufacturing method where a liquid binder material brings together powdered raw material layer by layer (Şahin & Turan, 2018). The structural material does not come directly from the printer but consists of a powdered raw material brought together by the binder. Although this method, first developed by the Massachusetts Institute of Technology (MIT), is called “3D Printing (3DP)” in the literature, it has not been registered as an official trademark. The licensing rights for the technology initially belonged to Z Corp, but they were later transferred to companies such as 3D Systems and ExOne. The method offers advantages such as support-free production and multi-color options, but it also has disadvantages such as high cost and limited mechanical strength. Ceramic, metal, plastic, sand and composite materials are commonly used in this technology (Eke, 2019).

PolyJet (Additive Modelling)

PolyJet technology is based on the principle of accumulating liquid polymers layer by layer by jetting them in fine droplets, and instantly curing each layer by UV light. This method enables the production of complex geometries with high precision and resolution, and stands out for its rapid prototyping capability, multi-material use, smooth surface quality, and user-friendly nature (Şahin & Turan, 2018). However, its main disadvantages include low mechanical strength, limited material variety, high cost, and the need for support structures (Gibson, et al., 2021). Photopolymer resins and acrylic

materials are used in this technology (Şahin & Turan, 2018).

Multi-Jet Printing (MJP)

Multi-Jet Printing (MJP) technology is based on the principle of depositing liquid photopolymer droplets layer by layer via print heads that operate on the logic of inkjet printers. The use of multiple nozzles makes it possible to print the main and support material simultaneously, and the ability to apply three different materials concurrently increases color and material variety. This method is prominent for its advantages of high resolution, smooth surface quality, multi-material combinations, and easily removable wax support material. However, it also has disadvantages such as limited production volume, high cost, and low mechanical strength. MJP technology can work with plastic, metal, and wax-based materials, and it is particularly preferred for low-volume end-use parts, prototype production, and assembly testing. Healthcare, automotive, consumer products, and household goods are among the common application areas of this technology (Eke, 2019).

Directed Energy Deposition (DED)

Directed Energy Deposition (DED) is an additive manufacturing technology based on the principle of melting and depositing metal powders or wires layer by layer with a high-energy heat source (laser, electron beam, or plasma arc) (Herzog et al., 2016). It is generally preferred for the production of large-scale parts, surface coatings, and repair applications. Functional gradient structures can be produced with multi-material printing, and the production process is not limited only to horizontal layers thanks to 4–5 axis systems (Eke, 2019). The main advantages of the method are its high production speed, suitability for large-part manufacturing, and the ability to combine different metal alloys in a single process. Its disadvantages are surface roughness, geometric limitations, high equipment cost, and the risk of porosity due to rapid solidification (DebRoy et al., 2018). Metallic materials such as titanium, aluminum, nickel, cobalt-chromium alloys, stainless steel, and similar materials are commonly used in the DED process (Liu et al., 2017).

Table 1

Comparison of 3D Working Principle, material properties and advantages and disadvantages of different 3D printing methods

3D Printing Technology	3D Working Principle	Basic Materials	Advantages	Disadvantages
FDM Fused Deposition Modeling	Filament melting and layering	Thermoplastic materials, ABS, PLA, Nylon, PC, ULTEM	The most popular technique, inexpensive, easy, complex geometry, flexible, resistant and durable, variety of materials	Rough product surface, low production speed, precision and material density

SLA Stereolithography Apparatus	Photo-polymerization	Resin-based materials, Liquid photopolymer, ABS-Like, PC-Like, PP, Like	high resolution and smooth surface quality, rapid prototyping, detailed models	Cost, long printing time, limited materials
SLS Selective Laser Sintering	combining powdered materials by distributing them in thin layers	Powder Material, Ceramic, Glass, Composites, Nylon PA, Aluminum, Steel, Sand, Paper,Wood	resistance to high heat, , high speed, durable print quality, complex geometries, chemical resistant, strong structure	Expensive, more complex, printing sensitivity is limited by the size of dust particles, rough surface finish due to the powder-based manufacturing process
SLM Selective Laser Melting	produced by melting metal powders with a laser and bonding them in layers	Metal powder and metal alloys,	Excellent surface quality performance, complex forming structure. the potential to replace welding applications, large and lightweight products	Limited size, high cost, The use of additional support elements in the production of complex geometries, Additional surface treatment processes must be applied to achieve a smooth surface.
LOM Laminated Object Manufacturing	Laser cutting and bonding of sheets	Plastic foam, Paper (new or recycled), Ceramic, Metal powder impregnated materials.	Rapid prototyping technology, cost-effectiveness, multi-colour usage	low precision, fragile material low precision and inadequacy in complex geometries
DMLS Direct Metal Laser Sintering	Powder bed fusion	Titanium, Aluminum, Nickel Alloy, Stainless Steel, Cobalt chrome, Maraging steel,	No mold requirement, cost efficiency, time savings, design flexibility, high surface quality, and mechanical strength	Surface roughness is high; final processing may be required, has limitations in the manufacture of large-volume parts,
DLP Digital Light Processing	Curing of photopolymer resin using UV light	Liquid photopolymer	Provides simultaneous production, complex shapes can be produced, provides high precision in production	Limited product variety, limited material variety
RLP Rapid Liquid Printing	Principle of direct liquid material injection within a gel suspension	Rubber, Foam, Plastic, Any industrial liquid material	Suitable for the production of complex geometries, fast and high-quality production	Limited production capacity on an industrial and commercial scale
3DCP (Concrete Printing)	Extrusion-based additive manufacturing	Concrete and Plastic, sand, metal, clay along with concrete	No formwork required, *Rapid production,* Material and cost savings, Design flexibility	Costs, limited material variety, weak interlayer bonding
BJ (Binder Jetting)	Filling powder-filled material sheets with adhesive liquid	Ceramics, sand, metal, plastic, composite	Unsupported material multi color	Cost, limited mechanical properties
PolyJet (Additive Modelling)	Photopolymer sputtering and UV curing	Acrylic, photopolymer resins	Complex geometry, high speed, high precision and resolution, easy to use, multi-material use, functional prototyping and suitable for office/home environments.	Low mechanical strength, cost, material limitations and support material requirements
MJP (Multi- Jet Printing)	layer-by-layer deposition of liquid photopolymer droplets	Plastic, metal, wax	High resolution and precision, use of resistant and flexible multi-materials, complex geometries,	limited material diversity, limited production volume, limited mechanical strength, high cost

DED (Directed Energy Deposition)	Layered deposition by feeding wire or powder through the nozzle and melting with laser/ beam	Metal, cobalt-chromium, nickel, titanium, stainless steel, aluminium	large-scale parts, durable and final product, fast production, material flexibility	Surface roughness is high, geometric limitations, high equipment costs, risk of porosity and residue

3D Printing Technologies in Furniture and Interior Design Elements

In recent years, 3D printing technology has made an impact across many sectors, especially food, construction, automotive, and healthcare. The number of sectors not directly affected by this technology has remained quite limited. This rapid development process has paved the way for radical transformations in the fields of interior design and furniture production (Eti Proto & Koç Sağlam, 2021). In this context, 3D printing technology not only offers an innovation in production methods but also initiates a new era in the design paradigm. Traditional furniture design and production methods are no longer considered sufficient alone and are being replaced by alternative approaches supported by innovative technologies. Accordingly, 3D printing technology presents significant potential by expanding the possibilities for original and personalized design in interiors (Yıldıztepe & Arabacıoğlu, 2024). This process, unlike traditional manufacturing in furniture and interior design, allows for production directly from digital data without the need for molds, assembly, or additional processing (Aydın, 2015). Within the context of interior design, 3D printing makes it possible to produce furniture pieces with personalized and complex geometries by enabling designers to seek original forms (Kang, 2015; Eti Proto & Koç Sağlam, 2021). This process, through rapid prototyping and small-scale production capabilities, allows designers to transform their ideas into physical form and experiment with different materials (Kang, 2015). Furthermore, the 3D printing process contributes to the development of efficiency in material use, sustainability, and a user-centered design approach (Cengiz & Aktepe, 2022). This technology, which goes beyond the mold-dependent production concept, allows furniture and spaces to acquire user-specific characteristics. Therefore, the use of 3D printing in interior design provides both transformation and advantages from various aspects in design practices (Yıldıztepe & Arabacıoğlu; 2024).

The emergence of new technologies has many advantages and disadvantages. This section will discuss the advantages and disadvantages of 3D printing technologies in furniture and interior design elements.

Advantages of 3D Printing Technologies in Furniture and Interior Design Elements

Personalization and Customization: This approach, which goes beyond standard production molds, allows for the development of innovative designs specific to each space and individual. Thus, it becomes possible to personalize interior spaces. It enables the 3D modeling and production of 3D designs, and in this way, it significantly contributes to

the development of customized products (Saad, 2016; Yıldıztepe & Arabacıoğlu, 2024).

Design Freedom and Production of Complex Geometry Products: 3D printing allows for the design and production of complex, organic, and unique forms that are difficult to achieve with traditional methods (Petrova & Jivkov, 2024).

Economic: Although 3D printing technology initially requires high equipment and setup costs, it eventually has a lower production cost compared to the labor-intensity and additional costs that arise in traditional production methods (Saad, 2016; Eti Proto & Koç Sağlam, 2021; Yıldıztepe & Arabacıoğlu, 2024).

Rapid Production and Prototyping: In contrast to the time-constraining nature of traditional production processes, 3D printers provides significant advantages in terms of both efficiency and continuity by rapidly converting designs into production (Aydın, 2015). Furthermore, the time to create a prototype from a model is shortened; the time elapsed from the modeling of the design to its physical realization is much lower compared to traditional methods (Petrova & Jivkov, 2024).

Reduced Material Waste and Sustainability: Traditional furniture production leads to high material waste due to cutting and shaping processes. In contrast, 3D printing technology reduces waste by using only the necessary amount of material and offers a sustainable production approach by allowing waste to be recycled and reused (Cengiz & Aktepe, 2022; URL-1). Moreover, parts produced with 3D printing can be up to 60% lighter compared to those produced with traditional methods, and provide an advantage in terms of both cost and environmental impact while maintaining the same strength (Saad, 2016).

Reduction of Storage Costs: Traditional mass production processes bring with them the need for storage and associated costs resulting from large-scale production. 3D printing technology significantly reduces storage requirements and costs in small-scale productions (Thomas & Gilbert, 2014).

New Material Combinations: 3D printing technology allows different raw materials to be used together by overcoming the limitations of traditional production methods regarding material combinations. Thanks to additive manufacturing, materials other than plastic have also become processable, and numerous materials with metal, ceramic, or glass appearances, various strengths, and heat resistance have become usable in design processes. This increases design freedom and supports functional and aesthetic diversity in production (Saad, 2016).

Disadvantages of 3D Printing Technologies in Furniture and Interior Design Elements

Surface Quality and Post-Processing Requirement: Due to additive manufacturing, layer lines on the final product can be visible, and the surface of the product produced with 3D printing is often rough. Therefore, the products require post-processing before use. Especially for interior design elements and furniture parts that are aesthetically prominent, post-processing activities such as painting, sanding, or coating are necessary (El-Sayegh et al., 2020).

Unauthorized Copying of Products: One of the most significant disadvantages of 3D printing technology is that it enables the production of counterfeit products. Consequently, this leads to intellectual property rights infringements. This technology allows any individual with access to the necessary design files and a 3D printer to become a producer. This situation complicates the detection of the source of counterfeit products and makes it significantly difficult for copyright and patent holders to protect their legal rights (Saad, 2016).

Scale Limitations and Production Speed: 3D printers have certain limitations regarding the dimensions of the objects created. While providing significant advantages in small and medium-scale projects, the production of large furniture pieces or high-volume mass production processes can take a long time. Consequently, in some cases, traditional production methods may be more efficient in terms of the advantages arising from the economic scale (URL-2).

Lack of Material Diversity: Compared to traditional materials used in furniture parts, the types of materials that can be used in 3D printing are still limited. Especially for advanced polymers, metals, and composites that can meet the requirements for durability, aesthetics, and mechanical performance, suitable options are either high in cost or have technical constraints in use (Petrova & Jivkov, 2024).

Furniture and Interior Design Elements Produced by 3D Printing Technologies and Their Analyses

In this section, furniture and interior design products manufactured using 3D printing technologies are distinguished. The analysis has been carried out in terms of the type of 3D printing technology examined, the material used and its properties, as well as the general application and presentation of the design. The evaluations of these analyses are provided in Table 2.

Table 2

Analyses of 3D Printed Products: Design, Designer, Design Concept, 3D Printer Materials, Material Properties, General Use, and 3D Printing Technology

Design Prototype/ Design Concept	**Design:** Bikechair **Designer:** Giorgio Gurioli.  **-Design and Collaboration:** The Bikechair was designed by Italian designer Giorgio Gurioli and produced using large-scale 3D printing technology; the project was realized in collaboration with WASP (World's Advanced Saving Project) (URL-3). **-Exhibition:** The product was exhibited at the Milan PLAST Fair in 2018. **-Design Objective:** The chair aims to provide an ergonomic and aesthetically pleasing seating experience while offering a posture suitable for passive exercise (URL-3). **-Production Process:** Large-scale printing was carried out using Delta WASP 3MT INDUSTRIAL 3D printers using thermoplastic granules provided by Eni Versalis; production time was approximately 10 hours (URL-3). **-Material and Technical Characteristics:** ABS (Acrylonitrile Butadiene Styrene) granules were used, with a 1 mm layer height ensuring detailed and smooth surface quality (URL-3). **-Aesthetics and Functionality:** The yellow ABS material provides a modern and dynamic aesthetic, while the ergonomic design offers user comfort. The design integrates digital production with traditional craftsmanship, reflecting the Maker Economy approach (URL-3).
Material	**ABS** (Optimized ABS in pellet form)
Material Properties	**- Surface Quality:** ABS models exhibit a rougher surface compared to other materials (Saad, 2016). **-Water and Heat Resistance:** ABS is water-permeable and can withstand temperatures up to approximately 105 °C (Saad, 2016; Şahin & Turan, 2018). **- Dimensional Accuracy:** The material allows for the production of precise and detailed parts (URL-4). **- Surface Treatments:** Smooth and aesthetic surfaces can be achieved by chemical treatment with acetone (Demircali et al., 2024). **- Cost:** ABS is a low-cost material (URL-5). **-Safety Warning:** It can release HCN gas at high temperatures; therefore, good ventilation is required during printing (Şahin & Turan, 2018).
General Use	-ABS filament is widely used in furniture connectors, prototypes, architectural models, consumer products, and component production (Petrova & Jivkov, 2024; Şahin & Turan, 2018). -Functional Capability: ABS is suitable for producing fully functional models; for example, Lego pieces are made from this material (Şahin & Turan, 2018). -Mechanical Properties: ABS is characterized by high strength and impact resistance (Demircali et al., 2024). -Material Advantages: The material is UV-resistant and is one of the closest options to real production materials (Saad, 2016).
3D Printing Technology	**FDM** (Fused Deposition Modeling)

Design Prototype/ Design Concept	**Design:** Voxel Chair V1.0 **Designer:** The design team is led by DCL's two co-directors, Manuel Jiménez Garcia and Gilles Retsin.
	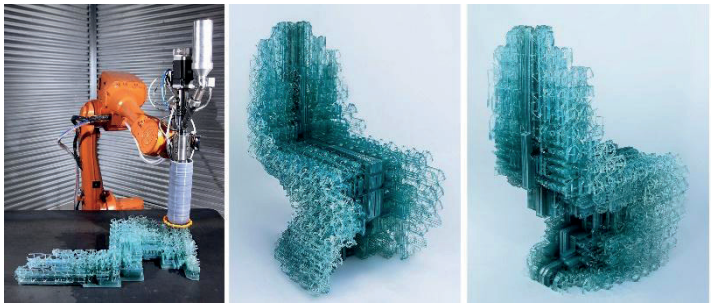 **-Production and Exhibition:** The Voxel Chair v1.0, produced in collaboration with Nagami. Design and Vicente Soler, is currently exhibited at Imprimer Le Monde at the Centre Pompidou, Paris (URL-6). **Design Inspiration:** The model was inspired by the iconic Panton Chair designed by Danish designer Verner Panton (URL-6). **-Production Method:** Unlike conventional additive manufacturing, software developed by the Bartlett Design Computation Laboratory (UCL) generates the design through robotic extrusion of a continuous 2.36 km-long PLA filament (URL-6). **-Structural Characteristics:** A robotic arm extrudes molten PLA directly into the air along computer-controlled paths; as the material cools and solidifies, it forms a lightweight, durable, and lattice-like structure (URL-6). **-Material and Color:** Transparent blue PLA filament was used in the prototype production (URL-6). **Contribution of the Software:** The system enables the fabrication of complex patterns while minimizing material consumption, thereby producing lightweight and efficient structures (URL-6).
Material	**PLA**
Material Properties	-PLA (polylactic acid) is a thermoplastic aliphatic polyester produced from renewable resources (URL- 7).
General Use	- PLA is a recyclable and environmentally friendly material (Şahin & Turan, 2018). - When mixed with different components, it can achieve wood- or plaster-like appearances (Şahin & Turan, 2018). - PLA material has lower strength compared to ABS material (Şahin & Turan, 2018). - Due to its slow solidification, printing errors may occur at high printing speeds; however, the use of cooling fans can mitigate these issues and enable higher printing speeds (Şahin & Turan, 2018). - It has lower heat resistance than ABS. (Şahin & Turan, 2018).
3D Printing Technology	**Robotic 3D Printer**

Design Prototype/ Design Concept	**Design:** Nadarra – 3D-Printed Sand Wall **Designer:** London-based architect and researcher Barry Wark.  - **Exhibition:**Nadarra is located at the entrance of the Dubai Future Museum (URL-8, URL-9). **- Dimension and Structure**: The wall measures 3X6 m and is composed of reusable modules (URL-8, URL-9). **- Modular Design:** The structure consists of puzzle-like panels that are easily assembled, manually transportable, and recyclable up to eight times (URL-8, URL-9). **- Production Technique:** The panels were produced using a binder jet printing method, which involves adding liquid binder to thin layers of sand particles (URL-8, URL-9). **- Sustainability:** The sand-based technology minimizes waste generation and enables the repeated fabrication, assembly, and recycling of the modules (URL-8, URL-9). **- Environmental and Design Contribution:** The prevention of material waste offers environmental benefits, while the method also allows the production of complex geometries without the need for molds (URL-8, URL-9).
Material	**SAND**
Material Properties	**Production Technology:** Production was carried out with the Voxeljet VX1000 3D printer used by the German 3D printer company Sandhelden; Quartz sand was used as the material (Kurşun & İpekoğlu, 1995). **- Post-processing:** After 3D printing, the object is strengthened and solidified by applying a liquid preservative, this process is called infiltration (Kurşun & İpekoğlu, 1995). **- Material Properties:** Quartz sand is a material found abundantly on earth (Kurşun & İpekoğlu, 1995).
General Use	-Quartz sand is used in different sectors such as glass, foundry and refractory industries (Kurşun and İpekoğlu, 1995). - In glass production, quartz sand must contain more than 99% SiO_2 and the amount of impurities must be stable (Aydın, 2021). - In casting systems, quartz sand must contain a minimum of 95-96% SiO_2 (URL-10). - When heated up to 1500 °C, quartz sand demonstrates high refractory performance (Kurşun and İpekoğlu, 1995).
3D Printing Technology	**BJ** (Binder Jetting)

Design Prototype/ Design Concept	**Design:** Gradient Fauteuil (3D printed concrete furniture), 2021 **Designer:** Philipp Aduatz  **Dimensions:** The dimensions of the design are 108 × 95 × 102 cm (URL-11). **- Production Technology:** The seating unit is produced using the 3D concrete printing method, enabling rapid production of complex forms without the need for molds (URL-11). **- Ecological and Economic Contribution:** Not using molds provides sustainability and cost advantages (URL-11). **- Aesthetic Feature:** During the printing process, pigments were injected into the concrete to create localized gradient color effects, resulting in each piece possessing a unique aesthetic transition (URL-11). **- Structural Strength:** The low tensile strength of concrete is strengthened by steel reinforcement in the design (URL-12).
Material	**CEMENT**
Material Properties	- Design Opportunities: 3D concrete printing enables the production of complex and innovative designs (URL-13). - Aesthetic Contribution: This method facilitates the creation of more aesthetic and original designs (URL-13).
General Use	-3D concrete printing enables free-form, organic, and innovative furniture designs by eliminating traditional constraints such as molding or prefabrication (Buswell et al., 2018; Bos et al., 2016). - Concrete provides high mechanical strength, resistance to weather conditions, and long service life, particularly for outdoor furniture applications (Wolfs et al., 2019). - Thanks to additive manufacturing, production can be done without using molds, which reduces material waste and additional costs (URL-13). - Designers can develop user-specific forms, patterns, and dimensions with 3D concrete printing; this provides advantages in indoor and outdoor applications (Yıldıztepe & Arabacıoğlu, 2024; URL-13). - The low tensile and impact strength of concrete may lead to structural weaknesses in furniture applications (URL-13).
3D Printing Technology	**Robotic arm-based 3D concrete extrusion printing method**

Design Prototype/ Design Concept	**Design:** Reform Lounge Chair **Designer:** Jurih Rahimkulov
	 **-Design Approach:** Reform Lounge Chair was designed with an aesthetic approach that integrates art, technology and sustainability (URL-14). **- Production Method:** Additive manufacturing (3D printing) technique, a computer-controlled process that deposits material in layers, was used in production (URL-14). **- Digital Infrastructure:** The design and software processes were developed using cloud-based platforms (URL-14). **- Area of Use:** The design can be used in both indoor and outdoor conditions (URL-14).
Material	**WOOD** (made of DuraSense®, a wood fiber-based biocomposite)
Material Properties	**-Material Composition:** The material contains cellulose fibers (URL-15). **-Mechanical and Production Advantages**: Cellulose fibers provide high strength, good printing performance and flexibility in finishing (URL-15). **- Sustainability:** The material is environmentally friendly and sustainable (URL-15).
General Use	-Wood and sawdust can be ground into fine powder and mixed with a binding material to be used in 3D printing (Cengiz & Aktepe, 2022). - Energy Efficiency: Wood exhibits lower energy consumption compared to steel and cement-based materials (Çankal & Şakar, 2021). - Wood is a natural and renewable resource and a sustainable building material with low carbon emissions and low energy requirements (Cengiz & Aktepe, 2022).
3D Printing Technology	**Large-Scale 3D Printing**

Design Prototype/ Design Concept	**Design:** Dragon Bench **Designer:** Joris Laarman (Joris Laarman Lab, Dutch, established 2004)  **- Technological Innovation:** Dragon Bench is one of the pioneering examples of 3D printing in metal processing. The design is produced with the MX3D robotic 3D printing system developed by Joris Laarman (URL-16, URL-17). **-Production Method:** The MX3D system is based on the principle of Wire Arc Additive Manufacturing (WAAM), which combines industrial robotic arms with welding technology (Canbolat & Aydın, 2019; Eke, 2019). **-Material Diversity:** This method enables the melting and solidification of metals such as stainless steel, aluminum, copper, and bronze into freeform lines without the need for support structures (URL-16, URL-17). **-Furniture Design:** Dragon Bench is one of the first examples of furniture produced with this technology and is considered as a hybrid research object that combines art, engineering and design (URL-16, URL-17). -**Advantages:** Compared to traditional furniture manufacturing, the method provides significant advantages in terms of cost and time efficiency by offering design freedom, material efficiency, parametric form generation, and the elimination of support structure requirements (URL-16, URL-17).
Material	**STEEL**
Material Properties	-Metal powders used in 3D printing technologies consist of micro- or nanoscale particles of metallic elements or alloys. These powders are employed in additive manufacturing processes through 3D printers (URL-18).
General Use	-Compared to conventional methods, 3D metal printing enables the production of more complex and flexible components (URL-18). -Metal powders are of critical importance for ensuring the desired alloy composition, properties, and mechanical strength (URL-18). -Metal tozlar lazer veya elektron ışını ile eritilir ve katmanlarla birleştirilir. -Various metal powders, such as titanium, aluminum, stainless steel, and nickel alloys, are utilized in this process (URL-18).
3D Printing Technology	**MX3D-Metal 3D-Printing Robot**

Design Prototype/ Design Concept	**Design:** Print To Build **Designer:** Gellert Olle (2017)  **-Design Series:** Gellert Olle's "Print to Build" series consists of modular connectors designed to join 8 mm thick plywood panels at angles of 90°, 45°, and 120° (URL-19). **-Assembly Feature:** The system is distinguished by its ability to be assembled without the use of screws or adhesives (URL-19). **-Production and Weight:** The connectors are produced via 3D printing, designed to accommodate different angles, with the heaviest component weighing approximately 30 grams (URL-19).
Material	**POLYAMIDE** (Powder)
Material Properties	**Material Properties**: Polyamide (nylon) is a widely used thermoplastic that provides toughness and flexibility, along with high impact and abrasion resistance (URL-20). **Economic Advantage:** Due to its low cost, polyamide is preferred in the production of functional parts using 3D printers (URL-21). **-Production Method:** Polyamide prints are produced from white, fine-grained powder (URL-22). **-Mechanical Properties:** The resulting products are durable and flexible, exhibiting resistance to minor impacts and bending (URL-23). **Surface Texture:** The surfaces have a sandy, granular, and slightly porous appearance (URL-24). **Usage Limitation:** Due to its moisture-absorbing property, polyamide is unsuitable for outdoor use; however, it can be rendered waterproof through specific treatments (URL-25).
General Use	-Application Area: Polyamide is suitable for the production of detailed and complex models (URL-24). Prototype Production: It is particularly preferred for small-scale prototypes (e.g., lamps, connectors) (URL-24).
3D Printing Technology	**FDM** (Fused Deposition Modeling)

Design Prototype/ Design Concept	**Design:** Aluminum Gradient Chair **Designer:** Joris Laarman  **- Exhibition:** The design is in the permanent collections of the National Gallery of Victoria in Australia and the Vitra Design Museum in Germany (URL-26). **- -Production Technology:** The Aluminum Gradient Chair is the first non-plastic 3D-printed furniture produced by layering aluminum powder and compressing it with a laser (URL-27). **- Design Feature:** The chair employs a gradient cellular density approach based on biomimetic and generative design principles, providing high structural strength and lightweight performance. Additionally, its permeable surfaces contribute to light transmission and aesthetic transparency (URL-27).
Material	**ALUMINUM** (Powder)
Material Properties	-Material Composition: Aluminum powder represents a finely particulate form of aluminum metal (URL-28). -Material Properties: Aluminum is a low-density, lightweight, durable metal with resistance to oxidation (URL-28).
General Use	-Industrial Applications: Aluminum powder is utilized in a variety of industrial and commercial applications, including additive manufacturing (3D metal printing), powder metallurgy, coatings, paint production, and rocket propellants (URL-28).
3D Printing Technology	**SLS** (Selective Laser Sintering)

Design Prototype/ Design Concept	**Design:** Cool Brick **Designer:** Virginia San Fratello & Ronald Rael, 2015
	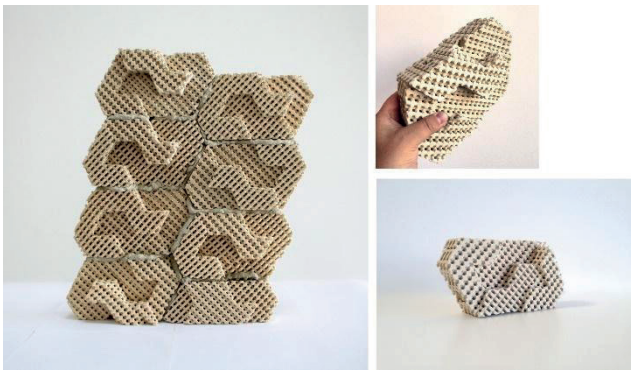 **-Design Inspiration:** Cool Brick was inspired by the Muscatese Evaporative Cooling Window, which combines wooden shutters with ceramic vessels filled with water to provide passive indoor cooling in desert environments (URL-29). **-Function:** Porous ceramic bricks, which can be used as partitions or curtain walls in interior, absorb water and enable passive cooling through evaporation (URL-29). **-Modular Production:** The bricks were produced as a modular system through 3D printing (URL-29). **-Working Mechanism:** The 3D-printed bricks are joined with mortar; as air passes through the bricks, the water within the ceramic's micro-pores evaporates, thereby lowering the indoor temperature (URL-29).
Material	**CERAMIC**
Material Properties	**-Production Method:** Ceramic-based models are manufactured using alumina–silica powder, with their surfaces coated in porcelain and silica layers (Saad, 2016). **-Aesthetics and Safety:** A lead-free and non-toxic glaze applied after production ensures both surface gloss and user safety (Saad, 2016). **-Heat Resistance:** Depending on the composition of the clay, ceramic materials can be fired at temperatures ranging between 800°C and 4215°C, providing high thermal resistance (Yıldırım, 2021).
General Use	- Ceramics are widely used in building materials (bricks, roof tiles, tiles, ceramic slabs), household items (porcelain plates, cups, decorative objects, and vases), and in the production of glass and porcelain products. Additionally, they are employed in advanced technological applications within biomedical, electronics, energy, and defense industries (Yıldırım, 2021).
3D Printing Technology	**LOM** (Laminated Object Manufacturing)

Design Prototype/ Design Concept	**Design:** Glass I & Glass II (2017-2018) **Designer:** Neri OXMAN & Mediated Matter Group 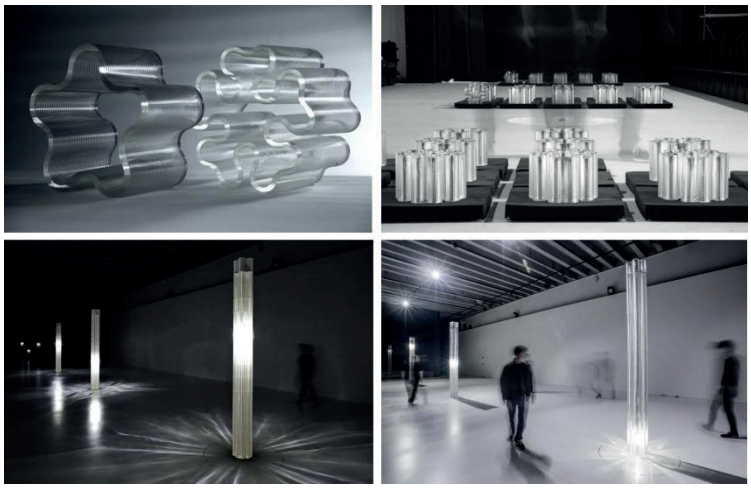 **-Exhibition and Installation:** At the Lexus Yet exhibition during the Milan Salone del Mobile, the scalability of the Glass 3D Printing II (G3DP2) technology, developed by the Mediated Matter Group at the MIT Media Lab, was showcased. The system presents a material processing method applicable from desktop scale to architectural scale and potentially to the construction industry (URL-30). **- Technological Advancement:** Building upon the first-generation printer design developed in 2015, the G3DP2 system was introduced. The new platform offers a production area four times larger and the capability to process up to 30 kg of molten glass in a single print. Its integrated thermal control system preserves structural integrity during annealing and printing, while four-axis motion control enables geometric precision and the production of complex glass forms with variable extrusion thicknesses (URL-30, URL-31). **-Architectural Forms:** The installation includes light-dynamic columns composed of modular glass units, each 20 cm in height, stacked to form three columns approximately 3 meters tall. The columns exhibit continuously shifting geometries, with multiple lobe profiles that organically transition toward the base (URL-30, URL-31). **- Structural and Aesthetic Features:** Structurally, the columns function similarly to the columns of a multi-story building. The varied geometric profiles of each layer generate caustic light patterns through programmable LED illumination. Dark mirrored surfaces further enhance the visual effect, creating an illusion of infinity and light integration within the spatial environment (URL-30, URL-31).
Material	**GLASS**
Material Properties	Potential: Glass-based materials hold significant potential in additive manufacturing due to their hardness, optical performance, economic accessibility, and widespread availability. However, existing studies on glass additive manufacturing remain limited. To date, two primary technologies have been applied, each with inherent disadvantages. In particular, the high melting temperature and viscosity of glass have led to the development of the binder jetting method. Although sintered glass objects produced through this approach are commercially available, they exhibit high brittleness and insufficient densification, resulting in low light transmittance and an opaque appearance (Klein, 2015).
General Use	-Application Areas: Glass materials are utilized in architecture and construction, furniture and interior design, optical and electronic applications, healthcare and laboratory equipment, the packaging industry, as well as in art and design (Belis et al., 2019; Demirci & Akçay, 2023; Wiederhorn & Clarke, 2022).
3D Printing Technology	**G3DP** (Nozzle Extrusion)

Conclusion

Developments in technology-based modern design and production methods have created a significant transformation in interior design elements and furniture applications. In this context, 3D printing technology has become one of the increasingly prominent methods in the field of furniture and interior design, thanks to the facilities it provides in production processes. This technology not only increases efficiency in production processes but also provides designers and interior architects with the opportunity to realize more original, personalized forms that are difficult to produce with traditional methods. These developments offer notable improvements in terms of both speed and quality, as well as productivity. The fact that many designers have preferred this method in recent years can be considered a strong indicator of the transition from mass production to a personal production model. Thus, thanks to 3D printing, designers have the opportunity to realize their products with a unique production process in their own workshops. The increasing widespread use of 3D printing technology in the production of interior design elements and furniture will continue to allow for the development of innovative and sustainable solutions in terms of aesthetics and functionality.

This study, conducted using the descriptive analysis method, examined the materials used in 3D printing technologies, the applications of these materials in furniture and interior design elements, and the effects of the aforementioned smart technology on design. Furthermore, the effects of various products used with 3D printing in the field of interior design and furniture on designers worldwide were also evaluated within this framework. As a result of all these examinations, the evaluations are as follows:

- Product development is possible in the design process thanks to 3D printing technology.
- 3D printing technology offers design freedom to designers by providing the opportunity for creativity and original design development.
- 3D printing technology continues to increase the creative potential of designers by offering new production methods in furniture manufacturing.
- It allows for the production of complex and detailed designs that are difficult to produce with traditional methods.
- It enables the transfer and application of natural forms and structural orders into the design process.
- It allows for the application of the parametric design approach.
- Personalization is prioritized in 3D printing methods. It is predicted that the demand for personalized products will increase over time due to the monotony of mass production, and in line with this, the use of 3D printing technology is

expected to become widespread.

- Time management in the design process is optimized through modeling and prototyping.
- 3D printing in the production of interior design elements and furniture has high potential for rapid prototyping, especially in the production of detailed products, and provides benefits in terms of design flexibility and the reduction of production risks. Furthermore, 3D printing technology provides significant time and cost advantages in scaled prototype production, especially for system solutions.
- The use of recycled or local materials through 3D printing in the production of interior design elements and furniture plays an important role in achieving sustainable production and consumption balances. In this context, material waste is observed to be almost completely eliminated in the 3D printing process.
- Changing color, design, and other personalization options does not create an additional cost during the printing process.
- In terms of production speed, 3D printing methods are relatively slower compared to mass production techniques and thus require further development.
- Since production can be performed locally with 3D printing technologies, the need for global logistics of raw materials and products is significantly reduced.
- 3D printing technology will significantly transform the habits of designers, manufacturers, and consumers by increasing production speed and will reshape the way furniture is purchased.
- It will be possible for consumers to quickly have products such as chairs, tables, and accessories produced in local 3D printing workshops.
- It should be noted that 3D printing technology is limited to certain material types.
- The advantages and disadvantages of each material to be used with 3D printing technology should be investigated. Furthermore, the type of objects to be printed and the functional requirements these objects will meet should be taken into account.
- Each design should be analyzed in terms of the mechanical properties of the materials before being offered for sale.
- Although 3D printing technology causes significant transformations in the furniture industry, it is not expected to completely eliminate traditional production methods. Designers and manufacturers will continue to use 3D printing by integrating it with their traditional production capabilities.

Based on the results of this study, in the context of the development of 3D printing

technology, it is recommended that further research should be conducted on expanding material diversity, production using hybrid materials, and increasing production speed. Furthermore, it is foreseen that 3D printing technology will offer an innovative perspective, primarily to designers, but also to educators, students, and professional sector employees, and will form a dataset or reference plane for other scientific studies.

References

Akbaba, A. İ., & Akbulut, E. (2021). 3 Boyutlu Yazıcılar ve Kullanım Alanları. *ETÜ Sentez İktisadi Ve İdari Bilimler Dergisi*, (3), 19-46.

Aydın, B. (2021). Düşük SiO_2 İçerikli Kuvars Kumunun Zenginleştirme İşlemleri ile Hammadde Kaynağı Olarak Kullanılabilirliğinin İncelenmesi. *Bilimsel Madencilik Dergisi*.

Aydın, M. (2015). Use of 3D Printing in Furniture Production. *Akademik Platform,* 590-599.

Belis, J., Louter, C., Nielsen, J. H., & Schneider, J. (2019). Architectural Glass. *In Springer Handbook of Glass*, 1781-1819.

Bos, F., Wolfs, R., Ahmed, Z., & Salet, T. (2016). Additive Manufacturing of Concrete in Construction: Potentials and Challenges of 3D Concrete Printing. *Virtual and physical prototyping*, 11(3), 209-225.

Buswell, R. A., De Silva, W. L., Jones, S. Z., & Dirrenberger, J. (2018). 3D Printing Using Concrete Extrusion: A Roadmap for Research. *Cement and concrete research*, 112, 37-49.

Canbolat, T. & Aydın, K. (2019). Mobilya Sektörü Özelinde Üç Boyutlu Yazıcılarla Tasarım ve Malzeme-Biçim-Üretim Yöntemi Üzerine İlişkisel Düşünme. *Çukurova Üniversitesi Mühendislik-Mimarlık Fakültesi Dergisi*, 34(4), 181-192.

Çankal, D., Şakar, G. (2021). Sürdürülebilir Yapılar İçin Ahşap ve Lamine Ahşabın Lifli Polimer (FRP) Malzemeler ile Güçlendirilmesinin Değerlendirilmesi. *Şehir Sağlığı Dergisi*, 2(2), 99-10.

Cengiz, Ö. & Aktepe, Ş. (2022). Üç Boyutlu (3D) Yazıcılarda Sürdürülebilir Malzeme Olarak Ahşap ve Proses Atıklarının Kullanım Potansiyelinin Değerlendirilmesi. *Avrupa Bilim ve Teknoloji Dergisi*, (38), 143-150.

Chen, C. C., Yang, W. Z., Teng, H. M., Liao, S. S., & Tsao, C. C. (2023). Study on the Application of 3d Printing to Wooden Furniture Connectors. *In Journal of Physics: Conference Series,* IOP Publishing, 2631(1), 012006.

DebRoy, T., Wei, H. L., Zuback, J. S., Mukherjee, T., Elmer, J. W., Milewski, J. O., Beese, A. M., Wilson-Heid, A., De, A. & Zhang, W. (2018). Additive Manufacturing of Metallic Components–Process, Structure and Properties. *Progress in Materials*

Science, 92, 112-224.

Demircali, A. A., Yilmaz, D., Yilmaz, A., Keskin, O., Keshavarz, M., & Uvet, H. (2024). Enhancing Mechanical Properties and Surface Quality of FDM-printed ABS: A Comprehensive Study on Cold Acetone Vapor Treatment. *The International Journal of Advanced Manufacturing Technology*, 130(7), 4027-4039.

Demirci, S., & Akçay, S. (2023). Bir Tasarım Malzemesi Olarak Kullanılan Camın Tasarımda Kullanım Alanları. *Turkish Journal of Fashion Design and Management*, 5(3), 207-225.

El-Sayegh, S., Romdhane, L., & Manjikian, S. (2020). A Critical Review of 3D Printing in Construction: Benefits, Challenges, and Risks. *Archives of Civil and Mechanical Engineering*, 20(2), 34.

Eke, T. E. (2019). Mobilya Tasarım ve Üretiminde Üç Boyutlu Yazıcı Teknolojisi. Yüksek Lisans Tezi, Marmara Üniversitesi, Türkiye.

Eti Proto, M., & Koç Sağlam, C. (2021). Furniture Design Education with 3D Printing Technology. In Makers at School, Educational Robotics and Innovative Learning Environments: Research and Experiences from FabLearn Italy 2019, in the Italian Schools and Beyond, 97-105. Cham: Springer International Publishing.

Gedik, E., Togay, A., Çoşkun, M., & Demirhan, E. (2018). Üç Boyutlu Baskının Mobilya Sektöründe Ürün Tasarımında Kullanım İmkanlarının Araştırılması. *International Journal of 3D Printing Technologies and Digital Industry*, 2(2), 16-25.

Gibson, I., Rosen, D., Stucker, B., Khorasani, M., Rosen, D., Stucker, B., & Khorasani, M. (2021). Additive Manufacturing Technologies. Cham, Switzerland: *Springer*, 17, 160-186.

Girskas, G., & Kligys, M. (2025). 3D Concrete Printing Review: Equipment, Materials, Mix Design, and Properties. *Buildings*, 15(12), 2049.

Herzog, D., Seyda, V., Wycisk, E., & Emmelmann, C. (2016). Additive manufacturing of metals. *Acta Materialia*, 117, 371-392.

Kang, H. D. (2015). Analysis of Furniture Design Cases Using 3D Printing Technique. *The Journal of the Korea Contents Association*, 15(2), 177-186.

Klein, J., Stern, M., Franchin, G., Kayser, M., Inamura, C., Dave, S., Weaver J. C., Houk, P., Colombo, P., Yang, M. & Oxman, N. (2015). Additive Manufacturing of Optically Transparent Glass. *3D printing and additive manufacturing*, 2(3), 92-105.

Kurşun, İ., & İpekoğlu, B. (1995). Türkiye Kuvars Kumu Potansiyeline Genel Bir Bakış. *Endüstriyel Hammaddeler Sempozyumu*, İzmir, Türkiye, 21-22.

Liu, R., Wang, Z., Sparks, T., Liou, F., & Newkirk, J. (2017). Aerospace Applications of Laser Additive Manufacturing. *In Laser additive manufacturing*, Woodhead Publishing, 351-371.

Nadarajah, N. (2018). Development of concrete 3D printing masters in Building Technology. Aalto University, Finlandiya.

Petrova, B., & Jivkov, V. (2024). Application of 3D Printing Technology in Furniture Construction. *Materials*, 17(19), 4848.

Saad, R. M. (2016). The Revolution of Materials Used in 3D Printing Applications in Furniture & Interior Design. *International Design Journal*, 6(3), 143-163.

Şahin, K., & Turan, B. O. (2018). Üç Boyutlu Yazıcı Teknolojilerinin Karşılaştırmalı Analizi. Stratejik ve Sosyal Araştırmalar Dergisi, 2(2), 97-116.

Thomas, D. S., & Gilbert, S. W. (2014). Costs and Cost Effectiveness of Additive Manufacturing. *NIST special publication*, 1176, 12.

Topal, S., & Kavut, İ. E. (2024). Mimari Tasarımda Üç Boyutlu Baskı Teknolojisinin Örnekler Üzerinden İncelenmesi. *Kırklareli Üniversitesi Mimarlık Fakültesi Dergisi*, 3(1), 13-26.

Venkatesh, K. V., & Nandini, V. V. (2013). Direct Metal Laser Sintering: A Digitised Metal Casting Technology. *The Journal of Indian Prosthodontic Society*, 13(4), 389-392.

Wiederhorn, S. M., & Clarke, D. R. (2022). Architectural Glass. *Annual Review of Materials Research*, 52, 561-592.

Wolfs, R. J. M., Bos, F. P., & Salet, T. A. M. (2019). Hardened Properties of 3D Printed Concrete: The Influence of Process Parameters on Interlayer Adhesion. *Cement and Concrete Research*, 119, 132-140.

Yang, S., & Du, P. (2022). The Application of 3D Printing Technology in Furniture Design. *Scientific Programming*, 2022(1), 1960038.

Yıldırım, B. (2021). Seramik Malzemenin Kullanım Alanları ve Ülkemizde "Seramik Üniversitesi" Kurulması Önerisi. *Yeni Fikir Dergisi*, 13(26), 18-34.

Yıldıztepe, B., & Arabacıoğlu, B. C. (2024). Üç Boyutlu Yazıcı Teknolojisi ile İç Mekanlarda Özgün Tasarımlar. *Kırklareli Üniversitesi Mimarlık Fakültesi Dergisi*, 3(1), 1-11.

Electronic References

URL-1 https://www.tmcnet.com/topics/articles/2023/05/04/455775-3d-printed-furniture-revolutionizing-home-decor-with-customization.htm

URL-2 https://techbullion.com/the-impact-of-3d-printing-on-furniture-design-and-

home-decor/?utm

URL-3 https://www.core77.com/posts/113714/3D-Printed-Alternative-to-Yoga-Ball-as-Chair

URL-4 https://3dinsider.com/pros-and-cons-3d-printing-filaments/?utm_source

URL-5 https://www.boyutkat.com/3d-yazici-filament/abs-filament-nedir/#abs-filamentinin-dezavantajlar%C4%B1-nelerdir

URL-6 https://www.dezeen.com/2017/05/17/robot-made-voxel-chair-new-software-bartlett-researchers-design-furniture-technology-chairs-robot

URL-7 https://en.wikipedia.org/wiki/Polylactic_acid?utm

URL-8 https://makerfairerome.eu/en/blog/the-most-intricate-3d-printed-wall-ever-manufactured/?utm

URL-9 https://www.dezeen.com/2023/12/12/3d-printed-sand-wall-barry-wark/

URL-10 https://www.tesisat.org/kuvars-kuvarsit-ve-kuvars-kumu.html?utm

URL-11 https://www.philippaduatz.com/portfolio-item/gradient-fauteuil/?utm

URL-12 https://designwanted.com/philipp-aduatz-3d-printed-gradient-furniture/

URL-13 https://confabric.com/tr/geleneksel-insaat-yontemlerine-karsi-3d-beton-baski-avantajlar-ve-dezavantajlar

URL-14 https://sixtysixmag.com/3d-printed-furniture/

URL-15https://kcl.fi/app/uploads/2025/04/KCL-Formi%E2%84%A2-3D-Nordic-Birch-product-brochure.pdf.

URL-16 https://www.jorislaarman.com/work/mx3d-metal/

URL-17 https://high.org/collection/mx3d-dragon-bench-prototype/

URL-18 https://grafen.com.tr/3d-metal-tozlari-nedir-kullanim-alanlari/

URL-19 https://competition.adesignaward.com/design.php?ID=58206&utm

URL-20 https://divanambalaj.com/polyamid-nedir-ozellikleri-nelerdir/

URL-21 https://xometry.pro/tr/makaleler/3d-baski-mjf-pa12/?utm

URL-22 https://i.materialise.com/blog/en/how-professional-3d-printing-works/?utm

URL-23 https://www.xometry.com/resources/materials/polyamide/?utm

URL-24 https://i.materialise.com/en/3d-printing-materials/polyamide?utm

URL-25 https://xometry.eu/en/3d-printing-water-resistance/?utm

URL-26 https://www.jorislaarman.com/work/gradient-chair/

URL-27 https://collectiononline.design-museum.de/#/en/object/40023?_k=ojimxj

URL-28 https://www.kimyadeposu.com/makaleler/aluminyum-tozu-ve-kullanim-alanlari

URL-29 https://emergingobjects.com/project/cool-brick/?utm

URL-30 https://www.media.mit.edu/projects/g3p-ii/overview/

URL-31 https://oxman.com/projects/glass-ii

About The Author

Tuba ARKAN DEMİRÖRS holds an integrated PhD degree in Architecture in 2023. She is guest instructor, in the Department of Interior Architecture at KTO Karatay University in Konya, Turkiye. Her main areas of interest are materials and technology in architecture and interior architecture, building materials and interior architecture design.
E-mail: tuba_arkan@hotmail.com , **ORCID:** 0000-0003-3278-9045

Similarity Index

The similarity index obtained from the plagiarism software for this book chapter is 11%.

Investigation of the Microstructure and Mechanical Properties of S355JR – S700MC Steels Welded by GMAW

Fatma Nur ŞAHİN
Necmettin Erbakan University

Hakan GÖKMEŞE
Necmettin Erbakan University

Şaban BÜLBÜL
Necmettin Erbakan University

To Cite This Chapter:
Şahin, F. N., Gökmeşe, H., & Bülbül, Ş. (2025). Investigation of the microstructure and mechanical properties of S355JR–S700MC steels welded by GMAW. In H. Gökmeşe, Ş. Bülbül, & Y. Uzun (Eds.), Current studies in basic sciences: *Innovative approaches in materials science and applications* (pp. 47–64). ISRES Book Series. ISRES Publishing.

Introduction

Following the Stone Age, the discovery of metals led to the development of processing methods. For the people of that era, who subsisted on hunting, metals used particularly in weapon production gained significant importance. After the discovery of gold, copper, silver, lead, and tin, iron was discovered around 1500 BC. Subsequently, many different types of metals, such as chromium, aluminium, and nickel, were discovered. As history progressed, the smelting of iron was discovered and used in the manufacture of tools and weapons. In the Bronze Age, the foundations of alloying were laid, and it was discovered that two different metals could be mixed to obtain a stronger metal.

With the technology that developed after the Industrial Revolution, steel was added to iron, which had been used since ancient times, forming the basis of industry. With this development, production techniques also changed. Welding, which enables two materials to be joined together in a strong manner, has also gained great importance in heavy industry. Known as blacksmithing in ancient times, this method has been developed using different techniques with the discovery of steel and other materials.

Welding, one of the most important production methods used in industry, involves melting and joining multiple materials using different techniques. Starting with joining by hammer blows, welded manufacturing was further developed with the discovery of sources such as oxygen and electricity. Applications were made using oxyacetylene, electric arc welding, TIG, GMAW (MIG and MAG welding) methods, respectively. With advancing technology, many different welding techniques have been developed,

such as submerged arc welding, resistance welding, and laser welding.

Due to the widespread use of steel as a raw material in industry, MIG/MAG welding applications are particularly prevalent. In many sectors, such as automotive and construction, the MAG welding method is preferred due to its cost and good welded joints in terms of mechanical and chemical properties. Since the effect of shielding gas is very high in this welding method, it has been the subject of many scientific studies. Argon-rich carbon dioxide and oxygen additives are particularly preferred for their high-quality weld seam, economy, and availability.

In addition to structural steels such as S235 and S355, which have a wide range of uses, the use of high-strength SSAB brand Strenx lightweight structural steels has also become widespread. They are particularly preferred in the automotive industry because they can carry more load than other steels of the same weight. Companies that choose these steels due to the expectation that load-bearing transport vehicles in Europe should be lighter are also achieving significant financial gains in exports.

In the automotive sector, the welded combination of S700MC and S355JR steel is a common application in trailer and body manufacturing. Deformations in the material are likely when incorrect application techniques are used. Experimental research was conducted in this thesis to understand the weld structure and mechanical properties of these products, which carry very high tonnages.

In this study, S355JR structural steel and S700MC fine-grained structural steel, which are widely used in industry, were welded using the MAG welding method, using SG2 welding wire with a diameter of 1.2 mm and protective gases of 86%Ar+12%CO_2+2%O_2 and 93%Ar+5%CO_2+2%O_2. The welded areas of the steels, the grain structure changes in the HAZ and parent metal, and the mechanical properties were examined.

Welding Methods

Welding is defined as metal or plastic welding, depending on the type of material to be applied. If heat input is involved in the applied method, it is fusion welding, and in some applications of this method, a filler metal is used to join the two materials. If welding is performed under pressure, it is called pressure welding. In pressure welding, the material is heated and joined under pressure in the area without the use of any filler metal.

When classified according to the purpose of welding, it is defined as joining and filling welding; it is classified according to the type of material as metal and plastic welding. The method used to join multiple materials into an inseparable whole is called joining welding. while the method used to fill a gap in a part or to enlarge a part is called filling welding (Anık, 1991).

Gas Metal Arc Welding (GMAW)

In gas metal arc welding, which is performed with a consumable electrode, a shielding gas is used to protect the weld pool from the adverse effects of the air. If the welding gas used is inert, it is called MIG (Metal Inert Gas) welding, and if it is active, it is called MAG (Metal Active Gas) welding (Koç, 2009). During welding, the welding gas passes through the welding torch over the wire and covers the weld pool. In this welding method, the arc is established between the welding wire and the contact nozzle and is transferred to the workpiece via the wire.

Argon and helium gases are commonly used as inert gases in MIG welding. In MAG welding, mixtures of gases consisting of carbon dioxide or inert gases mixed with carbon dioxide in specific proportions are used as active gases. In this method, depending on the intended use, electrodes can be made into cored wires by feeding them with various minerals to obtain a more efficient and higher-quality weld. The equipment and hardware used in MIG and MAG welding are identical; only the gas and electrode used differ. MIG welding is a suitable method for unalloyed and low-alloy steels. MAG welding can also be used for welding aluminium, copper, nickel, and titanium alloys (Toprak Şenol, 2020).

Figure 1

Principle of GMAW (Antonini, 2014)

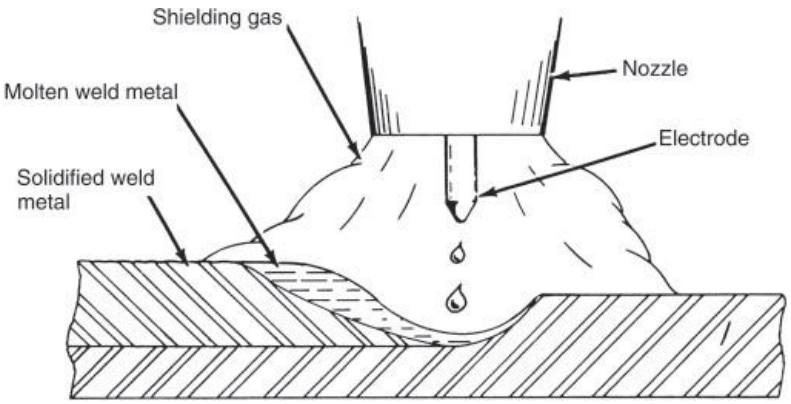

Principle of GMAW

In the GMAW method, a continuously fed consumable electrode is used together with a shielding gas. In semi-automatic welding machines, the free wire length and electrical characteristics of the arc set by the welder are automatically determined; the welder only controls the position of the welding torch and the feed rate.

The arc, which is created by the contact of the wire fed through the torch with the part, passes through an ionized gas with the electric current and melts with the heat generated. The energy generated by the movement of electrons travelling rapidly from the cathode to the anode releases heat, and the material in the heated area begins to melt. Atoms

that lose electrons become ionised and rapidly move towards the cathode. As a result, melting also occurs in that heated area. Melting continues in this manner continuously **(Figure 1)**. The metal and wire being welded melt with the heat created by this welding. The molten wire, protected by shielding gas, fills the weld pool, which is also protected by the gas, as filler metal. After the arc is extinguished in the fusion zone, the weld metal solidifies (Şık, 2002).

As shown in **Figure 2**, in GMAW, the transfer of metal droplets to the weld metal occurs through three different mechanisms:

- Short-circuit transfer
- Large droplet transfer (Globular Transfer)
- Spray transfer

The droplet transfer type varies depending on many parameters, such as the type of shielding gas, the properties of the welding wire, the free wire length, and the type and intensity of the welding current (Eryürek, Sevük, & Odabaş, 2007).

Figure 2

Droplet Transfer Mechanisms ('Morrow Welding', n.d.)

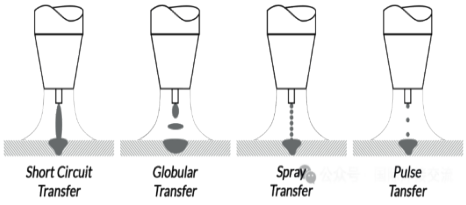

A short circuit transfer occurs in gas shielded welding performed at very low currents with low electrode diameters. Metal transfer to the workpiece does not occur in the arc gap; it only occurs when the electrode contacts the weld pool. In short-circuit transfer, the chemical composition of the shielding gas significantly affects the metal droplet diameter, arc characteristics, penetration into the workpiece, and short-circuit duration. Carbon dioxide provides deeper penetration than noble gases but causes more spatter. To achieve this balance, a mixture of carbon dioxide and argon is generally preferred. An argon-helium mixture also provides good penetration in metals other than iron. In large droplet transfer, the metal droplet diameter is larger than the electrode diameter. Large droplet transfer, where the type of shielding gas is not decisive, occurs at low welding currents with direct current and positive electrode polarity. It occurs at all welding currents when performed only with carbon dioxide and helium gases. In welds performed entirely with inert gas shielding, a globular transfer can be achieved at a current value slightly higher than the short circuit transfer current. Spray transfer can be achieved without spattering under argon gas shielding, with the electrode positively polarised in direct current, and when the current intensity is higher than the critical transition current value.

Metal transfer occurs when droplets smaller than the electrode diameter separate at a transfer rate of hundreds of droplets per second. The melting temperature and chemical composition of the shielding gas affect the transition current. Furthermore, the transition current is inversely proportional to the electrode diameter and free wire length. When spray transfer is performed under argon gas shielding, it can be used with almost all alloy metals (Eryürek et al., 2007).

GMAW Welding Equipment

The equipment used in gas shielded welding is divided into five main groups: the power unit, the shielding gas unit, the electrode feed unit, the welding torch, and the cable assembly **(Figure 3)**. Gas shielded arc welding equipment has a more complex structure than electric arc welding equipment (Küpeli, 2008).

Figure 3

GMAW Equipment (Stephanie Oostman, 2021)

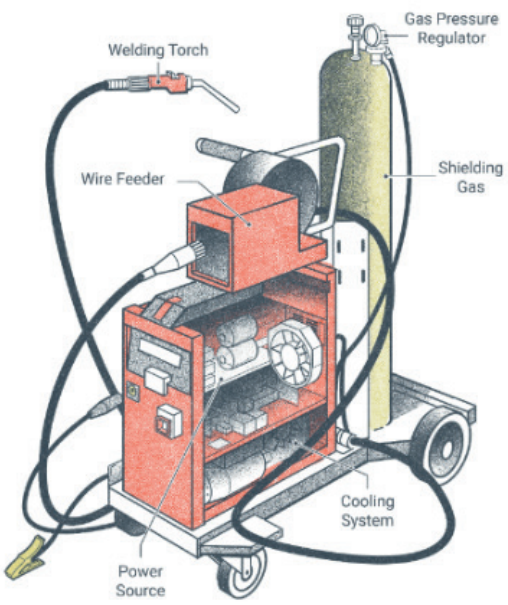

Electrodes (Welding Wires)

The wire-form electrodes used in GMAW are wound onto spools that meet specific standards (Durmuşoğlu, 2006). Electrodes are generally grouped according to their chemical composition and mechanical properties based on AWS standards, which are commonly used in the United States. According to German DIN standards, classification is based on wire diameter, surface tolerances and conditions, chemical composition, and application areas. The chemical compositions of electrodes used in the welding of steels commonly preferred in industry, according to DIN 8559 and TS 5618, are given in **Table 1**. Electrodes should be free of surface defects such as burrs, pits, and foreign matter that could impede their progression during welding; their surfaces should be completely

smooth (Geçmen, 2006).

Table 1

Chemical Composition of Some Electrodes Used in Welding Steels (Geçmen, 2006)

Symbol	Mat. No	C	Si	Mn	P <	S <	Cu <	Impurity
SG 1	15112	0.07-.0.12	0.5-0.7	1.0-1.3	0.025	0.025	0.30	Cr 0.15 V 0.05 Zr+Ti 0.15 Al 0.02 Ni 0.15 Mo 0.15
SG 2	15125	0.07-0.14	0.7-1.0	1.3-1.6	0.025	0.025	0.30	
SG 3	15130	0.07-0.14	0.8-1.20	1.6-1.9	0.025	0.030	0.30	

The selection of consumable electrodes used in GMAW is crucial because the combination with the shielding gas affects the physical and chemical properties of the weld metal. The physical and mechanical properties of the weld metal and its chemical composition are selected according to the type of shielding gas. This selection is facilitated by knowing the effect of the components in the structure of the electrodes used in welding steels on the weld. These components are carbon, silicon, manganese, aluminium, titanium, zirconium, nickel, chromium, and molybdenum elements (Durmuşoğlu, 2006).

Shielding Gases

In MIG welding, inert gases such as argon and helium, which do not react, are used, while in MAG welding, active or active-inert gas mixtures such as carbon dioxide are used. The primary purpose of the shielding gases used in GMAW is to protect the weld pool and the area affected by heat from contamination and oxidation caused by the atmosphere. The molten metals in the weld pool absorb oxygen and nitrogen from the atmosphere, and these gases dissolve within the metal. The shielding gases can prevent these dissolved elements from forming compounds with the alloying elements in the metal and disrupting its chemical and physical structure, causing brittleness through the formation of pores and cracks. In addition, shielding gases affect welding characteristics such as welding speed, metal transfer mode, penetration and bead geometry, arc characteristics, and burn-off. The protective gases to be used are selected based on criteria such as part thickness, desired weld geometry, and mechanical properties, chemical composition of the base metal, cost and availability, and welding speed (Durmuşoğlu, 2006).

Weld Structure

A welded composite obtained by gas metal arc welding consists of the base metal, the weld metal formed by the mixture of the base metal and the filler metal, and the heat-affected zone (HAZ) **(Figure 4)**. In fusion arc welding, the mixture in the weld zone is

complete and homogeneous. The amount of heat provided by the weld and the metal's ability to conduct this heat, as well as the weld speed, cause the width of the HAZ to vary (Karakoç, 2012).

Figure 4

Heat-affected Zone (HAZ) (Tukahirwa & Wandera, 2023)

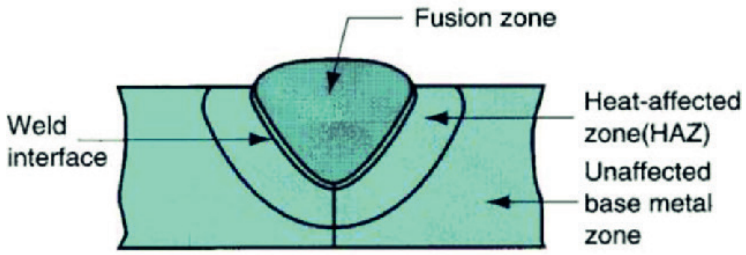

The weld metal is the region where the metal completely melts and then solidifies again during the welding process. The heat-affected zone (HAZ) is the non-melted region with different properties from the base metal due to the effect of the welding heat (Tukahirwa & Wandera, 2023).

Material and Methods

In this study, 4 mm thick S700MC and S355JR structural steels were used. Metal pieces measuring 200x200 mm were cut from sheet metal using plasma. The chemical compositions of S355JR2 are given in **Table 2,** and those of S700MC are given in **Table 3**.

Table 2

Chemical Composition of S355JR Structural Steel (%) (Dikeç, 2023)

C	Si	Mn	P	S	Al	Cu	Cr	N	Mo	Ni
0,186	0,13	1,426	0,011	0,008	0,036	0,121	0,042	0,0082	0,0002	0,059

Table 3

Chemical Composition of S700MC Structural Steel (%) (SSAB, 2023)

C	Si	Mn	P	S	Al	Nb	V	Ti
0,12	0,21	2,1	0,02	0,01	0,015	0,09	0,2	0,15

Of the steels whose mechanical properties are given in **Table 4,** S700MC steel has a stronger and harder structure than S355JR due to its fine-grained structure. Despite its high resistance under load, it is a very light steel. For this reason, it is widely preferred, especially in the automotive industry.

Table 4

Mechanical Properties of S355JR and S700MC Structural Steels (ChnÇelik, 2023)

Steel	Yield Strength (MPa)	Tensile Strength (MPa)	Elongation (%)
S355JR	355	470-630	22
S700MC	700	750-950	12

As O_2 gas was used during the cutting of the 200x200x4 mm metal parts, no further processing was required. Due to the low thickness of the parts to be butt welded, there was no need to open the weld joint. The parts were welded using 1.2 mm SG2 welding wire, which belongs to the ER70S-6 product group according to the AWS standard, under two different gas shields with composition ratios given in **Table 5**.

Table 5

Chemical Composition of HB205 ve HB212 (%)

	O_2	CO_2	Ar
HB 205	2	5	93
HB 212	2	12	86

The welding parameters were automatically set by the Kolarc M500 synergic welding machine by entering the material thickness of 4 mm, the type of welding gas, and the electrode diameter, and MAG welding was performed. Accordingly, the welding current intensity was set to approximately 200 A, the welding voltage to 20 V, and the wire feed speed to 7 m/min. The protective gas flow rate, one of the most important parameters determining the mechanical and chemical properties of the weld seam, was set to 12 m^3/s before starting the welding. The gas flow rate is theoretically calculated as 10 times the electrode diameter. In addition, to ensure full gas protection, the tip of the water-cooled torch is adjusted so that it does not lose its field of view and, when pulled perpendicular to the surface, is at most 20° from the surface.

In accordance with the standard ISO 5178:2019 Destructive tests on welds in metallic materials - Longitudinal tensile test on weld metal in fusion welded joints, two metal butt welds measuring 200x200 mm were welded on both sides using a thin material that was too thin to weld with the weld opening **(Figure 5a)**. Welding was performed in the PA (1G) position at a welding speed of 10 mm per second. Using a mixture of HB 205 and HB 212 gases, three samples each of 200x200 mm in size and 4 mm in thickness were welded under the same welding parameters: S355JR-S355JR, S355JR-S700MC, and S700MC-S700MC.

Figure 5
Welded Steel Samples

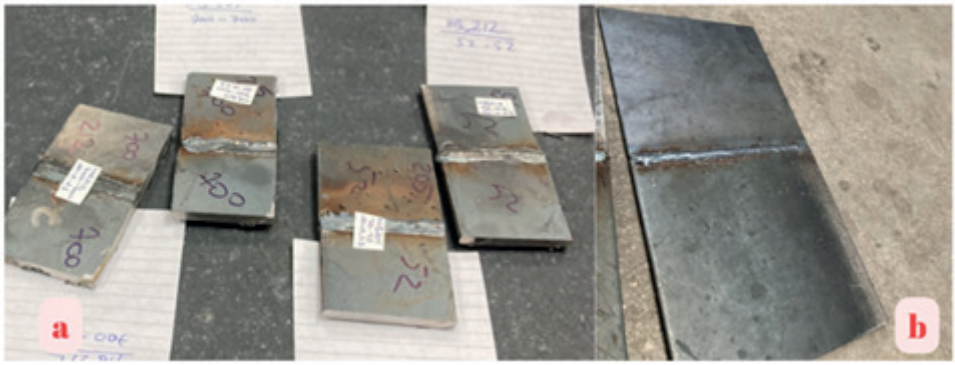

The samples were cut from the welded metal to approximately 50x90 mm as shown in **Figure 5b**. Due to the heat input, which would alter the properties of the material, the samples were cut to large dimensions. The flex-cut samples were prepared for water jet cutting for microstructure, microhardness, and XRD analysis. Small samples were cut to fit into the bakelite so that they would cover the base metal, HAZ, and weld zone of the material. Metal parts were placed in a moulding device together with two scales of Aka-Resin Acrylic bakelite powder. Samples processed in this device at 190 °C temperature and pressure for 15.5 minutes were ready for grinding.

For a clear image in microstructure examinations, the material's surface must be completely smooth, free of scratches and deformations. Therefore, the sample's surface was sanded using a sanding machine while submerged in water. The surface was processed with 400, 800, and 1200 grit sandpaper until it was completely smooth. Before each sanding, the surface of the sample was washed and cleaned with alcohol. As a final step, the felt was changed on the same machine, and the sample was polished dry. The polished samples were washed with soap, cleaned with alcohol, and dried.

Following metallographic studies conducted after the welding process, optical microscope examinations were performed to examine the microstructure of the test specimens. In particular, regarding the microstructural characterisation of the test specimens, the phase structures and their distributions, the examination of grains and grain boundaries, and the differences in the welding process in terms of HAZ and the base material were investigated.

In terms of welded manufacturing, phase transformation differences are important, particularly for the formation of the weld pool and HAZ region, within the scope of two different welding metals and welding parameter variables used. In this context, XRD analysis was performed to identify compounds that are likely to form depending on two different steel materials and welding parameters. The XRD analysis results were obtained using Cu-Kα radiation (λ= 1.544 Å) in the range of $10° < 2\theta < 70°$, using a

voltage of 40 kV and a current of 40 mA.

Microhardness measurements were performed to evaluate the hardness of the HAZ and weld metal of the test specimens as a result of the applied MAG welding method, depending on the difference in welding parameters. For these hardness measurements, studies were carried out under HV1 load on a Vickers-scale microhardness device. The microhardness measurement was automatically measured from the indentation mark left on the sample surface after pressing the diamond pyramid tip onto the sample surface for approximately 10 seconds with the load specified.

To perform the tensile test, the samples were designed in SolidWorks for cutting, as shown in **Figure 6a**, in accordance with the jaw dimensions of the tensile testing machine and the ISO 5178:2019 standard. In accordance with this standard, the laser method was preferred for cutting the specimens to be tested. The tensile bars were cut to the specified dimensions from each specimen, three pieces per specimen, as shown in **Figure 6b**, on a laser cutting bench programmed according to the design.

Figure 6

Tensile Test Samples

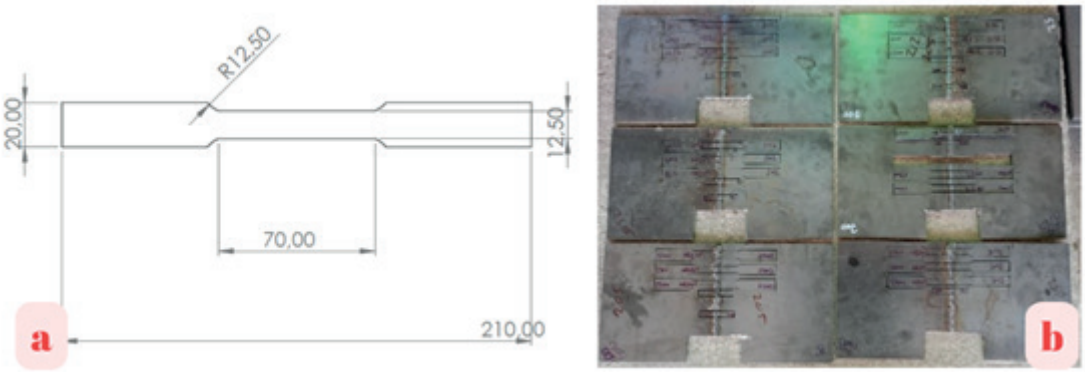

The test parameters were entered into the computer control programme compatible with the tensile testing machine, integrated with the ISO 6892-1 Metallic materials -Tensile testing- Part 1: Test method at ambient temperature standard. These parameters were set to a displacement speed of 5 mm/s and a loading speed of 0.2 kN/s, and the testing machine was started. Under these parameters, tensile tests were performed in triplicate for each sample, and the results obtained are given as average values.

Experimental Results

To describe the results obtained from the test specimens, the parts made of different steels welded under different gas shielding were named as follows:

- S355JR-S355JR steel sample welded with HB 20 gas S1
- S700MC-S700MC steel welded with HB 205 gas → S2
- S355JR-S700MC steel welded with HB 205 gas sample → S3

- S355JR-S355JR steel welded with HB 212 gas → S4
- S700MC-S700MC steel welded with HB 212 gas → S5
- S355JR-S700MC steel welded with HB 212 gas → → S6

The optical microstructure results obtained from the base metal, HAZ, and weld metal regions of S355JR and S700MC steel materials welded using the MAG welding method are shown in **Figure 7**, respectively.

Figure 7

Microstructural Analysis Results a)S1 b)S2 c)S3 d)S4 e)S5 f)S6

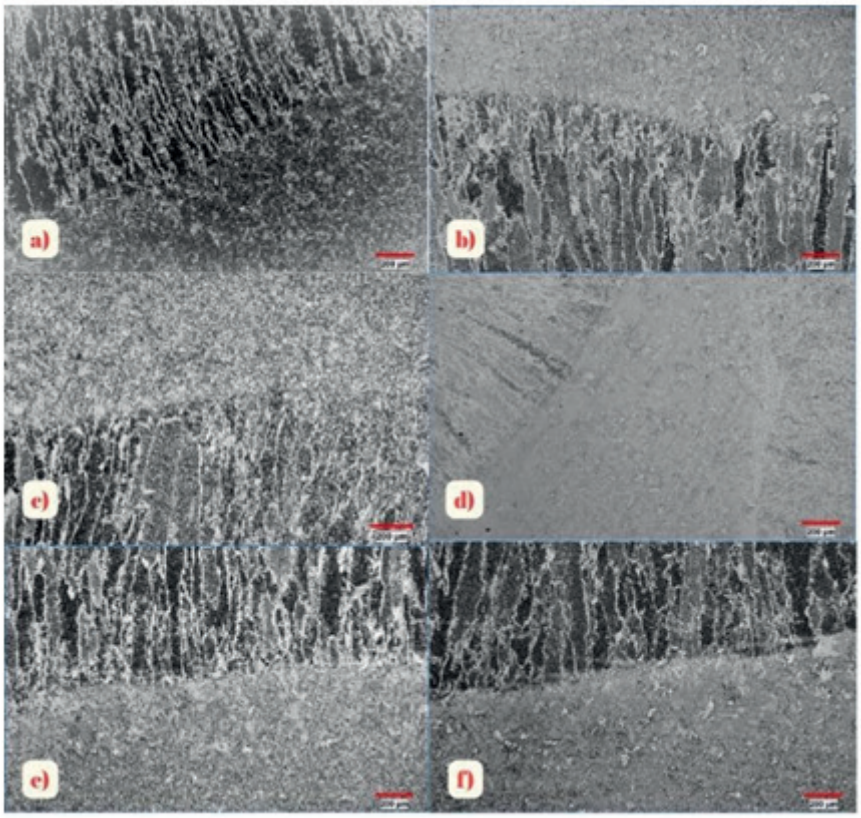

When examining the base metal of S355JR structural steel, it can be seen that the material consists of ferrite and pearlite phases. Moving to the HAZ and weld zone, this distinct structure is lost, and the grain size increases towards the weld metal. Coarse-grained dendritic arms are observed in the weld metal zone. Experimental studies in the literature indicate that grain growth in the weld metal zone is a result of increased heat input. Furthermore, it was observed that this heat causes grain orientation in the direction of flow (Kaya vd., 2020; Şık, 2007). Different composition ratios of the mixed gas did not create a significant difference in the microstructure. In S700MC steel, it was observed that the grain size increased as it progressed towards the HAZ and weld metal. As in S355JR steel, a dendritic structure was observed in the weld metal region. In these metals, the difference in welding gas also had no significant effect on the microstructure. A typical coarse-grained weld structure was also observed in the weld metal, which is

the fusion zone of the S355JR and S700MC steel welds made using two different metals.

Grain coarsening from the base material towards the HAZ is a result of the welding heat input. Similarly, in the weld metal, coarse dendritic arms forming from the base material towards the centre of the weld metal also occur due to high heat input. In S355JR steel, a more ductile and soft structure has also formed due to slow cooling (Ayyıldız, 2022). In S700MC steel, despite the same cooling rates, it is considered that the original microstructure exhibits a martensitic structure. Consequently, following the welding process, no significant microstructural change was observed due to heat input, indicating that the martensitic and brittle structure was relatively preserved.

Figure 8

XRD Analysis Result

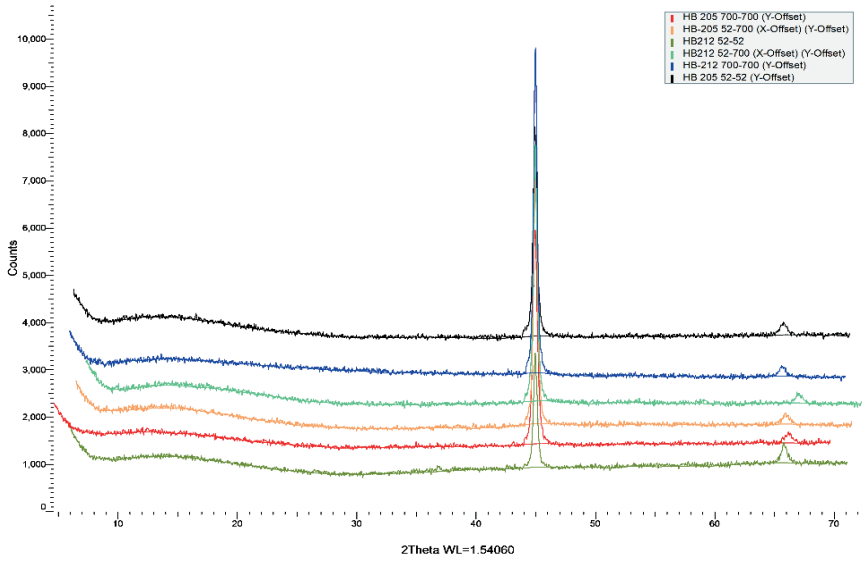

The results obtained from XRD analysis conducted to determine phase and phase transformations in the molten weld pool during the welding process of S355JR and S700MC steel materials using the MAG welding method, particularly under the influence of welding gas differences, were examined. The analysis revealed that the most intense fundamental peak in all materials was the iron (Fe) phase. Another intense but smaller peak can be seen to represent a small amount of iron phase. In materials of this type, the presence of austenitic alloying elements such as nickel and chromium in the weld metal indicates the presence of the iron phase (Górka & Stano, 2018). It is generally stated that in welded joints, the X-ray diffraction total intensity of iron and iron phases in terms of lattice plane can be limited to a range of 3-6% residual austenite content in the structure.

The combined XRD analysis results obtained in welded materials, depending on the HB 212 and HB 205 mixture gas difference, are given in **Figure 8**. Upon examination of the combined XRD analysis results, it can be stated that the microstructure of the base materials and welded joints consists of a ferrite phase. Another factor contributing to this situation is the use of the copper wavelength (1.544 Å) due to the XRD analysis device infrastructure used in the study. This is because the expected martensite structure has a smaller lattice parameter than a ferrite, and thus the martensite peaks cannot be displayed under the copper wavelength (Ekinci & Balalan, 2019).

When examining the microhardness results given in **Table 6**, considering that the hardness value is thought to be a maximum of 380 HV in the literature (Gür, 2022), it was determined that the obtained hardness values were below this value and consistent with the literature. The hardness values obtained in the base material after welded fabrication of S355JR materials were measured as 165-166 HV and 170-171 HV for HB 205 and HB 212 gas differences, respectively. Similarly, when the hardness values obtained in the S700MC base material were examined, they were measured as 305-310 HV and 304-301 HV for HB 205 and HB 212 gas differences, respectively. It can be stated that the hardness value of S700MC steel is higher than that of S355JR steel due to both the fine grain structure of the material and, in particular, the superior mechanical properties of this material and its high weldability (Çetin, 2019).

Looking at the microhardness measurement results according to the Vickers scale, an increase in hardness values is observed in S355JR steel due to high heat input. Conversely, in the more resistant S700 steel, a decrease in hardness is observed due to boron carbide precipitation at the austenite grain boundaries caused by its rolled structure (Eski, 2001).

When S355JR steel is welded with HB 212 mixed gas, the HAZ and weld metal are harder than when using HB 205 mixed gas. Based on this, it has been observed that HB 205 mixed gas gives better results when welding S355JR steel, as a 4 mm thick sheet metal is used. When looking at the weld of S700MC steel, in contrast to S355JR, higher hardness values were obtained when welding with HB 205 gas in the HAZ and weld metal. The increase in CO_2 content increased the heat input, causing a decrease in hardness due to the material's high hardness despite its low thickness. In this case, it was seen that the HB 205 mixture gas was more suitable for welding S700MC steels with each other and with S355JR steels.

Table 6

Microhardness Results of Welded Steel Samples

Sample Name	Base Metal	HAZ	Weld Metal	HAZ	Base Metal
S1	165	175	185	177	166
S4	170	208	239	201	171
S2	305	303	219	290	310
S5	304	298	198	261	301
S3	174	204	202	250	311
S6	177	222	209	223	312

Tensile tests were performed on three tensile bars from each sample, and the average values were taken to examine the yield and tensile strengths and the percentage elongation values. In addition to the test results obtained in the tensile test, the region where the tensile bar broke is also very important for interpreting the results. For the tensile specimens to be considered suitable, the fracture region must originate from the material itself, not the welded region (Özkan, 2019). When examining the samples obtained from the welds of S355JR steel with each other and with S700MC steel, a ductile fracture occurred appropriately on the S355JR material side. In the welds of S700MC steel with each other using both mixed gases, a fracture occurred inappropriately from the welded region. According to the data from the experimental studies, boron carbide precipitation causes a brittle structure at the grain boundaries, and the probability of intergranular fracture is high in this region where precipitation occurs (Eski, 2001). This has revealed the disadvantages of welding high-strength S700MC steel without preheating.

Figure 9

Tensile Test Results

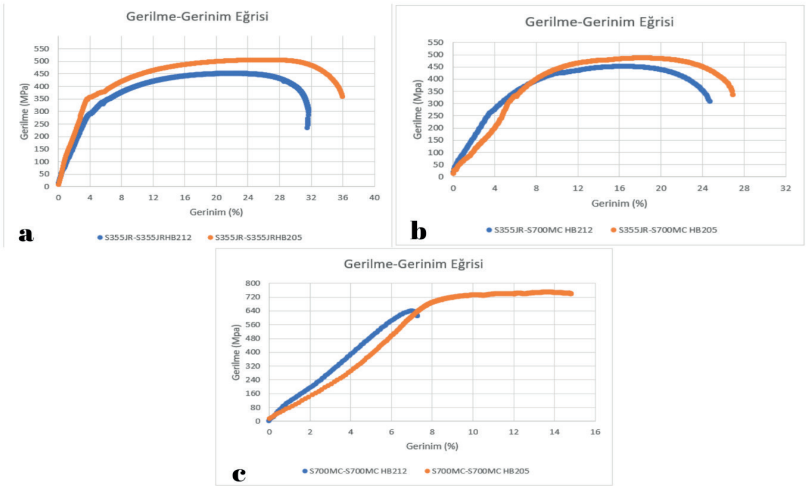

When examining the tensile test results of samples obtained from the source of S355JR structural steel under HB 205 mixed gas, the average yield strength was found to be 355 MPa, the tensile strength was 500 MPa, and the elongation (percentage elongation) was 36%. When examining the tensile test results of S355JR structural steel samples obtained from the same source under HB 212 mixed gas, the average yield strength was found to be 300 MPa, the tensile strength was 450 MPa, and the elongation (percentage elongation) was 31.5% **(Figure 9a)**. The S355JR steel exhibited performance above the percentage elongation values given in the material certificate. The yield stress, tensile stress, and strain values of the tensile bars welded with HB212 mixed gas were also low when compared to the samples welded with HB205 mixed gas, and consequently, a more brittle structure was observed. The high CO2 content in the HB212 mixture gas increased the hardness of the thin sheet metal structure, resulting in a more brittle material. The average yield strength of samples obtained from S355JR and S700MC structural steel welded with HB205 mixture gas was found to be 350 MPa, tensile strength 490 MPa, and elongation 27%. When looking at the values obtained from rods welded with HB212 mixed gas, they are relatively lower; the yield strength is 270 MPa, the tensile strength is 450 MPa, and the elongation is 24.7% **(Figure 9b)**.

It was observed that lower values were obtained when S700MC structural steel was welded with HB212 mixed gas, as was the case with other samples. The yield and tensile stresses and elongation values of the tensile bars welded with HB205 were 700 MPa, 740 MPa, and 15%, respectively, while those of the samples welded with HB212 were 610 MPa, 640 MPa, and 7.3% **(Figure 9c)**. Considering the requirements that the weld of the HB212 welded specimens must have a yield strength of 700 MPa, a tensile strength of 750-949 MPa, and a minimum elongation of 12%, as specified in the TS EN 10149-2 standard for S700MC steels, it was found that the weld was not suitable (Ulaştı, 2018). Although the test results of the specimens welded with HB205 fell within these values, their welds were found to be unsuitable due to fracture zones.

Conclusion

- It was observed that the chemical composition ratio of the gas used did not affect the grain size.
- It was observed that grain sizes increased in the HAZ and welded regions, and the equiaxed grain structure transformed into dendritic branches.
- Relatively lower hardness values were obtained in sample S1 compared to sample S4. Lower hardness values were obtained in sample S5 compared to sample S2.
- The hardness values of samples S3 and S6 are almost identical.
- It was observed that the hardness values of both metals in the HAZ and weld metal did not exceed the maximum hardness values required.
- Upon examining the XRD analysis results, it was determined that the most

intense fundamental peak in the phase analysis of all materials exhibited the iron (Fe) phase.

- In the XRD analysis, it can be stated that the microstructure of the main materials and welded joints consists of a ferrite phase.
- Although residual stresses are high after welding due to the high cooling rate caused by the thin material thickness, S355JR steel welded with HB205 mixed gas has good mechanical properties. The elongation and tensile strength meet the values specified in the material certificate. The high CO_2 content in the HB212 mixed gas resulted in a more brittle structure, reducing ductility.
- Although S700MC steel yielded better results in the HB205 mixed gas test, examination of the fracture zone revealed brittle fracture at the welded area. This demonstrates the necessity of heat treatment.
- Although the S355JR and S700MC combination has relatively better mechanical properties than the combination of S700MC steels, it has low mechanical properties. In the tensile test, the fracture occurred in the S355JR steel, which has a lower strength value.

References

Anık, S. (1991). *Kaynak tekniği el kitabı*. İstanbul: Gedik Eğitim Vakfı.

Ayyıldız, E. A. (2022). *Aşınmaya dirençli HBW450 Hardox çeliği ve S355J2 yapı çeliğinin robotik gazaltı kaynak yöntemi ile birleştirilmesi ve metalurjik özelliklerinin değerlendirilmesi* (Yüksek Lisans Tezi). Gazi Üniversitesi Fen Bilimleri Enstitüsü, Ankara.

Çetin, V. (2019). *Treyler şaselerinde kullanılan S700 MC çelik saclarının elektrik direnç nokta kaynağında mekanik özelliklerinin incelenmesi* (Yüksek Lisans Tezi). Sakarya Uygulamalı Bilimler Üniversitesi Lisansüstü Eğitim Enstitüsü, Sakarya.

ChnÇelik. (2023). Guide to citing Internet sources. Retrieved 24 December 2023, from https://www.chncelik.com.tr/teknik-dokumanlar/st-52-s355jr-celik-ozellikleri/

Demirci, D. (2010). *Muhtelif kaynak yöntemlerinde doğru akımlı kaynakta kutuplamanın kaynak dikiş formuna etkilerinin araştırılması* (Yüksek Lisans Tezi). Dokuz Eylül Üniversitesi Fen Bilimleri Enstitüsü, İzmir.

Dikeç, S. (2023). *Erdemir Test Sertifikası*. Kocaeli.

Durmuşoğlu, Ş. (2006). *Gazaltı kaynağında kaynak kalitesine tesir eden parametrelerin mekanik özelliklere etkisi* (Yüksek Lisans Tezi). Kocaeli Üniversitesi Fen Bilimleri Enstitüsü, Koaceli.

Ekinci, Ö., & Balalan, Z. (2019). Microhardness and microstructure of fiber laser welded S960 and S700 steels. *International Journal of Innovative Engineering Applications*, *3*, 15–21.

Eryürek, B., Sevük, A., & Odabaş, A. (2007). *Kaynak teknolojisi* (2nd ed.). İstanbul: Askaynak.

Eski, Ö. (2001). *Kaynak ısı girdisinin soğuk şekillendirilmiş S700MC çeliğinin mekanik özelliklerine etkisi* (Yüksek Lisans Tezi). İstanbul Teknik Üniversitesi Fen Bilimleri Enstitüsü, İstanbul.

Geçmen, İ. (2006). *Çeliklere gazaltı kaynağının uygulanması* (Yüksek Lisans Tezi). Marmara Üniversitesi Fen Bilimleri Enstitüsü, İstanbul.

Górka, J., & Stano, S. (2018). Microstructure and properties of hybrid laser arc welded joints (laser beam-MAG) in thermo-mechanical control processed S700MC steel. *Metals*, *8*(2). doi:10.3390/met8020132

Gür, Y. (2022). *MIG/MAG kaynağı ile birleştirilen S700 MC yüksek dayanımlı yapı çeliğinin mikroyapı ve mekanik özelliklerinin incelenmesi* (Yüksek Lisans Tezi). Gazi Üniversitesi Fen Bilimleri Enstitüsü, Ankara.

Karakoç, S. (2012). *Çeliklere gazaltı kaynağının uygulanması ve kaynağa etki eden parametreler* (Yüksek Lisans Tezi). Mustafa Kemal Üniversitesi Fen Bilimleri Enstitüsü, Hatay.

Kaya, Y., Çayırhan, G., Bökü, M., & Kahraman, N. (2020). Paslanmaz çelik ile düşük karbonlu çelik malzemelerin MIG kaynak yöntemiyle birleştirilebilirliğinin incelenmesi. *NWSA Academic Journals*, *15*(2), 89–99. doi:10.12739/nwsa.2020.15.2.1a0453

Koç, M. (2009). *Elektrik ark kaynağında kaynak gazı ve dumanının kaynak parametrelerine göre analizi* (Yüksek Lisans Tezi). Gazi Üniversitesi Fen Bilimleri Enstitüsü, Ankara.

Küpeli, G. (2008). *Alaşımsız çeliklere robotik gazaltı kaynağının uygulanması* (Yüksek Lisans Tezi). Marmara Üniversitesi Fen Bilimleri Enstitüsü, İstanbul.

Morrow Welding. (n.d.). Retrieved 2 September 2025, from https://www.morrowwelding.com/tr/news/classification-of-droplet-transition-in-gas-metal-arc-welding/

Özkan, E. (2019). *Kaynak sonrası S355J2N yapı çeliğinde oluşan gerilmeleri gidermek için uygulanan ısıl işlemin etkilerinin tahribatlı-tahribatsız muayene yöntemleriyle belirlenmesi* (Yüksek Lisans Tezi). Tekirdağ Namık Kemal Üniversitesi Fen Bilimleri Enstitüsü, Tekirdağ.

Şık, A. (2002). *Otomobil saclarının MIG/ MAG kaynağında gaz karışımlarının bağlantının mekanik özelliklerine etkisi* (Doktora Tezi). Gazi Üniversitesi Fen Bilimleri Enstitüsü, Ankara.

Şık, A. (2007). MIG/MAG kaynağı ile kaynatılan çelik yapılarda koruyucu gaz karışımlarının mekanik özelliklere etkilerinin araştırılması*. *Tujs Trakya Univ J*

Sci, *8*(1), 55–60. Retrieved from http://fbe.trakya.edu.tr/

Stephanie Oostman. (2021). GMAW Equipment and Setup. In *Introduction to Welding* (pp. 418–433). Washington: Washington Open Proftech.

Toprak Şenol, H. (2020). *Zeki sistemler ile ark kaynağı elektrotlarındaki kaynak parametrelerinin incelenmesi* (Yüksek Lisans Tezi). Muğla Sıtkı Koçman Üniversitesi Fen Bilimleri Enstitüsü, Muğla.

Tukahirwa, G., & Wandera, C. (2023). Influence of Process Parameters in Gas-Metal Arc Welding (GMAW) of Carbon Steels. In *Welding - Materials, Fabrication Processes, and Industry 5.0*. IntechOpen. doi:10.5772/intechopen.1002730

Ulaştı, E. (2018). *Termomekanik haddeleme ile S700MC kalite çeliklerin üretimi ve üretim parametrelerinin mekanik özelliklere etkisinin incelenmesi* (Yüksek Lisans Tezi). İstanbul Teknik Üniversitesi Fen Bilimleri Enstitüsü, İstanbul.

About The Authors

Fatma Nur ŞAHİN, MSc, graduated from Necmettin Erbakan University, Institute of Science, Department of Mechanical Engineering. She is a PhD student at Necmettin Erbakan University and worked as a quality and production manager in the forklift and trailer industry. She is worked in the supervision and management of welded manufacturing applications, which is her main area of expertise.
E-mail: fnursahin7@gmail.com **ORCID:** 0000-0001-6071-0168

Hakan GÖKMEŞE, PhD, is a Professor of Mechanical Engineering at Necmettin Erbakan University in Konya, Turkey. I have a master's degree in Metallurgical Education from Gazi University. His main areas of interest are casting technology, powder metallurgy, heat treatments, and composites and nanocomposites applications.
E-mail: hakan1440@gmail.com, **ORCID:** 0000-0003-0053-8444

Şaban BÜLBÜL, PhD, is an Associate Professor of Mechanical Engineering at Necmettin Erbakan University in Konya, Turkey. I have a master's degree in Metalurgical Education from Karabuk University. His main areas of interest are casting technology, powder metallurgy, polymer materials, and polymer applications.
E-mail: sabanbulbul42@hotmail.com , **ORCID:** 0000-0002-9268-1469

Similarity Index

The similarity index obtained from the plagiarism software for this book chapter is 10 %.

Investigation of Surface Shift Behavior Under Internal Pressure In Carbon Composite Tubes

Ahmet Faruk DOĞAN
Necmettin Erbakan University

Mehmet KAYRICI
Necmettin Erbakan University

Okan KILINÇ
Necmettin Erbakan University

To Cite This Chapter:
Doğan, A. F., Kayrıcı, M., & Kılınç, O. (2025). Investigation of surface shift behavior under internal pressure in carbon composite tubes. In H. Gokmese, S. Bulbul, & Y. Uzun (Eds.), *Innovative approaches in materials science and applications* (pp. 65–87). ISRES Book Series. ISRES Publishing.

Introduction

The biggest obstacle to technological development has been the failure of materials science to keep pace with technological developments. In other words, materials science is the foundation of technological developments. Advances and discoveries in materials science have always led to technological developments throughout history.

Given the importance of technology today, materials science is important at least as a technological innovation. For this reason, materials science has created sub-sectors that represent different industries within itself. Examples of these sub-sectors include metals, non-metals, chemicals, organic and inorganic materials, polymers, etc. However, composites are the most important of these sub-sectors in modern technology. Composites first emerged as a new field of materials science during World War II. Since then, composites have found widespread application in technology and are materials that are frequently used in leading industries such as aerospace, automotive, and textiles, and continue to evolve to meet the demands of these applications.

In general, composites are materials with the highest properties formed by combining two or more substances with different chemical and physical properties at the macro level. When designing parts made from composite materials, it is necessary to know where the part will be used and what the specific needs of the application are. During the planning stage, factors such as raw material properties, environmental conditions, and production methods must be evaluated along with cost. One of the greatest challenges in composite material design is that composite materials do not exhibit isotropic properties. Therefore, the person producing the structure must calculate how much load will be

applied to each part of the composite material and how much strength will be required, and position the fibers accordingly.

The matrix material prevents the propagation of cracks that may occur during plastic deformation and prevents damage to the composite material. Another purpose of the matrix material is to hold the fibrous material together under load and distribute the load evenly among the fibers. Thus, when forces causing plastic deformation of the fibrous material are applied, the propagation time of a crack that may occur will be extended. Various metal alloys can be used as the matrix, but resin matrices are more commonly used.

For a produced material to meet the definition of a composite material, it must possess certain properties. These include:

It must be produced using various methods. (Excluding composite structures such as bone, naturally occurring wood, etc.)

It must be formed by the combination of two or more materials with physically or chemically different properties.

It must achieve mechanical properties that cannot be obtained with a single component.

In this study, Atagün and colleagues addressed the detailed design of a filament winding machine, the design of composite pressure pipes, and the numerical analysis of their structural performance. The geometry of the pipe dome plays an important role in determining the performance of the structure. Therefore, the continuity theorem and mesh analysis methods were used to achieve the optimal dome geometry in the design. The optimal dome geometry was obtained using equations based on the radar radius, and the geometry of the resulting pipe was finalized. Various structural and modeling analyses were performed on the pipe geometry obtained during the study to determine the structural behavior and limits of the pipes. Since the burst pressure value, which is important for pipes, is related to the degree of detail of the dome geometry, there should be no structural deformation of the pipe from the side of the dome (rib). Any damage to the tip of the nozzle could cause the tube to rocket away under excessive internal pressure. Therefore, in designs, it is expected that the cylindrical region will bend outward beyond the limit load of the composite pressure tubes (Atagün, 2017).

Composite materials were examined within the scope of this project. When manufacturing a material using composites, there are many variables, such as resin and fiber, each with its own unique properties. However, the final product depends not only on the properties of these two variables but also on how the composite is manufactured, which greatly affects the final properties of the material. In this study, a fiber winding technique called

filament winding was used as a method for making composites. This method is used in many fields, from aviation to the military, as it enables the production of strong and lightweight parts. In this thesis study, research was conducted in the field of pressure vessel applications, one of the areas where composite materials obtained by fiber adsorption are used. Models of high-pressure vessels with composite structures produced using fiber production technology under various loads were examined (Pehlivan, 2017).

This study examines pressure vessels, which are used in many fields today and exhibit different performance under changes in temperature and pressure. Pressure vessels differ depending on the type of material they are made of, particularly due to their physical properties. While analyzing the behavior of structures whose material properties are temperature-dependent under various loads, the experimental results were validated by applying hydrostatic pressure tests to pressure vessels under internal pressure. Since pressure vessels may pose potential hazards that could affect human health and safety, any issues that may arise before use must be identified and addressed. This requires a comprehensive and detailed analysis of the pressure vessel design, accurately defining and considering all loads that could affect the system in calculations. Therefore, the solution of the theoretical approach for a cylindrical pressure vessel subjected to an axially symmetric load was compared with the displacements and pressures obtained from the Von-Mises stress analysis in SolidWorks software. The "COSMOXpress Analysis Wizard" computer program was used to perform the analysis using the finite element method (Mestan, 2010).

In another study, a pressure vessel design was created using steel-lined and glass fiber-reinforced epoxy resin material wrapped in circumferential and tangential composite material. Compressed natural gas storage tanks were used as a reference when designing these pressure vessels. Axial and circumferential deformations occurring on the vessel wall at different pressure values were investigated. Additionally, the results from the prototype were compared with real-world results and analysis results from a virtual environment (J., 2009).

In another academic study, a tank to be used in a satellite response system was designed and analyzed in a virtual environment. While designing this tank, it was desired to be lighter than metal tanks of the same volume. The design model consists of composite layers wrapped in aluminum foil. Before using thick-walled cylinders, the process of relieving residual stress in the wall is called autoclaving. This eliminates some of the stress under high pressure. As a result, the pressure-bearing capacity of pressure vessels increases. Autoclaving can be performed mechanically or hydraulically. Hydraulic autofrettage is more costly than mechanical autofrettage. Numerical values were determined by conducting strain and stress analyses of the parts forming the composite-wrapped pressure vessel, identifying the optimal angle for the wrap, autofrettage,

vibration, and model fiber analyses, and fatigue analyses of potential damage to the aluminum liner. The Ta-sai-Wu, Hashin, and Tsai-Hill criteria were used to determine these damages (Çetin, 2014).

Another study aimed to determine the burst pressure of cylinders exposed to environmental stresses during operation. In this study, HY 225 hardener was mixed with CY 225 epoxy and wound at an orientation angle of 55°. Repeated and single impacts were applied to hollow composite cylinders filled with water at different temperatures. In addition to the impact test, a static pressure test was also conducted. As a result, it was observed that the explosion pressure decreased as the impact energy and temperature increased. The number of repetitions did not affect this result. Finite element analyses were also conducted on samples that were not subjected to impact (İlki et al., 2008).

In another study, stress analyses under pressure were evaluated for two different steels in thin-walled pressure vessels. Designs were created using finite element software. Three-dimensional models were examined in two different ways. The explosion pressures were determined using maximum stress criteria on the damaged areas of the vessel. The damage results were evaluated using Von-Mises criteria. The importance of design effects in thin-walled pressure vessels was observed in the finite element analysis. It was determined that the explosion pressure was higher in the analysis than in the analytical results (Eruslu, 2008).

Another study aimed to investigate the fatigue behavior of filament-wrapped pipes under pressure. The wrapped pipes were obtained from four layers using a ±75° helical wrapping method with glass fiber and epoxy. The tests were conducted at a frequency of 0.42 Hz, a stress ratio of R:0.05, and in accordance with the ASTM D-2992 standard. Leakage and fracture tests were performed, and strength-time graphs were created based on the results of damage progression (Gemi et al., 2009).

In another study, the strength of composite pressure vessels for different layer arrangements was examined in real and virtual environments. As a result, it was determined that the first layer was the most significant factor in the damage to the pressure vessel. Graphite fiber and epoxy pressure vessels were used in this study. When examining the results, it was observed that the first layer burst pressure in analytical analyses was significantly higher than in real-world conditions. In real-world experiments, the value was lower. As a result, it was determined that the first-layer damage theory is an important theory for design (Khanna & W. P. Kuhn, 1997).

In another study, the stresses and deformations occurring in the wall of a composite-wrapped pressure tank with a metal liner under internal pressure were calculated for different layer arrangements. This study also used different composite materials. In addition, analytical studies were compared with real studies. The analyses utilized

Tsai-Wu damage criteria. According to the analyses, reducing the helical winding angle positively affects the burst pressure. The burst pressure values in the real-world experiments and analytical studies are similar. In the analytical studies, work was conducted on the cylindrical part of the pressurized container. In the real-world studies, two 6-liter prototypes made of Kevlar 49 fiber, epoxy, and carbon fiber, epoxy-coated metal were used (LD Landau et al., 1975).

In his academic work, the explosion pressures of composites produced with glass fiber and epoxy resin in anti-symmetrical and symmetrical layers with thin walls at different angles were examined, and as a result, the most suitable angle was evaluated. In other words, the effects of filament winding angles on composite pipes were evaluated. S.G. Lekhnitskii's theory was used as a numerical solution method to determine the damage condition in the container. The effects of different angles under the same temperature were calculated using this theory. The Tsai-Wu damage criterion was used for damage control. The results of this study showed that the optimal winding angle for composite pipes produced using the helical winding method was approximately 55°, while for pipes produced using the single-angle winding method, it was approximately 90° (Onder et al., 2009).

In another study, a stress analysis method was developed for thick- and thin-walled multilayer composite cylinders under hydrothermal stresses. The layers were designed to be anti-symmetric and symmetric at different angles. During the analysis, the plane stress condition and the boundary condition of open or closed pipe ends were evaluated. Parabolic and uniform temperature distributions were preferred for heat loads. All integration values were obtained from normal directional deformations and radial stresses. In addition to hydrothermal properties, other mechanical properties were also found on a glass fiber epoxy composite. It was observed that the finite element solutions obtained from the analysis were consistent with the analytical results (Sayman et al., 2011).

In his study, he examined the increase in strength by creating pressure within the material or by selecting materials to increase strength. The main objective is to evaluate the increase in strength by creating pressure cells within the designed product. In the study, pressurized air was placed inside cylindrical aluminum tubes with thin walls, and different strength and stress tests were performed. In these studies, a finite element analysis program was used for analytical calculations. The results obtained were compared with each other. It was determined that the results were consistent. Subsequently, studies and analyses were conducted using the finite element method on real models to prove their applicability in real life (Yıldırım, 2012).

Materials And Methods

Properties of Carbon Fiber

The density of carbon fibers varies depending on the processing temperature and raw material used in production. The densities of raw materials used in production range from 1.6 g/cm^3 to 2.2 g/cm^3. After fiber production, there is a slight increase in density depending on the raw material. The increase in the produced fibers varies depending on the graphitization temperature.

The technical properties of the carbon fiber used in this study are given in the table below;

Table 1

Technical specifications of 24 K-type carbon fiber rope

Features	Unit	Value
Fiber Type	Carbon	HT
Number of Filaments		24000
Linear Density	Dtex	1600
Sizing Ratio	%	1,5
Elongation at Break	%	1,5
Tensile Strength	MPa	3950
Modulus of elasticity	GPa	238
Density	g/cm^3	1,77
Diameter	micron	7
Electrical Conductivity	Ohm*cm	1,6*10^{-3}
Carbon Ratio	%	93
Coil Weight	kg	4

Figure 2

Carbon Fiber Rope 24K

Hexion brand LR160 epoxy resin and LH160 hardener are used together in a 4:1 ratio as the matrix material. Detailed information about the matrix material is available in the tables below.

Table 2

Resin LH160 technical specifications

Density (g/cm^3)	1,13-1,17
Viscosity (mPas)	700-900
Epoxy Equivalent (gr/equivalent)	166-182
Epoxy Value (equivalent/100gr)	0,55-0,60
Refractor İndex	1,5480-1,5530
Flexural Strength (MPa)	110-140
Tensile Strength (MPa)	3.2-3.5
Compression strength (MPa)	80-100
Poisson Ratio	0,36

Table 3

Hardener lh160 technical specifications

Density (g/cm^3)	0,96-1,00
Viscosity (mPas)	10-50
Amine Value	550-650
Refractor İndex	1,5200-1,5210

Carbon Nanotubes (CNTs)

Carbon nanotube polymer composites are the most important carbon nanotube composites. Materials that provide electrical conductivity can be produced with carbon nanotube polymer composites. When 5% carbon nanotubes are added to the produced material, the electrical conductivity of the material is between 0.01 and 0.1 S (YAĞLIKÇI, 2012).

In this study, multi-walled 10-20 nm 95% purity H carbon nanotubes were used. The technical specifications of the nanotubes used are listed in Table 4.

Table 4

Technical properties of carbon nanotubes

Purity%	>%95(carbon nanotube) >%97(carbon content)
Outer diameter	10-20 nm
İnner diameter	5-10nm
Length	10-30 µm
Surface area	>200m^2/g
Color	black
Ash	By mass<%1.5
Electrical conductivity	>100S/cm
Gravity(Tap)	0.22g/cm^3
Gravity(True)	~2,1g/cm^3

Manufacture of Pressure Vessels

In this study, composite tubes were produced at different nanotube reinforcement ratios using carbon fiber, epoxy, and carbon nanotube reinforcement with the filament winding technique and the wet winding method at ±55°. The carbon filament material used to form the composite tube has a diameter of 17 µm, while the matrix materials used are LR160 Hexion resin, Hardener MGS LH160, and Multi-walled Carbon Nanotubes 10-20 nm 95%.

Figure 3

Images of nanotube, resin, and hardener packaging are used

Figure 4

Image of the pressurized container (liner) connected to the machine before winding

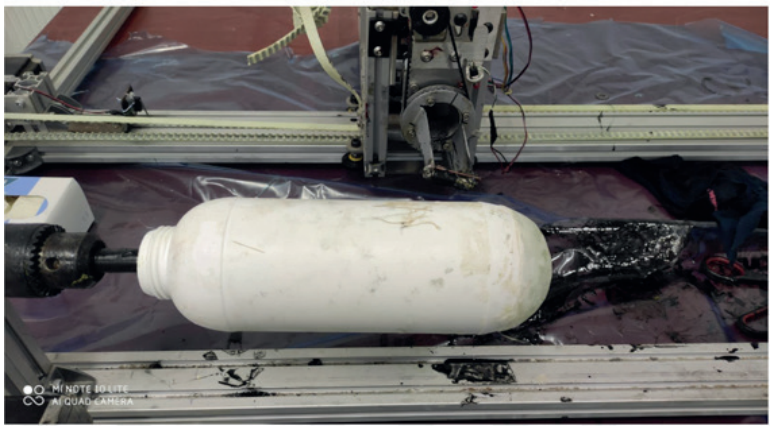

In this method and technique, carbon fibers passed through a resin pool were wound at an angle of ±55° onto plastic liners 30 cm long and 72 mm in diameter. Winding was continued until the desired outer diameter of 94.7 mm was achieved. Using these windings, three different samples with varying carbon nanotube reinforcement ratios were produced. The matrix ratios of these samples are provided in Table 6. The produced samples were subjected to surface finishing using a universal lathe to achieve an outer diameter of 94 mm.

Figure 5

Surface finishing of the produced sample

After the surface finishing process, the test apparatus was prepared for the samples to withstand internal pressure tests. To attach the samples to the test apparatus, threading was performed using a universal lathe. Connection equipment was produced using a universal lathe to connect the samples to the internal pressure test apparatus, and threading was applied to the base of the threads to ensure sealing with the resin mixtures used in the production of each sample. After securing, the curing time was waited for, and the test fixtures were set up by applying leak-proof Teflon tape to the test fixture.

Experimental Setup

The equipment used for the experimental setup is as follows:

Hydraulic Pump: An Anca ACP-01 manual oil pump was used to generate internal pressure for the purpose of examining surface shape changes under internal pressure. The technical specifications of the oil pump are listed in Table 5.

Table 5

Manual oil pump technical specifications

Model	Pump Type	Body	Available oil capacity	Tank oil capacity	High pressure flow rate(cm^3)	High-pressure piston diameter	working size	low-pressure flow rate	low-pressure piston diameter	maximum arm force	connection type	manometer	working pressure
ACP-01	Single-acting double speed	Al	0,5	0,7	0,8	7	21	10,3	25	29	3/8”-NPT	Ø63,1000 Bar	700 Bar

Datalogger: A D4 Micro-Measurements brand 4-channel digital data logger was used in the study. Data was recorded on a computer at a sampling rate of 8 Hz via RJ-45 connectors and at intervals of 0.125 seconds via a USB interface.

Strain gauges; In this study, the m-Bond 200 strain gauge mounting adhesive kit was used. The m-Bond 200 kit consists of a cyanoacrylate strain gauge adhesive that cures instantly at room temperature and a catalyst. The general-purpose adhesive properties commonly used in hot environmental conditions are listed in Table 6.

Table 6

General-purpose adhesive technical specifications

Maximum elongation (Strain in % at 75°F)	5
Lower temperature limit (FahrenheitH)	-25
Minimum curing temperature (FahrenheitH)	70
Container life	3 month
Shelf life	1 year
Upper temperature limit (FahrenheitH)	150

Badge: The CEA-06-062UR-120/P2 code badge product was used as a strain gauge in the study.

The P2 model is designed to be added to CEA series strain gauges with pre-installed main wires. No soldering is required during installation of the P2 model. The cables are color-coded, straight, and three-conductor. They are also manufactured with a thickness of 30 gauge (0.255 mm), vinyl-insulated multi-strand, and tin-plated copper solder. Each conductor of the cables has a nominal resistance of 0.1 ohm/ft (0.35 ohm/m). The temperature range for the connectors is –60° to +180°F (–50° to +80°C).

Figure 6

CEA-06-062UR-120/P2 coded badge scheme

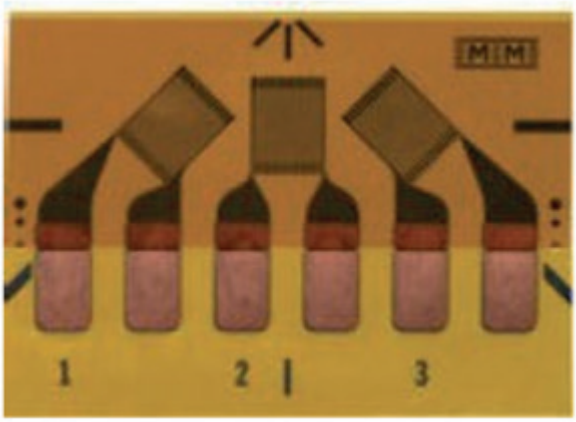

The experimental setup consists of a thin-walled cylindrical pressure vessel with a length of 38 cm, a wall thickness of 0,32 cm, and a diameter of 11.5 cm. In addition, there is an auxiliary system to increase the pressure of the thin-walled pressure vessel. The auxiliary system uses a hydraulic hand pump to increase the pressure of the vessel.

Strain gauges are used to measure the strain values that will occur on the vessel wall due to internal pressure. These strain gauges are attached to the outer surface of the vessel

with special adhesives. The stresses that will occur in the axial and circumferential directions are measured with the 1st and 3rd strain gauges, while the shear stress that may occur on the cylinder wall is calculated with the values read from the 1.2. and 3rd strain gauges.

The resistance values provided by the strain gauges will also be read using an auxiliary device. Additionally, a manometer integrated into a hydraulic hand pump is used to measure the pressure inside the vessel and to apply regular pressure increases.

The experiment aimed to determine and verify the axial and circumferential strain values of thin-walled pressure vessels under internal pressure using strain gauges. The oil-filled samples were connected to a manual hydraulic oil pump using a leak-proof band. Three strain gauges were attached to each sample. During the experiment, resistance data were measured at 0.125 ms intervals and recorded in real-time on a computer.

Research Findings And Discussıon

The aim of the tests conducted on composite cylindrical pressure vessels was to develop pressure vessel types. For this purpose, surface shape change tests were performed under internal pressure. The variables in the study were carbon nanotubes in the composite resin. The parameters covered in the study are shown in Table 7.

Table 7

Parameter charts

Parameter No	Carbon nanotube/Resin ratio
1	*0*
2	*%1*
3	*%3*

Parameter 1, Stress Test Results of Carbon Nanotube-Free Pressurized Containers Under Internal Pressure

Three pressure vessels made of carbon fiber wrapped with carbon-free resin were produced, and as a result of the application under internal pressure, the tubes burst at an average pressure of 45 bar. The experiments lasted an average of 24 minutes, and the data were recorded on a computer using a data collection device every 0.125 seconds. During the first 2-3 minutes of the experiments, a manual oil pump with its own mechanism evacuated the air to create internal pressure. The samples were monitored for stress sounds associated with internal pressure increases, and surface changes were observed during the experiments. Since the experimental setup included a manual manometer, pressure values were tracked manually, and the final values of the samples before rupture were recorded. Figure 6 and 7.

Figure 6

Experimental setup

Figure 7

Parameter 1 screenshot with instant results

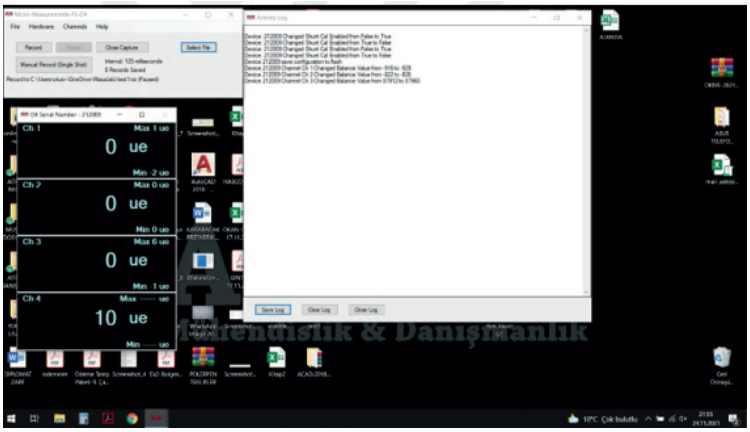

Figure 8 shows the stress-strain ratio graph for the carbon nanotube-free composite cylindrical pressure vessel. The maximum pressure resistance of the samples was found to be 45 bar, with an average axial elongation of 0.258286, an average radial elongation of 0.075429, and an average shear stress of 6.889905 corresponding to this resistance.

Figure 8

Parameter 1 stress/strain graph

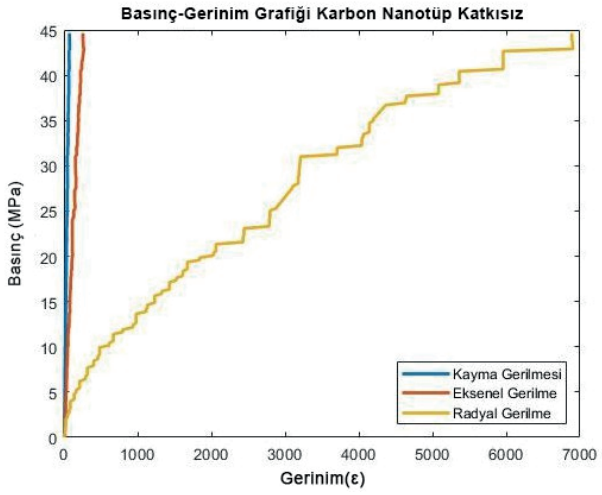

When the results of the Parameter 1 experiment are examined, it is seen that the numerical values of shear and axial elongation are approximately equal, and the numerical value of radial stress is high.

The samples were cut into two pieces with an automatic saw in order to examine the deformations in the cross sections. The cross-section images are shown in Figures 9 and 10.

Figure 9

Parameter 1 sample image

Figure 10

Parameter 1 cross-sectional image 1

Figure 11

Parameter 1 cross-sectional image 2

Figure 12

Parameter 1 section microscope image 1

Figure 13

Parameter 1 section microscope image 2

Figure 14

Parameter 1 section microscope image 3

Figure 15

Parameter 1 section microscope image 4

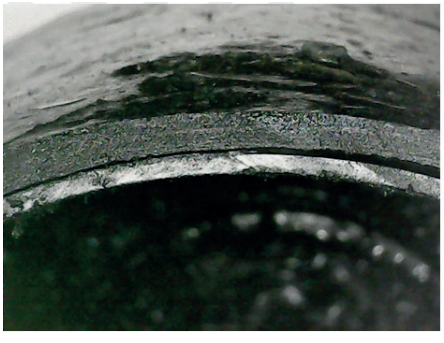

Parameter 2, Carbon Nanotube Ratio 1% Internal Pressure Surface Shape Change Test Results

In the pressure test on the 2nd sample, the tubes burst at an average pressure of 95 bar as a result of the stable application of load. The test duration averaged 38 minutes, and data were recorded on a computer using a data collection device every 0.125 seconds. During the first 2-3 minutes of the tests, a manual oil pump with its own mechanism evacuated the air to create internal pressure. Stress sounds associated with the increase in internal pressure in the tubes were monitored, and surface changes were observed during the test. Since the test setup included a manual manometer, pressure values were tracked manually, and the final values of the tubes before bursting were recorded.

Figure 16

Parameter 2 screenshot with instant results

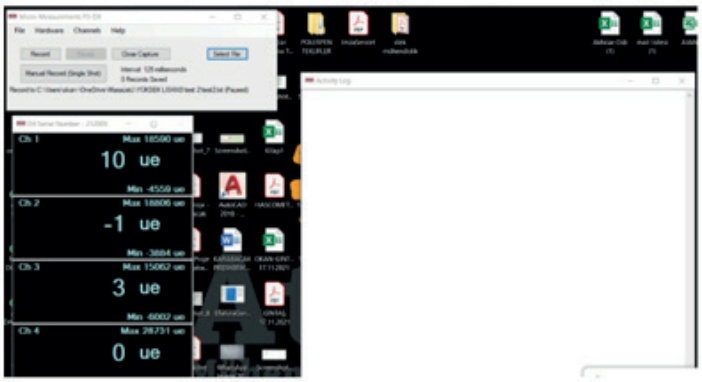

Figure 17 shows the stress-strain ratio graph for a composite cylindrical pressure vessel with a carbon nanotube ratio of 1%. The maximum pressure resistance of the sample was found to be 95 bar, with an average axial elongation of 7.315875, an average shear elongation of 5.725125, and an average radial stress of 3.299625 corresponding to this resistance.

Figure 17

Parameter 2 stress/strain graph

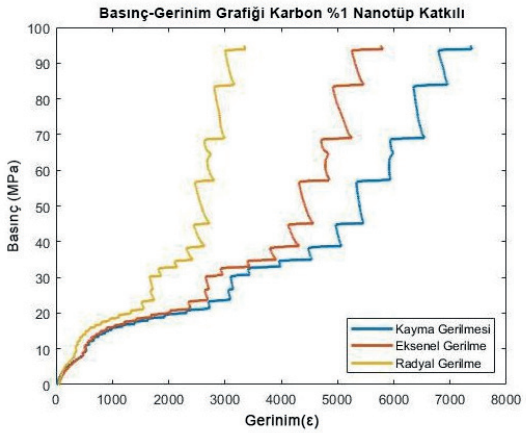

Figure 18

Parameter 2 sample image after experiment 1

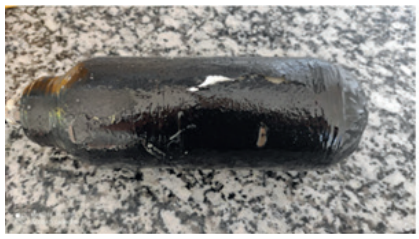

Figure 19

Parameter 2 sample image after experiment 2

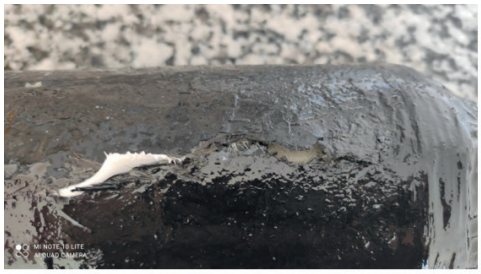

Figure 20

Parameter 2 cross-sectional image 1

Figure 21

Parameter 2 cross-sectional image 2

When the results of the Parameter 2 experiment are examined, it shows that the axial and shear strain values are approximately low, and the radial stress is low.

Figure 22

Parameter 2 section microscope image 1

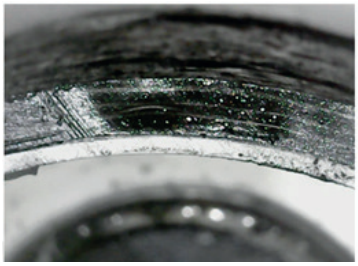

Figure 23

Parameter 2 section microscope image 2

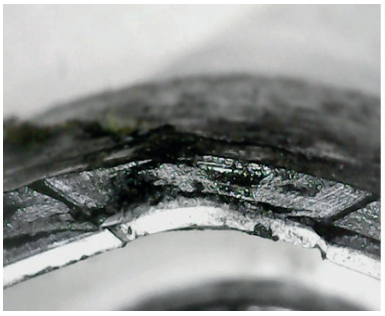

Figure 24

Parameter 2 section microscope image 3

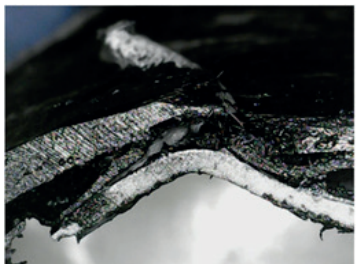

Figure 25

Parameter 2 section microscope image 4

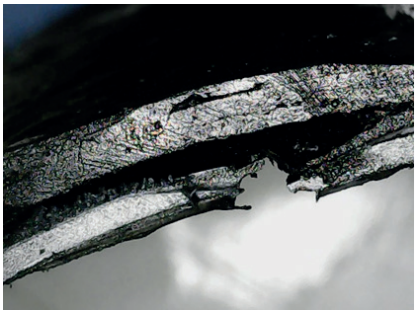

Parameter 3, Carbon Nanotube Ratio 3% Internal Pressure Surface Shape Change Test Results

Parameter 3 pressure test reached a value of 140 bar as a result of stable load application and exploded. The test lasted 42 minutes, and data were recorded on a computer using a data collection device every 0.125 seconds. During the first 2-3 minutes of the test, a manual oil pump with its own mechanism discharged the air to create internal pressure. Stress sounds associated with the increase in internal pressure were monitored, and surface changes were observed during the test. Since the test setup included a manual manometer, pressure values were tracked manually, and the final values of the samples before the explosion were recorded.

Figure 26

Parameter 3 screenshot with instant results

Figure 27 shows the stress-strain curve for a cylindrical pressure vessel made of a composite material containing 3% carbon nanotubes. The average maximum pressure resistance of tubes with parameter 3 is 140 bar, with an average axial elongation of 2.36775, an average shear elongation of 2.499, and an average radial stress of 0.947625 corresponding to this resistance.

Figure 27

Parameter 3 stress/strain graph

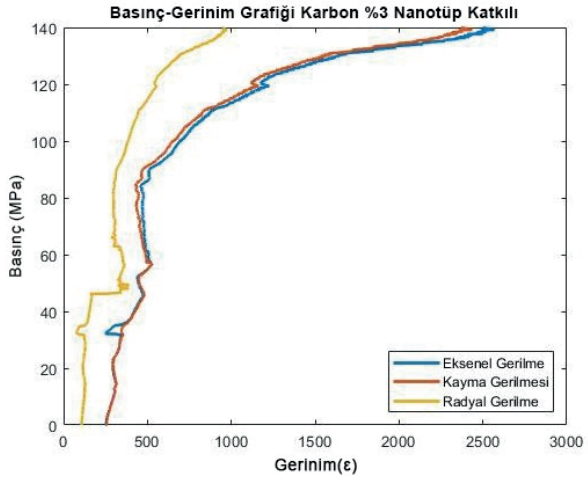

When the results of Parameter 3 experiments are examined, they show that the axial and shear strain values are approximately low, and the radial stress is low.

Figure 28

Parameter 3 sample image before experiment

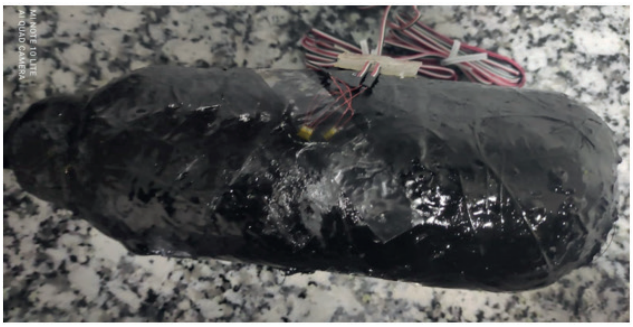

Figure 29

Parameter 3 cross-sectional image 1

Figure 30

Parameter 3 cross-sectional image 2

Figure 31

Parameter 3 section microscope image 1

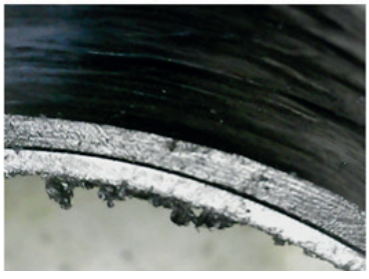

Figure 32

Parameter 3 section microscope image 2

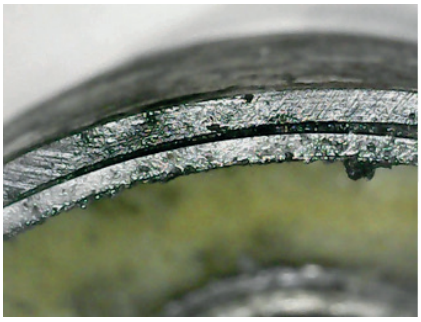

Figure 33

Parameter 3 section microscope image 3

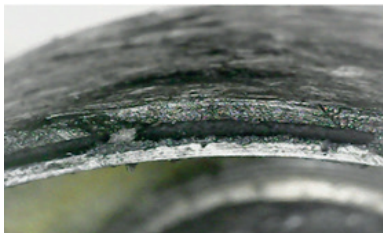

Figure 34

Parameter 3 section microscope image 4

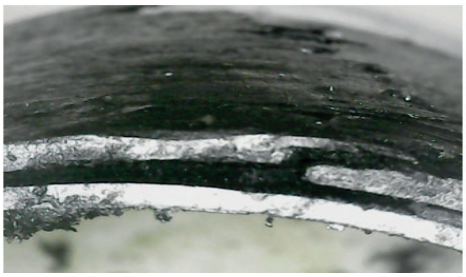

Results And Recommendations

- In internal pressure tests of carbon fiber-wrapped pressurized cylindrical composite tank samples, it was observed and confirmed by test results that carbon nanotube-reinforced composite materials and their ratios have a significant effect on surface stress displacement.
- When the carbon nanotube ratio, which is the experimental variable, increases, the strength of the composite samples increases compared to the carbon-nanotube-free composite tubes. This is because the carbon nanotubes are homogeneously mixed into the resin, giving the composite material new properties.
- The addition of carbon nanotubes has also increased the burst pressure of the tubes proportionally. There has been an average increase of 9.33 times between the empty liner and the composite tube with 3% additive. Here, carbon nanotubes have generally increased the strength of the material, making crack formation and fiber/matrix separation more difficult.
- In the study, damage was expected in the areas where teeth were cut into the material and connection and filling devices were mounted in the geometries of the tank's end sections, and the composite throat section was added later. However, since epoxy was used as a sealing and bonding agent, no damage was

encountered here. In the study, it was observed that the critical region of the tube suffered axial separation damage in the main body. The material did not show any geometric planar displacement while being damaged. It retained its cylindrical structure. This prevents negative effects on the environment during use and damage.

- As a result, it has been concluded that tubes or tanks made of composite materials using aluminum, plastic, or other liners can store much more gas (approximately 20 times more) in a much smaller volume, and that the use of much lighter materials creates an ideal combination of weight, volume, and pressure.

References

Onder, A., O Sayman, T Dogan, & N Tarakcioglu. (2009). Burst failure load of composite pressure vessels. *Composite Structures*, *89*(1).

İlki, A., Önder Peker, Emre Karamuk, Cem Demir, & Nahit Kumbasar. (2008). Düşük ve Orta Mukavemetli Dairesel ve Dikdörtgen Betonarme Kolonların FRP ile Güçlendirilmesi. *İnşaat Mühendisliği Malzemeleri Dergisi*, *20*(2).

Atagün, C. (2017). *Bir Filaman Sarım Makinenin Tasarım Ve Ürün Olarak Basınçlı Türlerin İncelenmesi*. Yüksek Lisans Tezi, İstanbul Teknik Üniversitesi Fen Bilimleri Enstitüsü.

Çetin, M. (2014). *Uzay Uygulamalarında Kullanılan Kompozit Sargılı Basınçlı Bir Tankın Yapısal Tasarımı ve Analizi*.

Eruslu, S. Ö. (2008). İnce Cidarlı Basınçlı Tüplerin Sonlu Elemanlar Yöntemiyle Analizi. *Pamukkale Üniversitesi Mühendislik Bilimleri Dergisi*, *14*(2), 169–174.

J., C. (2009). Large-Scale Pattern Growth of Graphene Films for Stretchable. *Nature 457*, 706–710.

Khanna, Y. P., & W. P. Kuhn. (1997). Measurement of crystalline index in nylons by DSC: Complexities and recommendations. *Journal of Polymer Science Part B: Polymer Physics*, *35*(14).

LD Landau, EM Lifshitz, & EM Lifshit͡s. (1975). *The Classical Theory of Fields* (Vol. 2).

Gemi, L., Necmettin Tarakçioğlu, Ahmet Akdemir, & Ömer Sinan Şahin. (2009). Progressive fatigue failure behavior of glass/epoxy (±75) 2 filament-wound pipes under pure internal pressure. *Materials & Design*, *30*(10).

Mestan, F. (2010). *Basınçlı Kapların Deneysel ve Teorik Olarak İncelenmesi*. Havacılık ve Uzay Teknolojileri Enstitüsü.

Sayman, O., ME Deniz, T Dogan, & E Yaylagan. (2011). Failure pressures of composite cylinders with a plastic liner. *Journal of Reinforced Plastics and Composites*, *30*(10).

Pehlivan, A. (2017). *Elyaf Sarma ile Üretilen Kompozit Yapıdaki Basınçlı Kapların Değişik Yüklemelerde Modellenmesi*. Yüksek lisans Tezi, İstanbul Teknik Üniversitesi Fen Bilimleri Enstitiüsü,İstanbul.

Yağlıkçı, S. (2012). *Karbon nanotüp üretiminde katalizörün gaz fazı derişim profiline etkisinin incelenmesi. Yüksek* Lisans Tezi, Ankara Üniversitesi Fen Bilimleri Enstitüsü.

Yıldırım, F. (2012). *İnce cidarlı basınçlı kapların yük altındaki mekanik davranışlarının deneysel ve sayısal analizi*. Yüksek Lisans Tezi, Karabük Üniversitesi Fen Bilimleri Enstitüsü.

About The Authors

Mehmet KAYRICI, PhD, is an Assistant Professor of Mechanical Engineering at Necmettin Erbakan University in Konya, Turkey. He holds a PhD in Mechanical Engineering from Necmettin Erbakan University. His main areas of interest are polymer materials, composite materials, and nanocomposites.
E-mail: mkayrici@erbakan.edu.tr, **ORCID:** 0000-0001-8553-1166.

Ahmet Faruk DOĞAN, Ms.C, is a general manager at Ali Kaan İnovasyon ısı makinaları ve sistemleri san.tic.ltd.şti. He holds a master's degree in Mechanical Engineering from NecmettİIn Erbakan University. His main areas of interest are polymer materials, composite materials, nanocomposites, and boiler systems.
E-mail: 22820713012@ogr.erbakan.edu.tr. **ORCID:** 0009-0007-8712-3431

Okan KILINÇ is a manager at Atimak Engineering Company, has a Master's Degree in Mechanical Engineering from Necmettin Erbakan University. My areas of interest are nanomaterials and polymers.
E-mail: okan@atimak.com.tr **ORCID:** 0009-0007-8320-172X

Similarity Index
The similarity index obtained from the plagiarism software for this book chapter is 4 %.

Advanced Exergy Analysis

Dilek Nur ÖZEN
Necmettin Erbakan University

To Cite This Chapter:
Özen, D. N. (2025). Advanced exergy analysis. In H. Gökmeşe, Ş. Bülbül, & Y. Uzun (Eds.), Current studies in basic sciences: *Innovative approaches in materials science and applications* (pp. 88–103). ISRES Book Series. ISRES Publishing.

Introduction

The persistent growth in global energy demand, largely driven by industrial expansion, population increase, and advances in technology, continues to exert tremendous pressure on current energy infrastructures. Simultaneously, the impacts of climate change and environmental degradation have intensified the urgency of adopting sustainable and efficient energy strategies. According to the International Energy Agency (IEA, 2022), the energy sector remains the dominant source of global greenhouse gas emissions, responsible for approximately three-quarters of the total. In this light, enhancing the performance of energy systems is therefore not only an economic objective but a strategic necessity aligned with international frameworks such as the Paris Agreement and the United Nations Sustainable Development Goals.

In the field of engineering sciences, numerous performance indicators and analytical techniques have been developed to evaluate and improve system efficiency. Among them, exergy analysis has emerged as one of the most comprehensive and insightful thermodynamic approaches. Unlike traditional energy balances, which are based solely on the first law of thermodynamics and treat all forms of energy equivalently, exergy analysis incorporates the second law. This allows for an assessment of energy quality and the inevitable irreversibilities that occur during energy conversion processes. As a result, exergy analysis provides a more meaningful evaluation of not only the quantity of energy consumed but also the effectiveness with which it is transformed into useful work.

The principal strength of conventional exergy analysis (CEA) lies in its ability to highlight the true thermodynamic inefficiencies of a system by quantifying irreversibilities. Over the past several decades, CEA has been extensively applied to diverse energy systems, including gas turbines, steam power plants, refrigeration cycles, and renewable energy technologies (Bejan, 2017; Ozen et al., 2020; Rosen & Dincer, 2001). These studies have consistently demonstrated that exergy analysis delivers deeper insights into system performance compared to analyses based solely on the first law. For example, in combined cycle power plants, while the reported energy efficiency may reach 55-

60%, exergy efficiency values often fall within the range of 35-45%, clearly exposing significant hidden irreversibilities that a first-law perspective fails to capture.

Nonetheless, despite its recognized benefits, CEA suffers from notable limitations. While it provides the total magnitude of exergy destruction within a system, it does not distinguish between avoidable and unavoidable portions of irreversibility. In practical terms, this means that CEA cannot differentiate losses that may be realistically reduced through improved designs or operational strategies from those that are inherently irreducible due to thermodynamic constraints. Furthermore, conventional analysis does not separate endogenous irreversibilities, which arise from within a specific component, from exogenous ones, which are caused by the interaction of that component with others. This lack of resolution diminishes the decision-making power of CEA, particularly in complex systems with high levels of integration.

To illustrate this issue, consider a gas turbine within a broader power generation system. Conventional exergy analysis may reveal that the turbine exhibits the largest share of exergy destruction. Yet such a result leaves key questions unanswered: How much of the destruction is unavoidable due to the fundamental physics of gas expansion, how much is avoidable through design modifications such as advanced blade geometry, cooling techniques, or optimized operation, and importantly, what share of the destruction originates internally within the turbine itself, and what share is imposed by other components such as upstream compressors or downstream heat exchangers? Because CEA cannot provide these distinctions, it falls short of guiding targeted engineering interventions.

To overcome these shortcomings, Advanced Exergy Analysis (AEA) was developed as a refinement of conventional methods. Its origins can be traced to the pioneering contributions of George Tsatsaronis in the late 1980s and early 1990s, who emphasized the need to classify different types of irreversibilities for improved decision-making in design and optimization (Tsatsaronis, 1993). The methodology was subsequently extended and formalized through the work of Morosuk and Tsatsaronis (2009), Vučković et al. (2012), and numerous others. Over time, AEA has matured into a robust framework widely recognized for its ability to deliver deeper insights into system inefficiencies and to support decision-making at both the component and system levels.

The essence of AEA lies in its two-dimensional classification of exergy destruction. It separates irreversibilities into avoidable versus unavoidable and endogenous versus exogenous categories. When combined, these classifications generate a fourfold partition: avoidable-endogenous, avoidable-exogenous, unavoidable-endogenous, and unavoidable-exogenous. This refined categorization not only quantifies the overall magnitude of losses but also identifies their origin and reducibility, thereby offering

engineers actionable insights into where system improvements can most effectively be pursued.

In this way, AEA transforms exergy analysis from a diagnostic tool into a decision-support framework. By revealing the nature and source of inefficiencies, it provides clear guidance for prioritizing engineering strategies. For instance, if analysis reveals that a compressor's losses are predominantly avoidable-exogenous, this indicates that upstream components are the true focus for improvement, as their inefficiencies propagate downstream. Conversely, if the majority of losses are avoidable-endogenous, direct efforts on the compressor's design or operation will be most effective.

Since its introduction, AEA has been applied to a broad array of energy systems. In industrial processes such as natural gas liquid (NGL) recovery, AEA has helped pinpoint compressors and heat exchangers as critical targets for improvement(Jovijari, Kosarineia, Mehrpooya, & Nabhani, 2022a). In power generation applications, including organic Rankine cycles (ORC) and combined heat and power (CHP) systems, it has clarified the distribution of irreversibilities and guided optimization of system integration(Azubuike, Njoku, Eke, & Ekechukwu, 2025; Yan et al., 2019). More recently, the method has also been adopted in unconventional sectors such as food processing, where Bühler et al. (2018) demonstrated its utility in identifying hidden inefficiencies in milk processing plants-opportunities that conventional analysis had overlooked.

Beyond thermodynamic insights, AEA has been extended into the economic and environmental domains. The development of advanced exergoeconomic analysis (AECA) and advanced exergoenvironmental analysis (AEEA) allows simultaneous consideration of cost-related and environmental implications of irreversibilities(Petrakopoulou, Tsatsaronis, Morosuk, & Paitazoglou, 2012; Qi et al., 2024). These integrated approaches are particularly valuable in the context of the global energy transition, where technical efficiency must align with economic feasibility and sustainability objectives.

AEA has also proven valuable in education. Introducing students to the distinctions between avoidable and unavoidable, and endogenous and exogenous irreversibilities, nurtures a deeper understanding of energy systems and promotes systems-oriented thinking. This prepares future engineers and scientists to confront the complex realities of modern energy infrastructures, where interactions among components often dictate overall performance more than individual component efficiencies.

In conclusion, Advanced Exergy Analysis represents a paradigm shift in the assessment of energy systems. By distinguishing between the nature and reducibility of irreversibilities, it generates actionable insights for the design, optimization, and operation of energy technologies. Its successful application across a wide range of industrial, renewable, and unconventional systems highlights its versatility, while its extensions to economic

and environmental dimensions demonstrate its broad relevance. The following sections of this work will provide a detailed account of the methodological framework of AEA, beginning with a closer examination of the limitations of conventional exergy analysis, and then elaborating on the theoretical foundations, decomposition strategies, and hybrid cycle approaches employed in advanced applications.

Limitations of Conventional Exergy Analysis

Conventional exergy analysis (CEA) has long been recognized as a significant step beyond traditional energy balances, as it incorporates the second law of thermodynamics and evaluates not only the quantity but also the quality of energy flows. It quantifies the irreversibilities within a system and indicates where thermodynamic performance is being compromised. Despite these advantages, however, CEA presents several important limitations that restrict its usefulness as a decision-support tool in engineering practice. These limitations become particularly critical when dealing with complex energy systems such as combined heat and power (CHP) units, gas turbine plants, or novel cycles integrating renewable and cryogenic sources.

Aggregated representation of irreversibilities

One of the primary shortcomings of CEA is that it provides only the total magnitude of exergy destruction in each system component. While this information highlights the most inefficient components, it does not clarify the nature of these inefficiencies. For instance, in a simple Brayton cycle, CEA may show that the combustion chamber exhibits the largest share of exergy destruction. Yet this result alone does not explain whether these losses are fundamentally unavoidable due to entropy generation inherent in combustion or whether they can be significantly reduced through better design or operational improvements. Thus, the aggregated representation of irreversibilities prevents engineers from identifying realistic improvement potentials (Kelly, Tsatsaronis, & Morosuk, 2009).

Lack of distinction between avoidable and unavoidable losses

CEA does not distinguish between avoidable irreversibilities, which can be reduced through engineering actions, and unavoidable irreversibilities, which are constrained by thermodynamics or the current state of technology. This lack of distinction often leads to misleading conclusions. For example, when analyzing a heat exchanger, conventional exergy analysis may report a certain level of exergy destruction. However, part of this destruction is unavoidable due to the finite temperature difference required for heat transfer, while another part could be avoided with better heat exchanger design or operating conditions. Without separating these two, CEA risks overstating or understating the true improvement potential of the component (Morosuk & Tsatsaronis, 2009).

Inability to differentiate endogenous and exogenous contributions

A further limitation lies in the inability of CEA to account for interactions between components. Exergy destruction in a given component is not always the result of its own inefficiencies; rather, it can also be influenced by upstream or downstream components. For instance, a turbine may appear highly irreversible under conventional analysis. Yet a portion of this irreversibility may be caused by non-ideal performance of the upstream compressor, which alters the inlet conditions to the turbine. Since CEA attributes all irreversibilities to the turbine itself, it fails to capture such exogenous effects, leading to inaccurate or incomplete diagnostics (Yousefizadeh Dibazar, Salehi, & Davarpanah, 2020).

Limited decision-making value in complex systems

Because of the above limitations, the practical decision-making value of CEA is restricted. In real-world engineering practice, decision-makers require precise answers to questions such as:

- Which losses should be prioritized for improvement?
- Which losses are technologically unavoidable and therefore not worth further investment?
- Are the inefficiencies caused by the component itself, or are they imposed by interactions with other parts of the system?

CEA cannot provide definitive answers to these questions. As a result, it may misdirect investment and design efforts. For example, in a combined cycle power plant, CEA may suggest focusing on the gas turbine due to its high exergy destruction. However, without distinguishing avoidable from unavoidable losses and endogenous from exogenous contributions, such an approach could lead to costly design modifications with limited actual benefit (Kelly et al., 2009).

Illustrative examples from literature

Numerous studies have highlighted these limitations. Petrakopoulou et al. (2012) demonstrated that in a combined cycle power plant, conventional exergy analysis identified the heat recovery steam generator (HRSG) as one of the dominant sources of inefficiency. However, when advanced exergy analysis was applied, it was revealed that a large fraction of the HRSG's losses were unavoidable, thereby shifting the focus of improvement efforts to other components such as the turbine and condenser. Similarly, Kelly et al. (2009) showed that in gas turbine systems, CEA often overstated the contribution of certain components (e.g., combustion chamber) to total exergy destruction, while AEA clarified that much of this destruction was unavoidable and endogenous, leaving only a smaller fraction as truly avoidable.

Another example is provided by Yousefizadeh Dibazar et al. (2020), who analyzed three different organic Rankine cycles (ORCs). Conventional analysis indicated the expander as the most critical component. However, advanced analysis showed that a significant part of the expander's irreversibilities originated from exogenous interactions with the evaporator, highlighting the need for system-level improvements rather than component-level redesign.

Summary of limitations

In summary, the main limitations of conventional exergy analysis can be outlined as follows:

1. It provides only aggregated values of irreversibilities without explaining their causes.
2. It does not separate avoidable from unavoidable losses, making it impossible to quantify true improvement potentials.
3. It cannot differentiate between endogenous inefficiencies and exogenous interactions, limiting its diagnostic accuracy.
4. It offers limited decision-making support in the design and optimization of complex energy systems.

For these reasons, while CEA remains a valuable preliminary tool, it is insufficient for guiding detailed design improvements or strategic decisions. This recognition paved the way for the development of Advanced Exergy Analysis (AEA), which directly addresses these shortcomings by introducing a refined framework capable of decomposing exergy destruction into more meaningful categories. The theoretical basis of this framework is presented in the following section.

Conceptual Framework of Advanced Exergy Analysis

Advanced Exergy Analysis (AEA) goes beyond conventional exergy analysis by not only measuring the magnitude of irreversibilities but also clarifying why and where they occur and to what extent they can be reduced. To achieve this, AEA employs a two-dimensional classification:

- Avoidable and Unavoidable
- Endogenous and Exogenous

The combination of these two dimensions results in a fourfold categorization that has become the conceptual backbone of modern exergy research.

Avoidable and unavoidable destruction

This dimension addresses the most practical question for engineers: *"How much of this loss can actually be reduced?"*

- Avoidable destruction refers to the portion of losses that can be reduced by technological improvements, better component design, or optimized operation strategies. For instance, pressure losses in a heat exchanger due to outdated design can be minimized with compact modern geometries.

- Unavoidable destruction represents irreversibilities that remain even under the best available technology and are fundamentally constrained by thermodynamics. An example is the minimum entropy generation that inevitably occurs in compression processes. This classification was systematically introduced by Tsatsaronis (1999), providing a foundation for later AEA studies.

Endogenous and exogenous destruction

The second dimension deals with the origin of losses:

- Endogenous destruction originates within the component itself, such as aerodynamic or frictional losses in turbine blades.
- Exogenous destruction, on the other hand, arises due to the influence of other system components. For example, a compressor receiving non-ideal inlet conditions from an upstream heat exchanger suffers exogenous penalties.

This classification highlights the importance of system integration and was further clarified by Vučković et al. (2012) in their analyses of industrial plants.

Fourfold classification

By combining both dimensions, AEA provides a comprehensive four-part framework:

1. Avoidable-Endogenous (AV-EN): Internal inefficiencies that can be reduced by redesign or improved operation.
2. Avoidable-Exogenous (AV-EX): Losses induced by other components but still reducible, often by better system integration.
3. Unavoidable-Endogenous (UN-EN): Intrinsic irreversibilities of a component that cannot be further reduced with current technology.
4. Unavoidable-Exogenous (UN-EX): External inefficiencies imposed by other subsystems, persisting even if the component itself operates ideally.

Studies such as Petrakopoulou et al. (2012) have shown the relevance of this categorization in real applications, illustrating its diagnostic and optimization potential.

Practical value of the conceptual framework

The importance of this framework lies in its guidance for engineering decisions. When the dominant share of losses falls into the avoidable-endogenous category, redesign of the component is a rational priority. If avoidable-exogenous losses dominate, then system-level integration and coordination strategies should be emphasized. Conversely, high

unavoidable fractions indicate that significant improvements would require technological breakthroughs rather than incremental modifications.

In this sense, AEA becomes more than an analytical tool it acts as a strategic compass for engineers and researchers, pointing not only to where inefficiencies occur but also to which losses can realistically be reduced and how system performance can be improved in practice (Alibaba et al., 2020).

Theoretical Foundations of Advanced Exergy Analysis

Theoretical foundations of advanced exergy analysis

The theoretical basis of Advanced Exergy Analysis (AEA) lies in the second law of thermodynamics and the concept of irreversibility. Conventional exergy balances provide information about the total exergy destruction in a component or system, but they do not explain whether these losses are reducible, to what extent they originate from the component itself, or how much is induced by interactions with other system elements. AEA addresses these shortcomings by decomposing total exergy destruction into two dimensions: avoidable vs. unavoidable and endogenous vs. exogenous. The combination of these two dimensions leads to four distinct categories: avoidable-endogenous (AV-EN), avoidable–exogenous (AV-EX), unavoidable–endogenous (UN-EN), and unavoidable-exogenous (UN-EX).

Over the years, several methodological approaches have been proposed in the literature to perform this decomposition. The most common ones are the engineering approach, the thermodynamic approach, and the hybrid cycle approach. Each differs in terms of accuracy, computational effort, and the type of information it can provide.

Engineering approach

The engineering approach represents the simplest and most approximate method. In this framework, the endogenous destruction of a component is estimated based on assumed values, such as typical isentropic efficiencies or design catalog data. For example, if a compressor is considered to have a nominal efficiency of 85%, the irreversibilities corresponding to this efficiency are assigned as endogenous. The exogenous destruction is then calculated as the difference between the real destruction and the assumed endogenous part (Morosuk & Tsatsaronis, 2009):

$$\dot{Ex}_{D,k}^{EX} = \dot{Ex}_{D,k} - \dot{Ex}_{D,k}^{EN} \quad (1)$$

This method does not simulate interactions explicitly and thus provides only rough approximations. While it requires minimal computational effort and is useful for preliminary assessments or educational purposes, it lacks accuracy and may be misleading

for highly integrated systems (Kelly et al., 2009; Morosuk & Tsatsaronis, 2009).

Thermodynamic approach

The thermodynamic approach provides a more rigorous distinction between endogenous and exogenous destruction. The procedure is as follows:

1. The real system is simulated to obtain the total exergy destruction for each component: $\dot{Ex}_{D,k}$
2. The component under study is kept at its real performance, while all other components are assumed to operate under ideal reversible conditions. The resulting destruction is the endogenous part: $\dot{Ex}^{EN}_{D,k}$
3. The exogenous destruction is obtained by subtraction:

$$\dot{Ex}^{EX}_{D,k} = \dot{Ex}_{D,k} - \dot{Ex}^{EN}_{D,k} \tag{2}$$

This approach improves the understanding of interactions among system components and provides useful information for improving an exergy conversion system. However, as highlighted by Kelly et al. (2009), this method only splits exergy destruction into endogenous and exogenous parts, and information about avoidable and unavoidable fractions must be obtained separately through additional analysis.

Hybrid cycle approach

The hybrid cycle approach builds upon the thermodynamic approach and is now considered the most comprehensive and reliable method. It retains the endogenous–exogenous decomposition but extends the framework by incorporating the avoidable/unavoidable distinction through simulations under unavoidable operating conditions (Liu, Liu, Cao, Luo, & Yang, 2020; Yousefizadeh Dibazar et al., 2020).

The stepwise procedure is outlined below for a component k:

Step 0 – Real cycle

The system is solved under actual operating conditions: $\dot{Ex}_{D,k}$

Step 1 – Endogenous destruction (EN)

Component k operates at its real performance, while all other components are ideal (reversible). The resulting destruction is the endogenous part: $\dot{Ex}^{EN}_{D,k}$

Step 2 – Exogenous destruction (EX)

The exogenous part $\dot{Ex}^{EX}_{D,k}$ is found using the following equation after the endogenous part is found.

$$\dot{Ex}_{D,k}^{EX} = \dot{Ex}_{D,k} - \dot{Ex}_{D,k}^{EN} \quad (3)$$

Step 3 – Unavoidable destruction (UN)

Unavoidable operating conditions are defined based on technological limits (e.g., maximum achievable efficiencies, minimum temperature differences (Petrakopoulou, Tsatsaronis, Morosuk, & Carassai, 2012; Tsatsaronis, 1999): $\dot{Ex}_{D,k}^{UN}$

Step 4 – Avoidable destruction (AV)

The avoidable part $\dot{Ex}_{D,k}^{AV}$ is found using the following equation after the unavoidable part is found.

$$\dot{Ex}_{D,k}^{AV} = \dot{Ex}_{D,k} - \dot{Ex}_{D,k}^{UN} \quad (4)$$

Step 5 – Partitioning of UN into UN-EN and UN-EX

Component k operates at its unavoidable performance, while all other components are ideal (reversible). The resulting destruction is the endogenous part $\dot{Ex}_{D,k}^{UN,EN}$ (Hançer Güleryüz & Özen, 2022; Morosuk & Tsatsaronis, 2009):

The exogenous part $\dot{Ex}_{D,k}^{UN,EX}$ is found using the following equation after the endogenous part is found.

$$\dot{Ex}_{D,k}^{UN,EX} = \dot{Ex}_{D,k}^{UN} - \dot{Ex}_{D,k}^{UN,EN} \quad (5)$$

Step 6 – Partitioning of AV into AV-EN and AV-EX (Morosuk & Tsatsaronis, 2009; Özen, Hançer Güleryüz, & Acılar, 2024)

$$\dot{Ex}_{D,k}^{AV,EN} = \dot{Ex}_{D,k}^{EN} - \dot{Ex}_{D,k}^{UN,EN} \quad (6)$$

$$\dot{Ex}_{D,k}^{AV,EX} = \dot{Ex}_{D,k}^{AV} - \dot{Ex}_{D,k}^{AV,EN} \text{ or } \dot{Ex}_{D,k}^{AV,EX} = \dot{Ex}_{D,k}^{AV} - \dot{Ex}_{D,k}^{AV,EN} \quad (7)$$

Finally, the complete decomposition is obtained:

$$\dot{Ex}_{D,k} = \dot{Ex}_{D,k}^{AV,EN} + \dot{Ex}_{D,k}^{AV,EX} + \dot{Ex}_{D,k}^{UN,EN} + \dot{Ex}_{D,k}^{UN,EX} \quad (8)$$

This approach allows engineers to distinguish not only the origin of irreversibilities (EN/EX) but also their reducibility (AV/UN). As a result, it provides precise guidance on whether design improvements should target the component itself or system-level

integration.

Comparative Summary

In summary, the engineering approach estimates endogenous destruction based on assumptions or typical efficiencies and assigns the remainder as exogenous, without any avoidable/unavoidable split. The thermodynamic approach rigorously calculates endogenous destruction by assuming the component real and all others ideal, and exogenous as the difference, but it also stops short of avoidable/unavoidable classification. The hybrid cycle approach combines both dimensions, producing a fourfold subdivision (AV-EN, AV-EX, UN-EN, UN-EX) that is now the standard in advanced exergy studies (Liu et al., 2020; Petrakopoulou, Tsatsaronis, Morosuk, & Carassai, 2012; Yousefizadeh Dibazar et al., 2020).

The development of these methods can be traced through several key contributions. The idea of distinguishing avoidable and unavoidable exergy destruction was first systematically presented by Tsatsaronis (1999), who emphasized the importance of separating losses imposed by technological limits from those that could be reduced by improved design or operation. The methodological treatment of endogenous and exogenous exergy destruction was provided in detail by Kelly et al. (2009), who compared different ways of calculating endogenous destruction and explicitly described the principle of "keeping the studied component real while assuming the others ideal."

Later studies integrated these concepts within a single framework, giving rise to the hybrid cycle method. A landmark application was presented by Petrakopoulou et al. (2012), who analyzed a combined cycle power plant and demonstrated how both AV/UN and EN/EX distinctions could be performed within one consistent procedure. Their work also illustrated how exogenous destruction could be traced back to specific upstream or downstream components, adding diagnostic depth. Since then, the hybrid cycle method has been widely adopted, with applications in systems such as organic Rankine cycles, refrigeration, and LNG-based plants (Özen & Koçak, 2022). Recent works by Yousefizadeh Dibazar et al. (2020) and Liu et al. (2020) confirmed its practicality and reliability in modern energy system evaluations.

From a broader perspective, Morosuk and Tsatsaronis (2019) provided a comprehensive review of advanced exergy-based methods, highlighting how exergy, exergoeconomic, and exergoenvironmental extensions each address different questions. Their synthesis shows that AEA has evolved into a multidimensional framework that supports not only thermodynamic optimization but also economic and environmental decision-making. Taken together, the literature demonstrates that today's advanced exergy analysis is the result of integrating the AV/UN and EN/EX concepts into a unified methodology, which is why it is now regarded as one of the most powerful diagnostic tools for energy system analysis.

From a broader perspective, Morosuk and Tsatsaronis (2019) provided a comprehensive overview of advanced exergy-based methods, including exergoeconomic and exergoenvironmental extensions, clarifying how each tool addresses different questions. Altogether, the literature shows that today's AEA framework is

Applications of AEA in Energy Systems

Industrial processes

AEA has found impactful applications in industrial settings, where seemingly small gains in efficiency can lead to major economic and environmental returns. For instance, in natural gas liquid (NGL) recovery plants, Jovijari et al. (2022b) conducted a detailed AEA and found that while conventional exergy analysis pointed to compressors and heat exchangers as the primary loss contributors, the advanced analysis revealed that a significant portion of the heat exchangers' losses were unavoidable helping prioritize where actual improvements should be targeted.

In ORC systems, AEA has enabled decomposition of exergy destruction into component-origin and interaction-origin categories. A recent "thermodynamic cycle" study by Wang et al. (2021) meticulously modeled the expander and heat exchanger, showing that exergy losses were not only within the expander but also significantly influenced by upstream components like the evaporator

Unconventional sectors

AEA's adaptability has also been demonstrated in non-traditional fields. For example, in a milk processing facility, both conventional and advanced exergy analyses were conducted. While the conventional analysis offered a broad overview of losses, AEA provided a detailed partitioning into avoidable and interaction-driven inefficiencies, revealing opportunities for targeted improvements (Bühler et al., 2018).

Renewable and hybrid systems

In renewable energy systems such as combined heat and power (CHP) units and solar-assisted cycles, AEA has clarified hidden inefficiencies and synergies, thus guiding the integration of renewable resources into complex systems (Jani, Kachhwaha, Nagababu, Das, & Ehyaei, 2022; Özen, 2024; Özen & Koçak, 2022).

Integration of Economic and Environmental Dimensions

Over time, AEA has expanded to include economic and environmental dimensions, offering a more comprehensive framework for evaluating and improving energy systems. These extensions allow engineers not only to understand thermodynamic inefficiencies but also to assess their economic and ecological implications.

- **Advanced exergoeconomic analysis (AECA):** This approach evaluates the

costs associated with exergy destruction, providing guidance for cost-effective system improvements. For instance, Güler (2023) applied AECA to a dual-binary geothermal power plant and demonstrated how identifying cost-intensive losses helps reduce both operating costs and CO_2 emission-related expenses.

- **Advanced exergoenvironmental analysis (AEEA):** AEEA connects irreversibilities to environmental impacts, enabling design strategies that prioritize sustainability. Benavides Gamero et al. (2023) performed AEEA on an ORC waste-heat recovery system, showing that the majority of environmental impacts were endogenous and largely avoidable.
- **Combined AECA and AEEA:** Recent studies integrate both perspectives within a single methodological framework. A notable example is the work of Özen (2024), who applied advanced exergoeconomic and exergoenvironmental analyses to a geothermal-based power system using the Modified Productive Structure Analysis (MOPSA) method. This study highlighted how combining the two approaches provides a multidimensional understanding of system performance, revealing improvement opportunities that remain hidden when only one dimension is considered.

Together, these contributions show that AEA has become not only a diagnostic tool but also a comprehensive sustainability framework, integrating thermodynamic efficiency with economic and environmental decision-making.

Educational Contributions of AEA

Including the advanced approaches of AEA in engineering education helps students develop both critical thinking and a systems-oriented perspective. In this way, they not only gain theoretical knowledge but also learn to better understand the complexities and interdependencies of real-world energy systems, preparing them to deal with these challenges in practice.

Conclusion and Future Outlook

Advanced Exergy Analysis has emerged as a powerful approach that connects the principles of thermodynamics with real engineering practice. By separating avoidable, unavoidable, endogenous, and exogenous irreversibilities, it offers a unique diagnostic capability that supports both broad system-level improvements and targeted component optimizations.

Its wide use in industrial, renewable, and even unconventional applications, together with its extensions into economic and environmental fields, demonstrates its flexibility and relevance. At the same time, its role in education helps prepare future engineers and scientists to think critically about sustainability and efficiency.

Looking ahead, AEA is expected to become a central framework for next-generation energy systems. As the global energy transition demands higher efficiency, lower

emissions, and sustainable design, AEA provides the precision and multidimensional insight needed to meet these challenges.

References

Alibaba, M., Pourdarbani, R., Hasan Khoshgoftar Manesh, M., Herrera-Miranda, I., Gallardo-Bernal, I., & Hernández-Hernández, J. L. (2020). Conventional and advanced exergy-based analysis of hybrid geothermal–solar power plant based on ORC cycle. *Applied Sciences*, *10*(15), 5206.

Azubuike, U. G., Njoku, H. O., Eke, M. N., & Ekechukwu, O. V. (2025). Advanced Exergy Analysis and Performance Ranking of Components of a Combined Cycle Power Plant. *Thermal Engineering*, *72*(1), 17–31.

Bejan, Adrian. (2017). *Advanced engineering thermodynamics*. John Wiley & Sons Inc.

Benavides Gamero, A., Camargo Vanegas, J., Duarte Forero, J., Valencia Ochoa, G., & Diaz Herazo, R. (2023). Advanced exergo-environmental assessments of an organic rankine cycle as waste heat recovery system from a natural gas engine. *Energies*, *16*(7), 2975.

Bühler, F., Nguyen, T.-V., Jensen, J. K., Holm, F. M., & Elmegaard, B. (2018). Energy, exergy and advanced exergy analysis of a milk processing factory. *Energy*, *162*, 576–592.

Güler, O. V., Gürbüz, E. Y., Georgiev, A. G., & Keçebaş, A. (2023). Advanced Exergoeconomic Assessment of CO2 Emissions, Geo-Fluid and Electricity in Dual Loop Geothermal Power Plant. *Energies*, *16*(8). doi:10.3390/en16083466

Hançer Güleryüz, E., & Özen, D. N. (2022). Advanced exergy and exergo-economic analyses of an advanced adiabatic compressed air energy storage system. *Journal of Energy Storage*, *55*. doi:10.1016/j.est.2022.105845

Jani, Hardik K, Kachhwaha, Surendra Singh, Nagababu, Garlapati, Das, Alok, & Ehyaei, MA. (2022). Energy, exergy, economic, environmental, advanced exergy and exergoeconomic (extended exergy) analysis of hybrid wind-solar power plant. *Energy & Environment*, *34*(7), 2668–2704. doi:10.1177/0958305X221115095

Jovijari, F., Kosarineia, A., Mehrpooya, M., & Nabhani, N. (2022a). Advanced exergy analysis of the natural gas liquid recovery process. *Thermal Science*, *26*(3 Part A), 2287–2300.

Jovijari, F., Kosarineia, A., Mehrpooya, M., & Nabhani, N. (2022b). Advanced exergy analysis of the natural gas liquid recovery process. *Thermal Science*, *26*(3 Part A), 2287–2300.

Kelly, S., Tsatsaronis, G., & Morosuk, T. (2009). Advanced exergetic analysis: Approaches for splitting the exergy destruction into endogenous and exogenous

parts. *Energy*, *34*(3), 384–391.

Liu, Z., Liu, Z., Cao, X., Luo, T., & Yang, X. (2020). Advanced exergoeconomic evaluation on supercritical carbon dioxide recompression Brayton cycle. *Journal of Cleaner Production*, *256*, 120537. doi:10.1016/J.JCLEPRO.2020.120537

Morosuk, T., & Tsatsaronis, G. (2009). Advanced exergy analysis for chemically reacting systems–application to a simple open gas-turbine system. *International Journal of Thermodynamics*, *12*(3), 105–111.

Morosuk, T., & Tsatsaronis, G. (2019). Advanced exergy-based methods used to understand and improve energy-conversion systems. *Energy*, *169*, 238–246. doi:10.1016/J.ENERGY.2018.11.123

Ozen, D. N., Uysal, C., & Balli, O. (2020). Thermoeconomic analysis of t56 turboprop engine under different load conditions. *Isi Bilimi Ve Teknigi Dergisi/ Journal of Thermal Science and Technology*, *40*(2), 251–265. https://doi.org/10.47480/isibted.817013

Özen, D. N. (2024). Advanced exergo-economic and exergo-environmental analyses of a geothermal sourced power system with the modified productive structure analysis method (MOPSA). *Renewable Energy*, *237*. doi:10.1016/j.renene.2024.121715

Özen, D. N., Hançer Güleryüz, E., & Acılar, A. M. (2024). Advanced exergo-economic analysis of an advanced adiabatic compressed air energy storage system with the modified productive structure analysis method and multi-objective optimization study. *Journal of Energy Storage*, *81*. doi:10.1016/j.est.2023.110380

Özen, D. N., & Koçak, B. (2022). Advanced exergy and exergo-economic analyses of a novel combined power system using the cold energy of liquefied natural gas. *Energy*, *248*. doi:10.1016/j.energy.2022.123531

Petrakopoulou, F., Tsatsaronis, G., Morosuk, T., & Carassai, A. (2012). Conventional and advanced exergetic analyses applied to a combined cycle power plant. *Energy*, *41*(1), 146–152. doi:10.1016/J.ENERGY.2011.05.028

Petrakopoulou, F., Tsatsaronis, G., Morosuk, T., & Paitazoglou, C. (2012). Environmental evaluation of a power plant using conventional and advanced exergy-based methods. *Energy*, *45*(1), 23–30.

Qi, X., Yang, C., Huang, M., Ma, Z., Hnydiuk-Stefan, A., Feng, K., … Li, Z. (2024). Conventional and advanced exergy-exergoeconomic-exergoenvironmental analyses of an organic Rankine cycle integrated with solar and biomass energy sources. *Energy*, *288*, 129657.

Rosen, M. A., & Dincer, I. (2001). Exergy as the confluence of energy, environment and sustainable development. *Exergy, an International Journal*, *1*(1), 3–13.

Tsatsaronis, G. (1993). Thermoeconomic analysis and optimization of energy systems. *Progress in Energy and Combustion Science*, *19*(3), 227–257.

Tsatsaronis, G. (1999). Strengths and limitations of exergy analysis. In *Thermodynamic optimization of complex energy systems* (pp. 93–100). Springer.

Vučković, G. D., Vukić, M. V, Stojiljković, M. M., & Vučković, D. D. (2012). Avoidable and unavoidable exergy destruction and exergoeconomic evaluation of the thermal processes in a real industrial plant. *Thermal Science*, *16*(suppl. 2), 433–446.

Wang, Y., Qin, G., Zhang, Y., Yang, S., Liu, C., Jia, C., & Cui, Q. (2021). Conventional and advanced exergy analyses of an organic Rankine cycle by using the thermodynamic cycle approach. *Energy Science & Engineering*, *9*(12), 2474–2492.

Yan, C., Yang, A., Chien, I.-L., Wei, S., Shen, W., & Ren, J. (2019). Advanced exergy analysis of organic Rankine Cycles for Fischer-Tropsch syngas production with parallel dry and steam methane reforming. *Energy Conversion and Management*, *199*, 111963.

Yousefizadeh Dibazar, S., Salehi, G., & Davarpanah, A. (2020). Comparison of exergy and advanced exergy analysis in three different organic rankine cycles. *Processes*, *8*(5), 586.

About the Author

Dilek Nur ÖZEN, PhD is an Associate Professor of Mechanical Engineering at Necmettin Erbakan University in Konya, Turkey. She holds a PhD in Mechanical Engineering from Selcuk University. Her main areas of interest are exergy and exergo-economic analyses of energy plants.

E-mail: dnozen@erbakan.edu.tr, **ORCID:** 0000-0002-8622-4990

Similarity Index

The similarity index obtained from the plagiarism software for this book chapter is 10%.

Development of Composite Materials Reinforced with Hybrid GNP and B_4C

Melik ÇETİN
Karabük University

Hayrettin AHLATÇI
Karabük University

Kenza DJEBARI
Karabük University

To Cite This Chapter:
Çetin, M., Ahlatci, H., & Djebari, K. (2025). Development of composite materials reinforced with hybrid GNP and B4C. In H. Gokmese, S. Bulbul, & Y. Uzun (Eds.), *Innovative approaches in materials science and applications* (pp. 104–127). ISRES Book Series. ISRES Publishing.

Introduction

Composite materials hold a significant position in modern industry due to their high hardness-to-density and strength-to-density ratios. These materials are widely used in sectors where weight is critical, such as the aerospace and aviation industries. The high efficiency and performance enhancement provided by composite structures have rendered them indispensable in these fields (Liu et al., 2016).

In practical applications, randomly oriented particle-reinforced metal matrix composites (MMCs) are frequently preferred. The primary reason for this preference is the desire to obtain isotropic properties (Miyazaki et al., 2004). MMCs combine the ductility and toughness of metals with the high strength of ceramics, enabling their use in essential engineering applications (Asthana et al., 2006). Particle reinforcement is an effective method for improving the mechanical properties of composites, providing a noticeable increase in strength compared to the unreinforced metal matrix.

Although the production of composite materials generally involves liquid-state processes such as casting, solid-state techniques, including powder metallurgy, have been gaining increasing importance (Del Monte et.al., 1999). With recent technological advancements, there has been a shift from traditional methods toward advanced manufacturing techniques, and powder metallurgy has become particularly prominent in the fabrication of particle-reinforced MMCs (Ma et al., 2020; Zhang et al., 2020). However, the oxidation-sensitive nature of Mg and Mg-based alloys remains a critical factor that increases production costs (Blawert et al., 2004).

Among the expected properties of composite matrix materials are low density, corrosion resistance, fracture toughness, and compatibility with the reinforcement phases. While the matrix transfers the applied load to the reinforcing phases, it also protects them from corrosive environmental effects and limits the propagation of brittle cracks. Therefore, the matrix material plays a critical role in the mechanical and thermomechanical performance of composite structures.

Light metals are frequently chosen as matrix materials due to their high toughness and excellent mechanical properties. Owing to its low density, magnesium (Mg) has gained prominence in modern lightweight structural design (Monticelli et al., 2019). In armoured vehicles, mobility and multidirectional manoeuvring capability are closely associated with the use of lightweight materials. For this reason, Mg alloys are increasingly preferred in armor systems that require high ballistic resistance (Alaneme et al., 2021; Luo et al., 2013). In recent years, Mg alloys have become increasingly competitive with Al alloys, offering environmentally friendly and efficient solutions for engineering applications where weight reduction is critical (Liu et al., 2024). Mg provides strength levels close to those of Al while offering advantages in many fields due to its lightweight nature combined with adequate strength (Alaneme et al., 2021; Liu et al., 2024).

Aluminium and its alloys are widely used in automotive, aerospace, construction, and energy sectors owing to their high corrosion resistance, low density, and favourable mechanical properties. Aluminium matrix composites (AMCs) are distinguished by their high specific strength and hardness, as well as their superior wear and temperature resistance. The Al5754 alloy is particularly known for its high ductility, strength, and corrosion resistance; however, it may be susceptible to certain forms of corrosion under harsh environmental conditions, such as marine atmospheres. Ceramic reinforcements such as B_4C and GNP (graphene nanoplatelets) are commonly incorporated into AA5754 matrix composites, offering advantages including high melting temperatures, low densities, and high elastic moduli.

However, incorporating GNP into an Al matrix is quite challenging due to wetting difficulties. Although the literature includes studies on GNP reinforcement in Mg-based composites, research on GNP reinforcement in AA5754 remains limited (Zhang et al., 2020; Zhang et al., 2017; Prakash et al., 2011). This study aims to investigate the structural characteristics of nano-sized ceramic-reinforced composites based on the Al5754 matrix, thereby addressing this gap in the literature and enhancing the commercial application potential of these materials. In this study, the Al5754 alloy was reinforced with various proportions of GNP, B_4C, and GNP+B_4C mixtures. The composites were produced via the stir-casting method, cold-rolled to 30%, and subsequently subjected to a recrystallization heat treatment.

Materials and Methods

The Al5754 Al–Mg wrought alloy, whose chemical composition is given in Table 1, was procured as plates from SEYKOÇ ALUMINIUM. The initial quantities of the reinforcements (GNP and B_4C) used for producing the composites namely Al5754+0.5% GNP, Al5754+0.5% GNP+15% B_4C, Al5754+1% GNP+15% B_4C, and Al5754+15% B_4C are presented in Table 2. Before induction melting, the nano-sized carbon GNP and B_4C ceramic reinforcements were mixed both dry in a V-type ball mixer and magnetically ultrasonically in alcohol. The steps of the homogeneous mixing process are shown in Figure 1. Finally, to ensure complete removal of ethanol from the system, the mixed powders were placed in a furnace at a controlled temperature and dried for 12 hours. The prepared GNP- and B_4C-containing mixtures were then pressed in a 30-ton capacity hydraulic press at 350 °C to form compacts of 32×30 mm diameter within a mold, and these compacts were partially sintered at 500 °C for 3 hours.

Together with the sintered compacts, the Al5754 Al–Mg alloy (initial masses provided in Table 2) was melted in an S6 gas-shielded induction melting furnace using an alumina-lined graphite crucible, and the stir-casting method was applied to ensure homogeneous incorporation of the added reinforcements. The melt was poured into rectangular steel molds preheated to 300 °C, with dimensions of 35×25×200 mm as shown in Figure 2(b), producing the as-cast AA5754 alloy and the Al-matrix GNP- and B_4C-reinforced composites. The cast composites were then wrapped in Al foil and subjected to a homogenization heat treatment at 490 °C for 5 hours in an atmosphere containing B_4C and graphite powders.

Table 1

Chemical composition of Al5754 alloy.

Alloy	Mg	Mn	Si	Cr	Fe	Al
Al 5754	3.650	0.526	0.349	0.112	0.348	Rest.

Table. 2

The amount (in grams) of carbon- and ceramic-reinforced Al5754 matrix composites produced in this study.

Alloy	GNP (g)	B_4C (g)	Gd-Nd (g)	AA5754 (g)
Al+%0,5GNP	5	0	10	985
Al+%0.5 GNP+%15 B_4C	5	150	10	835
Al+%1 GNP+%15 B_4C	10	150	10	830
Al+%15 B_4C	0	150	10	840

Figure 1

Preparation process of powder mixtures.

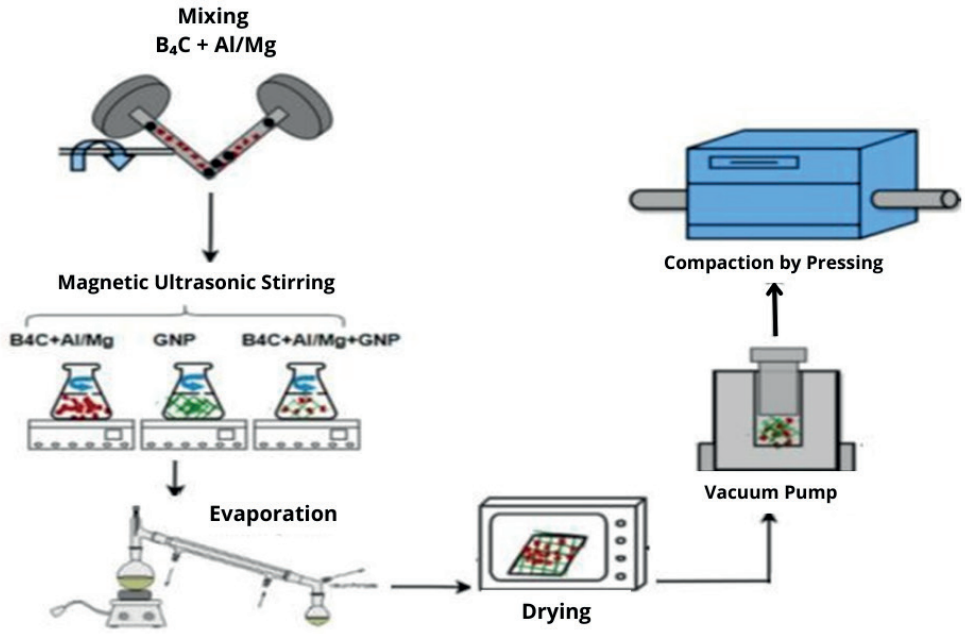

Figure 2

Induction melting furnace and specimen production mold.

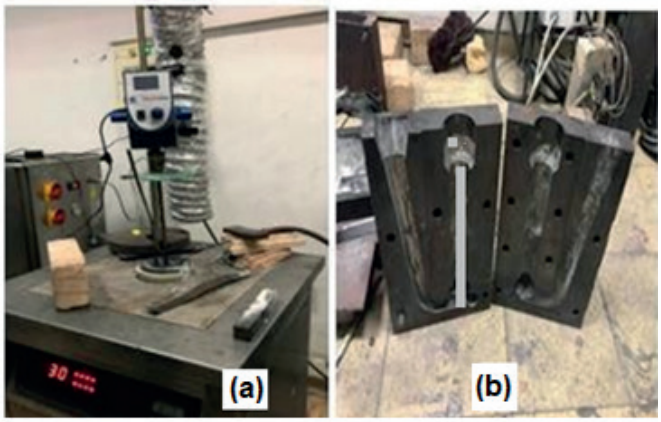

The specimens were prepared using standard metallographic procedures, involving sequential grinding with SiC papers ranging from 240 to 2500 mesh, followed by final polishing with a 1 μm alumina suspension. They were then etched using 100 mL of Keller's solution (1 cm^3 hydrofluoric acid; 1.5 cm^3 hydrochloric acid; 2.5 cm^3 nitric acid; 95 cm^3 water), rinsed with water and alcohol, and dried with hot air. The microstructures of the specimens were examined using a Nikon optical microscope and SEM-EDAX analyses. The hardness of the as-cast specimens was measured in Brinell units using an HB-3000B Brinell hardness tester. In contrast, the hardness of the rolled and subsequently recrystallized specimens was measured using an FV-700 model FUTURETECHCOPP Vickers hardness tester.

The rolling process for the unprocessed AA5754 alloy and composites reinforced with varying amounts of GNP and B_4C was carried out on a double-cold roller mill. Specimens measuring 10 × 25 × 55 mm were rolled at room temperature with 10% reductions per pass, resulting in a total decrease of 30%. To investigate the diffusion and recrystallization behaviour of the 30% cold-rolled unreinforced AA5754 and GNP- and B_4C-reinforced composites, and to evaluate the effect of heat treatment on hardness and corrosion resistance, the specimens were held at 300 °C for 1 hour and then cooled to room temperature outside the furnace.

Wear tests were conducted on the reciprocating wear test apparatus shown in Figure 3 under a constant load of 20 N, a sliding speed of 0.1 m/s, and a total sliding distance of 1000 m. Wear was measured and recorded every 200 m of sliding distance. The friction force generated during testing was measured instantaneously using a load cell attached to the tribometer arm and transferred to a computer. A 6 mm-diameter AISI 52100-grade steel ball was used as the counter material. Specimen weight measurements were performed using a RADWAG AS 220.R2 balance with a precision of 10^{-4}.

Figure 3

Schematic representation of the reciprocating wear test apparatus.

The worn surfaces of the specimens were examined in detail using a Scanning Electron Microscope (SEM), and the corresponding wear mechanisms were identified. Five wear tests were performed for each specimen, and the results were evaluated based on the average values obtained. To investigate the corrosion behaviour of Al5754 aluminium composites, an immersion corrosion test was conducted in a mixed solution of 3.5% NaCl and 3.5% HCl, using the glass containers shown in Figure 4. The initial weights and surface areas of all specimens were measured before immersion. The specimens were left in the solution for 3, 6, and 24 hours, respectively. At the end of each exposure period, the specimens were reweighed, and their surface measurements were recorded. Images of the corrosion specimens before and after immersion in 3.5% NaCl and 3.5% NaCl + HCl solutions are presented in Figure 5.

Figure 4

Immersion of the specimens.

Figure 5

Appearance of the deformed-rolled Al5754 composites before and after the immersion corrosion test.

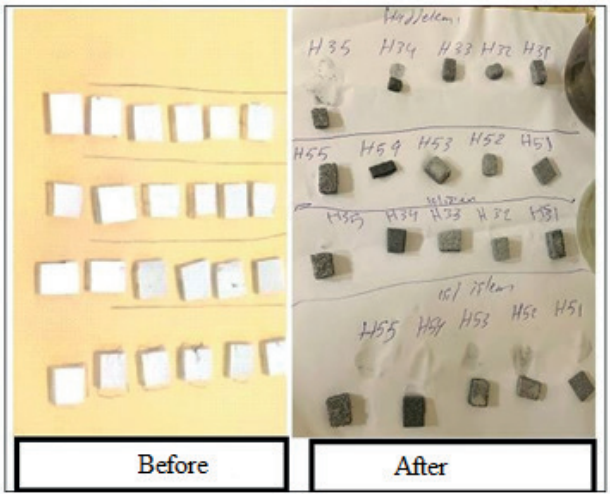

Characterization Results and Discussion

The X-ray diffraction (XRD) analyses of the as-cast unreinforced specimen and the composites reinforced with 0.5% GNP and 15% B_4C are presented in Figures 6(a-c). According to these results, when the alloy and composites are evaluated as a whole, the presence of binary intermetallic phases formed by Al, Cu, Mn, Mg, B, Cr, Ni, Zn, and C, namely AlMn, AlFe, and B_4C intermetallic, was identified. The findings are consistent with the literature (Hamid et al., 2025).

Figure 6

(a) X-ray diffraction analysis of the as-cast specimen, (b) the 0.5% GNP-reinforced specimen, and (c) the 15% B_4C-reinforced specimen.

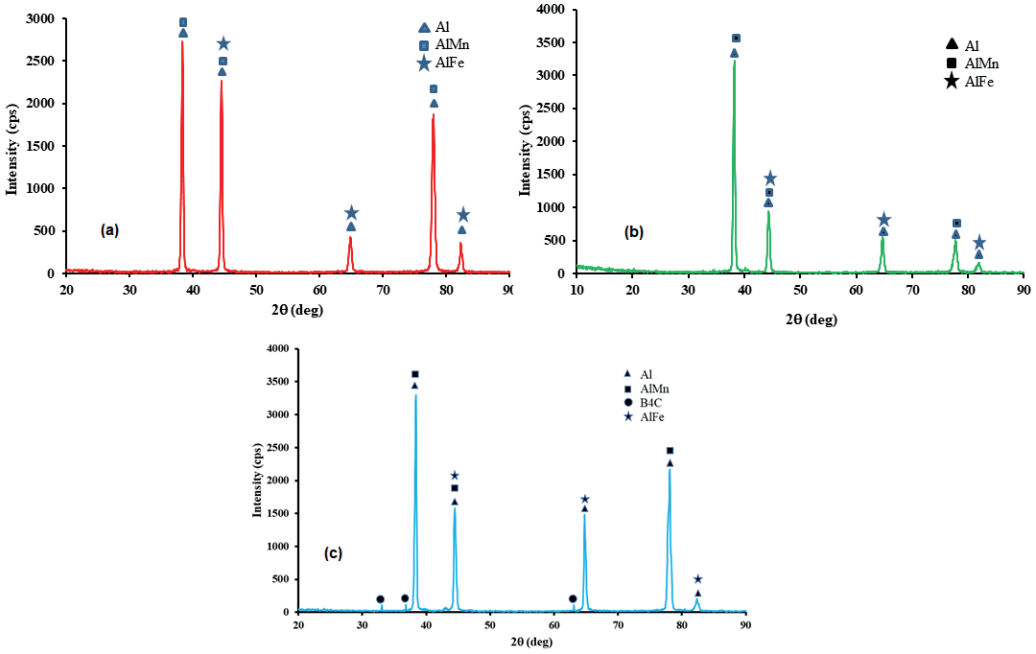

The optical microscope images of the as-cast alloy and composite specimens are presented in Figure 7. In Figure 7(a), the microstructure of the as-cast Al5754 specimen exhibits a typical granular morphology consisting of randomly distributed, irregularly shaped, and large intermetallic particles, along with evidence of dendritic structure formation. In Figures 7(b) and 7(c), the microstructure of the Al5754 composites containing GNP and B_4C shows that both reinforcements are uniformly distributed as dark-coloured phases within the matrix. The exceptionally uniform distribution of B_4C results in higher hardness values for this specimen than for either the other reinforced samples or the unreinforced alloy (Figure 8). As observed, B_4C particles appear dark and exhibit a regular distribution throughout the microstructure. In the microstructure of the AA5754 composite reinforced with 0.5% GNP and 15% B_4C, the dark and homogeneous distribution of the reinforcements has also been reported. Furthermore, the increase in hardness observed for the specimen reinforced with 0.5% GNP + 15% B_4C is evident in Figure 8 (Liu et al., 2024).

Figure 7

Optical microscope images of (a) as-cast AA5754, (b) the 1% GNP + 15% B_4C composite, and (c) the 0.5% GNP + 15% B_4C composite.

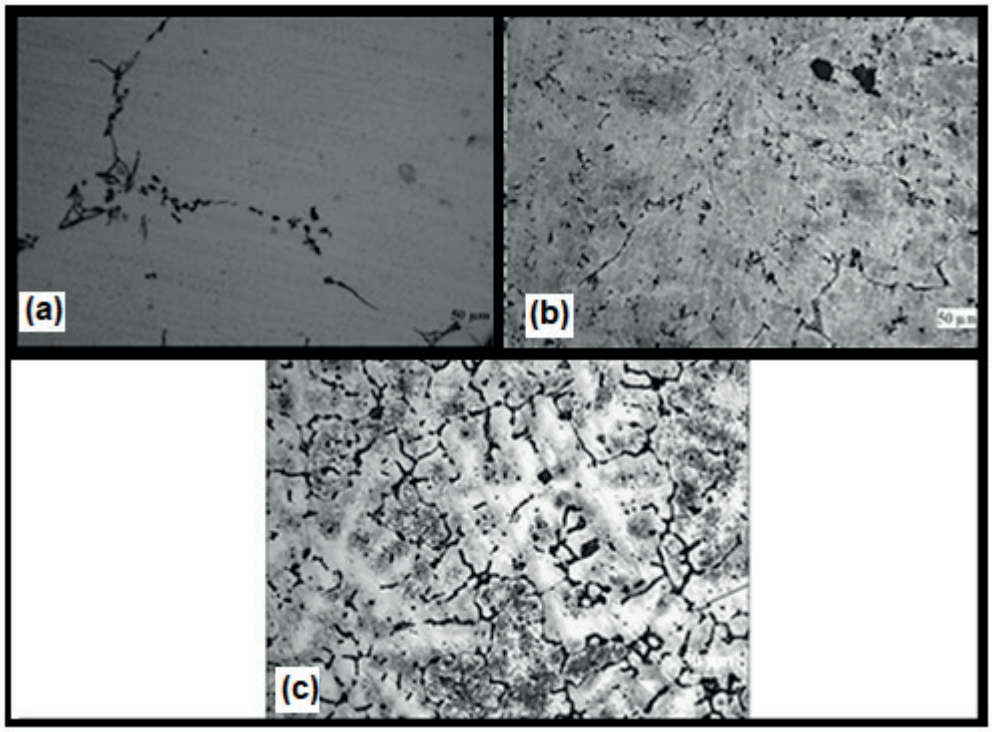

As shown in Figure 8, the highest hardness was measured for the composite specimen reinforced with 1% GNP and 15% B_4C, yielding 86.54 HB. This was followed by the specimen reinforced with 0.5% GNP + 15% B_4C, which exhibited a hardness of 73.6 HB. The specimens reinforced with 15% B_4C and 0.5% GNP, as well as the unreinforced specimen, showed hardness values of 53.4 HB, 49.2 HB, and 47.4 HB, respectively. The superior hardness of the as-cast specimen containing 1% GNP + 15% B_4C is attributed to the combined effect of GNP and B_4C reinforcement, as well as the presence of B_4C in the microstructure, which is evident in the X-ray diffraction patterns shown in Figure 6. Although B_4C is present in the microstructures of both specimens shown in Figure 6, the combined effect of 0.5% GNP + 15% B_4C in the initially produced composite is determined to be more influential than the individual contributions of 15% B_4C or 0.5% GNP alone. Examination of the XRD profiles (Figure 6) reveals that the common diffraction peaks in all specimens correspond to Al, AlMn, and AlFe phases.

Upon further evaluation of Figure 8, the highest hardness value was again observed for the composite specimen reinforced with 1% GNP + 15% B_4C, at 87.4 HB. The specimen containing 0.5% GNP + 15% B_4C exhibited a hardness of 82.33 HB, while the composites reinforced with 15% B_4C and 0.5% GNP, and the unreinforced specimen, recorded hardness values of 77.6 HB, 72.6 HB, and 66.2 HB, respectively.

Figure 8

Average hardness variation of the as-cast unreinforced and composite specimens.

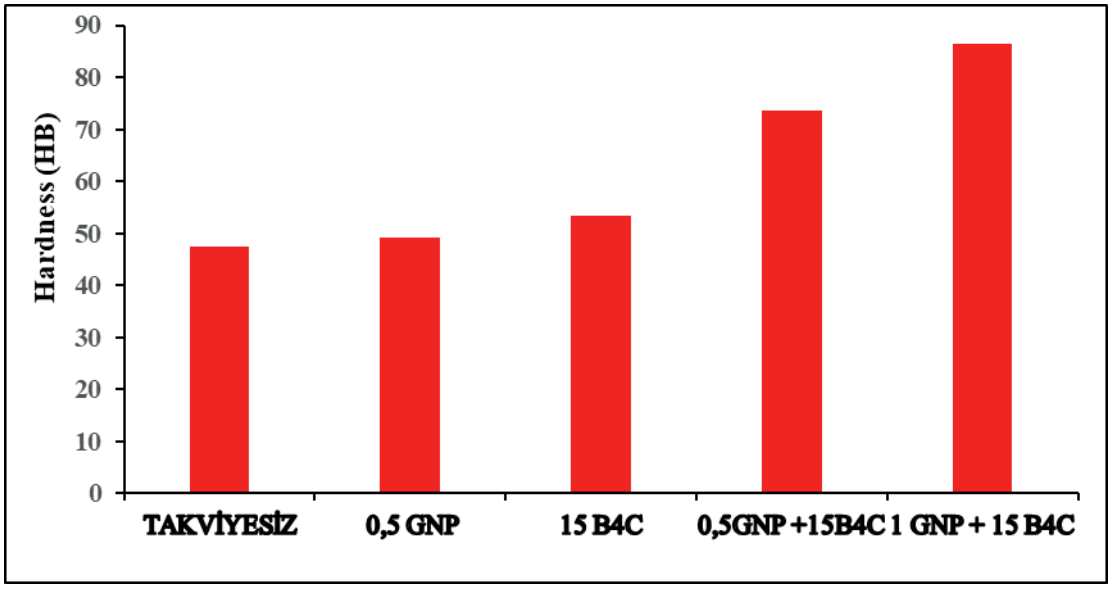

According to Figure 8, the hardness of the unreinforced AA5754 specimen produced by stir casting was measured as 47.35 HB. The addition of 0.5% GNP to Al5754 increased the hardness by 1.01 HB, to 49.17 HB. The hardness of the specimen reinforced with 0.5% GNP + 15% B_4C increased 1.56-fold compared with unreinforced AA5754, reaching 73.7 HB. When the nano-reinforcement ratio was 1% GNP + 15% B_4C and 15% B_4C alone, the hardness increased relative to unreinforced AA5754, yielding values of 86.45 HB and 53.36 HB, respectively. The comparison of hardness values clearly shows that the highest hardness was obtained in the specimens reinforced with 1% GNP and 15% B_4C. After the addition of 1% GNP + 15% B_4C, the hardness of the composite increased approximately 1.83 times compared with the unprocessed Al5754.

From the graphs, it can be observed that adding GNP and B_4C to Al5754 significantly increases hardness. The results indicate that the maximum hardness improvement occurs with a volumetric addition of 1% GNP and 15% B_4C, whereas varying the reinforcement ratio decreases hardness. This behavior can be explained by increased porosity due to the combined reinforcement effect and, in the case of the 1% GNP nanocomposite, potential GNP agglomeration/clustering (Liu et al., 2024). The presence of tough reinforcement phases within AA5754+15% B_4C, AA5754+0.5% GNP+15% B_4C, and AA5754+1% GNP+15% B_4C also contributed to increased hardness values. Literature reports confirm that similar trends have been observed in numerous studies (Wang et al., 2021; Sivakaruna et al., 2017; Rebba et.al., 2014). Figure 9 illustrates the effect of different reinforcement types (GNP and B_4C) on the hardness of specimens heat-treated at 300 °C.

Figure 9

Effect of the 300 °C recrystallization treatment on the hardness of the 30% cold-rolled specimens.

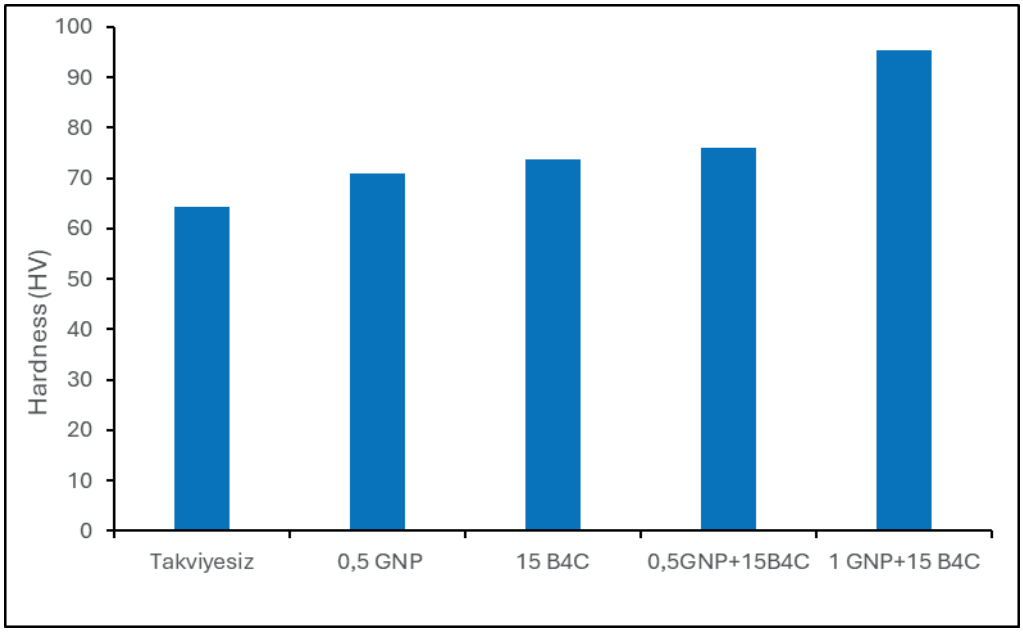

Examination of Figures 10 and 11 shows the steady-state wear rates of the unreinforced and nano-reinforced composites after 30% cold-rolling, followed by a recrystallization heat treatment. As seen in Figure 10, after a sliding distance of 1000 m, the nano-reinforced composite containing 0.5% GNP + 15% B_4C exhibited the highest at 0.022 g, while the composite containing 1% GNP + 15% B_4C showed the lowest wear loss at 0.016 g. Overall, it can be stated that the 30% cold-rolling + recrystallization heat treatment improved the wear-loss performance of both the 0.5% GNP + 15% B_4C and 1% GNP + 15% B_4C nano-reinforced composites and simultaneously enhanced their mechanical strength.

When the hardness and steady-state wear rates (g/m) of the specimens subjected to 30% rolling + recrystallization are evaluated together (Figure 11), the unreinforced AA5754 specimen, which had the lowest hardness (65.25 HV), exhibited a steady-state wear rate of 0.000017814 g/m. In contrast, the AA5754 + 1% GNP + 15% B_4C composite, which had the highest hardness (90.99 HV), showed a wear rate of 0.000014943 g/m. However, the composite with the second-highest hardness (86.28 HV), AA5754 + 0.5% GNP + 15% B_4C, exhibited the highest wear rate of 0.000021071 g/m. These findings indicate that although 30% rolling + recrystallization increased the hardness of the specimens, it also increased their wear rates.

Literature reports (Baradeswaran et al., 2014). indicate that B_4C-reinforced composites generally exhibit higher wear loss compared to GNP-reinforced ones. The dry sliding test results in this study similarly demonstrate that the addition of 0.5% GNP is more

effective than 15% B_4C in improving wear resistance. High amounts of B_4C alone are believed to make the composite more brittle, thereby reducing its resistance to wear. Graphene's high wear resistance and solid-lubrication behaviour reduce friction during sliding, thereby decreasing wear loss. shows that using B_4C up to 5% improves wear behaviour, whereas increasing the B_4C ratio beyond this level negatively affects wear performance. (Sathish Kumar et al., 2020).

Figure 10

of the specimens subjected to 30% cold rolling and recrystallization treatment.

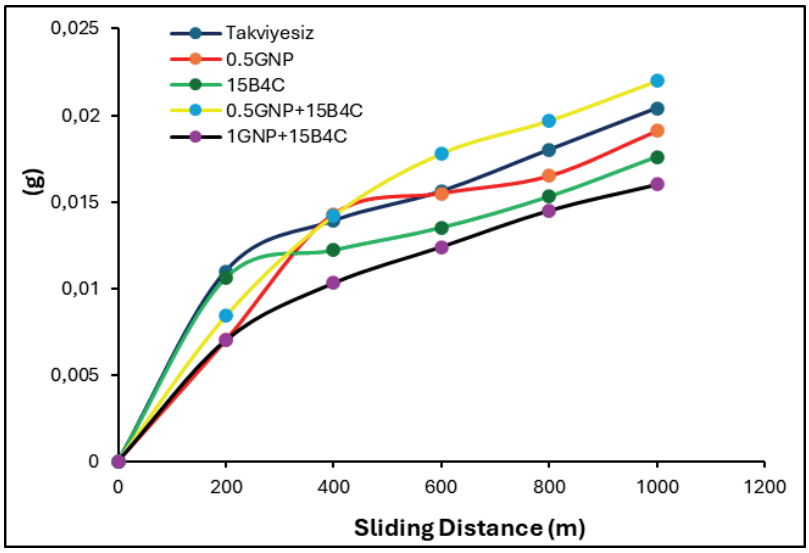

Figure 11

Steady-state wear rate of specimens subjected to 30% cold rolling and recrystallization treatment.

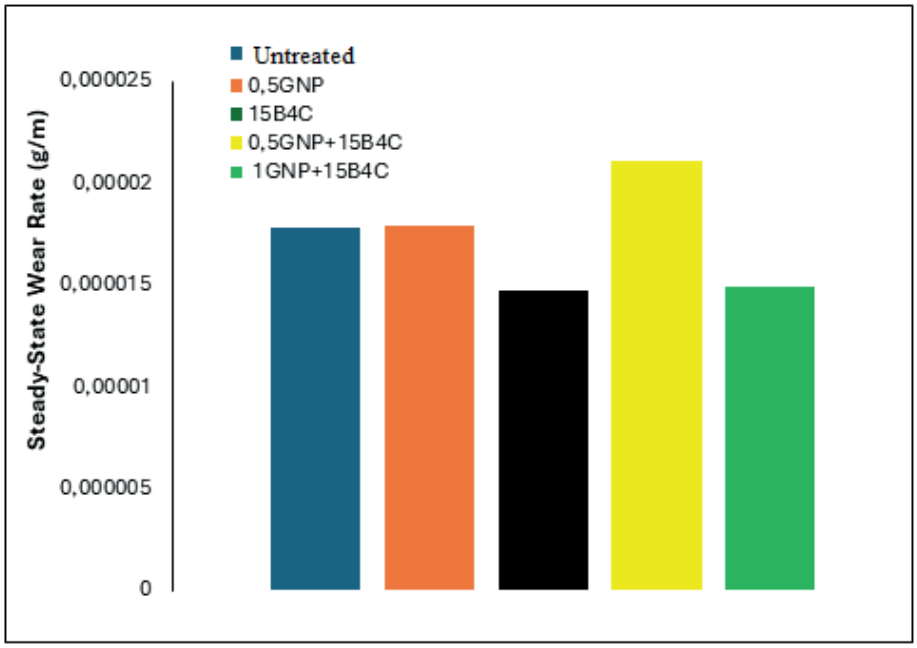

The reciprocating wear tests conducted in this study enabled a comparative evaluation of the wear performance of specimens processed with different reinforcement materials

(GNP graphene nanoplatelets and 15% B_4C boron carbide) and subjected to various thermomechanical treatments. The findings demonstrate that the reinforcement phases and thermomechanical processing significantly influence microstructural integrity, hardness, and wear resistance. Compared with the unprocessed specimen, all GNP- and B_4C-reinforced specimens exhibited lower es. Notably, the specimen containing 1% GNP + 15% B_4C showed a total of 0.0167 g at the end of the sliding distance, indicating a clear improvement over the unreinforced 5754 Al specimen. This result is consistent with the literature. According to Tang et al., aluminium matrix composites reinforced with graphene exhibit substantially enhanced tribological properties, where the formation of a transfer film on the sliding surface increases wear resistance (Chawla et al., 2006).

The addition of boron carbide also resulted in significant improvements in hardness. The 15% B_4C specimen, with a hardness of 75.45 HB, demonstrated greater structural resistance than the unreinforced specimen. This increase in hardness reduced surface deformation during wear. According to Chawla, harder surfaces exhibit greater resistance to mechanisms such as micro-cutting and plastic deformation (Kumar et al., 2015).

Specimens subjected to rolling generally exhibited lower steady-state wear rates. The 15% B_4C specimen exhibited a steady-state wear rate of 0.00002005 g/m, indicating improved performance compared to the unprocessed specimen. Kumar and Srivastava reported that grain refinement and a more homogeneous microstructure after rolling improve surface strength and reduce wear (Tjong et al., 2007).

The results obtained from heat-treated specimens were also highly favourable. The specimen reinforced with 1% GNP + 15% B_4C exhibited the best performance, with a steady-state wear rate of 0.000014943 g/m and a hardness of 90.99 HB. According to Tjong, precipitation structures formed after heat treatment promote a more stable distribution of reinforcement phases within the matrix, thereby enhancing wear resistance (Zhang et al.,2014).

The obtained findings show that both the amount of reinforcement and the applied thermomechanical treatments have a direct influence on wear performance. However, improvements become limited beyond a certain level of reinforcement. This behaviour is attributed to phase saturation and the deterioration of distribution homogeneity. Zhang and Chen reported similar observations in the wear analyses of graphene-reinforced composites (Mishra et al., 2005). The average steady-state coefficient of friction for specimens subjected to a 30% rolling + recrystallization heat treatment is shown in Figure 12. Although the 30% rolled specimens, the 30% rolled + recrystallized specimens, and the as-cast specimens exhibited similar trends in friction coefficient, the overall steady-state friction coefficient values were lower in the 30% rolled + recrystallized specimens.

Figure 12

Average steady-state friction coefficient of specimens subjected to 30% cold rolling and recrystallization.

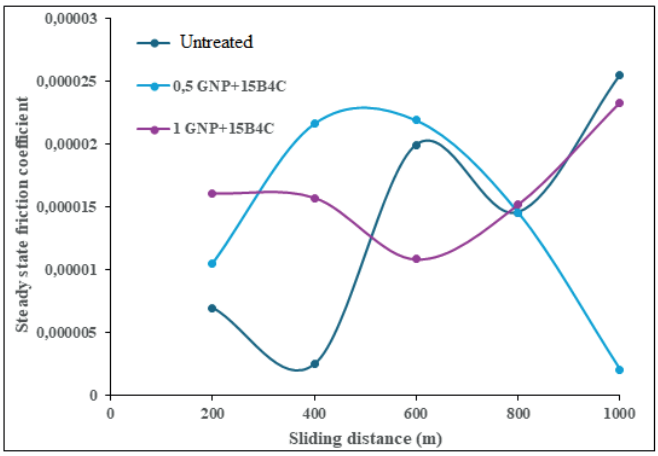

The friction coefficient values obtained from different reinforcement materials and processing routes (as-cast condition, 30% cold rolling, and recrystallization heat treatment) were comparatively evaluated in this study. The friction coefficient is a critical parameter for understanding how surface properties and interfacial interactions influence wear behaviour. Compared with the as-cast matrix material, lower friction coefficient values were generally observed in the hybrid-reinforced composites (0.5% GNP + 15% B_4C and 1% GNP + 15% B_4C). This behaviour may be attributed to the formation of a protective surface film by the reinforcement phases or to increases in microhardness, both of which reduce surface contact (Tang et al.,2017). Similarly, after 30% rolling, notable variations in friction coefficient values were observed depending on the reinforcement type and amount. In particular, the composite containing 1% GNP + 15% B_4C exhibited lower friction coefficients under most loading conditions than the composite containing 0.5% GNP + 15% B_4C, indicating that cold rolling improves reinforcement distribution and enhances frictional resistance. This observation is consistent with the literature, which reports that plastic deformation enhances the homogeneity of reinforcement particle dispersion (Zhou et al., 2018).

In the specimens subjected to recrystallization heat treatment, friction coefficient values were generally lower and more stable. This is attributed to heat treatment's ability to refine and reorganize the grain structure, thereby reducing surface energy and limiting surface wear. The friction coefficient values of the 0.5% GNP + 15% B_4C and 1% GNP + 15% B_4C specimens after heat treatment further indicate a synergistic effect of hybrid reinforcement on surface behaviour (Rajmohan et al., 2013).

Figure 13 presents the SEM images of the dry-sliding wear surfaces of the AA5754 + 0.5% GNP + 15% B_4C + 30% cold rolled + recrystallized composite and the AA5754 + 1% GNP + 15% B_4C + 30% cold rolled + recrystallized composite. In the composite

reinforced with 1% GNP and 15% B_4C, subjected to cold rolling and recrystallization, mild abrasive wear was observed on the worn surface. A high carbon/graphene signal was detected on the worn region, indicating the presence of reduced graphene oxide particles after wear. This suggests that GNP particles detached during wear reattached to the surface, influencing the wear characteristics.

Examination of Figure 13 further shows that adhesive wear dominates the worn surface of the AA5754 + 0.5% GNP + 15% B_4C + 30% cold rolled + recrystallized composite. This adhesion-dominated wear mode is typically associated with the transfer of counter-material particles (originating from the steel ball) onto the specimen surface during sliding.The presence of oxygen in the structure shown in Figure 14 was confirmed by EDX analysis. Regions 1-7 contain high Al levels, corresponding to the matrix. Examination of Figure 14 shows that EDX analysis performed on the worn surface of the AA5754 + 1% GNP + 15% B_4C composite revealed a high carbon content in region 4. The increased elemental carbon content is associated with complete particle fracture and pullout from the matrix, leading to the formation of a brittle interfacial layer and crack-assisted wear. Additionally, carbon detachment from widely distributed B_4C particles contributed to adhesion, thereby increasing the wear rate. In regions labelled 3, the high Mg concentration indicates the formation of a thick MgO layer on the surface, which contributed to increased mass loss.

Figure 13

SEM images of the wear surfaces of the as-cast unreinforced and composite specimens.

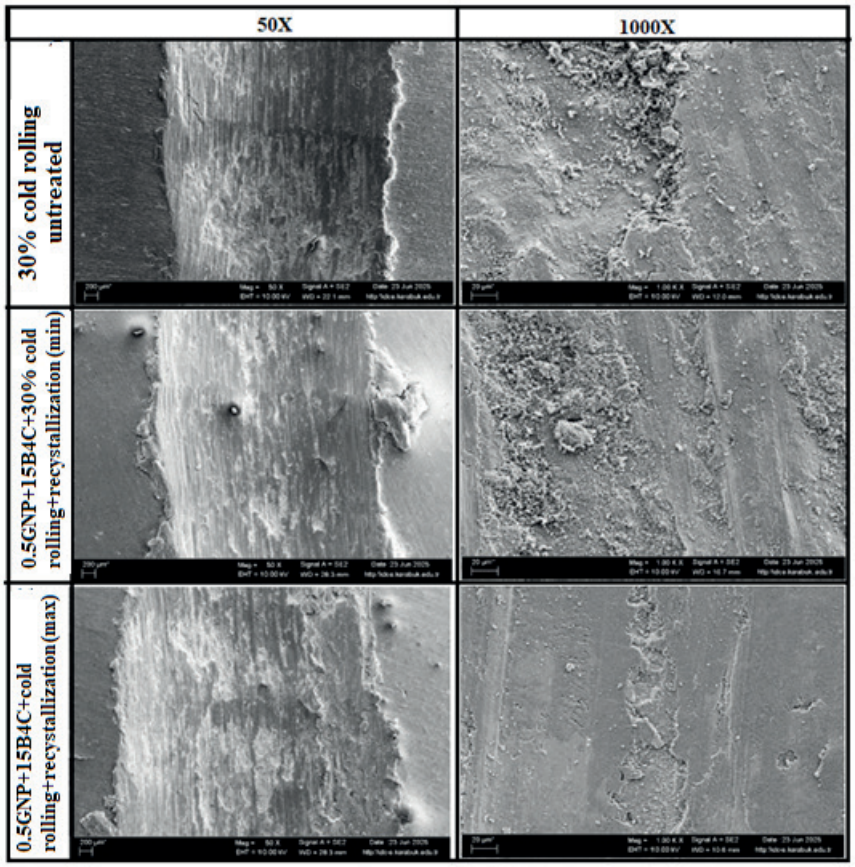

Figure 14

SEM–EDAX elemental analysis of the most severely worn specimen containing 0.5% GNP + 15% B_4C after 30% rolling and recrystallization.

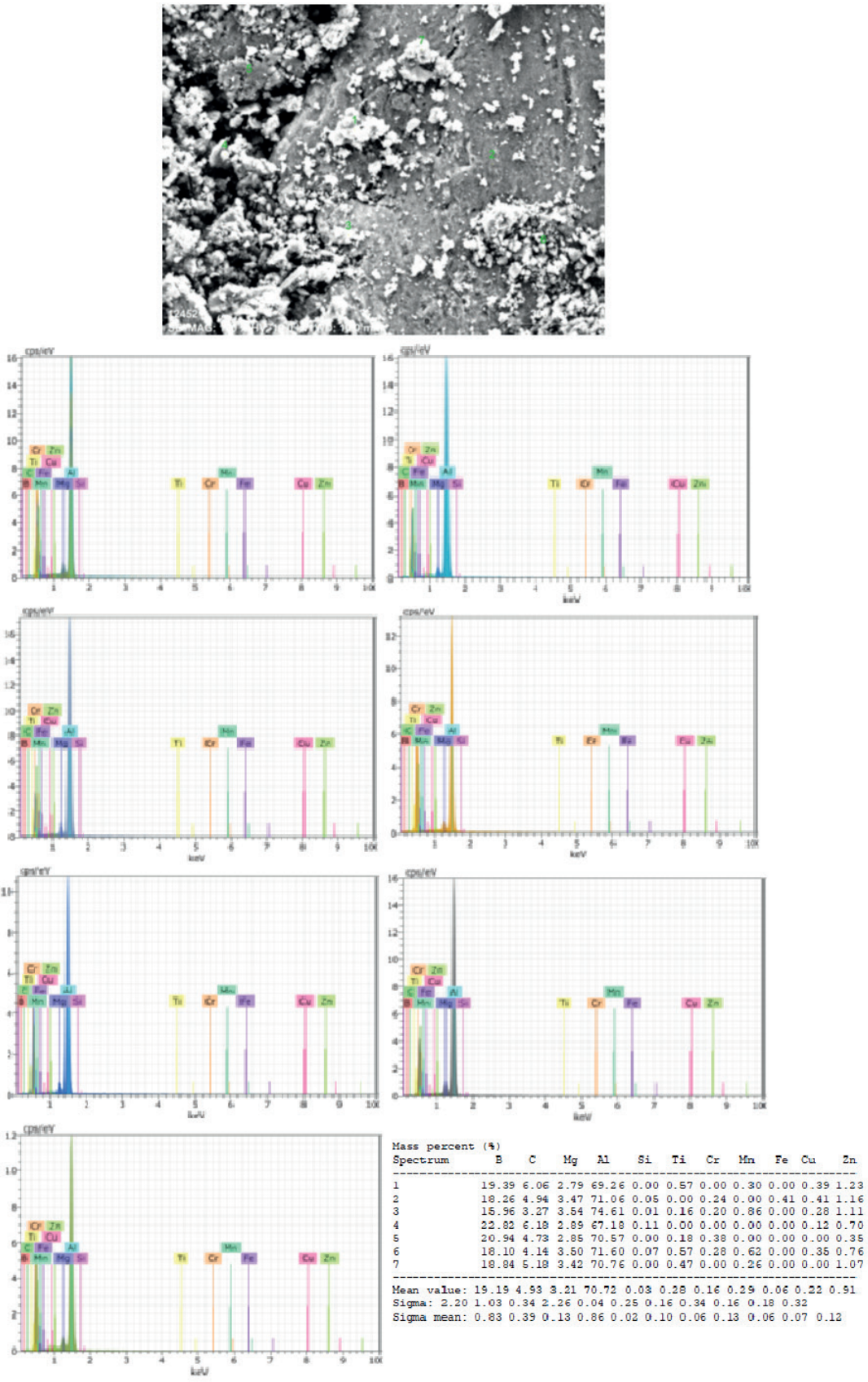

Mass percent (%)

Spectrum	B	C	Mg	Al	Si	Ti	Cr	Mn	Fe	Cu	Zn
1	19.39	6.06	2.79	69.26	0.00	0.57	0.00	0.30	0.00	0.39	1.23
2	18.26	4.94	3.47	71.06	0.05	0.00	0.24	0.00	0.41	0.41	1.16
3	15.96	3.27	3.54	74.61	0.01	0.16	0.20	0.86	0.00	0.28	1.11
4	22.82	6.18	2.89	67.18	0.11	0.00	0.00	0.00	0.00	0.12	0.70
5	20.94	4.73	2.85	70.57	0.00	0.18	0.38	0.00	0.00	0.00	0.35
6	18.10	4.14	3.50	71.60	0.07	0.57	0.28	0.62	0.00	0.35	0.76
7	18.84	5.18	3.42	70.76	0.00	0.47	0.00	0.26	0.00	0.00	1.07
Mean value:	19.19	4.93	3.21	70.72	0.03	0.28	0.16	0.29	0.06	0.22	0.91
Sigma:	2.20	1.03	0.34	2.26	0.04	0.25	0.16	0.34	0.16	0.18	0.32
Sigma mean:	0.83	0.39	0.13	0.86	0.02	0.10	0.06	0.13	0.06	0.07	0.12

The es measured after the 24-hour immersion corrosion test for the specimens subjected

to 30% rolling and recrystallization are presented in Figure 15. Examination of Figure 15 shows that the unreinforced AA5754 specimen experienced a value of 0.01849784 mg/dm². The composite with the highest value was the AA5754 + 0.5% GNP specimen, with a value of 0.02955899 mg/dm². The of the AA5754 + 15% B_4C composite specimen was measured as 0.0202653 mg/dm², while the AA5754 + 0.5% GNP + 15% B_4C composite exhibited a of 0.02937684 mg/dm². The lowest value was observed in the AA5754 + 1% GNP + 15% B_4C composite specimen, at 0.01594177 mg/dm².

Figure 15
of specimens subjected to 30% rolling and recrystallization after the 24-hour immersion corrosion test.

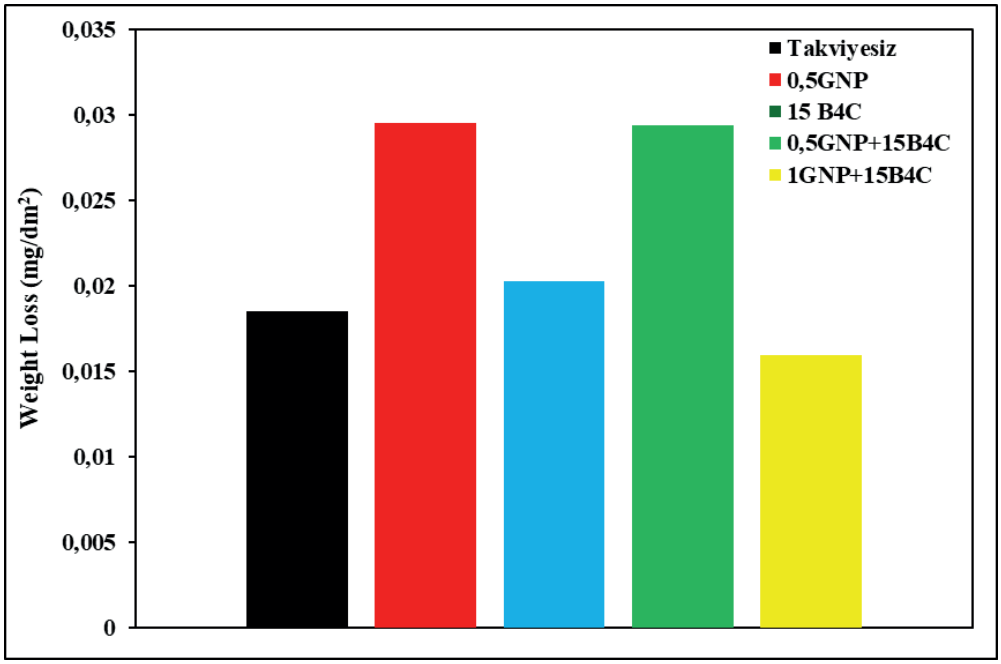

The corrosion behaviour of Al5754 aluminium matrix composites reinforced with different proportions of graphene nanoplatelets (GNP) and boron carbide (B_4C) was evaluated in this study using the immersion method. The tests were carried out on specimens subjected to 30% rolling followed by recrystallization heat treatment. The corrosion rate (mg/dm²), calculated from, was used as the basis for discussion. In immersion tests using a more aggressive solution prepared by adding HCl to NaCl, the acidic medium rapidly activated the electrochemical cells, leading to significant mass loss. This finding is consistent with the literature, which reports that aluminium alloys exhibit more severe localized corrosion (particularly pitting corrosion) in NaCl + HCl environments (Nagaral et al., 2015, El Garchani et al., 2024).

Among the as-cast composites, the lowest corrosion rate was observed in the unreinforced Al5754 specimen, at 0.011 mg/dm². The addition of individual GNP and/or B_4C to the Al5754 matrix increased corrosion rates. The highest corrosion rate, 0.029 mg/dm², was recorded for the Al5754 + 0.5% GNP composite. This behaviour can be explained

by the possibility that GNP promotes the formation of anodic–cathodic cells, thereby accelerating microgalvanic corrosion (Zheng et al.,2021). Interestingly, however, in the composites containing Al5754 + 0.5% GNP + 15% B_4C and Al5754 + 1% GNP + 15% B_4C, the increase in corrosion rate remained more limited, and the corrosion values were comparatively lower. This suggests that a synergistic interaction between GNP and B_4C may partly contribute to improved corrosion resistance.

The observed increase in corrosion rate in specimens subjected to 30% cold rolling can be attributed to the higher density of grain boundaries, accumulation of internal stresses, and formation of microcracks during cold rolling, which increases the surface area exposed to the corrosive medium (Yu et al., 2018). Notably, the Al5754 + 0.5% GNP composite exhibited a markedly higher corrosion rate of 0.050 mg/dm². The heterogeneous distribution of GNP on the surface and the microstructural differences it introduces may contribute to this increase.

In the specimens subjected to 30% rolling followed by recrystallization heat treatment, a reduction in corrosion rates was observed in some cases. This can be attributed to heat treatment's ability to relieve microstresses, reorganize grain boundaries, and improve surface homogeneity (Tang et al.,2017). For example, the corrosion rate of the 30% cold-rolled unreinforced AA5754 specimen decreased to 0.018 mg/dm², whereas the AA5754 + 1% GNP + 15% B_4C composite exhibited the lowest corrosion rate at 0.015 mg/dm². This result indicates that the appropriate combination of reinforcement content and recrystallization heat treatment can enhance corrosion resistance. When used alone, GNP may reduce corrosion resistance due to microgalvanic cell formation; however, its use in combination with B_4C may help mitigate this effect. The 30% cold rolling process increases structural stresses and surface defects, thereby increasing corrosion rates; therefore, an appropriate post-cold rolling heat treatment is essential. The AA5754 + 1% GNP + 15% B_4C composite, after 30% cold rolling and recrystallization, exhibited the best corrosion resistance and can be considered the optimum reinforcement combination.

Figures 16 and 17 show that, at the beginning of the test, the primary corrosion attack in both undeformed and deformed specimens occurred around Si-rich intermetallic particles, while Fe-rich particles remained unreactive. Local corrosion around Si-rich constituents led to cavitation around these particles, consistent with previous observations (Eckermann et al.,2008). As exposure time increased, crystallographically enlarged pits were observed more frequently in the original material compared with the deformed regions. Such crystallographically enlarged pits, bounded by steep walls of the crystal lattice, have been reported in Al and Al alloys, and their pit-growth kinetics have been previously described (Eckermann et al.,2008; Zaid et al., 2008). Furthermore, in acidic chloride-containing solutions, corrosion tunnelling has been identified as the dominant mode of pit propagation (Eckermann et al.,2008).

Considering the corrosion behaviour in chloride-containing solutions, the chemical composition of coarse particles is also essential. The Si-rich coarse intermetallic observed in AA5754 also contained Mg and Al. Previous reports have clearly shown that Mg dissolves rapidly from intermetallic particles during exposure, leading to their rapid disintegration (Yasakau et al., 2007; Zhu et al., 2018). The findings of earlier studies (Zhu et al., 2018, Zheng et al.,2020) explain the dissolution mechanism of Mg and Al from coarse particles predominantly composed of Mg and Si in Al–Mg–Si alloys. The results of this investigation demonstrate that, at the beginning of immersion, preferential and selective dissolution of Mg occurs, which alters the Volta potential of the particle. This transformation changes the nature of Mg-containing particles from anodic to cathodic, thereby forming a galvanic couple with the Al matrix. As these locally formed galvanic cells approach equilibrium, the cathodic particle promotes the galvanic dissolution of the anodic matrix, resulting in matrix corrosion.

The increased dislocation density near the coarse particles promotes corrosion reactions, leading to more pronounced trench formation around Mg- and Si-rich particles. This behavior is attributed to the higher dislocation density formed in the bent (deformed) region of the specimen, which, due to its less regular structure, facilitates the propagation of deeper pits (Brunner et al.,2010, Pouraliakbar et al., 201).

Figure 16

SEM–EDAX elemental analysis of the surface of the as-cast unreinforced specimen, showing the lowest corrosion.

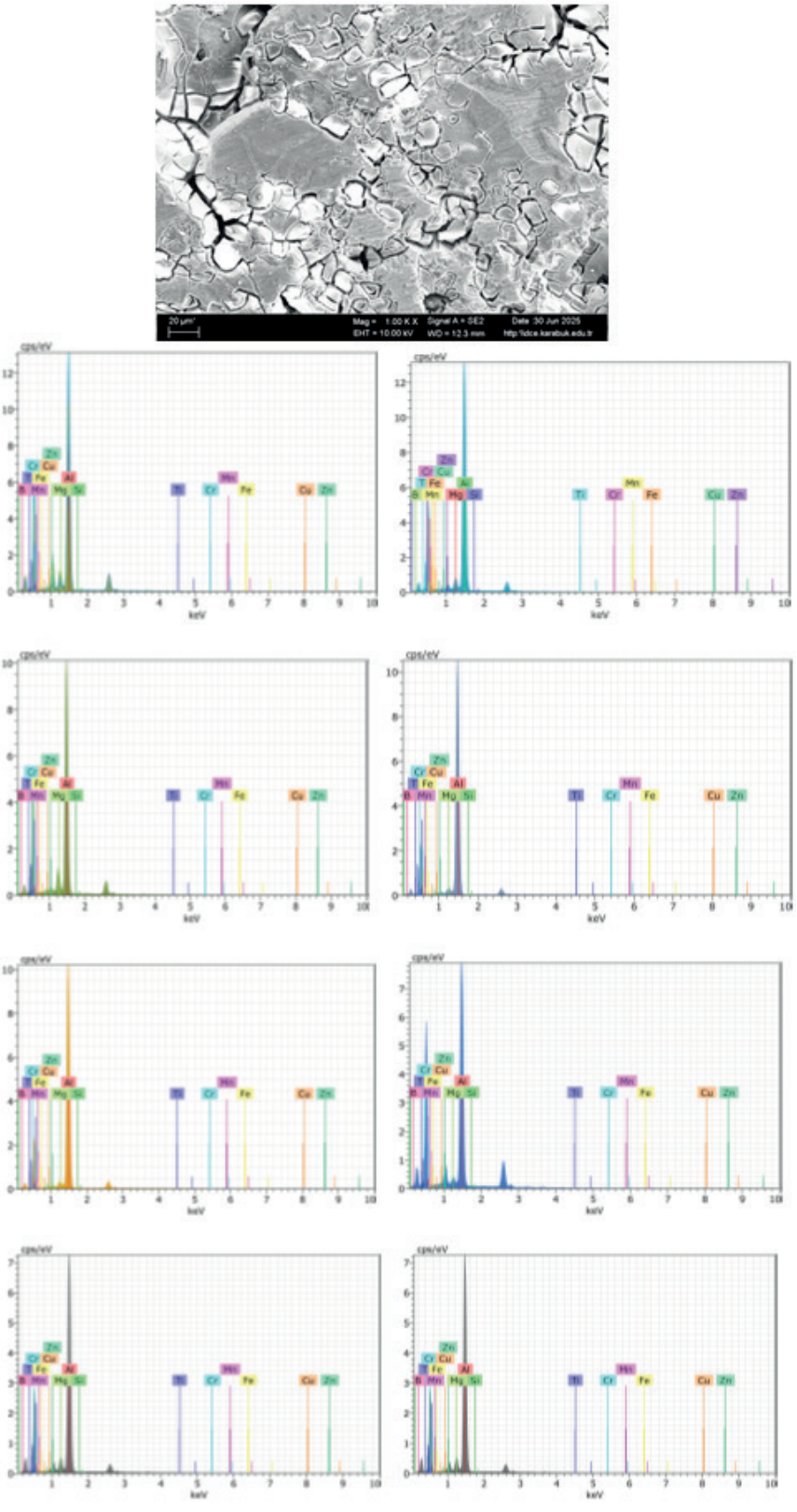

Figure 17

SEM–EDAX elemental analysis of the surface of the AA5754 + 15% B_4C composite specimen rolled by 30% showing the lowest corrosion.

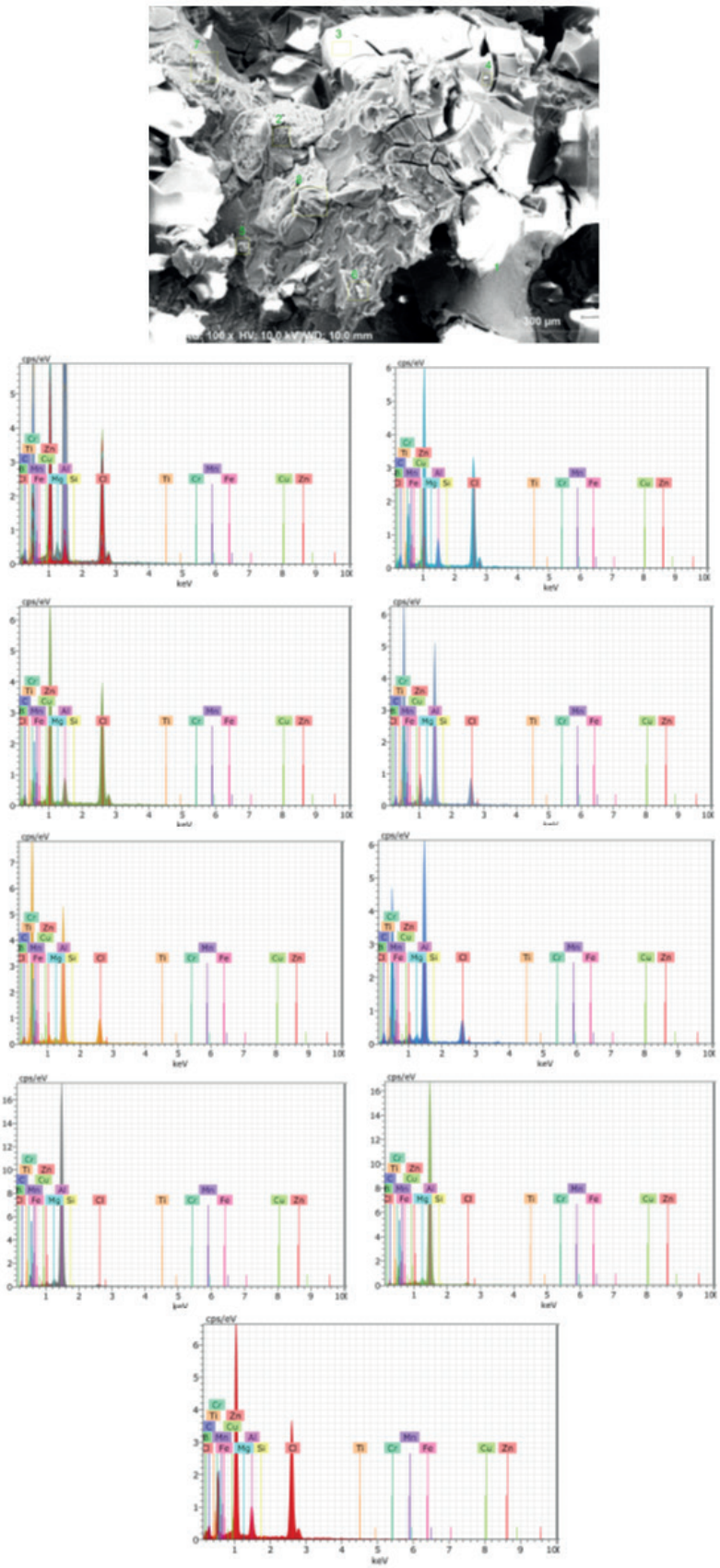

Acknowledgement

This study was supported by Karabük University Scientific Research Projects Coordination with the project code KBÜBAP-24-YL-110. The authors would like to thank the KBÜ-BAP unit for their financial support. They would also like to thank Hiba Waleed Hamid HAMID for his contributions.

References

Alaneme, K.K., Babalola, S.A., Bodunrin, M.O., Chown, L.H., Okotete, E.A., Maledi, N.B. (2021) Hot deformation of nickel particles reinforced aluminium based composites: flow behaviour, microstructural evolution and processing map analyses, Mater. Res. Express, 8, 016510. (https://doi.org/10.1088/2053-1591/ABD5A3)

Asthana, R., Tewari, S.N., Lin, N.T.(2006) Metal-matrix composites, Mater. Sci. Eng., 23, 53–64.

Baradeswaran, A., Vettivel, S.C., Perumal, A.E., Selvakumar, N., Issac, R.F. (2014) Experimental investigation on mechanical behaviour, modelling and optimization of wear parameters of B4C and graphite reinforced aluminium hybrid composites, Mater. Des., 63, 620-632.

Blawert, C., Hort, N., Kainer, K.U. (2004) Automotive applications of magnesium and its alloys, Trans. Indian Inst. Met., 57(4), 397–408.

Brunner, J.G., May, J., Höppel, H.W., Göken, M., Virtanen, S. (2010) Localized corrosion of ultrafine-grained Al-Mg model alloys, Electrochim. Acta, 55, 1966–1970.

Chawla, N., Chawla, K.K. (2006) Metal matrix composites, J. Mater. Sci., 41(3), 793–815.

Del Monte, F., Bernal, M.M., Wenk, H.R. (1999) Metal matrix composites processed by powder metallurgy, Mater. Sci. Forum, 312–314, 453–460.

Eckermann, F., Suter, T., Uggowitzer, P.J., Afseth, A., Schmutz, P. (2008) The influence of MgSi particle reactivity and dissolution processes on corrosion in Al-Mg-Si alloys, Electrochim. Acta, 54, 844–855.

El Garchani, F.E., Kabiri, M.R., Moulay, R. (2024) Effects of heat treatment on the corrosion behavior and mechanical properties of aluminum alloy 2024, ResearchGate Preprint, 1356–1370.

Hamid, H.W.H., Çetin, M., Ahlatçı, H., Al-Mekhlafi, O.H.S. (2025) Karıştırma döküm yöntemiyle nano boyut takviyeli metal matrisli hibrit kompozit üretimi, 10. Latin Amerika Uluslararası Bilimsel Araştırmalar Konferansı, Havana, ISBN: 978-625-5962-70-6.

Kumar, S., Srivastava, V.C. (2015) Effect of rolling deformation on wear behavior of Al-

based composites, Mater. Sci. Eng. A, 628, 152–160.

Liu, J., Zhao, Z., Gao, F., Liu, C., Liu, X., Li, C., Zhang, Y. (2024) Effects of Rolling Deformation on the Microstructure and Properties of GNPs/2024Al Composite Materials, Prot. Met. Phys. Chem. Surf., 60(4), 734–742. (https://doi.org/10.1134/S207020512470206X)

Liu, J., Zhao, Z., Gao, F., Liu, C., Liu, X., Li, C., Zhang, Y. (2024) Effects of rolling deformation on the microstructure and properties of GNPs/2024Al composite materials, Protection of Metals and Physical Chemistry of Surfaces, 60(4), 734–742.

Liu, J.H., Khan, U., Coleman, J., Fernandez, B., Rodriguez, P., Naher, S., Brabazon, D. (2016). Powder processing methodology for production of graphene oxide reinforced aluminium matrix composites, Mater. Des., 94, 87, (https://doi.org/10.1080/2374068X.2016.1244389)

Luo, A.A. (2013) Magnesium casting technology for structural applications, J. Magnes. Alloys, 1, 2–22.

Ma, Y.L., Xiong, H.W., Chen, B.Y.(2020) Preparation and corrosion resistance of short basalt fiber/7075 aluminum composite, Mater. Corros., 71, 1824. (https://doi.org/10.1002/maco.202011771)

Mishra, R.S., Ma, Z.Y. (2005) Friction stir welding and processing, Mater. Sci. Eng. R Rep., 18, 1-78.

Miyazaki, T., Matsuura, H. (2004) Development and applications of metal matrix composites, J. Mater. Sci., 39, 4289–4295.

Monticelli, C., Zucchi, F., Bonollo, F., Brunoro, G., Frignani, A., Trabanelli, G. (2019) Application of Electrochemical Noise Analysis to Study the Corrosion Behavior of Aluminum Composites J. Electrochem. Soc., 142, 405. (https://doi.org/10.1149/1.2044035)

Nagaral, M., Attar, S., Reddappa, H.N., Auradi, V., Kumar, S.S., Raghu, S. (2015) Mechanical Behavior of Al7025- B4C Particulate Reinforced Composites, J. Appl. Mech. Eng., 4(6), 1000186.

Pouraliakbar, H., Jandaghi, M.R., Khalaj, G. (2017) Constrained groove pressing and subsequent annealing of Al-Mn-Si alloy: Microstructure evolutions, crystallographic transformations, mechanical properties, electrical conductivity and corrosion resistance, Mater. Des., 124, 34–46.

Prakash, A., Gupta, M. (2011) Processing and properties of rare-earth reinforced Mg-based composites, Mater. Sci. Eng. A, 528, 4489–4494.

Rajmohan, T., Palanikumar, K., Shankar, S. (2013) Development of hybrid metal

matrix composites through stir casting – Statistical analysis of friction and wear characteristics, Mater. Des., 48, 92–97.

Rebba, B., Ramanaiah, N. (2014) Studies on mechanical properties of 2024 Al-B4C composites, Adv. Mater. Manuf. Character., 4(1), 42-46.

Sathish Kumar, G., Rajaguru, K., Ramkumar, R., Ranjithkumar, M. (2020) Evaluation of Al-C-B4C composites fabricated by powder metallurgy for hardness and wear behaviour, K. Ramakrishnan College of Technology, Tiruchirappalli, 621112, India.

Sivakaruna, G., Babu, P.S. (2017) A Survey on effects of reinforcement on aluminum metal matrix composites, Int. J. Mech. Eng. Technol., 8(9), 112-131.

Tang, L., Zhang, C., Zhang, Y., Xie, H. (2017) Graphene reinforced aluminum matrix composites with enhanced tribological properties, Wear, 376-377, 653–659.

Tang, L., Zhang, C., Zhang, Y., Xie, H. (2017) Graphene reinforced aluminum matrix composites with enhanced tribological properties, Wear, 376–377, 653–659.

Tjong, S.C. (2007) Recent progress in development and properties of novel metal matrix nanocomposites reinforced with carbon nanotubes and graphene nanosheets, Mater. Sci. Eng. R Rep., 45(1-2), 1–88.

Wang, L.W., Zhang, Y., Su, Y., Li, J. (2021) Initial corrosion behavior and mechanism of 7B04 aluminum alloy in NaCl solution, Trans. Nonferrous Met. Soc. China, 31(4), 1000–1010.

Yasakau, K.A., Zheludkevich, M.L., Lamaka, S.V., Ferreira, M.G.S. (2007) Role of intermetallic phases in localized corrosion of AA5083, Electrochim. Acta, 52, 7651–7659.

Yu, F., Camilli, L., Wang, T., Mackenzie, D.M.A., Curioni, M., Akid, R., Bøggild, P. (2018) Complete long-term corrosion protection with chemical vapor deposited graphene, arXiv Preprint, arXiv:1805.05102, 1–10.

Zhang et al., 2017-14. Zhang, Y., Wang, X., Wang, L. (2017) Microstructure and mechanical properties of graphene nanoplatelets reinforced AZ magnesium alloy composites, Compos. Part B Eng., 109, 19–26.

Zhang, X., Chen, D. (2014) Microstructure and wear properties of graphene/aluminum composites, Compos. Part A Appl. Sci. Manuf., 66, 107–115.

Zhang, Z., Chen, G., Wang, Y. (2020) Powder metallurgy of magnesium matrix composites: A review, J. Mater. Sci. Technol., 40, 42–56.

Zheng, S., Li, C., Zhang, Y., Xiang, T., Cao, Y., Li, Q., Chen, Z. (2021) A general strategy towards superhydrophobic self-cleaning and anti-corrosion metallic surfaces: An example with aluminum alloy, Coatings, 11(7), 788.

Zheng, Y.Y., Luo, B.H., He, C., Gao, Y., Bai, Z.H. (2020) Corrosion evolution and behaviour of Al–2.1Mg–1.6Si alloy in chloride media, Rare Met..

Zhou, W., Xu, Z., Liu, C. (2018) Effect of rolling process on the tribological properties of particle-reinforced aluminum composites, Mater. Sci. Eng. A, 710, 92–100.

Zhu, Y., Sun, K., Frankel, G.S. (2018) Intermetallic Phases in Aluminum Alloys and Their Roles in Localized Corrosion, J. Electrochem. Soc., 165, C807–C820.

About Thhe Authors

Melik ÇETİN is a Professor of Metalurgical and Materials Engineering at Karabuk University. He has a Master's and doctoral degree in Metal Education from Gazi University. His main areas of interest are casting technology, corrosion and wear behaviors, and composite materials.
Email: mcetin@karabuk.edu.tr, **ORCID:** 0000-0002-6952-2523

Hayrettin AHLATCI is a Professor of Metalurgical and Materials Engineering at Karabuk University. He has a Master's and doctoral degree in Metalurgical and Materials Engineering from İstanbul Technical University. His main areas of interest are the mechanical behavior of materials, corrosion and wear, casting technology, and composite materials.
Email: hahlatci@karabuk.edu.tr, **ORCID:** 0000-0002-6766-4974

Dr. Kenza DJEBARI is a Materials Engineer with a Ph.D. in Metallurgical and Materials Engineering from Karabük University and an M.Sc. in Computational Pharmaceutical Chemistry. Her work focuses on alloy development, corrosion behavior of biodegradable metals, and microstructural and mechanical characterization.
Email: kenzadjebari@gmail.com, **ORCID:** ORCID: 0000-0003-0158-4741

Similarity Index

The similarity index obtained from the plagiarism software for this book chapter is 10 %.

Investigation of The Effect of Surface Hardening Process Applied to Crankshafts on Mechanical Properties

Yavuz SUN
Karabük University

Hayrettin AHLATÇI
Karabük University

To Cite This Chapter:
Sun, Y., & Ahlatci, H. (2025). Investigation of the effect of surface hardening process applied to crankshafts on mechanical properties. In H. Gokmese, S. Bulbul, & Y. Uzun (Eds.), *Innovative approaches in materials science and applications* (pp. 128–137). ISRES Book Series. ISRES Publishing.

Introduction

The crankshaft is the metal rod on which the engine pistons are mounted. The crankshaft converts the linear motion from the pistons into rotary motion using a simple formula, thus becoming the primary hub for all rotational power transmitted to the wheels. Nitriding is the diffusion of nitrogen onto the steel surface, resulting in the formation of a hard, highly wear-resistant layer on the material's surface. Every material has a nitriding capability. Nitriding increases corrosion resistance and fatigue strength in some steels (Polat et al., 2011; Winter et al., 2013; Chen et al., 2019).

Wear is one of the types of damage that reduces the operating efficiency of machine elements and increases production costs. With the advancement of technology from past to present, the operating tolerances of machine elements have decreased significantly, more complex and precise parts are needed, and damage investigations due to wear have become very important as a result of the necessity to work with low error in the aviation, space and defense fields (Castro et al., 2007; Whitney et al., 1986).

This study investigated the effects of gas nitriding on the mechanical properties of a crankshaft. For this purpose, the crankshaft was subjected to gas nitriding at 520°C for 15 hours. Following the gas nitriding process, hardness and microstructure characterization studies were conducted separately on unnitrated and nitrided samples. Wear tests on the examined samples were conducted in a reciprocating wear tester under loads of 20N, 40N, and 60N. The tests revealed that the nitriding process applied to the crankshafts resulted in an approximately 20% increase in the wear resistance of the examined samples.

Materials and Methods

Gas Nitration

The chemical composition of the crankshaft used in the studies is given in Table 1. The

nitriding process of the steels was carried out at the Manksan A.Ş. facilities. The process involved nitriding to prevent white layer formation. The nitriding process was carried out in the oven shown in Figure 1. under an ammonia atmosphere at 520°C for 15 hours.

Table 1

Chemical analysis results of the examined sample

C	Si	Mo	Cr	Mn	P	S
0,41	0,33	0,19	0,99	0,62	0,021	0,019

In the gas nitriding process, ammonia gas is introduced into the furnace. The system calculates the adequacy of the gas based on the furnace volume and the delivered gas flow. The furnace heats up to 520°C in approximately four hours. To achieve the Kn value, which depends on the amount of ammonia decomposition during all process steps, the system's temperature and gas flow are controlled. Additionally, the ammonia decomposer in the furnace breaks down the ammonia. When the temperature reaches 520°C, the nitriding process begins. Meanwhile, the ammonia released into the environment continues to decompose. After the nitriding process, the cooling fan is automatically activated, and the system cools to 100°C in approximately four hours. The entire nitriding process takes approximately 23 hours; however, the actual nitriding time is 15 hours, excluding the system's heating and cooling periods.

Figure 1

Gas nitriding furnace and its working principle

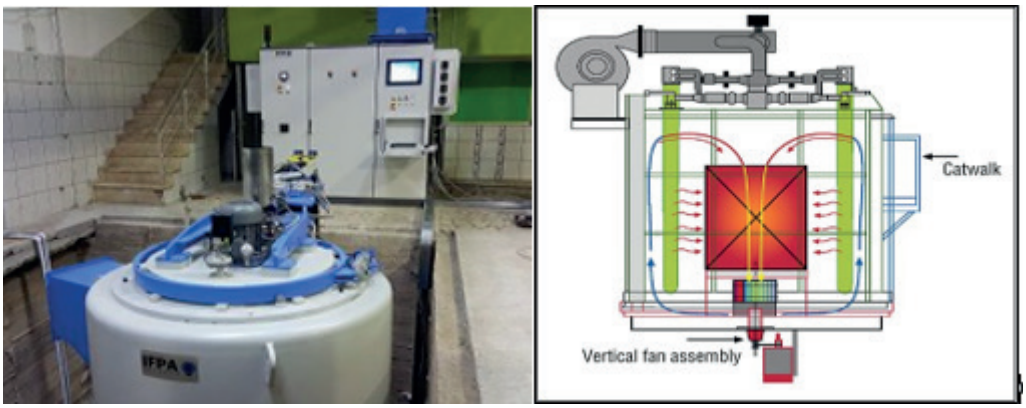

Microstructural And Mechanical Characterization

For metallographic processing, a 25x15x10 mm sample was cut from the crankshaft. The prepared samples were prepared for polishing by grinding to a 400-2500 mesh and polished with 3 micron Al2O3. Microstructure images were taken after etching with 3% nital. Microstructure images were taken longitudinally and in cross-section using a Nikon Eclipse 200 optical light microscope (Figure 2).

Figure 2

Sanding device (a) and optical microscope (b)

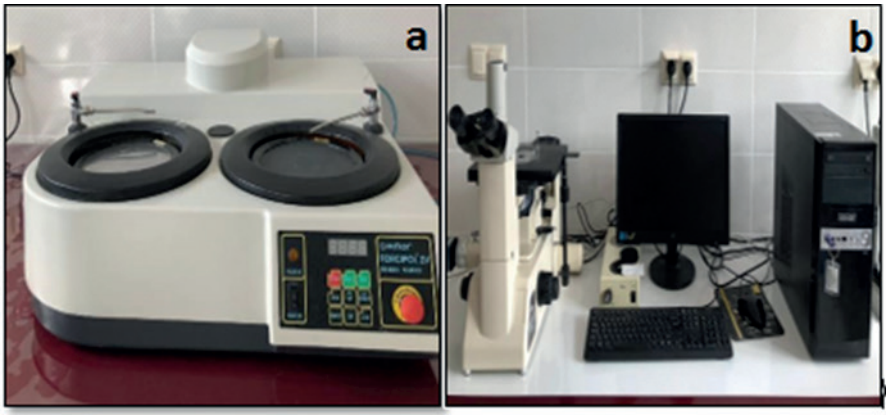

Hardness measurements were taken on the surface of nitrided crankshaft samples using a Vickers hardness tester at five different loads ranging from 0.20 to 5 kg. A picture of the test device is shown in Figure 3. During the test, hardness was measured at HV 0.5 using a diamond square pyramid tip with a 136° apex angle.

Figure 3

Vickers Hardness Tester

During the wear tests of the examined samples, 100Cr6 ball bearings and a 25x15x10 mm test sample were used as counter materials. The samples were designed to travel an average of 3 m under loads of 20N, 40N, and 60N. Dry-weather wear tests were conducted on the reciprocating wear device shown in Figure 4. Before and after the tests, the samples were weighed on an electronic scale with a precision of 0.0001 g, and the test results were evaluated according to weight loss. After the wear tests, the sample surfaces were examined with a scanning electron microscope (SEM) to determine the wear mechanisms, and surface roughness was measured with a profilometer.

Figure 4

Reciprocating wear device

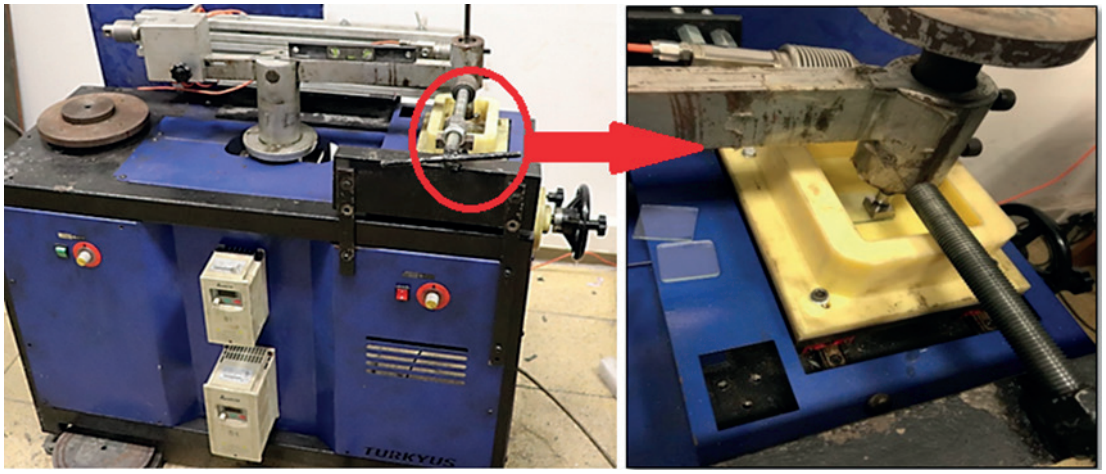

Characterization Results and Discussion

The microstructure images of the steel examined before and after nitriding are given in Table 2. An examination of the figure reveals tempered martensite phases in the pre-nitridation microstructure. An examination of the post-nitridation microstructure images (Table 2) reveals a more equiaxed grain structure. This is thought to be due to the nitriding process being carried out at 520°C and then slowly cooling to 100°C over 4 hours.

Table 2

Optical Microscope (LOM) and Scanning Electron Microscope (SEM) images of the examined alloys

	Non-nitrided	Nitrided
LOM	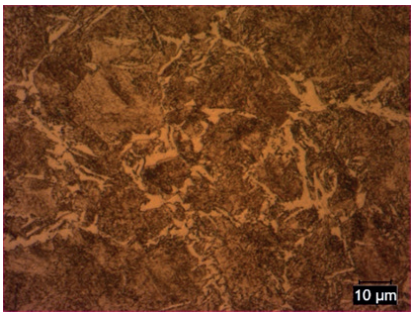	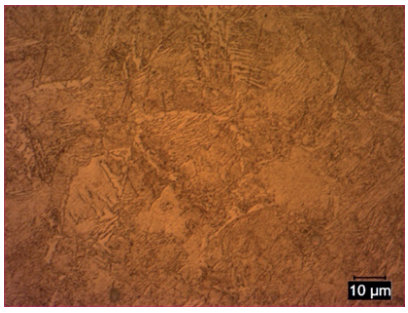
SEM	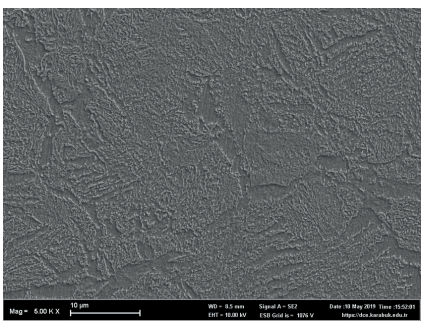	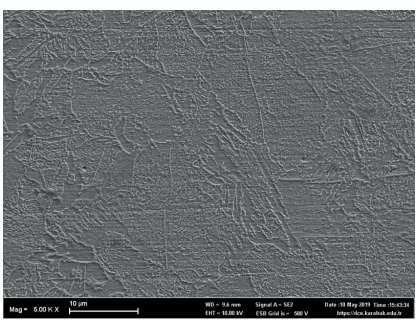

As mentioned in the literature, the low amount of strong nitride formers such as Cr and

Mo in the chemical composition of the crankshaft sample and the complete absence of V in the chemical analysis play a major role in the absence of a diffusion layer. The average thickness of the white layer seen in Figure 5 was measured as 23 µm. The SEM images shown in Figure 6 also support this view.

Figure 5

Optical microscope image of the nitriding layer.

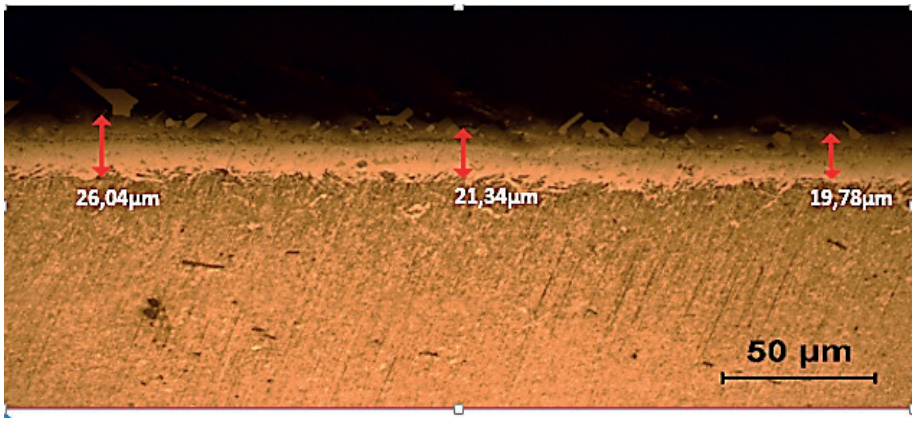

Figure 6

SEM image of the nitriding layer.

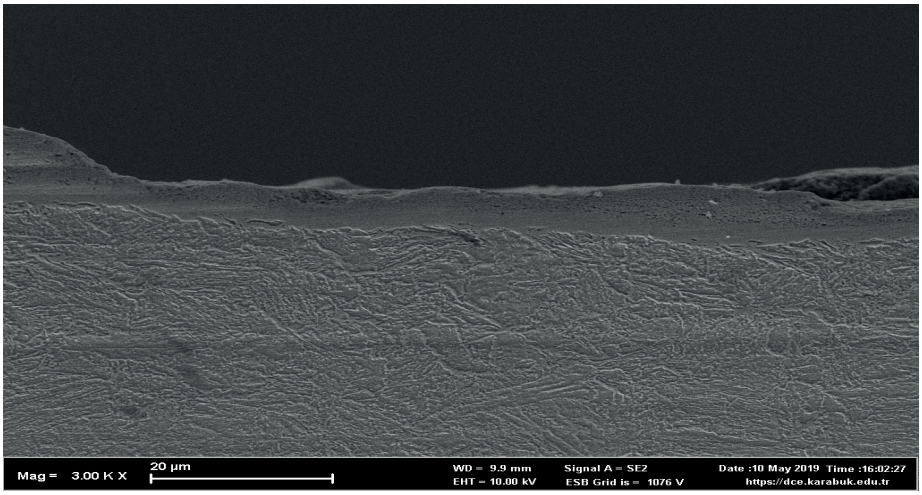

The average hardness value of the examined crankshafts without nitriding is 384 HV0.5. Table 3 shows the hardness values and indentation depths of the nitrided samples at different loads. A Vickers hardness indentation taken from the surface of the nitrided sample under a 5 kg load indicates that the indentation layer has passed through and reached the base material.

Table 3

Hardness results obtained from the nitriding layer

Applied Load	Hardness	Trace Depth (µm)
0,20	741	4,52
0,50	549	8,30
1,00	471	12,69
5,00	416	30,09

In the study, wear tests were applied to nitrided and non-nitrided crankshafts under 20-60N loads and a sliding distance of 1-4 m. As a result of the wear test, weight losses were determined before and after the test using an electronic scale with a sensitivity of 0.0001 g (0.1 mg) and were proportional to the sliding distance. Figure 7 shows the weight loss graph for the non-nitrided material, while Figure 8 shows the weight loss graph for the nitrided sample.

Figure 7

Weight loss graph of samples non-nitrided

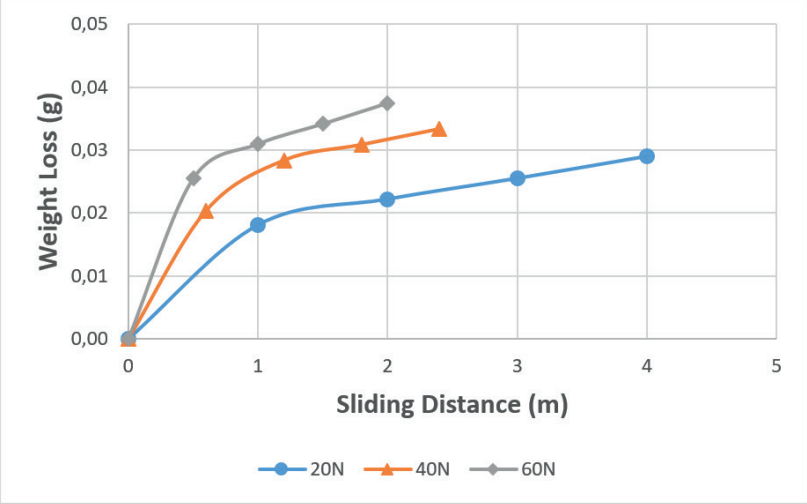

As seen in Figure 7, the non-nitrided samples experienced a weight loss that initially increased up to 1 meter and then varied linearly with the applied load and distance travelled. An examination of the weight loss graph of the nitrided samples (Figure 8) reveals a weight loss that varies linearly with the applied load and distance traveled. Examining these figures, it can be concluded that the nitrided samples exhibited less weight loss compared to the non-nitrided samples. The wear resistance of the sample increased by approximately 20% after the nitriding heat treatment. The wear behaviour of the examined crankshaft depends on the applied nitriding heat treatment, the applied load, and the hardness of the crankshaft. As a result, the hardness of the crankshaft increases, and therefore, its wear resistance also increases (Telesang et al., 2015; Uzun, 2002).

As the distance traveled during the wear test on crankshaft samples increases, weight loss increases. Wear rates were calculated by proportioning these weight losses to the sliding distance. Figure 9 shows the wear rate graph.

Figure 8

Wear rate graph depending on applied load

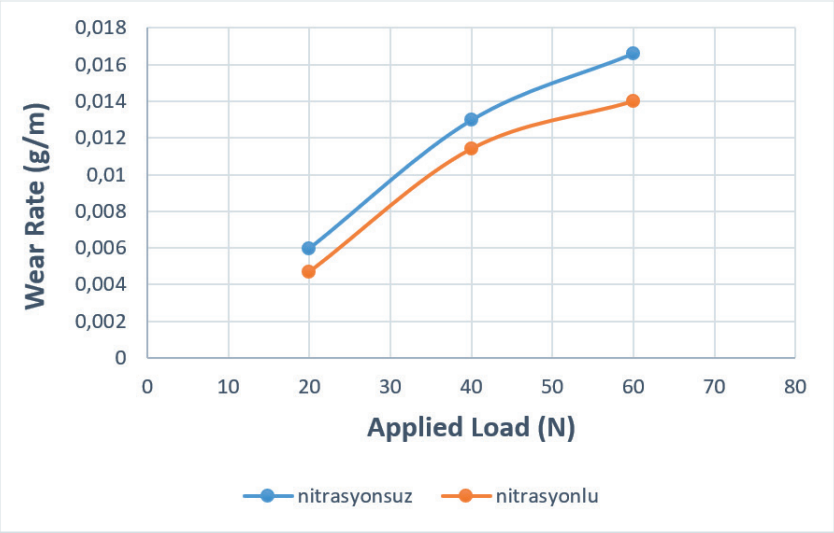

SEM images and EDX results of the worn surfaces of the non-nitrated and nitrided samples subjected to wear under 20 N and 60 N loads after the wear test are given in Tables 4 and 5, respectively. The samples subjected to wear under a 20 N load were relatively narrow and shallow in depth. The samples subjected to wear under a 60 N load were observed to have wider and deeper scars.

Figure 9

Weight loss graph of nitrided samples

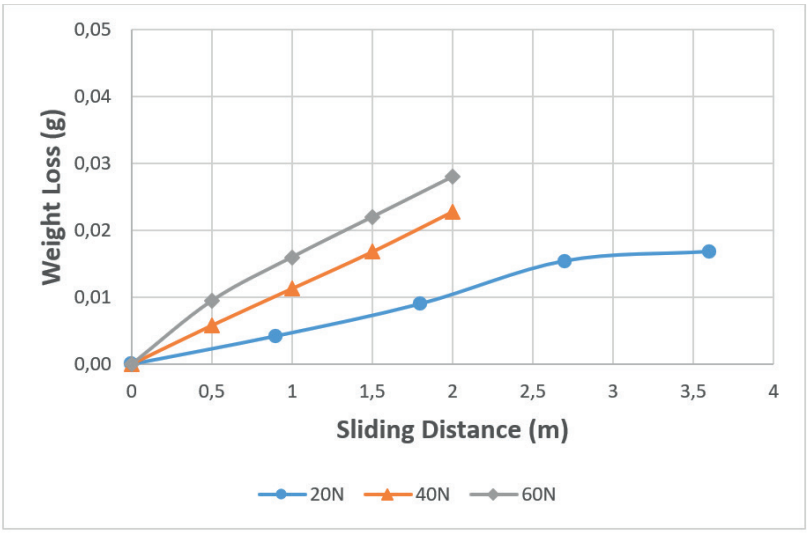

Table 4

SEM Image and EDX Results of Worn Surface for Non-Nitrided Samples

	SEM	EDS

20 N

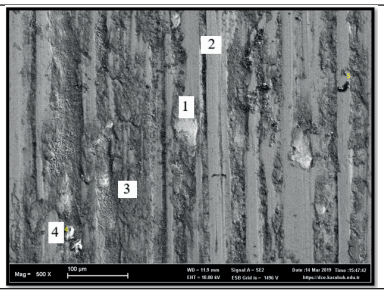

Selected Points	C	N	O	Na	S	CI	Cr	Mn	Fe
1	13.68	2.27	42.36	0.73	0.08	0.12	0.12	0.56	40.08
2	3.70	0.65	0.27	0.10	0.02	0.17	0.26	1.03	93.80
3	14.43	1.36	37.86	0.75	0.20	0.47	0.17	0.00	44.75
4	59.65	12.28	22.10	1.91	0.88	0.90	0.00	0.56	1.72

60 N

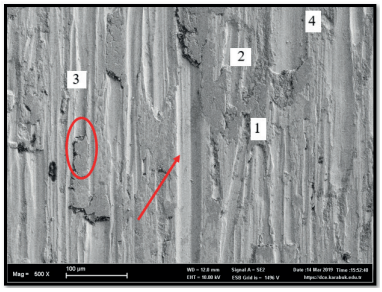

Selected Points	C	N	O	Na	S	CI	Cr	Mn	Fe
1	2.69	1.16	31.68	0.00	0.07	0.00	0.00	0.00	64.40
2	48.40	5.03	29.68	6.35	0.64	5.71	0.06	0.10	4.02
3	3.70	1.38	2.80	0.45	0.01	0.09	0.00	0.11	91.47
4	71.48	5.02	19.07	0.74	0.96	1.17	0.00	0.31	1.25

Table 5

SEM Image and EDX Results of Worn Surface for Nitrided Samples

	SEM	EDS

20 N

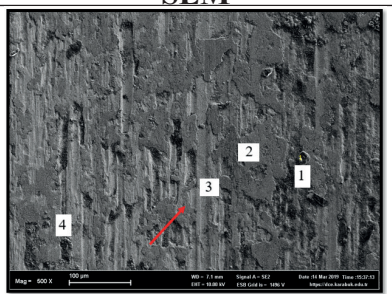

Selected Points	C	N	O	NA	S	CI	Cr	Mn	Fe
1	48.81	10.01	14.66	2.74	0.71	18.63	0.00	0.41	4.03
2	4.02	1.08	30.94	0.02	0.00	0.02	0.34	0.27	63.32
3	5.20	0.96	7.42	0.00	0.05	0.00	0.11	0.66	85.60
4	18.88	0.00	18.36	0.26	0.00	0.78	0.36	0.25	61.10

60 N

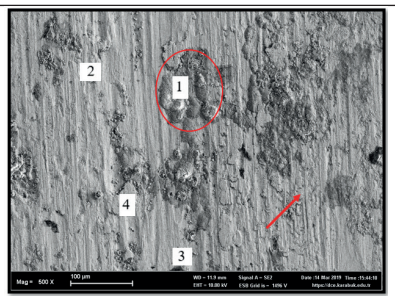

Selected Points	C	N	O	Na	S	Cl	Cr	Mn	Fe
1	8.80	2.70	44.47	0.27	0.00	0.53	0.23	0.00	43.01
2	17.73	2.55	3.22	0.23	0.04	0.38	0.03	1.65	74.17
3	58.55	13.50	21.33	0.61	0.77	1.84	0.44	0.00	2.97
4	2.95	0.76	11.19	0.00	0.00	0.08	0.17	0.63	84.21

In nitrided samples, under low and high loads, mild adhesion fracture marks were observed, and fine grooves formed at the location marked with the arrow in Table 5 (20N). In non-nitrated samples, under high loads, fragments broke off from the surface in the circled area (60N) in Table 4, and coarse grooves formed at the location marked with the arrow indicate excessive fracture. While deep and wide grooves formed after abrasion in the non-nitrated sample (Table 4) under a 60N load, finer grooves were

observed in the nitrided sample marked with the arrow in Table 5. Furthermore, under a 60N load, localized abrasive tearing and ruptures occurred in the nitrided sample, and it was determined that an oxide film had formed on the surface following this localized abrasion test. The formation of the oxide film increased wear resistance. The formation and propagation of surface cracks with a high degree of fracture at high loads are symptoms of fragment breakage resulting from the formation and propagation of severely fractured surfaces (Uma et al., 1999; Wang et al., 2020; Qiang et al., 2000).

Acknowledgement

This study was supported by Karabük University Scientific Research Projects Coordination with the project code FDT-2019-2104. The authors would like to thank the KBÜ-BAP unit for their financial support. They would also like to thank Emre Küçük for his contributions.

References

Castro, G., Fernández-Vicente & A., Cid, J., 2007. "Influence of The Nitriding Time in The Wear Behavior of An AISI H13 Steel During A Crankshaft Forging Process" *Wear*, 263, 1375–1385.

J-M. Winter & J. Kalucki, 2013. "Gas Nitriding and Gas Carburizing of Steels", Volume 4A, Steel Heat Treating Fundamentals and Processes, J. Dossett and G.E. Totten, editors, *ASM Handbook*, pp. 647-679.

Li WH, Chen HL & Yang SQ., 2009. "Surface Integrity Research on Barrel Finishing of Crankshafts" Key Engineering Materials, pp.655–660.

Qiang Y. H., Ge S. R. & Xue Q. J., 2000. "Microstructure and Tribological Properties of Complex Nitrocarburized Steel", *J. Mater. Process. Technol*. 101: 180.

Ş. Polat, Ş. H. Atapek & H. Topaç, 2011. "Gaz Nitrasyon ile Yüzeyleri Sertleştirilmiş AISI 4140 ve DIN 1.2344 Çeliklerinde Mikroyapısal Karakterizasyon", *6 th International Advanced Technologies Symposium (IATS'11)*, Elazığ, Turkey.

Telasang, G., Dutta Majumdar, J., Padmanabham, G. & Manna, I., 2015. "Wear and Corrosion Behavior Laser Surface Engineered AISI H13 Hot Working Tool Steel", *Surface and Coatings Technology* 261, 69–78.

Uma Devi M., Chakraborty T. K. & Mohanty O.N. 1999. "Wear Behaviour of Plasma Nitrided Tool Steels", *Surface and Coatings Technology*, 116–119: 212-221.

Uzun H., 2002. ''Borlama İle Yüzeyleri Sertleştirilen Çeliklerin Aşınma Ve Korozyona Karşı Dayanımları'', Yüksek Lisans Tezi, Süleyman Demirel Üniversitesi Fen Bilimleri Enstitüsü Makina Mühendisliği Anabilim Dalı, Isparta.

Whitney WJ Jr & Schwab BE., 1986. "Crankshaft Surfaces: Finishing Methods, Surface Characterization and Their İnfluence on Wear", *Wear* ; 108: 345–356.

Z. Wang, B.X. Huang, H. Chen, C.Z. Wang, J. Ma & X.C. Zhao, 2020. "The Effect of Quenching and Partitioning Heat Treatment on the Wear Resistance of Ductile Cast Iron", *J. Mater. Eng. Perform*., 29 (7), pp. 4370-4378.

About The Authors

Yavuz SUN is a Professor of Metalurgical and Materials Engineering at Karabuk University. I have a Master's and doctoral degree in Metalurgical and Materials Engineering from İstanbul Technical University. His main areas of interest are iron and steel alloys, non-ferrous metals, casting technology, and composite materials.
Email : ysun@karabuk.edu.tr, **ORCID:** 0000-0002-7336-5591

Hayrettin AHLATCI is a Professor of Metalurgical and Materials Engineering at Karabuk University. I have a Master's and doctoral degree in Metalurgical and Materials Engineering from İstanbul Technical University. His main areas of interest are mechanical behaviors of materials, corrosion and wear behaviors, casting technology, and composite materials.
Email : hahlatci@karabuk.edu.tr, **ORCID:** 0000-0002-6766-4974

Similarity Index

The similarity index obtained from the plagiarism software fort his book chapter is 9 %.

Analysis of UO2+5% Cr Fuel Performance Under Normal and Accident Operating Reactor Conditions for VBER 300

Mustafa ARAT
Peter the Great St. Petersburg Polytechnic University

To Cite This Chapter:
Arat, M. (2025). Analysis of UO_2 + 5% Cr fuel performance under normal and accident operating reactor conditions for VBER-300. In H. Gokmese, S. Bulbul, & Y. Uzun (Eds.), *Innovative approaches in materials science and applications* (pp. 138–151). ISRES Book Series. ISRES Publishing.

Introduction

One of the most important sectors of the energy that determines the prosperity of a country is energy. The human equivalent of energy today is primarily electricity. The majority of global electricity is produced in various types of power plants, including thermal, natural gas, nuclear, solar, wind, geothermal, and hydroelectric facilities. Ensuring reliable, safe, and economical operation of the global nuclear reactor fleet has consistently been a fundamental objective of the nuclear industry. The continuous advancement of technology-particularly in the areas of innovative materials and nuclear fuels-remains essential to achieving this goal. Over decades, extensive research and operational experience have driven significant technological progress and generated a comprehensive body of data and knowledge regarding the behavior of light water reactors (LWRs) under both normal operating and accident conditions. In the aftermath of the 2011 Great East Japan Earthquake and the subsequent tsunami that led to the Fukushima Daiichi nuclear accident, improving the accident tolerance of light water reactors (LWRs) became a central theme in international research and policy discussions.

The current atomic power industry depends on innovation and has a phenomenal record of safety and functionality. Classic used UO_2 – zirconium combination framework (for example, fuel bar) meets all presentation or wellbeing necessities while keeping thermal power a financially serious clean-energy choice. Accident-tolerant fuel (ATF) advancement is to distinguish elective fuel framework innovations for additional improving the security, efficiency, and financial matters of business atomic power. Any new fuel idea might be thought about in contrast to the current plan, functional, financial, and security requirements to assess the administrative well-being consistency with functional and monetary imperatives. It is necessary to carry out an extensive assessment of the potential effects of ATF concepts across the whole nuclear fuel cycle.

The complex multi-physical science conduct of LWR atomic fuel makes characterizing explicit material or plan upgrades troublesome. Subsequently, building up beneficial execution credits is essential in directing the plan and advancement of fills and cladding

with improved accident resistance. ATF plans would persevere through a serious accident situation in the reactor center for a more drawn-out time of fuel framework while keeping up with or further developing fuel execution during typical activities. Key prerequisites for cutting-edge fills identify with atomic fuel execution, cladding execution, and adherence to framework imperatives.

This document outlines a unified set of global metrics, standardized tests, and representative severe accident scenarios for assessing ATF concepts across PWR, BWR, and VVER reactor types. Derived from a comprehensive U.S. assessment framework (Bragg-Sitton et al., 2016) and adapted for international use, the proposed methodology evaluates each concept's capability to achieve performance and safety objectives relative to the conventional UO_2–zirconium system. It also summarizes the current development status of fuel performance and severe accident analysis codes to inform future model enhancements, along with the internationally agreed accident scenarios for ATF evaluation (Agency and OECD, 2018; Bragg-Sitton et al., 2016).

Design Limitations and Performance Objectives of ATF Systems

Enhanced Accident-Tolerant Fuels (ATFs) refer to advanced nuclear fuels designed to endure severe reactor core accidents for a longer duration compared with the standard UO_2–zirconium alloy fuel system, while achieving comparable or superior performance under normal and transient operating conditions. In order to evaluate their compliance with regulatory safety requirements as well as operational and economic constraints, each new fuel must be thoroughly assessed compared with existing economic, safety, design, and operational criteria. The development and implementation of ATF concepts in commercial nuclear reactors are subject to several limitations and constraints, including those imposed by current nuclear fuel development and deployment practices.

- *Backward compatibility:* refers to the capacity of a new fuel design to be utilized within existing and future Light Water Reactors (LWRs) without requiring significant modifications. This includes compatibility with current fuel handling systems, fuel rod and assembly geometries, as well as the ability to operate alongside existing fuel types within the reactor core.
- *Plant operations*: refer to the requirement that new fuel designs should sustain or extend existing plant operating cycles, reactor control system configurations, and reactor power output. Any fuel system proposed for regulatory approval must demonstrate reliable performance not only under normal operating conditions but also during operational transients, i.e., anticipated operational occurrences.
- *Safety:* achieves performance comparable to or exceeding that of existing fuel systems under normal operation.
- *Front end of the nuclear fuel cycle:* complies with equipment, regulatory,

technical, and fuel performance requirements and rules.

- *Back end of the nuclear fuel cycle:* must not adversely affect the fuel's performance during transportation, interim wet or dry storage, or final disposal; should consider usage inside a closed fuel cycle.

To estimate the possibilities of the fuel system being accepted by the industry, the economics of a suggested ATF idea should be analyzed. However, because of high uncertainty in fabrication costs and materials during this research period, evaluating novel materials at early development stages is inherently challenging for ATFs. Therefore, separating economic analyses from technical and safety evaluations is essential for prioritizing fuel concepts. Technical performance results will serve as the basis for subsequent assessments of economic viability, which may differ across regional energy markets. It is important to emphasize that ensuring the economic viability of new fuel concepts is crucial in terms of additional costs (such as fabrication expenses) and potential cost savings achieved through enhanced performance, including higher burn-up capability, extended operating cycles, power uprates, reduced waste generation, or improved safety margins. Depending on the regulatory environment of the specific country, this safety margin and higher performance may be an economic advantage in terms of resource removal or plant equipment, risk reclassification (Lin et al., 2022).

Cladding Materials

Zirconium alloys, optimized through decades of LWR operation, remain the standard cladding materials. For ATF applications, alternative claddings-ranging from ceramics to metals-are being explored, each with unique material and neutronic characteristics. These candidates require systematic evaluation to determine feasibility and identify designs offering the best balance of properties and performance under both normal and accident conditions (Radford, 1979).

The nuclear fuel rod cladding serves two primary functions:

- The nuclear fuel cladding primarily serves to contain the fissile material and fission products within the fuel rod while maintaining compatibility with the nuclear process.
- allow for effective thermal transfer from fuel to coolant.

All ideal qualities and behaviors will not be present in an actual cladding material. As a result, a baseline for evaluating and assessing candidate materials that conforms to the criteria given below must be developed. These measures will assist researchers in making the optimal choice by analyzing the cladding material with the best combination of features and behaviors (Oguma, 1982).

Loss-of-coolant accidents (LOCAs) constitute a well-studied category of reactor incidents

and represent the scenarios for which protective systems and operational procedures are primarily designed. As the term suggests, a LOCA occurs when coolant is lost from the reactor system. Among these, a large-break LOCA (LBLOCA) represents the most severe scenario, characterized by a double-ended rupture (guillotine failure). LBLOCAs are generally defined for break areas exceeding 0.1 m^2 (Joyce, 2018).

In LOCA, the pressure within the primary circuit drives a rapid expulsion of coolant from the reactor vessel-a phenomenon known as coolant blowdown-accompanied by a swift depressurization of the system. This process may occur within a matter of seconds. In the absence of effective mitigating measures, the reactor core may be deprived of adequate cooling, rendering it susceptible to overheating, while a substantial quantity of vaporized coolant may accumulate within the containment structure. Most remedial strategies for mitigating the consequences of a large-break LOCA (LBLOCA) rely on rapid and continuous delivery of emergency coolant to maintain core coverage and prevent damage. These measures are typically designed to be implemented sequentially, depending on the core's pressurization status during blowdown.

Additional LOCA scenarios have been analyzed. For instance, if the rupture-and consequently the coolant loss rate-is significantly lower than in the LBLOCA case, the resulting events are classified as small-break LOCAs (SBLOCAs), generally associated with break areas smaller than 0.1 m^2. Although minor leaks capable of causing SBLOCAs are more probable than a large pipe rupture, their consequences can nonetheless be severe, even under slower coolant loss conditions.

Given the necessity of controlling decay heat, many LOCA scenarios are relevant not only to operating reactors but also to freshly shut-down reactors. This is an important consideration for LOCA countermeasures, as most LOCA events involve automatic reactor shutdown triggered by core overpressure, excessive temperature, or low coolant levels. Consequently, by the time LOCA mitigation measures are implemented, the reactor is likely to be safely shut down, and the primary focus shifts to decay heat management. Additional classifications, such as small LOCA (SLOCA) and medium-break LOCA (MBLOCA), are used to describe coolant losses that do not result from major pipe ruptures (Joyce, 2018).

Since light water serves as the primary coolant and moderator in most modern commercial reactors, as well as in the majority of existing operational nuclear plants, LOCAs have been extensively investigated in the context of Light Water Reactor (LWR) design. Nonetheless, LOCA events remain plausible in any reactor design if the fuel is vulnerable to overheating. Contemporary reactor designs often incorporate additional features to mitigate LOCA risks, including reduced piping (to lower the probability of pipe rupture) and enhanced countermeasure systems. Examples include passive natural

circulation cooling, isolation cooling systems capable of sustained operation, auxiliary make-up tanks, and high-pressure injection systems (Joyce, 2018).

Fuel Materials

UO_2, enriched to about 4.0-4.95% ^{235}U, remains the standard fuel for water-cooled reactors (PWRs, BWRs, and VVERs). ATF development explores both incremental improvements to UO_2 and advanced alternatives with enhanced fission product retention. Fuel performance and accident tolerance are assessed through material properties-thermal, mechanical, chemical, and neutronic-which must be optimized considering their effects on existing fuel systems and irradiation behavior. Due to complex interdependencies among these variables, establishing quantitative target values for multiple attributes is challenging; thus, any advanced fuel design requires assessment of the combined effects of material characteristics to ensure reliable operation within the overall reactor system.

Thermal Properties of Light Water Reactor Fuel

The thermal properties of LWR fuel-such as melting point, conductivity, expansion, and specific heat-govern its overall thermal behavior, which is also affected by fuel density and porosity. These characteristics influence fission product release, fuel swelling, and rod integrity. Fuel design must control swelling and emissions while maintaining acceptable thermal performance under normal conditions before evaluating accident tolerance. Desirable safety-enhancing trends for these properties are outlined below.

- *Melting Point:* A higher melting point is desirable, as it defines fuel performance under AOOs, RIAs, and LOCA conditions. The temperature margin to melting depends primarily on the melting point and thermal conductivity for a given power level. Since alternative fuels may operate at different temperatures, the margin between operating and melting temperatures is more critical than the absolute melting temperature itself.
- *Thermal Conductivity:* High thermal conductivity is desirable, as it lowers the fuel centerline temperature for a given linear power and thermal barriers in the gap and cladding. Reduced centerline temperatures decrease diffusion-driven processes, including fission gas release. Furthermore, lower thermal energy storage at equivalent density and specific heat reduces fuel and cladding temperatures during coolant failures.
- *Specific Heat Capacity:* A lower specific heat capacity is advantageous, as it limits the energy retained in the fuel during accident conditions such as LOCAs or DNB-related transients, thereby helping to reduce peak fuel temperatures in rapid events.
- *Pellet Density and Porosity*: Pellet density influences the initial energy storage

during LOCA events and affects DNB behavior under loss-of-flow conditions. The type and distribution of porosity should be optimized to minimize fission gas release, reduce fuel-water interaction, and enhance overall fuel performance.

- *Coefficient of Thermal Expansion (CTE):* A low thermal expansion coefficient is desirable, as expansion strongly affects pellet–cladding interaction (PCI) during overpower conditions, as excessive expansion can exacerbate mechanical stresses between the pellet and cladding (Agency, N.E. and OECD, 2018).

VBER-300

The VBER-300 is a Russian type of reactor with a proposed generating capacity of 325 MWe, intended for deployment in remote areas. Its external containment structure stands 16 meters tall, while the operational section, constructed from transportable modules, has a total weight of 1300 tonnes. Reactor plant of medium and low power VBER on thermal neutrons, designed based on block marine pressurized water reactors, is an improved setup, allowing it to be used as part of nuclear power plants for the production of heat and electricity. Such energy sources are designed to provide energy to regions that are not equipped with a centralized power supply. It's possible to use power units as energy sources as part of complexes for desalination of seawater. The VVER reactor plant implements the mastered technologies of ship block reactors, verified by many years of experience in operation in difficult navigation conditions, as well as the technology and experience of operating VVER-type reactors (Agency, I.A.E., 2006).

A general view of the VBER-300 reactor plant is shown.

Figure 1

Schematic diagram of VBER-300 (Agency, I.A.E., 2006)

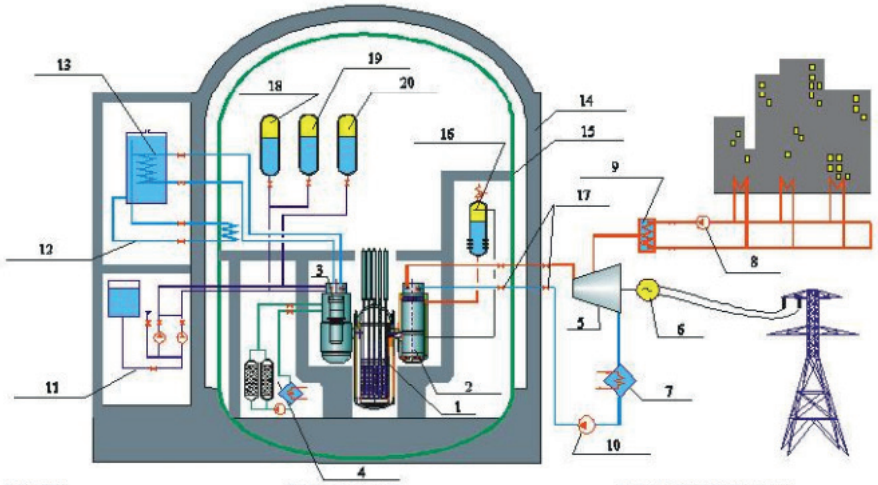

The power unit of VBER includes a reactor and steam turbine installations. The generation and receipt of energy is carried out according to the traditional and proven scheme: reactor plant-turbine-generator-power transmission line. For heat transfer, the necessary thermal and mechanical equipment and thermal networks connecting the speaker with the consumer are provided.

The main technical solutions of the VBER project:

- Direct-flow SG (steam generator);
- Sealed MCPs (main circulation pump);
- Active zone of reduced energy intensity;
- An optimal integration of passive and active safety systems.

What sets this project apart is its implementation of diverse, well-established technical solutions derived from decades of experience in both naval reactor construction and VVER-type reactors.

The main advantages of a VVER-type reactor plant include:

- The possibility of using the technology for nuclear power plants.
- Application of proven technologies of marine reactors, technical solutions of VVER reactors;
- Exclusion of the class of accidents of large and medium leaks, because there are no large-diameter pipelines;
- Increased strength and operability under;
- Operational loads, achieved due to the circulation of the primary circuit coolant through the connecting pipes of the main tract according to the “pipe in pipe” scheme;
- Minimum weight and size characteristics associated with the block execution of the reactor, allowing for the reduction of construction volumes, material consumption, and, as a result, achieving minimum capital investment, duration, and cost of installation work;
- The possibility of regulating the power range of the source using only standardized VBER equipment (Dimitriev et al., 2020).

VBER-300 core’s the fuel assemblies (FAs) are shroudless and of the TVSA (Advanced shroudless fuel assembly for VVER reactors) type (Fig. 2) (Samojlov et al., 2010).

Figure 2

VBER 300 TVSA FA (Samojlov et al., 2010)

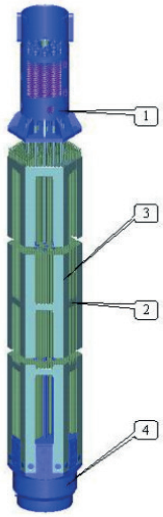

Thermal Calculation of the Reactor Core VBER 300

The input data for the calculation are presented in Table 1.

Table 1

Initial Data

Parameter		Value
Q_R, MWt		917
P_1, MPa		16.3
T_{inlet}, °C		292
T_{outlet}, °C		327.5
ΔT_s, °C		21.4
ΔT_1, °C		35.5
Fuel	d_{fuel}, mm	9.1
	Type of fuel	UO_2
	Cladding Material	Zr110
	$\delta_{thicness\ of\ cladding\ mat.}$	0.685
	δ_{gap}	0.065
Fuel Assembly	$n_{number\ of\ fuel} \mid n_{absorbsion\ element\ number} \mid n_{center}$	312|18|1
	Distance of fuel element, mm	12.75
	The distance between the faces of the fuel assembly, mm	4
	$m = \frac{H_{high\ of\ core}}{D_{diameter\ of\ core}}$	1.2

Table 2 shows the thermophysical parameters of the coolant at the outlet and inlet of the reactor.

Table 2

Thermophysical properties of the coolant

Parameter	Parameter Name, Dimension	Parameter Value
T_s	Saturation temperature, ℃	348.9
T_{inlet}	Inlet Coolant Temperature, ℃	292
T_{outlet}	Outlet Coolant Temperature, ℃	327.5
$T_{average}$	Average water temperature in the core, ℃	309.75
h_{inlet}	Enthalpy at the reactor inlet, $\frac{KJ}{kg}$	1294
h_{outlet}	Enthalpy at the reactor outlet, $\frac{KJ}{kg}$	1498
Δh	Enthalpy change, $\frac{KJ}{kg}$	204
ρ_{inlet}	The density of water at the reactor inlet, $\frac{kg}{m^3}$	751.9
ρ_{outlet}	The density of water at the outlet of the reactor, $\frac{kg}{m^3}$	659
$\rho_{average}$	Average density of water in the core, $\frac{kg}{m^3}$	705.45
μ_{inlet}	Dynamic viscosity of the inlet coolant, $Pa.s$	$9.37 \cdot 10^{-5}$
μ_{outlet}	Dynamic viscosity of the outlet coolant, $Pa.s$	$7.72 \cdot 10^{-5}$
$\mu_{average}$	Average dynamic viscosity of water in the core, $Pa.s$	$8.54 \cdot 10^{-5}$
$k_{average}$	Average thermal conductivity of water, $\frac{Watt}{m*K}$	0.541
$Pr_{average}$	The average number of Prandtl of water	0.92

Given in Tables 1 and 2, the required calculations were carried out, and a nuclear fuel simulation was developed using the ANSYS software package.

During the thermal calculation, the core parameters were determined, which are in good agreement with the data (Table 3) for the VBER 300 reactor.

Table 3

Geometric characteristics of the active zone

Parameter	$D_{a.z}, m$	$H_{a.z}, m$	$N_{fuel\ assembly}$	$W_{coolant}, \frac{m}{s}$
Value	2.42	2.9	85	3

The distribution of temperatures along the height of the active zone makes it possible to find the volumetric heat flux in the fuel pellet $q_v = 570 \frac{MW}{m^3}$.

Using the volumetric heat release, the heat transfer coefficient from the outer surface of the fuel element $\alpha_{convection}^{fuel\ assembly} = 37055 \frac{W}{m^2 \cdot ℃}$ and the coolant temperature near the fuel element wall (assumed to be average) $T_{avarage} = 309{,}75℃$, the temperature distribution inside the fuel element in the center of the active zone (z=0) was obtained in Figure 3.

To reduce the volume of calculations, we neglect the calculations for emergency-resistant fuel and claddings, since the thermal calculation and obtaining the temperature distribution is similar for all types of fuel and claddings (only thermal conductivity changes).

Figure 3

Temperature distribution inside a fuel element with UO_2 and Zr+1%Nb cladding

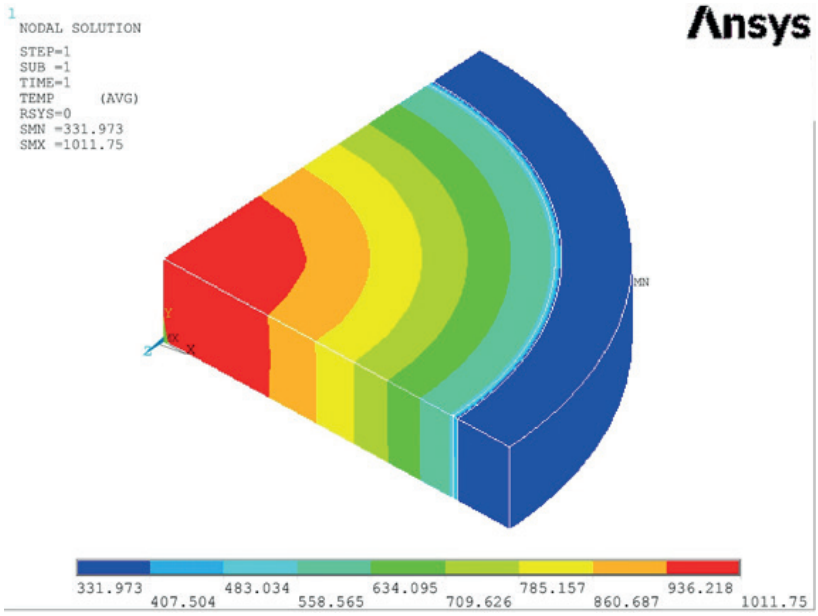

When using classic fuel, the temperature in the center of the pellet was obtained $T_{center} = 1011.75\ ℃$. On the surface $T_{surface} = 558.5\ ℃$, the temperature difference between the pellet and the cladding is approximately 150 °C (in the gas gap).

The following shows the temperature distribution with UO_2-5% Cr (CERMET) fuel and a Zr+1%Nb cladding of standard thickness, while maintaining the gas gap between the cladding and the pellet.

Figure 4

Temperature distribution inside a fuel element with $UO_2 - 5\%Cr$ (CERMET)

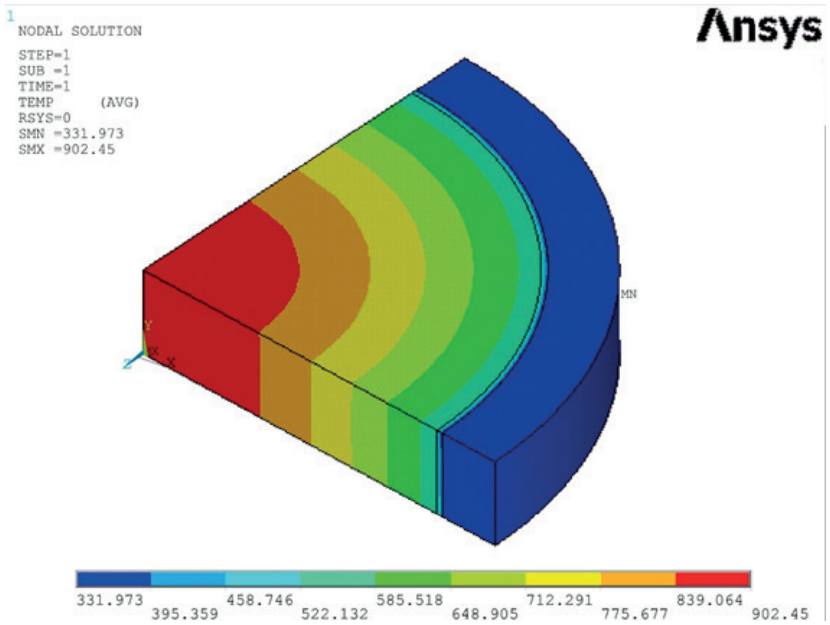

As illustrated in Figure 4, the temperature at the center of the fuel decreased by 109 ℃ and amounted to 902.45 ℃.

At the surface of the fuel pellet, the temperature decreased and amounted to 585.5 ℃.

$UO_2 + 5\%Cr$ fuel showed better results compared to UO_2, which is attributed to its high thermal conductivity.

According to the literature, the melting temperature of UO_2 is approximately 2865 ℃ (Hausner, 1965). The maximum operating temperature for UO_2 in operation is 1011.75 ℃. Since the operating temperature is lower than the melting temperature, we can say that the fuel works safely in the reactor.

The melting point of Zr+1%Nb typically ranges between 1726.85 ℃ and 1976.85 ℃, depending on the oxygen content and alloy. Just above 1726.85 ℃, the Zr+1%Nb cladding material can melt, in some cases, drain into the lower core regions (Pöml et al., 2012). The operating temperature of the cladding is 331.973 ℃, and it is safe for operation as this operating temperature is lower than the melting temperature (1726.85 ℃).

The operating temperature of fuel $UO_2 + 5\%Cr$ (CERMET) is 902.45 ℃, which is safe as it is lower than the melting temperature of uranium dioxide.

For a fuel element with $UO_2 + 5\%Cr$ and a zirconium cladding, there are no studies on the diffusion contact between the cladding and fuel, although the swelling of this type of fuel is less than that of dioxide, so it is not advisable to carry out the calculation without a gas gap, as there is no evidence to suggest that Cr will not form intermetallic compounds with Zr.

Conclusion

Figure 5

The temperature at the center of the fuel element depends on the fuel system

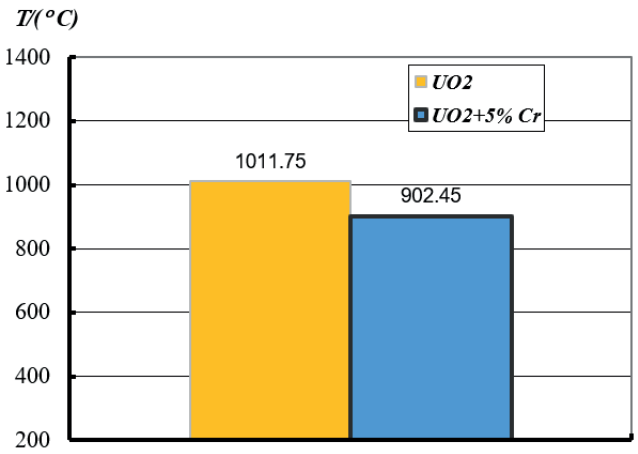

As illustrated in Figure 5, the classical UO_2|Zr fuel system has the highest temperature

compared with UO_2-5% Cr fuel with Zr.

In the final qualifying work, the analysis of the ATF system was carried out, and thermal calculations for the core were performed.

Materials (fuel and cladding) are proposed that can potentially be used in the VBER 300 project reactor.

The advantages that the ATF system provides are clearly shown:

- providing lower operating temperature;
- ensuring security.

In this study, the main geometric characteristics of the VBER 300 reactor plant were considered, as well as the parameters of the fuel cycle, were indicated: the duration of the campaign, the number of fuel assemblies, enrichment, etc.

The application of a block reactor in various fields of energy is considered.

Also, the study was devoted to an overview of the concepts of an accident-tolerant fuel system. A review of various accident-resistant fissile materials and cladding materials was carried out (their thermophysical properties, behavior in normal operating conditions were described, and production technology was studied).

The second chapter contains the thermal calculation of the reactor core: determination of the coolant velocity (3 m/s) and core geometry ($D_{a.z} = 2.42\ m; H_{a.z} = 2.42\ m$), determination of the number of fuel assemblies, determination of fuel temperatures for different systems (902℃- 1011℃), and comparison of the obtained data with VVER 300.

The analysis and comparison of the temperature distribution configurations for UO_2 $UO_2 + 5\%Cr$ fuels have been performed.

It can be said that they are safe for both Uranium dioxide and cladding, as well as CERMET and cladding, because their operating temperatures are lower than their melting (decomposition) temperatures.

Further research can be directed to a more detailed study of the strength characteristics of ATF systems, as well as optimization of the process for their production.

References

Agency, N.E. and OECD, State-of-the-Art Report on Light Water Reactor Accident-Tolerant Fuels. Vol. 7317. 2018.

Agency, I.A.E., Status of Innovative Small and Medium Sized Reactor Designs: Reactors with Conventional Refuelling Schemes. IAEA-TECDOC. Vol. 1485. 2006, Vienna.

Bragg-Sitton, S.M., et al., Metrics for the Technical Performance Evaluation of Light Water Reactor Accident-Tolerant Fuel. Nuclear Technology, 2016. 195(2): p. 111-123.

Dmitriev, S., et al., Investigation of Coolant Local Hydrodynamics in the Mixed Core of the VVER Reactor. ENERGETIKA. Proceedings of CIS higher education institutions and power engineering associations, 2020. 63: p. 151-162.

Hausner, H., Determination of the melting point of uranium dioxide. Journal of Nuclear Materials, 1965. 15(3): p. 179-183.

Joyce, M., Chapter 14- Nuclear Safety and Regulation, in Nuclear Engineering, M. Joyce, Editor. 2018, Butterworth-Heinemann. p. 323-355.

Lin, C., et al., Mechano-electrochemical phase field modeling for formation and modulation of dendritic Pattern: Application to uranium recovery from spent nuclear fuel. Materials & Design, 2022. 213: p. 110322.

Oguma, M., Microstructure Effects on Fracture Strength of U02 Fuel Pellets. Journal of Nuclear Science and Technology, 1982. 19(12): p. 1005-1014.

Pöml, P., et al., 3.09- Inert Matrix Fuel, in Comprehensive Nuclear Materials, R.J.M. Konings, Editor. 2012, Elsevier: Oxford. p. 237-256.

Radford, K.C., Effect of fabrication parameters and microstructure on the mechanical strength of UO_2 fuel pellets. Journal of Nuclear Materials, 1979. 84(1): p. 222-236.

About The Author

Mustafa ARAT, Ph.D., is an engineer at the Department of Thermal Power Plants in the Directorate General of Electricity Generation Corporation in Ankara. He completed his master's degree in Metallurgical and Materials Engineering at Selçuk University and his master's degree in Nuclear Power Engineering at Peter the Great St. Petersburg Polytechnic University. He completed his PhD in Metallurgical and Materials Engineering at Gazi University. His main areas of expertise are nuclear fuel, composite materials, metal casting processes, and materials characterization.

E-mail: mustafaarat199@gmail.com **ORCID:** 0000-0001-8783-6043

Similarity Index:
The similarity index obtained from the plagiarism software for this book chapter is 6 %.

Introduction to Composite Solid Rocket Propellants

Selva ASTAN
Mechanical and Chemical Industry Corporation

Ahmet Burçin BATIBAY
Mechanical and Chemical Industry Corporation

To Cite This Chapter:
Astan, S., & Batibay, A. B. (2025). Introduction to composite solid rocket propellants. In H. Gokmese, S. Bulbul, & Y. Uzun (Eds.), *Innovative approaches in materials science and applications* (pp. 152–169). ISRES Book Series. ISRES Publishing.

Introduction

Composite solid rocket propellants are a crucial technology in aerospace propulsion, functioning as the primary propulsion system for a wide array of civilian and military applications. Their significance stems from their capability to deliver high energy output and reliability, essential for launching vehicles and tactical missiles (Bekhouche & Luo, 2014; Ling et al., 2025; Shi et al., 2025)

These propellants are heterogeneous mixtures engineered to combine multiple constituent materials with distinct physical and chemical properties, producing materials with characteristics significantly different from their individual components (Mourdikoudis, Kostopoulou, & LaGrow, 2021). These propellants consist of a mixture that combines oxidizers, such as ammonium perchlorate, fuels like aluminum powder, and binders such as hydroxyl-terminated polybutadiene (HTPB), which together facilitate efficient energy release during combustion (Bekhouche & Luo, 2014; Campos et al., 2010; Mingireanu, Jula, Miclos, Baschir, & Savastru, 2018).

The mechanical properties and performance characteristics of composite solid rocket propellants are vital for their effective use in different operational contexts. Their formulation enables adaptability to various missions, illustrating their importance not only in aerospace operations but also in defense strategies (Alemayehu & Solomon, 2020; Ling et al., 2025; Thakre & Yang, 2010).

Solid rocket motors employing these propellants are known for their simplicity and operational reliability, making them a favored choice in both commercial and military sectors (Lichthardt et al., 2022; Mingireanu et al., 2018; Unni et al., 2020). With ongoing research aimed at enhancing their performance and safety attributes, composite solid rocket propellants remain a focal point of advancement in propulsion technologies (Runtu, Setiani, Utami, & Review, 2023; Said, Maraden, Elhedery, Abd Elall, &

Elbasuney, 2023).

Thus, composite solid rocket propellants symbolize a foundational technology in aerospace propulsion, serving critical roles in numerous applications across both civilian and military domains (Koizumi et al., 2010; Remissa et al., 2023; Singh & Shekhar, 2016).

The development of composite solid rocket propellants emerged from the need for reliable, storable propulsion systems that could provide consistent performance across a wide range of applications. The historical preference for ammonium perchlorate (AP) as the oxidizer in composite propellants stems from its well-established thermal decomposition characteristics and proven performance in flight applications. However, the combustion of AP-based propellants produces undesirable byproducts, most notably hydrogen chloride (HCl), which presents environmental and operational challenges (De Amicis, Scalia, Accettura, & AERONAUTICS, 2008). This limitation has driven significant research into alternative oxidizer systems, including ammonium dinitramide (ADN), hydrazinium nitroformate (HNF), and ammonium nitrate (AN)-based formulations (Elzaki & Zhang, 2016).

The evolution of composite solid rocket propellant technology has been characterized by continuous refinement of component selection, processing methodologies, and performance optimization. Modern propellant formulations increasingly incorporate advanced additives and catalytic systems designed to enhance thermal decomposition efficiency, improve combustion characteristics, and reduce environmental impact (Mani, 2025). The field has also witnessed the emergence of energetic binders—polymeric materials that contribute to the overall energy content of the propellant rather than serving merely as inert binding agents (Jarosz, Stolarczyk, Wawrzkiewicz-Jalowiecka, Pawlus, & Miszczyszyn, 2019).

Fundamentals and Classification of Propellants

Primary explosives are very sensitive to initiation. They can be set off by friction, impact, heat, electrical discharge, and shock. Secondary explosives, on the other hand, are more powerful because they have higher detonation pressures and speeds. Even though they are quite sensitive, primary explosives are employed a lot in the military and in commercial settings (Agrawal, 2010; Arun Kumar, Purayil Dhanya, Venugopal, Vargeese, & Krishnamurthy, 2024; Singh & Shekhar, 2016).

Propellants, which are also called low explosives, burn slowly and in a controlled way, creating a lot of hot gases that can be used for a variety of explosive applications, such as pushing projectiles (bullets, shells, rockets, or missiles). Propellants don't explode like primary explosives do. Instead, they burn, which creates heat (Agrawal, 2010;

Arun Kumar et al., 2024). The classification of chemical propellants is based on their respective physical states, which are liquid, solid, polymer, or hybrid (Mishra, 2017).

Solid propellants are favored over liquid propellants due to their safety, reliability, simplicity, and long storage life (Agrawal, 2010; Mishra, 2017). It is important to note that a solid propellant must have a minimum ignition temperature for ignition to occur. The distribution of fuel and oxidizer in solid propellants can be broadly classified into two categories: homogeneous (or colloidal), and heterogeneous. Fuel and oxidizer are both present in the same molecule of homogeneous propellants. Solid fuel and oxidizer maintain their respective physical identities in the context of heterogeneous propellants (Mishra, 2017; Singh & Shekhar, 2016).

Homogeneous propellants, also known as double-base (DB) propellants, mainly consist of nitrocellulose (NC) and nitroglycerine (NG). Additional substances are often added in small quantities to enhance properties, serving as stabilizers, plasticizers, coolants, lubricants, opacifiers, or burning-rate modifiers. These propellants are shaped using extrusion or casting techniques and are commonly used in anti-tank missiles (Agrawal, 2010; Mishra, 2017).

Heterogeneous propellants primarily include composite propellants, which consist of a fuel or binder and oxidizer. The binder, which forms the base matrix, retains solid oxidizers like ammonium nitrate (AN) or ammonium perchlorate (AP). The choice of binder is influenced by factors such as availability, cost, processing ease, and required specific impulse (I_{sp}) (Agrawal, 2010; Singh & Shekhar, 2016; Sutton & Biblarz, 2011).

Properties of Composite Solid Rocket Propellants (CSRPs)

Composite solid rocket propellants (CSRPs) are integral to modern propulsion systems, widely utilized across military and civilian applications for their reliability, efficiency, and adaptability. This discussion presents an in-depth exploration of the components, formulation, performance characteristics, recent advancements, and future directions for CSRPs (Singh & Shekhar, 2016).

Composite solid rocket propellants are engineered materials composed of multiple discrete phases that function synergistically to produce controlled combustion and thrust generation (De Amicis et al., 2008). Understanding the classification of propellants and their respective advantages and limitations provides foundational context for CSRPs. Each component plays a critical role in determining the propellant's performance characteristics, including burn rate, specific impulse, combustion stability, and environmental compatibility (Singh & Shekhar, 2016).

Composite solid rocket propellants generally consist of a fuel component, an oxidizer, and a polymer binder. Most commonly, hydroxyl-terminated polybutadiene (HTPB) is

used as the binder due to its favorable mechanical properties and compatibility with various additives (Bekhouche & Luo, 2014; Rao, Solanke, Bihari, Singh, & Bhattacharya, 2016). The oxidizing agent most frequently utilized in CSRP is ammonium perchlorate (AP), which plays a critical role in enhancing the propellant's energy output through efficient combustion (Lu et al., 2023; Park, Choi, Kim, Kim, & Park, 2020).

Composite propellants differ from other types, such as double-base or homogeneous propellants, by the incorporation of solid oxidizers mixed with metallic fuels within a polymer matrix, resulting in heterogeneous structures (Navalino, Muda, Hafizah, & Ruyat, 2024; Shekhar, 2012). This allows for tailored performance characteristics such as burn rate, thrust, and stability.

Modern rockets and missiles mainly utilize composite propellants. These composite propellants comprise three essential components: an organic polymer that acts as a binder and a gas-generating combustible fuel; an oxygen-rich solid oxidizer that supplies the requisite oxygen for oxidation; and a combustible metal additive that functions as the primary source of additional thermal energy, thereby improving their performance (Agrawal, 2010).

The integration of these components into a cohesive propellant formulation requires careful consideration of particle size distribution, volume fraction of each constituent, and the chemical compatibility between components. The heterogeneous nature of composite propellants necessitates sophisticated processing techniques to ensure uniform distribution of particles and consistent propellant properties throughout the grain (Singh & Shekhar, 2016). Additionally, various additives are incorporated into the formulation to enhance specific performance characteristics, including catalysts to accelerate oxidizer decomposition, plasticizers to improve mechanical properties, and stabilizers to enhance long-term storage stability (Agrawal, 2010).

Oxidizers of Composite Solid Rocket Propellants (CSRPs)

Oxidizer constitutes a vital element in composite propellants, accounting for more than 70% of their mass. The essential attributes of an optimal oxidizer encompass compatibility with other constituents, elevated oxygen content, little heat of creation, high density, thermal stability, and low hygroscopicity. Safety in handling and extended shelf life, which entails preserving its qualities without phase alterations, are critical factors (De Amicis et al., 2008; Mani, 2025).

The oxidizer's function is essential, as it influences the propellant's physical, chemical, and mechanical properties. Upon decomposition, the oxidizer releases oxygen, facilitating the oxidation of the fuel, thereby generating the necessary energy through exothermic reactions and yielding significant volumes of gas. Historically, various

inorganic compounds, including sodium perchlorate and potassium perchlorate, were evaluated; however, ammonium perchlorate (AP) has emerged as the primary oxidizer for composite solid propellants, particularly in launch vehicles. The quest for environmentally sustainable energetic oxidizers has led to the development of innovative molecules, including dinitramide salts paired with diverse counter cations such as ammonium, guanidinium, and hydrazinium (Agrawal, 2010; Sutton & Biblarz, 2011).

Ammonium perchlorate (NH_4ClO_4) has historically dominated the composite solid rocket propellant industry as the primary oxidizer of choice. With a density of 1.95 g/cm³, AP provides excellent oxygen balance and well-characterized thermal decomposition kinetics that have been extensively studied and optimized over decades of aerospace applications. During combustion, AP undergoes thermal decomposition to release oxygen-rich species, including nitrogen oxides and chlorine-containing compounds, which subsequently participate in diffusive flame combustion with the fuel and binder components (Chen, Xue, & Yu, 2024; De Amicis et al., 2008).

The thermal decomposition of AP is highly sensitive to the presence of additives, which can significantly influence the decomposition temperature and reaction pathway (Mani, 2025). The primary limitation of AP-based propellants is the production of hydrogen chloride (HCl) during combustion (De Amicis et al., 2008). The release of HCl presents multiple challenges: environmental concerns regarding atmospheric chlorine chemistry, corrosion issues in rocket engine hardware, and operational constraints related to exhaust plume visibility and environmental regulations. These limitations have motivated substantial research into alternative oxidizer systems that can provide comparable or superior performance while eliminating or significantly reducing the production of toxic chlorine-containing byproducts (Elzaki & Zhang, 2016; Gettwert, Tagliabue, & Weiser, 2017).

Ammonium dinitramide (ADN) represents a promising alternative to ammonium perchlorate, offering the potential for significantly improved environmental performance (Harimech, Salah, Amrousse, & Evaluation, 2025). ADN-based composite propellants are attractive from an environmental perspective because their combustion products do not include toxic chlorine-containing species (Elzaki & Zhang, 2016). The thermal decomposition of ADN has been the subject of intensive research, with particular focus on developing efficient catalyst systems to optimize decomposition kinetics and thermal stability (Gettwert et al., 2017; Harimech et al., 2025).

Recent advances in ADN propellant technology have centered on the development of sophisticated catalyst systems incorporating metal oxides, transition metal complexes, and nanomaterials. Iron and copper oxides have emerged as particularly effective catalysts for ADN decomposition, demonstrating the ability to significantly lower decomposition

temperatures while maintaining thermal stability (Harimech et al., 2025). These catalytic systems are crucial for developing energy-efficient ADN-based propellant compositions that can achieve performance levels comparable to or exceeding those of conventional AP-based formulations. The implementation of ADN as a replacement for AP requires careful consideration of its different thermal and chemical properties. ADN exhibits different decomposition mechanisms compared to AP, necessitating reformulation of the complete propellant system to optimize performance (Elzaki & Zhang, 2016; Gołofit, Cieślak, & Chmielarek, 2023; Harimech et al., 2025).

Hydrazinium nitroformate (HNF) and hydrazinium dinitramide (HDN) are energetic oxidizer alternatives that have been investigated for composite propellant applications (Elzaki & Zhang, 2016). These oxidizers can offer potential advantages in terms of specific impulse and environmental compatibility compared to conventional AP-based systems. However, their practical implementation has been limited by factors including availability, cost, and the need for comprehensive characterization of their thermal decomposition behavior and compatibility with standard binder systems. Continued research is required to fully quantify their benefits, understand processing constraints, and evaluate long-term storage and handling safety (Elzaki & Zhang, 2016; Singh & Shekhar, 2016).

Ammonium nitrate (AN)-based composite propellants have attracted significant attention as environmentally benign alternatives to AP-based formulations. The primary advantage of AN-based propellants is that their combustion products are free of toxic gases, particularly HCl, making them attractive from environmental and operational perspectives. These characteristic addresses one of the most significant limitations of AP-based propellants and aligns with regulatory trends toward greener propulsion technologies (Elzaki & Zhang, 2016; Singh & Shekhar, 2016).

The development of AN-based composite propellants requires careful formulation optimization to achieve performance levels comparable to established AP-based systems. The thermal decomposition characteristics of AN differ substantially from those of AP, necessitating adjustments to binder chemistry, fuel particle size distribution, and additive packages to optimize combustion kinetics and propellant performance. Despite these challenges, AN-based propellants represent a promising direction for future composite propellant development, particularly for applications where environmental considerations are paramount (Elzaki & Zhang, 2016).

Fuels of Composite Solid Rocket Propellants (CSRPs)

The fuel component, conventionally consisting of aluminum particles, provides the primary energy source for combustion and contributes substantially to the propellant's specific impulse. Alternative fuel materials, including magnesium, have been investigated to achieve enhanced performance characteristics, though aluminum remains the industry standard for most applications (Sahimi, 2003).

Aluminum has established itself as the dominant fuel material in composite solid rocket propellants due to its exceptional combination of properties (Sahimi, 2003). Aluminum particles provide high energy density, well-characterized combustion kinetics, and excellent compatibility with standard binder systems and oxidizers (De Amicis et al., 2008). The combustion of aluminum in the oxygen-rich environment created by oxidizer decomposition produces aluminum oxide (Al_2O_3), which contributes substantially to the propellant's specific impulse and exhaust temperature (Sahimi, 2003).

The selection of aluminum particle size and size distribution critically influences propellant performance characteristics. Smaller aluminum particles exhibit higher surface area and faster combustion kinetics, potentially enhancing burn rate and specific impulse. However, particle size must be carefully controlled to ensure adequate mixing with oxidizer and binder components during propellant processing and to maintain consistent combustion characteristics throughout the burn duration. Aluminum particles typically constitute 10–20% of the total propellant mass, with the exact percentage determined through thermochemical calculations to achieve optimal energy release and combustion temperature. The heterogeneous distribution of aluminum particles throughout the propellant matrix ensures combustion occurs in a distributed manner throughout the grain volume, contributing to the stable and predictable burn characteristics that characterize composite propellants (Agrawal, 2010; Sahimi, 2003; Sutton & Biblarz, 2011).

Magnesium has been investigated as an alternative or supplementary fuel material in composite propellants, offering potential advantages in terms of specific impulse and combustion temperature compared to aluminum alone. Magnesium exhibits higher energy density per unit mass than aluminum, and its combustion products (magnesium oxide) can contribute to enhanced exhaust temperature. However, the implementation of magnesium in composite propellants presents challenges related to particle reactivity, oxidation during processing, and compatibility with binder systems. The use of magnesium in composite propellants requires careful control of processing conditions to prevent premature oxidation and to ensure adequate dispersion throughout the propellant matrix. Additionally, magnesium particles exhibit different combustion kinetics compared to aluminum, potentially affecting the overall burn rate and combustion stability of the propellant. Other alternative fuel materials, including boron and boron compounds, have been explored for composite propellant applications. These materials offer potential

advantages in terms of energy density and specific impulse, but present significant challenges related to particle reactivity, processing complexity, and environmental considerations. The combustion of boron-containing fuels produces boron oxide particles that can affect exhaust plume characteristics and environmental impact, limiting their applicability in many operational scenarios (Sahimi, 2003).

Binders of Composite Solid Rocket Propellants (CSRPs)

Binders are very important to the performance of solid propellants because they control how much solid can be loaded and how well the materials are put together. Asphalt and a variety of polymers, including polyethylene and polyester, were among the traditional binders. However, these early alternatives are now considered outdated due to their inferior mechanical properties and lower specific impulse characteristics. The introduction of advanced materials such as polybutadiene with functional groups and other energetic binders has substantially facilitated the development of energetic polymer binders over the past two decades.

A polymer suitable as a binder for composite rocket propellants must possess a range of desirable attributes, the most critical of which include:

- The binder must be compatible with the propellant's supplementary components, including an oxidizer, metal powder, plasticizer, bonding agent, stabilizer, and ballistic modifier, among others.
- The binder must possess a polymer backbone characterized by a high carbon-hydrogen ratio.
- The average molecular weight (M_n) and weight (M_w) must range from 2000 to 3500, with the molecular weight distribution being as narrow as possible to enhance the mechanical properties of propellants and ensure reproducibility.
- The binder must possess low viscosity to provide enhanced solids loading (oxidizer and metal fuel), hence yielding a higher specific impulse (I_{sp}).
- Upon the incorporation of solids (85-90%), the binder must exhibit elevated tensile strength, elongation, and Young's modulus to maintain the structural integrity of rocket propellant grains during flight.
- The binder should possess a low glass transition temperature ($_{Tg}$) and an extended shelf life (Agrawal, 2010; Jarosz et al., 2019; Sutton & Biblarz, 2011).

Hydroxyl-terminated polybutadiene (HTPB) has emerged as the industry-standard binder material for composite solid rocket propellants, serving as the primary polymeric matrix that holds oxidizers and fuel particles in a cohesive structure. HTPB is a synthetic rubber

polymer with terminal hydroxyl groups that enable cross-linking through reaction with isocyanate curing agents, forming a three-dimensional polymeric network. The resulting cured propellant exhibits rubbery mechanical properties that provide structural integrity to the propellant grain while accommodating the thermal stresses generated during combustion (De Amicis et al., 2008).

The selection of HTPB as the standard binder reflects its favorable combination of properties: excellent mechanical properties in both cured and uncured states, well-characterized curing kinetics, good compatibility with oxidizer and fuel particles, and proven long-term storage stability (De Amicis et al., 2008). HTPB-based propellants have been extensively characterized through decades of aerospace applications, providing a comprehensive database of performance characteristics and processing parameters that facilitate reliable propellant formulation and manufacturing. The mechanical properties of HTPB-based propellants can be tailored through adjustment of the polymer molecular weight, cross-link density, and incorporation of plasticizers (Sutton & Biblarz, 2011). These adjustments allow propellant engineers to optimize the balance between mechanical strength and flexibility, ensuring that the propellant grain can withstand the mechanical stresses imposed during motor operation while maintaining structural integrity throughout the burn duration (Chen et al., 2024; Gligorijević et al., 2016).

Carboxyl-terminated polybutadiene (CTPB) represents an alternative polymeric binder system that offers certain advantages over HTPB in specific applications. CTPB contains terminal carboxyl groups that enable cross-linking through different curing mechanisms compared to HTPB, potentially offering enhanced mechanical properties and improved compatibility with certain oxidizer and fuel systems. The use of CTPB allows for alternative curing chemistry that may provide advantages in processing flexibility and final propellant properties (De Amicis et al., 2008; Sutton & Biblarz, 2011).

Glycidyl Azide Polymer (GAP) is a notable energetic polymer created in 1972 by a reaction between NaN_3 and polyepichlorohydrin (PECH-triol) in DMF. It has garnered significant scientific interest for its application as an energetic plasticizer and binder owing to its beneficial qualities. GAP possesses a density of 1.3 $g \cdot cm^{-3}$, a positive heat of formation of +42 $kcal \cdot mol^{-1}$, and the capacity to desensitize nitroglycerine (NG), an essential element in rocket propellants. It is easily produced and economical, demonstrating superior binder qualities in its unadulterated state. It functions in propellants as both a plasticizer (molecular weight M_n = 400–500) and a binder (M_n ≈ 2500–3000), markedly improving the specific impulse (I_{sp}) (Agrawal, 2010; Hafner, Keicher, & Klapötke, 2018).

GAP represents a paradigm shift in composite propellant binder technology, transitioning from inert polymeric materials to energetic binders that actively contribute to the overall

energy content of the propellant (Jarosz et al., 2019). The incorporation of GAP as a binder enables the development of higher-performance propellants with enhanced specific impulse and combustion temperature compared to conventional HTPB-based formulations (Gligorijević et al., 2016; Gołofit et al., 2023).

The fundamental distinction between energetic and non-energetic binders lies in their chemical composition and role in the combustion process (Jarosz et al., 2019). While traditional binders such as HTPB serve primarily as mechanical binding agents with minimal energy contribution, energetic binders like GAP participate directly in the combustion reaction, releasing substantial energy that enhances overall propellant performance. Compared to HTPB, GAP not only provides structural and mechanical support but also contributes to the propellant's total energy content, resulting in higher specific impulse and increased combustion temperature. This distinction has profound implications for propellant formulation, as the incorporation of energetic binders allows for optimization of the overall energy balance and combustion characteristics of the propellant system (Gołofit et al., 2023; Jarosz et al., 2019).

NiMMO is produced via the selective nitration of the hydroxyl group in 3-hydroxymethyl-3-methyloxetane (HyMMO) utilizing N_2O_5, aided by a flow nitration method that improves yield and purity in dichloromethane. Through cationic polymerization with an initiator system of BF_3 and a diol, NiMMO yields poly(NiMMO), a pale-yellow viscous liquid. The cationic polymerization process is affected by several factors, including reaction temperature, initiator system, reaction duration, and monomer addition rate, all of which influence the resulting molecular weight, polydispersity, viscosity, hydroxyl functionality, and the formation of cyclic species (Agrawal, 2010; Gołofit et al., 2023).

Polynitropolymers, including polyNiMMO (poly(3-nitratomethyl-3-methyloxirane)), represent another class of energetic binders that have been investigated for composite propellant applications. These materials incorporate nitrate ester functional groups into the polymer backbone, providing energetic content while maintaining the structural and mechanical functions required of a binder material. PolyNiMMO and related polynitropolymers offer potential advantages in terms of specific impulse and combustion characteristics compared to conventional binders, though their implementation requires careful consideration of thermal stability and compatibility with oxidizer and fuel components (Gołofit et al., 2023; Jarosz et al., 2019).

The incorporation of energetic binders into composite propellants offers significant potential advantages, including enhanced specific impulse, higher combustion temperature, and improved volumetric energy density (Jarosz et al., 2019). These improvements can translate into enhanced rocket motor performance, increased payload capacity, or extended mission duration for space applications. Additionally, the

use of energetic binders can facilitate the development of propellants with improved environmental characteristics, as the enhanced energy content may allow for reduced oxidizer loading or the substitution of environmentally problematic oxidizers with greener alternatives. However, energetic binders present substantial challenges related to safety, processing, and long-term stability. Their energetic nature requires enhanced safety protocols during manufacturing, handling, and storage. Thermal stability must be carefully characterized to ensure consistent propellant performance throughout its intended service life. Furthermore, interactions between energetic binders and other propellant components, particularly oxidizers and catalytic additives, must be thoroughly understood to ensure predictable and safe propellant behavior (Agrawal, 2010; Jarosz et al., 2019; Sutton & Biblarz, 2011).

Additives of Composite Solid Rocket Propellants (CSRPs)

The incorporation of catalytic additives into composite propellants represents a sophisticated approach to optimizing combustion kinetics and enhancing overall propellant performance. Catalytic additives function by accelerating the thermal decomposition of the oxidizer, reducing the decomposition temperature and enhancing the rate of oxygen release during combustion. This acceleration of oxidizer decomposition leads to improved combustion efficiency, enhanced burn rate stability, and potentially increased specific impulse (Mani, 2025). Advanced catalytic systems incorporating nanomaterials have been investigated for composite propellant applications, offering the potential for enhanced catalytic activity through increased surface area and unique nanoscale effects. Nano-scale iron oxides and other transition metal oxide nanoparticles demonstrate enhanced catalytic potency compared to conventional micrometer-scale catalysts, potentially enabling improved propellant performance through reduced catalyst loading (Harimech et al., 2025; Mani, 2025).

Thermite systems, consisting of metal fuels (typically aluminum) combined with metal oxides (such as iron oxide), have been investigated as additives to enhance the combustion characteristics of composite propellants. Aluminum/iron oxide (Al/Fe_2O_3) thermites demonstrate enhanced combustion-supporting ability for AP/HTPB propellants compared to iron oxide alone or other thermite formulations. The thermite reaction between aluminum and iron oxide generates substantial heat and produces molten products that can enhance the combustion of the surrounding propellant matrix (Chen et al., 2024; Zhao et al., 2016).

The effectiveness of thermite additives depends critically on the particle morphology and size distribution of the constituent materials. Granular iron oxide structures and corresponding thermites exhibit higher burning rates due to larger surface area associated with smaller particle sizes. Optimization of thermite additive systems requires careful

consideration of particle size, morphology, and loading to achieve enhanced combustion characteristics without adversely affecting propellant mechanical properties or processing characteristics (Zhao et al., 2016).

Plasticizers are incorporated into composite propellants to modify the mechanical properties of the cured binder, typically reducing stiffness and increasing flexibility. These additives function by disrupting polymer chain interactions, reducing the glass transition temperature, and enhancing the elasticity of the cured propellant. Common plasticizers include dioctyl phthalate (DOP), diisodecyl phthalate (DIDP), and other organic compounds that are compatible with the binder polymer and do not adversely affect propellant performance (De Amicis et al., 2008).

The selection and loading of plasticizers must be carefully optimized to achieve the desired mechanical properties while maintaining adequate structural strength and long-term stability. Excessive plasticizer loading can compromise propellant strength and increase the risk of mechanical failure during motor operation, while insufficient plasticizer may result in a propellant that is too brittle and susceptible to cracking during thermal cycling or mechanical stress (Thakre & Yang, 2010).

Stabilizers are incorporated into composite propellants to enhance long-term storage stability and prevent degradation of the propellant components during extended storage periods. These additives function by inhibiting oxidation reactions, preventing hydrolysis of the polymer binder, and maintaining the chemical stability of the oxidizer and fuel components. Common stabilizers include hindered phenols, aminic compounds, and other antioxidants that are compatible with the propellant matrix (De Amicis et al., 2008).

The incorporation of stabilizers is particularly important for propellants intended for long-term storage, as the oxidizer and fuel components can undergo slow chemical reactions that degrade propellant performance over time. The selection of appropriate stabilizers and their loading must be carefully optimized to ensure that the propellant maintains consistent performance characteristics throughout its intended service life, which may span decades for military and space applications (Singh & Shekhar, 2016; Thakre & Yang, 2010).

Beyond catalysts, plasticizers, and stabilizers, various other additives have been investigated for composite propellants to achieve specific performance objectives. These include burn rate modifiers (e.g., metal-based or organometallic burn-rate agents, inorganic nanoparticle promoters) to adjust the propellant's burn rate to meet specific motor design requirements, smoke suppressants (e.g., condensable mineral fillers, expandable graphitic materials, reduced metal loading approaches) to reduce exhaust plume visibility, and environmental modifiers (e.g., halogen-free/"green" oxidizer systems, acid-scavenging additives, alloying strategies to alter combustion product) to

minimize the production of toxic combustion products. The strategic incorporation of these additives allows propellant engineers to tailor the propellant's characteristics to meet specific application requirements while maintaining compatibility with the primary propellant components (Singh & Shekhar, 2016).

Performance Characteritics of Composite Solid Rocket Propellants (CSRPs)

Performance assessment of CSRP encompasses several critical parameters, including mechanical properties, thermal performance, and combustion characteristics. The mechanical stability of propellants during service is paramount. Studies on stress-strain behavior, using methods like indentation techniques, reveal the impact of aging and environmental factors on mechanical integrity (Kumar Bihari, Kumaraswamy, Jain, & Murthy, 2022). A comprehensive evaluation of mechanical properties throughout the lifecycle ensures safety and reliability during storage and operation (Gligorijević et al., 2016).

Beyond mechanical properties, thermal stability is essential for propellant safety. Thermal analyses, including differential scanning calorimetry (DSC) and thermogravimetric analysis (TGA), assess the decomposition temperatures and relevant thermal transitions of the materials, thereby ensuring safe operating conditions during propellant use (Gaur et al., 2017; Tsyshevsky et al., 2015).

The combustion behavior of CSRP is significantly influenced by the oxidizer-fuel ratio, the presence of additives, and the physical characteristics of the oxidizer. Advanced testing methodologies, such as X-ray computed tomography, provide insights into the mixing state and distribution of components, impacting performance and combustion efficiency (Hosomi et al., 2019).

Recent Developments and Future Trends of Composite Solid Rocket Propellants (CSRPs)

Recent advancements in CSRP technology focus on improving performance while ensuring reliability and safety. The incorporation of nanomaterials, such as carbon nanotubes and metal nanoparticles, enhances the mechanical and thermal properties of propellants while increasing energy output through improved combustion kinetics (Navalino et al., 2024). Research into reactive nanocomposites has demonstrated their potential in advancing propellant formulations (Tawfik, Saleh, Elbeih, & Klapötke, 2016).

Studies have shown that varying the particle size distribution of ammonium perchlorate can significantly impact the combustion rates and stability of CSRP. Understanding these correlations aids in optimizing propellant formulations for specific mission profiles (Park et al., 2020). Ongoing research investigates the aging characteristics of composite

propellants and their performance over time. The effects of environmental conditions such as temperature, humidity, and storage duration on mechanical properties and sensitivity are critical for maintaining reliable and robust rocket systems (Bogusz & Magnuszewska, 2019; Hawass, Kim, & Kwon, 2024).

Recent developments have focused on burn rate modifiers that can adjust the propellant's performance dynamically. Such modifications can enhance thrust profiles and adaptability across varying mission requirements, addressing the need for versatility in modern propulsion systems (Lu et al., 2023).

Conclusion

Composite solid rocket propellants are an established and mature technology that keeps developing in response to environmental factors, performance demands, and technical advancements. Over decades of operational experience, the basic design of these propellants—which consists of oxidizer, fuel, and binder components—has demonstrated efficacy for a wide range of aerospace applications. Significant gains in performance, manufacturing efficiency, and environmental compatibility are anticipated from ongoing research into enhanced catalytic systems, energetic binders, and alternate oxidizers.

Environmental restrictions and operational considerations have led to a considerable evolution in propellant technology, with the shift from traditional AP-based propellants to ecologically benign alternatives like ADN-based or AN-based systems. While enabling the use of more environmentally friendly oxidizer systems, the addition of active binders and sophisticated catalytic additives gives the possibility of improved performance. With continuous research tackling basic issues in combustion kinetics, environmental compatibility, and production efficiency, the field of composite solid rocket propellants is still vibrant and inventive. For upcoming military, commercial, and aerospace applications, the combination of advanced materials, complex catalyst systems, and creative processing methods promises to produce propellants with better environmental qualities, increased manufacturing efficiency, and improved performance.

References

Agrawal, J. P. (2010). High energy materials: propellants, explosives and pyrotechnics: John Wiley & Sons.

Alemayehu, A. Y., & Solomon, L. G. J. I. J. A. A. R. (2020). Design of a solid rocket propulsion system. 7(2), 224-229.

Arun Kumar, M., Purayil Dhanya, B., Venugopal, S., Vargeese, A. A., & Krishnamurthy, V. J. P., Explosives, Pyrotechnics. (2024). Development of Green Energetic Oxidizers for Solid Propellant Applications: Present Status. 49(12), e202400076.

Bekhouche, S., & Luo, Y. J. J. A. M. R. (2014). Research of formulation and processing

of Hydroxyl-Terminated Polybutadiene (HTPB) propellants. 1030, 155-160.

Bogusz, R., & Magnuszewska, P. J. P., Explosives, Pyrotechnics. (2019). The Aging Studies of the Low HCl Content Composite Rocket Propellant. 44(9), 1193-1198.

Campos, E. A., Dutra, R. d. C. L., Rezende, L. C., Diniz, M. F., Nawa, W. M. D., Iha, K. J. J. o. A. T., & Management. (2010). Performance evaluation of commercial copper chromites as burning rate catalyst for solid propellants. 2(3), 323-330.

Chen, K., Xue, X., & Yu, Y. J. P., Explosives, Pyrotechnics. (2024). A model for the combustion behavior of AP/HTPB propellant containing ultrafine aluminum. 49(7), e202400049.

De Amicis, R., Scalia, T., Accettura, A. J. P. I. A., & AERONAUTICS. (2008). Advanced solid rocket motors. 223, 19.

Elzaki, B. I., & Zhang, Y. J. J. M. (2016). Coating methods for surface modification of ammonium nitrate: A mini-review. 9(7), 502.

Gaur, P., Dev, S., Kumar, S., Kumar, M., Vargeese, A. A., Soni, P., . . . Ghosh, S. J. A. o. (2017). Dendritic polynitrato energetic motifs: development and exploration of physicochemical behavior through theoretical and experimental approach. 2(11), 8227-8233.

Gettwert, V., Tagliabue, C., & Weiser, V. (2017). Burning behavior of aluminized ADN/PSAN propellants. Paper presented at the 7th European Conf. for Aeronautics and Space Science (EUCASS), July.

Gligorijević, N. I., Rodić, V. Ž., Živković, S. Ž., Pavković, B. M., Nikolić, M. M., Kozomara, S. M., & Subotić, S. D. J. H. i. (2016). Mechanical characterization of composite solid rocket propellant based on hydroxy-terminated polybutadiene. 70(5), 581-594.

Gołofit, T., Cieślak, K., & Chmielarek, M. J. M. W. (2023). Theoretical analysis of the use of glycidyl polyazide and polynitratomethylmethyloxetane in high-performance reduced-smoke rocket propellants. 15, 36-47.

Hafner, S., Keicher, T., & Klapötke, T. M. J. P., Explosives, Pyrotechnics. (2018). Copolymers based on GAP and 1, 2-Epoxyhexane as Promising Prepolymers for Energetic Binder Systems. 43(2), 126-135.

Harimech, Z., Salah, M., Amrousse, R. J. I. M. f. I. A. S., Characterization, & Evaluation. (2025). Ammonium Dinitramide (ADN) Decomposition as Green Propellant: Overview of Synthesized Catalysts. 169-194.

Hawass, A., Kim, J. W., & Kwon, S. J. E. J. o. C. (2024). Novel method for Investigation the mass of different pyrotechnics MTV Compositions for rocket motor igniter. 67(3), 203-207.

Hosomi, N., Otake, K., Uegaki, N., Iwasaki, A., Matsumoto, K., Asakawa, M. R., . . . Space Sciences, A. T. J. (2019). Analysis of mixed state of AP/HTPB composite propellant by X-ray computed tomography. 17(1), 14-18.

Jarosz, T., Stolarczyk, A., Wawrzkiewicz-Jalowiecka, A., Pawlus, K., & Miszczyszyn, K. J. M. (2019). Glycidyl azide polymer and its derivatives-versatile binders for explosives and pyrotechnics: tutorial review of recent progress. 24(24), 4475.

Koizumi, H., Hamasaki, K., Kondo, R., Okada, K., Nakano, M., & Arakawa, Y. J. J. S. o. A. S. S. (2010). Effect of the Thruster Configurations on a Laser Ignition Microthruster. 58(677), 178-186.

Kumar Bihari, B., Kumaraswamy, A., Jain, M., & Murthy, K. P. J. P., Explosives, Pyrotechnics. (2022). Assessment of Mechanical Properties of Aged Composite Propellant Using Non-Destructive Indentation Technique in Solid Propellant Rocket Motor. 47(6), e202100339.

Lichthardt, J. P., Tappan, B. C., De, N. N., Novak, A. M., Baca, E. V., Oschwald, D. M., & Risha, G. A. J. P., Explosives, Pyrotechnics. (2022). Novel Segregated Solid Propulsion System with Separately Stored Fuel and Oxidizer. 47(11), e202200142.

Ling, C., Zhang, X., Li, X., Mou, G., Guo, X., Yuan, B., & Yang, K. J. P. (2025). Molecular Simulations of Interface-Driven Crosslinked Network Formation and Mechanical Response in Composite Propellants. 17(13), 1863.

Lu, H., Wang, H., Chen, X., Bai, X., Xu, Z., Wei, Y., & Fan, L. (2023). Improved mass flow rate regulation methods based on variable frequency control: a case study of oxidizer agent weighing for solid propellants. Paper presented at the Actuators.

Mani, G. J. M. R. F. (2025). Earth-Abundant Transition Metal Oxide-based Catalysts for Composite Solid Propellants. 179.

Mingireanu, F., Jula, N., Miclos, S., Baschir, L., & Savastru, D. (2018). Solid rocket motors internal ballistic model with erosive and condensed phase considerations. Paper presented at the The International Conference on Applied Mechanics and Mechanical Engineering.

Mishra, D. P. (2017). Fundamentals of rocket propulsion: CRC Press.

Mourdikoudis, S., Kostopoulou, A., & LaGrow, A. P. J. A. S. (2021). Magnetic nanoparticle composites: synergistic effects and applications. 8(12), 2004951.

Navalino, R., Muda, N. R. S., Hafizah, M., & Ruyat, Y. J. F. (2024). Analysis of carbon nano particle variant as the propellant fuel to increase specific impulses of rockets. 12, 1414.

Park, S., Choi, S., Kim, K., Kim, W., & Park, J. J. P., Explosives, Pyrotechnics. (2020).

Effects of ammonium perchlorate particle size, ratio, and total contents on the properties of a composite solid propellant. 45(9), 1376-1381.

Rao, N. P., Solanke, C., Bihari, B. K., Singh, P. P., & Bhattacharya, B. J. P., Explosives, Pyrotechnics. (2016). Evaluation of mechanical properties of solid propellants in rocket motors by indentation technique. 41(2), 281-285.

Remissa, I., Jabri, H., Hairch, Y., Toshtay, K., Atamanov, M., Azat, S., & Amrousse, R. J. E. C.-T. J. (2023). Propulsion systems, propellants, green propulsion subsystems and their applications: a review. 25(1), 3-19.

Runtu, K. R., Setiani, W., Utami, M. J. I. J. o. S. S. R., & Review. (2023). Application energetic materials for solid composite propellant to support defense rocket development. 6(1), 153-159.

Sahimi, M. (2003). Heterogeneous Materials I: Linear transport and optical properties: Springer.

Said, A., Maraden, A., Elhedery, T., Abd Elall, A., & Elbasuney, S. (2023). Propulsion theoretical and experimental analysis of composite propellants motors. Paper presented at the Journal of Physics: Conference Series.

Shekhar, H. J. D. S. J. (2012). Studies on Stress-Strain Curves of Aged Composite Solid Rocket Propellants. 62(2).

Shi, J., Liang, J., Sun, X., Li, Y., Zhang, H., Guo, X., . . . Nie, J. J. N. (2025). Synergistic Regulation of Combustion Behavior and Safety Characteristics of Graphene Modified Core–Shell Al@ AP Composites. 15(11), 853.

Singh, H., & Shekhar, H. (2016). Solid rocket propellants: science and technology challenges: Royal Society of Chemistry.

Sutton, G. P., & Biblarz, O. (2011). Rocket propulsion elements: John Wiley & Sons.

Tawfik, S. M., Saleh, A., Elbeih, A., & Klapötke, T. M. J. Z. f. a. u. a. C. (2016). Reactive nanocomposites as versatile additives for composite propellants. 642(21), 1222-1229.

Thakre, P., & Yang, V. J. E. o. a. e. (2010). Solid propellants.

Tsyshevsky, R., Pagoria, P., Zhang, M., Racoveanu, A., DeHope, A., Parrish, D., & Kuklja, M. M. J. T. J. o. P. C. C. (2015). Searching for low-sensitivity cast-melt high-energy-density materials: Synthesis, characterization, and decomposition kinetics of 3, 4-bis (4-nitro-1, 2, 5-oxadiazol-3-yl)-1, 2, 5-oxadiazole-2-oxide. 119(7), 3509-3521.

Unni, A. A., Kulkarni, R., Singh, C., Singh, V., Varshini, V. M. P., & Shanmugaraj, G. (2020). Effects of adding powdered metals with the solid propellants–A review. Paper presented at the Journal of Physics: Conference Series.

Zhao, N., Li, J., Zhao, F., An, T., Hu, R., & Ma, H. J. D. C. T. (2016). Combustion catalyst: Nano-fe2o3 and nano-thermite al/fe2o3 with different shapes. 325(10.5772), 64748.

About The Authors

Selva ASTAN is an R&D Engineer at the Mechanical and Chemical Industries Corporation, R&D and Technology Directorate in Ankara, working in the field of energetic materials for defense industry projects. She holds a master's degree in Metallurgical and Materials Engineering from Sivas Cumhuriyet University. Her master's research focused on the electroceramic fabrication of high-temperature stable piezoelectric materials, including dielectric and electromechanical characterization and advanced microstructure analysis. She earned a bachelor's degree in Materials Science and Engineering from Gebze Technical University, where she was a member of the Piezodevices Research Group.

E-mail : selvaastan@gmail.com, **ORCID :** 0009-0007-3075-1410

Ahmet Burçin BATIBAY, PhD, works as a Senior Engineer at the Energetic Materials Research Center, which is part of the R&D and Technology Directorate located within the Mechanical and Chemical Industry Cooperation in Ankara, Turkey. He earned a master's degree in Materials Science and Engineering from Istanbul Technical University and subsequently obtained his PhD in the same field from Afyon Kocatepe University. His primary research interests encompass powder metallurgy, biomaterials, energetic materials, and materials characterization.

E-mail : batybay@gmail.com, **ORCID :** 0000-0002-2606-5115

Similarity Index:

The similarity index obtained from the plagiarism software for this book chapter is 10%.

Characterization of Energetic Materials

Ahmet Burçin BATIBAY
Mechanical and Chemical Industries Corporation

To Cite This Chapter:
Batibay, A. B. (2025). Characterization of energetic materials. In H. Gokmese, S. Bulbul, & Y. Uzun (Eds.), *Innovative approaches in materials science and applications* (pp. 170–181). ISRES Book Series. ISRES Publishing.

Introduction

Energetic materials (EMs) play a vital role in various applications, ranging from military munitions to civilian explosives for construction and resource extraction. The continuous enhancement of these materials is driven by the demand for higher performance, safety, and stability. Owing to their composition and properties, energetic materials can generally be divided into categories based on their chemical makeup and intended use (Badgujar, Talawar, Asthana, & Mahulikar, 2008).

Energetic materials can be broadly classified into several categories. The primary distinction lies between low explosives and high explosives. Low explosives, like black powder, deflagrate, burning relatively slowly and producing a rapid expansion of gases. In contrast, high explosives, such as TNT or RDX, detonate, resulting in a supersonic shockwave. Further distinctions can include:

- Propellants: used in rockets, propellants burn to produce thrust. Solid propellants consist of a fuel and an oxidizer mixed into a solid form, whereas liquid propellants combine liquid fuel with an oxidizer.
- Explosives: high explosives induce rapid combustion a detonation that produces a shockwave capable of causing destruction.
- Pyrotechnics: these include materials that burn or explode and are often used for signaling (e.g., flares, fireworks) (Klapötke, 2025).

Properties of EMs

Energetic materials (EMs) represent a critical class of chemical compounds that undergo rapid exothermic reactions, generating heat and gas—predominantly nitrogen—essential for various applications such as explosives, propellants, and pyrotechnics. Their utility spans a wide range of fields, including military uses (e.g., munitions and missiles), aerospace applications (e.g., rocket fuels), and civilian activities (e.g., construction and mining explosives). As the demand for EMs continues to evolve, the field relies on advancements that strike a careful balance between high energy density and the paramount concerns of safety, stability, and environmental impact (Chen et al.,

2021; Chun et al., 2020). Recent research efforts have intensified, focusing on various classes of energetic materials, such as high-nitrogen compounds, ionic liquids, and advanced organic frameworks, which are tailored to meet these evolving requirements (X. Liu, Ortmeyer, Bodach, Petersen, & Felderhoff, 2025; Zhou et al., 2014). This trend highlights the significance of ongoing innovations in EMs, ensuring that they remain safe and effective for both military and civilian applications (S. Zhang et al., 2020), while addressing challenges associated with environmental sustainability (Goncalves, Iha, & Rocco, 2018). Thus, the quest for novel energetic compounds continues, with an emphasis on synthesizing materials that not only enhance performance but are also safer and more environmentally friendly (An et al., 2009; Feng, Qiu, Yang, Du, & Zhang, 2016).

One of the significant trends in the development of high-performance EMs is the incorporation of nitrogen-rich compounds. Materials rich in nitrogen are desirable due to their high heat of formation, which leads to increased energetic performance. For instance, Du et al. highlight that compounds based on 1,3,4-oxadiazoles present excellent candidates for high-performing EMs due to their stability and favorable oxygen-balance properties (Du, Qu, Wang, Cui, & Wang, 2021). Similarly, Zhang et al. emphasize the role of fused triazole-tetrazine compounds that showcase versatile energetic performance, reflecting the growing trend towards advanced organic chemistry in EM development influenced by military and civilian needs (H. Zhang et al., 2024). Additionally, the focus on dinitrophenyl and tetrazole derivatives illustrates the continual exploration of new frameworks with optimized performance attributes (Zhao et al., 2024).

High-nitrogen compounds are a significant focus within the realm of EMs due to their favorable energy profiles and environmentally friendly byproducts, primarily nitrogen gas upon decomposition. Ionic liquids have emerged as promising alternatives to traditional solid explosives and propellant fuels, possessing unique properties that allow for tunable energy densities and mitigated volatility (Q. Wang, Wang, Zhou, & Gao, 2023; Q. Zhang & Shreeve, 2014). The adoption of such materials can potentially reduce the sensitivity associated with conventional explosives, offering safer handling without compromising performance. Recent advancements demonstrate that integrating high nitrogen content in energetic salts can yield materials with enhanced stability and performance traits (He et al., 2016; Q. Wang et al., 2023).

Another area of significant interest is the advancement of fused heterocycles, particularly those constructed through innovative synthetic methodologies. Studies indicate that incorporating fused-ring systems contributes to improved energetic performance while addressing safety concerns linked to traditional materials (Gao, Zhang, & Jean'ne, 2020; L. Yang et al., 2022). Fused compounds typically present a structurally resilient framework, which can stabilize the energetic content without the high sensitivity

often observed in their linear counterparts (Bu, Xiong, Zhang, & Design, 2020). The exploration of new synthetic pathways continues to provide fresh insights into designing advanced EMs that meet the rigorous demands of modern applications.

The focus has also been directed towards using metal-organic frameworks (MOFs) and nano-sized composite materials. MOFs are recognized for their tunable porosity and functionality, allowing for the encapsulation of energetic materials and optimized release profiles (Li et al., 2013; J. Liu et al., 2022). Research indicates that MOFs can serve as platforms for high-performance EMs, enhancing properties such as stability, energy output, and lower sensitivity to external stimuli (Gettings, Zeller, Byrd, & Piercey, 2019; J. Liu et al., 2022). Similarly, nano-sized composite energetic materials (nano-CEMs) present a breakthrough, leveraging their high surface area and reactivity to refine detonation characteristics and reduce the environmental impact of EMs (Jiang, Cai, Mao, & Wang, 2019; Pang et al., 2020).

Recent advancements in material science, particularly through the development of metal-organic frameworks (MOFs) and composite materials, have facilitated the production of EMs with enhanced properties. For example, Yang et al. explore the potential of multifunctional materials based on 1-aminotetrazol-5-one ligands, highlighting their broad range of sensitivities and reactivity (J. Yang et al., 2018). Furthermore, the incorporation of nanoscale additives has been shown to improve the performance of existing EMs, as demonstrated by Cheng et al., whose work reveals the positive effects of boron powders on the detonation performance of explosives (Cheng, Yao, Li, Li, & Yao, 2023).

Safety remains a paramount concern in the design of energetic materials. The challenge lies in balancing high energy density with sufficient thermal and mechanical stability, crucial for safe handling and storage. For example, Lin et al. and Liu et al. underscore the importance of developing heat-resistant EMs that can perform reliably at elevated temperatures, particularly in applications like oil and gas extraction where thermal stability is vital (Lin, Chen, Xu, Zheng, & Wen, 2019; N. Liu et al., 2020). Alongside this, the development of insensitive materials has become a focal area of research, as reflected in the studies of Dippold and Klapötke, which investigate the design of high-performance insensitive EMs through strategic molecular modifications (Dippold & Klapötke, 2013).

The importance of thermal stability in EMs cannot be overstated, as it directly influences their performance across various operational environments. The development of heat-resistant energetic materials, such as those derived from specific heterocyclic structures, has been pivotal in ensuring reliability at elevated temperatures (Stolarczyk & Jarosz, 2022; Z. Zhang et al., 2021). Advancements have led to the discovery of heat-resistant

compounds that maintain stability in ascent scenarios experienced in aerospace applications, thus meeting modern equipment demands designed for extreme conditions (Stolarczyk & Jarosz, 2022).

Thermal stability of EMs is a critical factor determining their usability in extreme conditions. Stability depends significantly on the molecular structure and the presence of stabilizing agents. Extensive studies have focused on creating heat-resistant EMs through structural modifications (Bu et al., 2020). For instance, the addition of halogens or the strategic placement of nitrogen-rich groups within molecular frameworks often results in improved stability (Li et al., 2013; J. Liu et al., 2022).

Compounds like 1,3,5-triamino-2,4,6-trinitrobenzene (TATB) have gained attention for their thermal stability, able to resist initiation under high temperatures while maintaining good energetic outputs (Gettings et al., 2019). These findings underscore the importance of material innovations focused on retaining performance under varied environmental conditions.

Collaboration between chemists and material scientists has facilitated a better understanding of the underlying mechanisms governing impact sensitivity, stability, and energetic performance of these materials. As new compounds are synthesized, cheminformatics approaches are being integrated to model and predict the behaviors of these substances under various conditions, which is imperative to enhancing safety profiles and improving predictability in applications (Fayet & Rotureau, 2022; B. Wang et al., 2018).

The field of energetic materials is rapidly evolving, driven by the need for improved performance, safety, and environmental considerations. The synthesis of high-nitrogen compounds, exploration of ionic liquids, utilization of complex frameworks such as MOFs, and advancements in heat-resistant materials exemplify the dynamic nature of this research area. As new methodologies and materials continue to emerge, the implications for both military and civilian applications could be substantial, transforming how energetic materials are utilized across multiple industries.

Another critical aspect of EMs is the characterization of their performance characteristics under various operational conditions. Various studies have consistently demonstrated that structural modifications can significantly impact the thermal stability and detonation performance of EMs. For instance, Yao et al. discussed the effectiveness of micro-encapsulation to enhance the thermal safety of high-energy emulsion explosives (Yao et al., 2021), while Lei et al. explored integration of pyrazole compounds that have shown promise in yielding new classes of insensitive EMs without compromising safety (Lei, Yang, & Cheng, 2020; Yin, Mitchell, Parrish, & Shreeve, 2017).

In conclusion, the evolution of energetic materials is characterized by an intricate interplay of chemical innovation, safety considerations, and performance optimization. Continued research efforts aim to balance these factors while addressing the specific demands of both military and civilian applications. The synthesis of nitrogen-rich compounds, the development of heat-resistant formulations, and advances in composite materials demonstrate the dynamic nature of this field, positioning it as a critical area of both fundamental chemistry and applied sciences.

Structural, Mechanical, and Thermal Characterization of EMs

Energetic materials (EMs) are vital for various applications, including military munitions, propellants for aerospace applications, and demolition explosives in civil engineering. An accurate and comprehensive characterization of these materials is essential for ensuring their reliability, performance, and safety. Characterization encompasses a range of physical and chemical techniques aimed at understanding the materials' structure, sensitivity to external stimuli, mechanical behavior, thermal properties, and overall stability.

Structural characterization techniques such as X-ray Crystallography and Nuclear Magnetic Resonance (NMR) are pivotal in determining the molecular and crystal structures of energetic materials. These methods help elucidate the arrangement of atoms within the material, which directly relates to its energy release mechanisms during detonation. For example, Wozniak et al. highlighted the importance of identifying structural motifs by employing NMR and infrared spectroscopy coupled with crystallography to validate the structural integrity of newly synthesized energetic compounds (Wozniak, Salfer, Zeller, Byrd, & Piercey, 2020).

Additionally, infrared (IR) spectroscopy can be employed to identify functional groups and study bond formations in energetic materials, offering insights into intermolecular interactions and assessing the stability of particular chemical functionalities within the material (Pedreira et al., 2016).

The mechanical properties of EMs significantly influence their performance, particularly in terms of shock sensitivity and internal defect management. Nanoindentation provides a means to measure hardness and elastic modulus at the nanoscale, allowing researchers to understand how EMs respond to mechanical loads. Olokun et al. explored the mechanical anisotropy of β-HMX crystals through nanoindentation and small-scale dynamic impact tests, emphasizing the importance of understanding deformation mechanisms that could alter the safety parameters of explosives (Olokun, Dillard, Dhiman, & Tomar, 2021).

Dynamic mechanical analysis (DMA) provides additional insights into the elastic properties of EMs under varying temperature and frequency conditions. It helps determine

the materials' responses to dynamic loads, which is essential for evaluating potential failure under high-stress conditions (Kaneshige, Rabbi, Mach, Catzin, & Stewart, 2017).

Thermal analysis techniques, such as Differential Scanning Calorimetry (DSC) and Thermogravimetric Analysis (TGA), provide critical information regarding the thermal stability, decomposition temperatures, and energetic performance of EMs. These techniques help ascertain the temperature ranges within which the materials are stable and their decomposition profiles during thermal exposure. For instance, Gaur et al. utilized TGA and DSC to analyze the thermal stability and gas evolution of triazole-based energetic motifs, allowing for an understanding of their energetic properties (Gaur et al., 2017).

Accelerated aging tests involve subjecting EMs to elevated temperatures and humidity to simulate long-term storage conditions. By monitoring performance changes, researchers can predict shelf life and operational stability, guiding formulations for military and commercial applications (Tsyshevsky et al., 2015).

Examples of novel characterization techniques such as multiaxial testing, energetic coordination polymers, and cocrystallization. Kaneshige et al. introduced novel methods for modeling the multiaxial constitutive and damage responses of energetic materials, facilitating a thorough understanding of their behavior under various loading conditions, which is essential for practical applications (Kaneshige et al., 2017).

The synthesis and characterization of Energetic Coordination Polymers (ECPs) have gained momentum, especially in achieving a balance between high energy density and low sensitivity. These materials present unique opportunities due to their tunable mechanical and energetic properties (Qu et al., 2015; J. Yang et al., 2018).

Cocrystallization has emerged as a promising method for tuning the physicochemical properties of EMs. Wiscons and Matzger discussed the challenges of characterizing cocrystals compared to physical mixtures, underscoring the necessity for comprehensive methods such as single-crystal X-ray diffraction to ensure accurate analysis (Wiscons, Matzger, & Design, 2017).

Performance Characterization of EMs

To ensure the reliability of EMs across various applications, robust performance characterization becomes essential. Standard tests typically assess crucial characteristics of EMs, such as detonation velocity, brisance (shattering capability), sensitivity (impact, friction, and thermal), and thermal decomposition temperatures.

Detonation tests measure the speed at which the shock wave travels through an explosive; higher velocities indicate more powerful explosives. The characterization often employs

empirical correlations and thermochemical calculations to determine performance (Pang et al., 2020). The detonation velocity (Dv) is a crucial property for assessing the energetic performance of explosives. Various experimental setups, employing detonators and pressure gauges, facilitate the measurement of Dv, yielding critical insights into the efficiency and power of the material (Yan et al., 2021).

Impact Sensitivity testing methods that simulate impacts and friction provide insights into the stability and safety associated with specific EMs. Areas of interest include how structural modifications affect the energetic material's propensity for accidental detonation (Jiang et al., 2019). Impact sensitivity tests measure the threshold energy required for detonation or deflagration when exposed to mechanical shock. For instance, Wozniak et al. characterized newly developed N-amino compounds for their impact sensitivity, classifying them among primary explosives (Wozniak et al., 2020).

Friction sensitivity tests, testing the response of EMs to friction, involve applying various loads and assessing the resulting frictional interactions, which guide the design of formulations that minimize the risk of unintended initiation during handling and storage (Lal, Staples, & Jean'ne, 2024).

With increasing environmental awareness, the development of "green" energetic materials is crucial. Assessments focus on the byproducts of explosions, emphasizing formulations that yield minimal ecological damage. This has led researchers to explore eco-friendly additives and greener chemical processes to reduce toxicity (Z. Zhang et al., 2021).

Future Directions in Energetic Materials Research

The future of EMs holds immense potential as new synthetic strategies and materials continue to be developed. Much research will focus on: Computational modelling, machine learning approaches, collaboration across disciplines, and sustainability-environmental conditions.

Advances in computational chemistry have led to the development of predictive models that can simulate the performance and stability of EMs before synthesis. For example, Tsyshevsky et al. described a comprehensive approach combining synthesis, characterization, and quantum-chemical modeling to design novel energetic materials effectively (Tsyshevsky et al., 2017). This predictive capability can significantly expedite the design process by circumventing the costly synthesis of ineffective compounds.

Recent efforts have integrated machine learning techniques to enhance screening processes for EMs. Utilizing thermochemical data and properties such as cohesive energy and oxygen balance enables machine learning to predict energetic performance efficiently, aiding in the identification of promising compounds (Kang, Liu, Abou-Rachid, & Guo, 2020). This approach holds potential for optimizing formulations tailored to

specific performance metrics while reducing trial-and-error methodologies in physical laboratories. The application of machine learning algorithms can expedite the discovery of new EMs by predicting the performance of molecular structures based on existing databases, optimizing formulations based on historical data (Stolarczyk & Jarosz, 2022).

The future of EMs will likely see heightened cooperation among chemists, material scientists, and engineers, culminating in innovative approaches to EM design, synthesis, and performance testing (Fayet & Rotureau, 2022). Finding sustainable paths for the synthesis and application of EMs will become increasingly essential, pushing research towards utilizing renewable resources and minimizing hazardous waste production.

Conclusion

The field of energetic materials is evolving rapidly, reflecting the complex interplay of performance demands, safety requirements, and environmental issues. Innovations driven by high-nitrogen chemistry, advanced composite materials, synthetic pathways, and a vigorous focus on safety are shaping the future of both military and civilian applications. The ongoing exploration of materials with tailored properties, enhanced stability, and reduced sensitivities promises a new era for the development of EMs, catering to the diverse and dynamic needs across multiple sectors.

The characterization of energetic materials is a multifaceted process encompassing various techniques tailored to understanding the materials' structural, thermal, mechanical, and energetic properties. Advances in computational modeling and machine learning further enhance the research landscape, allowing predictions of performance outcomes that inform the design of next-generation EMs. Continuous innovation in analytical techniques not only aids in developing safer and more efficient energetic materials but also ensures compliance with stringent safety regulations, paving the way for broader applications in both military and civilian domains.

References

An, C. W., Li, F. S., Song, X. L., Wang, Y., Guo, X. D. J. P., Explosives, Pyrotechnics: An International Journal Dealing with Scientific, & Materials, T. A. o. E. (2009). Surface Coating of RDX with a Composite of TNT and an Energetic-Polymer and its Safety Investigation. 34(5), 400-405.

Badgujar, D., Talawar, M., Asthana, S., & Mahulikar, P. J. J. o. h. m. (2008). Advances in science and technology of modern energetic materials: an overview. 151(2-3), 289-305.

Bu, R., Xiong, Y., Zhang, C. J. C. G., & Design. (2020). π–π stacking contributing to the low or reduced impact sensitivity of energetic materials. 20(5), 2824-2841.

Chen, L., Cao, X., Gao, J., Wang, Y., Zhang, Y., Liu, J., & He, W. J. P., Explosives,

Pyrotechnics. (2021). Synthesis of 3D Porous Network Nanostructure of Nitrated Bacterial Cellulose Gel with Eminent Heat-Release, Thermal Decomposition Behaviour and Mechanism. 46(8), 1292-1303.

Cheng, Y. F., Yao, Y. L., Li, D. Y., Li, Z. H., & Yao, Y. K. J. P., Explosives, Pyrotechnics. (2023). Effects of boron powders on the detonation performance of emulsion explosives. 48(3), e202200277.

Chun, S., Roy, S., Nguyen, Y. T., Choi, J. B., Udaykumar, H. S., & Baek, S. S. J. S. r. (2020). Deep learning for synthetic microstructure generation in a materials-by-design framework for heterogeneous energetic materials. 10(1), 13307.

Dippold, A. A., & Klapötke, T. M. J. J. o. t. A. C. S. (2013). A study of dinitro-bis-1, 2, 4-triazole-1, 1′-diol and derivatives: design of high-performance insensitive energetic materials by the introduction of N-oxides. 135(26), 9931-9938.

Du, Y., Qu, Z., Wang, H., Cui, H., & Wang, X. J. P., Explosives, Pyrotechnics. (2021). Review on the synthesis and performance for 1, 3, 4-oxadiazole-based energetic materials. 46(6), 860-874.

Fayet, G., & Rotureau, P. J. M. I. (2022). Chemoinformatics for the safety of energetic and reactive materials at Ineris. 41(1), 2000190.

Feng, Y.-a., Qiu, H., Yang, S.-s., Du, J., & Zhang, T.-l. J. D. T. (2016). Carbonyl-bridged energetic materials: biomimetic synthesis, organic catalytic synthesis, and energetic performances. 45(43), 17117-17122.

Gao, H., Zhang, Q., & Jean'ne, M. S. J. J. o. M. C. A. (2020). Fused heterocycle-based energetic materials (2012–2019). 8(8), 4193-4216.

Gaur, P., Dev, S., Kumar, S., Kumar, M., Vargeese, A. A., Soni, P., . . . Ghosh, S. J. A. o. (2017). Dendritic polynitrato energetic motifs: development and exploration of physicochemical behavior through theoretical and experimental approach. 2(11), 8227-8233.

Gettings, M. L., Zeller, M., Byrd, E., & Piercey, D. G. J. Z. f. a. u. a. C. (2019). Synthesis and characterization of salts of the 3, 6-Dinitro-[1, 2, 4] triazolo [4, 3-b][1, 2, 4] triazolate Anion: insensitive energetic materials available from economical precursors. 645(20), 1197-1204.

Goncalves, R. F. B., Iha, K., & Rocco, J. A. (2018). Enhancement of Energetic Materials Combustion Process. In Energetic Materials Research, Applications, and New Technologies (pp. 25-50): IGI Global Scientific Publishing.

He, P., Zhang, J. G., Yin, X., Wu, J. T., Wu, L., Zhou, Z. N., & Zhang, T. L. J. C. A. E. J. (2016). Energetic Salts Based on Tetrazole N-oxide. 22(23), 7670-7685.

Jiang, C., Cai, S., Mao, L., & Wang, Z. J. M. (2019). Effect of porosity on dynamic

mechanical properties and impact response characteristics of high aluminum content PTFE/Al energetic materials. 13(1), 140.

Kaneshige, M. J., Rabbi, M. F., Mach, R., Catzin, C. A., & Stewart, C. M. (2017). Novel Method to Characterize and Model the Multiaxial Constitutive and Damage Response of Energetic Materials. Retrieved from

Kang, P., Liu, Z., Abou-Rachid, H., & Guo, H. J. T. J. o. P. C. A. (2020). Machine-learning assisted screening of energetic materials. 124(26), 5341-5351.

Klapötke, T. M. (2025). Chemistry of High-Energy Materials: Explosives, Propellants, Pyrotechnics: Walter de Gruyter GmbH & Co KG.

Lal, S., Staples, R. J., & Jean'ne, M. S. J. D. T. (2024). Nitroiminotriazole (NIT) based potential solid propellants: synthesis, characterization, and applications. 53(3), 903-907.

Lei, C., Yang, H., & Cheng, G. J. D. T. (2020). New pyrazole energetic materials and their energetic salts: combining the dinitromethyl group with nitropyrazole. 49(5), 1660-1667.

Li, S., Wang, Y., Qi, C., Zhao, X., Zhang, J., Zhang, S., & Pang, S. J. A. C., Int. Ed. (2013). 3D energetic metal–organic frameworks: synthesis and properties of high energy materials. 52(52), 14031-14035.

Lin, J.-D., Chen, F., Xu, J.-G., Zheng, F.-K., & Wen, N. J. A. A. N. M. (2019). Framework-interpenetrated nitrogen-rich Zn (II) metal–organic frameworks for energetic materials. 2(8), 5116-5124.

Liu, J., Lei, T., Xue, Y., Wang, X., Yan, Q.-l., Fu, X., . . . Guo, Z. J. L. (2022). Modulation of crystal growth of an energetic metal–organic framework on the surfaces of graphene derivatives for improved detonation performance. 38(48), 14959-14968.

Liu, N., Xiao, C., Duan, B., Lu, X., Wang, B., Zhang, J., & Yan, Q.-L. J. A. A. E. M. (2020). Highly thermostable insensitive energetic polynitrophenyl-substituted furazan (furoxan)-annelated azepines. 3(7), 7129-7137.

Liu, X., Ortmeyer, J., Bodach, A., Petersen, H., & Felderhoff, M. J. C. A. E. J. (2025). Amine-AlH3 Adducts as Energetic Materials for a New Generation of Solid Fuels. e202501163.

Olokun, A., Dillard, T., Dhiman, A., & Tomar, V. J. S. A. S. (2021). Experimental study of anisotropic constitutive behavior of β-HMX crystals via nanoindentation and small-scale dynamic impact. 3(12), 875.

Pang, W., Fan, X., Wang, K., Chao, Y., Xu, H., Qin, Z., & Zhao, F. J. N. (2020). Al-based nano-sized composite energetic materials (nano-CEMs): Preparation,

characterization, and performance. 10(6), 1039.

Pedreira, S. M., Pinto, J. R. A., Campos, E. A., Mattos, E. d. C., Oliveira Junior, M. S. d., Oliveira, J. I. S. d., . . . Management. (2016). Methodologies for characterization of aerospace polymers/energetic materials–a short review. 8, 18-25.

Qu, X., Zhang, S., Yang, Q., Su, Z., Wei, Q., Xie, G., & Chen, S. J. N. J. o. C. (2015). Silver (I)-based energetic coordination polymers: synthesis, structure and energy performance. 39(10), 7849-7857.

Stolarczyk, A., & Jarosz, T. J. F. (2022). Thermal Properties of Energetic Materials—What Are the Sources of Discrepancies? , 5(6), 206.

Tsyshevsky, R., Pagoria, P., Zhang, M., Racoveanu, A., DeHope, A., Parrish, D., & Kuklja, M. M. J. T. J. o. P. C. C. (2015). Searching for low-sensitivity cast-melt high-energy-density materials: Synthesis, characterization, and decomposition kinetics of 3, 4-bis (4-nitro-1, 2, 5-oxadiazol-3-yl)-1, 2, 5-oxadiazole-2-oxide. 119(7), 3509-3521.

Tsyshevsky, R., Pagoria, P., Zhang, M., Racoveanu, A., Parrish, D. A., Smirnov, A. S., & Kuklja, M. M. J. T. J. o. P. C. C. (2017). Comprehensive end-to-end design of novel high energy density materials: I. Synthesis and characterization of oxadiazole based heterocycles. 121(43), 23853-23864.

Wang, B., Feng, Y., Qi, X., Deng, M., Tian, J., & Zhang, Q. J. C. A. E. J. (2018). Designing explosive poly (ionic liquid) s as novel energetic polymers. 24(59), 15897-15902.

Wang, Q., Wang, T., Zhou, Y., & Gao, H. (2023). Method and apparatus for automatic high-throughput synthesis of energetic salts. Paper presented at the Journal of Physics: Conference Series.

Wiscons, R. A., Matzger, A. J. J. C. G., & Design. (2017). Evaluation of the appropriate use of characterization methods for differentiation between cocrystals and physical mixtures in the context of energetic materials. 17(2), 901-906.

Wozniak, D. R., Salfer, B., Zeller, M., Byrd, E. F., & Piercey, D. G. J. C. (2020). Sensitive energetics from the N-amination of 4-nitro-1, 2, 3-triazole. 9(8), 806-811.

Yan, P., Zhao, X., Rui, J., Zhao, J., Xu, M., & Zhai, L. J. C. (2021). Molecular dynamics simulation of the influence of RDX internal defects on sensitivity. 11(4), 329.

Yang, J., Yin, X., Wu, L., Wu, J., Zhang, J., & Gozin, M. J. I. C. (2018). Alkaline and earth alkaline energetic materials based on a versatile and multifunctional 1-aminotetrazol-5-one ligand. 57(24), 15105-15111.

Yang, L., Zhang, Z.-Q., Yang, W., Ma, Q., Li, W., Li, J. J. C. G., & Design. (2022). Iodine-mediated furoxan formation facilitates the synthesis of high-density

tricyclic fused energetic materials. 23(1), 532-538.

Yao, Y. l., Cheng, Y. f., Liu, R., Hu, F. f., Zhang, Q. w., Xia, Y., & Chen, Y. J. P., Explosives, Pyrotechnics. (2021). Effects of Micro-Encapsulation Treatment on the Thermal Safety of High Energy Emulsion Explosives with Boron Powders. 46(3), 389-397.

Yin, P., Mitchell, L. A., Parrish, D. A., & Shreeve, J. n. M. J. C. A. A. J. (2017). Comparative Study of Various Pyrazole-based Anions: A Promising Family of Ionic Derivatives as Insensitive Energetic Materials. 12(3), 378-384.

Zhang, H., Du, X., Liu, Y., Lei, G., Yin, P., & Pang, S. J. A. o. (2024). Fused triazole-tetrazine assembled with different functional moieties: construction of multipurpose energetic materials. 9(31), 33557-33562.

Zhang, Q., & Shreeve, J. n. M. J. C. r. (2014). Energetic ionic liquids as explosives and propellant fuels: a new journey of ionic liquid chemistry. 114(20), 10527-10574.

Zhang, S., Gao, Z., Lan, D., Jia, Q., Liu, N., Zhang, J., & Kou, K. J. M. (2020). Recent advances in synthesis and properties of nitrated-pyrazoles based energetic compounds. 25(15), 3475.

Zhang, Z., Geng, W., Yang, W., Ma, Q., Li, W., Fan, G., & Chen, Y. J. P., Explosives, Pyrotechnics. (2021). Heat-resistant energetic materials deriving from benzopyridotetraazapentalene: Halogen bonding effects on the outcome of crystal structure, thermal stability and sensitivity. 46(4), 593-599.

Zhao, B., Kuang, B., Sun, M., Wang, T., Zhang, C., Xu, M., . . . Zhang, J.-g. J. C. (2024). 3-(3, 5-Dinitrophenyl)-5-amino-1, 2, 4-oxadiazole: synthesis, structure and properties of a novel insensitive energetic material. 26(19), 2491-2497.

Zhou, X., Torabi, M., Lu, J., Shen, R., Zhang, K. J. A. a. m., & interfaces. (2014). Nanostructured energetic composites: synthesis, ignition/combustion modeling, and applications. 6(5), 3058-3074.

About The Author

Ahmet Burçin BATIBAY, PhD, works as a Senior Engineer at the Energetic Materials Research Center, which is part of the R&D and Technology Directorate located within the Mechanical and Chemical Industry Cooperation in Ankara, Turkey. He earned a master's degree in Materials Science and Engineering from Istanbul Technical University and subsequently obtained his PhD in the same field from Afyon Kocatepe University. His primary research interests encompass powder metallurgy, biomaterials, energetic materials, and materials characterization.

E-mail : batybay@gmail.com, **ORCID :** 0000-0002-2606-5115

Similarity Index

The similarity index obtained from the plagiarism software for this book chapter is 2%.

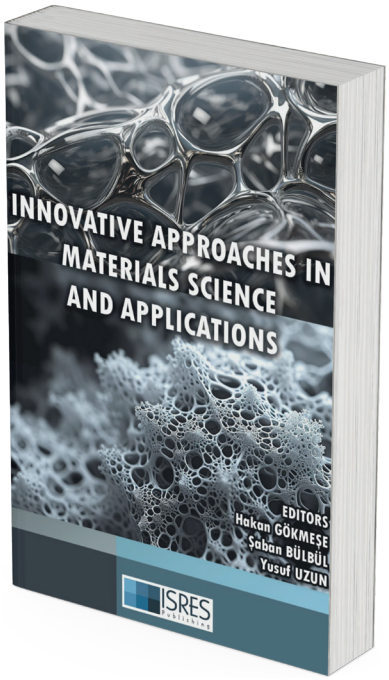

Innovative Approaches in Materials Science and Applications were published from selected articles invited by the editors.

This scholarly volume entitled **"*Innovative Approaches in Materials Science and Applications,*"** consists of 10 chapters that systematically present the latest discoveries and transformative applications in the field. All applications are reviewed by at least two international referees. It covers all groundbreaking aspects of materials science, from engineering materials and adaptive materials to the mechanical and physical properties of materials and sustainable and environmentally friendly composites.

Innovative Approaches in Materials Science and Applications are published by ISRES Publications.

ISRES Publishing